Chem Soc Rev

Functionalization of phosphorescent emitters and their host materials by main-group elements for phosphorescent organic light-emitting devices

Journal:	*Chemical Society Reviews*
Manuscript ID:	CS-REV-05-2015-000424.R1
Article Type:	Review Article
Date Submitted by the Author:	19-Jul-2015
Complete List of Authors:	Yang, Xiaolong; Xi'an Jiaotong University, Department of chemistry, School of science Zhou, Guijiang; MOE Key Laboratory for Nonequilibrium Synthesis and Modulation of Condensed Matter, State Key Laboratory for Mechanical Behavior of Materials, Department of Chemistry, Faculty of Science, Xi'an Jiaotong University, Xi'an 710049, P.R. China., Wong, Wai-Yeung (Raymond); Hong Kong Baptist University, Department of Chemistry

Functionalization of phosphorescent emitters and their host materials by main-group elements for phosphorescent organic light-emitting devices

Xiaolong Yang,[a] Guijiang Zhou*[a] and Wai-Yeung Wong*[bc]

[a] MOE Key Laboratory for Nonequilibrium Synthesis and Modulation of Condensed Matter, State Key Laboratory for Mechanical Behavior of Materials, Department of Chemistry, Faculty of Science, Xi'an Jiaotong University, Xi'an 710049, P.R. China. E-mail: zhougj@mail.xjtu.edu.cn

[b] Institute of Molecular Functional Materials, Department of Chemistry and Institute of Advanced Materials, Hong Kong Baptist University, Waterloo Road, Kowloon Tong, Hong Kong, P.R. China. E-mail: rwywong@hkbu.edu.hk

[c] HKBU Institute of Research and Continuing Education, Shenzhen Virtual University Park, Shenzhen, 518057, P.R. China.

Phosphorescent organic light-emitting devices (OLEDs) have attracted increased attention from both academic and industrial communities due to their potential practical application in high-resolution full-color displays and energy-saving solid-state lightings. The performance of phosphorescent OLEDs is mainly limited by the phosphorescent transition metal complex (such as iridium(III), platinum(II), gold(III), ruthenium(II), copper(I) and osmium(II) complexes, *etc.*) which can play a crucial role in furnishing efficient energy transfer, balanced charge injection/transporting character and high quantum efficiency in the devices. It has been shown that functionalized main-group element (such as boron, silicon, nitrogen, phosphorus, oxygen, sulfur and fluorine, *etc.*) moieties can be incorporated into phosphorescent emitters and their host materials to tune their triplet energies, frontier molecular orbital energies, charge injection/transporting behavior, photophysical properties and thermal stability and hence bring about highly efficient phosphorescent OLEDs. So, in this review, the recent advances on the phosphorescent emitters and their host materials functionalized with various main-group moieties will be introduced from the point of view of their structure-property relationship. The main emphasis lies on the important role played by the main-group element groups in addressing the key issues of both phosphorescent emitters and their host materials to fulfill high-performance phosphorescent OLEDs.

1. Introduction

Organic light-emitting devices or diodes (OLEDs) can convert electrical energy into light energy via electroluminescence (EL) by employing luminescent organic semiconductors, which have great potential in developing new-generation flat panel displays and energy-saving solid lighting sources.[1-4] Clearly, the luminescent organic semiconductors, *i.e.*, emitters, should represent the most crucial component in OLEDs. At the early stage, OLEDs were fabricated using fluorescent materials (singlet emitters), which can only utilize excitons in singlet state, corresponding to 25% of all the electronically generated excitons, and leave the other 75% excitons in triplet state unused through non-radiative transition pathways, leading to the internal quantum efficiency (IQE) of OLEDs based on singlet emitters no more than 25% theoretically.[5, 6] Fortunately, the bottleneck of the 25% limited IQE was broken in 1998 by the observation of EL from triplet metal-to-ligand charge-transfer (^{3}MLCT) excited states of both Os(II) and Pt(II) complexes,[7, 8] since these complexes are capable of utilizing both singlet and triplet excitons to enhance the EL efficiencies substantially. These two studies have opened a totally new outlet to develop new-generation highly efficient emitters: phosphorescent emitters (triplet emitters). It has been shown that incorporation of the heavy transition metal ions into the organic skeletons is the most effective way of developing the phosphorescent emitters, since the heavy atoms will induce the strong spin-orbit coupling (SOC) effect to promote the intersystem crossing (ISC) process and hence increase the triplet state manifold. To date, numerous triplet emitters including Ir(III),[9] Pt(II),[10] Os(II),[11] Au(III),[12] Ru(II),[13] and Cu(I) complexes[14] displaying intense phosphorescence at room temperature have been applied to construct highly efficient phosphorescent OLEDs (PHOLEDs), which can reach the 100% IQE

theoretically.[15-22] Generally speaking, the discovery of phosphorescent emitters has brought forth the bright commercial prospects of OLEDs.

Owing to the long lifetime of triplet excited states, the phosphorescent emitters are typically doped into host materials at low concentration to effectively suppress the triplet-triplet annihilation (TTA) and/or concentration quenching effects in the emission layer (EML) of PHOLEDs (Fig. 1).[23, 24] During the operation of PHOLEDs, the holes and electrons are injected and transported to the doped EML where they can either recombine on host molecules to form exctions which will subsquently be harnessed by the phosphorescent emitters or be trapped directly by the phopshorescent emitters, representing the two major excitation pathways of triplet emitters in the doped EML of PHOLEDs (Fig. 1). Hence, both the phosphorescent emitters and host materials are very critical for the PHOLEDs for modulating the charge carrier injection/transporting and excitation processes. Thus, the design and synthesis of new phosphorescent emitters and their host materials represent two research focuses in PHOLED field to improve the device performance. The state-of-the-art PHOLEDs can realize monochromatic or white emissions with very high efficiencies.[25-27] Clear, conferment of charge carrier injection/transporting abilities to both phosphorescent emitters and host materials should be an effective way of enhancing the EL performance of PHOLEDs. It is well known that non-metallic main-group elements can exhibit distinct electronic features according to their intrinsic nature. In addition, the electronic characters of some elements in these main groups, such as P and S, can be tuned dramatically by suitable chemical modifications. Hence, these main-group moieties can show inherent advantages in furnishing desirable electronic characters to both phosphorescent emitters and host materials to realize highly

efficient PHOLEDs. Based on the recent literature reports, there is an increasing number of original research papers on using main-group moieties to control the properties of both phosphorescent emitters and host materials in PHOLEDs. For example, besides the function of coordinating to the central metal ions,[28, 29] functional units containing nitrogen atom can be used to enhance the hole injection/transporting (HI/HT) abilities[30-32] or electron injection/transporting (EI/ET) properties[33-35] of phosphorescent emitters and host materials depending on the different hybrid mode of the nitrogen atom.

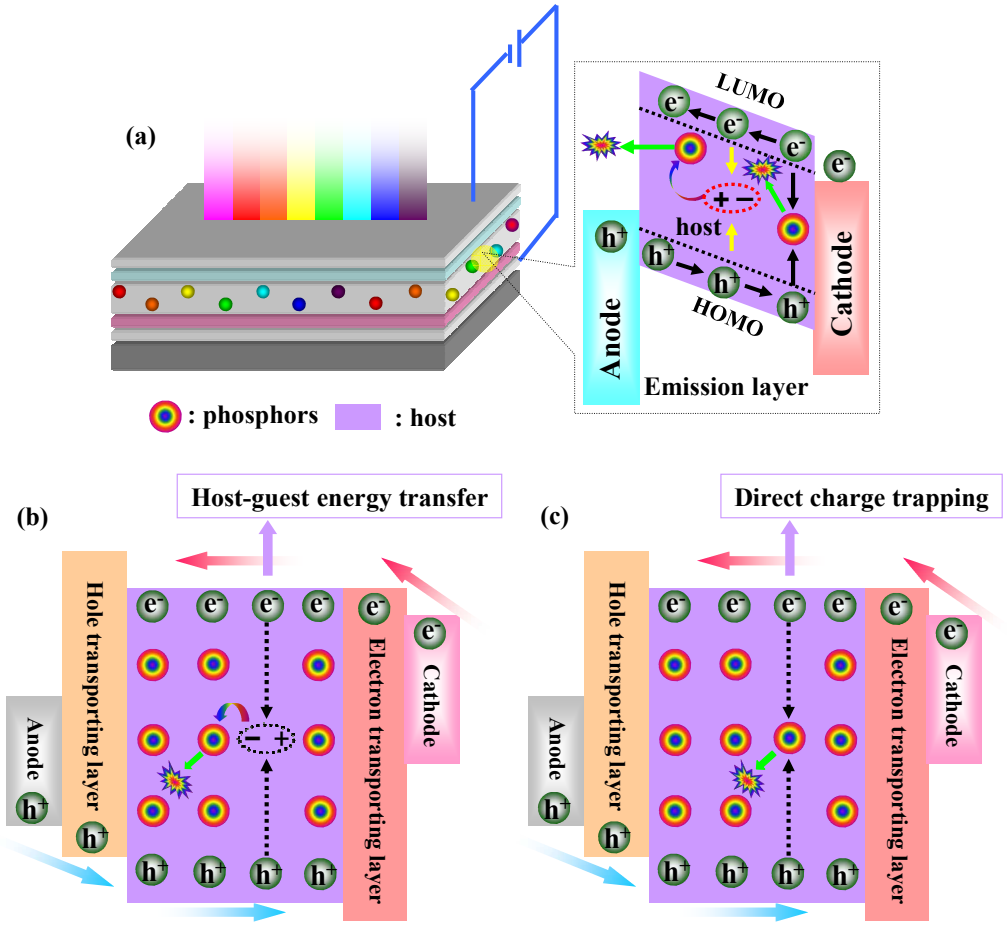

Fig. 1 (a) The typical device structure of a PHOLED and emission mechanisms: (b) host-guest energy transfer and (c) direct charge trapping.

For the time being, the previous review articles about the progress on phosphorescent emitters and host materials typically summarize the results from the perspective of either the molecular structures, *i.e.*, the pattern of ligand coordination[10, 36] and identity of central metal ions,[37, 38] or the molecular configuration, *i.e.*, small molecules,[39, 40] dendrimers[41] and polymers.[42, 43] However, no review paper has given comments on the crucial role played by the non-metallic main-group moieties in tuning the properties of the phosphorescent emitters and host materials in PHOLEDs from the structure-property relationship point of view, *i.e.* how the functional moieties containing non-metallic main-group elements affect the properties of phosphorescent emitters and host materials. Herein, in this critical review, the crucial functions of the moieties containing non-metallic main-group elements (*e.g.*, B, Si, Ge, N, P, O, S and F) in adjusting the properties of phosphorescent emitters and host materials will be fully addressed. The structure-property relationship will be emphasized to provide more precise information for the design and synthesis of high-performance host materials and phosphorescent emitters with desirable properties to furnish highly efficient PHOLEDs.

2. Critical roles played by host materials and phosphorescent emitters in PHOLEDs

As aforementioned, the guest phosphorescent emitters in the doped EML of PHOLEDs can be electrically excited by either host-guest energy transfer[44, 45] or direct charge carrier trapping[46, 47] to induce the electrophosphorescence (Fig. 1). Clearly, in order to guarantee high EL efficiencies, all excitons in the EML should be harnessed effectively by the radiative triplet states of the guest phosphorescent emitters during the operation of the PHOLEDs.[48] In other words, it is the triplet

states of the phosphorescent emitter that hold the final position to relax to the ground state and therefore decide the emission color. Hence, one of the critical roles played by the host materials is to have them being excited by the recombination of holes and electrons migrated from the charge transporting layers and then to effectively transfer the energies to the guest emitters. Therefore, the first condition that a good host material must meet is that the triplet energy (E_T) of the host material should be higher than that of the guest emitter to avoid the undesired reverse energy transfer from the guests to the host materials and to effectively confine triplet excitons on the guest molecules. The E_T has been regarded as a very critical parameter for the host materials, especially the ones for blue phosphorescent emitters. In order to block the reverse energy transfer, the PHOLEDs involving blue phosphorescent emitters will require host materials with very large band gap (E_g) and thereby high E_T level, typically > 2.8 eV. Therefore, developing host materials for blue phosphorescent emitters, especially the deep-blue ones, represents a very tough task.

According to the working mechanism of PHOLEDs, the charge carrier injection/transporting ability of the host materials is very crucial as well. A high and balanced mobility for both hole and electron is preferred for the host materials, since this merit can not only increase the recombination efficiency of charge carriers but also broaden the charge carrier recombination zone to relieve triplet-triplet annihilation (TTA). Accordingly, furnishing high and balanced charge carrier injection/transporting ability to the host materials with functional groups should be a very effective way to improve the EL performance of PHOLEDs. Unfortunately, the host materials for blue phosphorescent emitters typically possess poor charge injection/transporting features due to their large E_g. This situation has seriously impeded the EL performance of the blue phosphorescent

emitters. Thus, development of high performance host materials, especially the ones for blue or even deep-blue phosphorescent emitters, with enhanced charge injection/transporting ability is highly desired.

The EML in PHOLEDs is a thin layer in which phosphorescent molecules in a small amount are homodisperse that can prevent the TTA and aggregation quenching effects. Hence, another critical role played by host materials is to keep the homogeneous dispersion system stable to suppress the detrimental de-excitation effects in the EML. To meet this requirement, the host materials should possess good thermal and morphological stability as well as good compatibility with guest emitters to avoid the phase separation and chemical degradation. Hence, high decomposition temperature (T_d) and glass transition temperature (T_g) are indispensible characters for the well qualified host materials as far as the lifespan of the PHOLEDs is concerned.

As the most essential component of the PHOLEDs, the phosphorescent emitters can decide the EL performance of the pertinent devices to a large extent. The relatively short phosphorescent lifetime (τ_P), high phosphorescent quantum yield (Φ_P) and good stability should represent the most crucial features for the high-performance phosphorescent emitters. The short τ_P can relieve the TTA effect within the EML and hence cope with efficiency roll-off problem at high current density/luminance. The high Φ_P should be one of the prerequisite features associated with the phosphorescent emitters to realize high EL efficiencies. The good stability of the phosphorescent emitters can benefit service life of the PHOLEDs.

Another critical issue about the phosphorescent emitters is the emission color. In developing high quality displays as well as solid light sources, blue-emitting materials, especially the deep-blue ones,

are essential. Considering the OLEDs as the promising candidates for full-color displays, the Commission Internationale de l'Éclairage (CIE) coordinates of the blue EL should be or very close to (0.14, 0.08) specified in the National Television System Committee (NTSC) standard or (0.15, 0.06) by the European Broadcast Union (EBU) television display criterion. It means that the phosphorescent emitters should possess vey wide E_g to give the desired blue EL, which can only be fulfilled by the judicious molecular design. However, in order to achieve high E_g, the phosphorescent complexes must have both very large intra-ligand $^3\pi$–π^* and ^{3}MLCT transition energies, which will approach the higher-lying metal-centered deactivating states or other unspecified quenching states. All these possible disadvantages can lower the Φ_P of blue phosphorescent emitters. Hence, development of blue phosphorescent emitters represents a much more challenging work than searching the phosphorescent emitters with other emission colors. To date, a lot of sky-blue phosphorescent emitters have been developed, but the deep-blue phosphorescent emitters are still much less.

In order to improve the stability, the chemical structures of the phosphorescent emitters should be carefully optimized. It has been indicated that the C−F bonds are liable to undergo decomposition during the operation of the PHOLEDs. However, the F-containing groups are frequently employed to tune the properties of the phosphorescent emitters, especially their critical role in fulfilling blue phosphorescent emission, since the strongly electron-withdrawing fluorine atom at the proper position of the organic ligands can effectively increase the E_T of the phosphorescent emitters. This will incur serious problem on the stability for the blue phosphorescent emitters. Thus, developing blue phosphorescent emitters free of C−F bonds should be a formidable task which is of great value

for the practical application of the PHOLEDs.

Extraordinary progresses have been made for all the aforementioned critical issues associated with both host materials and phosphorescent emitters. Owing to their unique electronic features, the nonmetallic main-group functional moieties have shown their great potential in making these achievements. In the following sections, the critical role played by the nonmetallic main-group moieties in addressing the critical issues of PHOLEDs will be summarized and discussed.

3. Main-group moiety functionalized host materials in PHOLEDs

As mentioned above, host materials are indispensable for state-of-the-art PHOLEDs in most cases. In this section, the critical roles played by different main-group moieties in addressing the issues associated with host materials will be discussed, which includes tuning the triplet-energy level, promoting and balancing charge carrier injection/transporting, and improving device stability, *etc*.

3.1 Host materials containing triarylboron moiety

Owing to the strong electron-accepting ability afforded by the empty p-orbital on the central boron atom,[49, 50] triarylboron compounds can show the electron-transporting (ET) properties.[51-53] Thus, the expectation of utilizing the triarylboron moiety to improve the electron-transporting ability of host materials is quite feasible. Following this approach, host materials bearing a triarylboron moiety core and three oligofluorene arms were synthesized.[54] The E_T of **DBF1** (Fig. 2 and Table 1) is estimated as 2.76 eV, which is high enough for effective energy transfer from **DBF1** to green phosphorescent emitters. Accordingly, the solution-processed PHOLED using **DBF1** as the host and **Ir(ppy)$_3$** as the guest displays pure green emission with the maximum external quantum efficiency (EQE), power efficiency

(PE) and current efficiency (CE) of 7.38%, 13.14 lm W^{-1} and 25.10 cd A^{-1}, respectively. The absence of clear reduction wave in the cyclic voltammogram implies that the ET ability of **DBF1** should be insufficient, which might be ascribed to the fact that the long fluorene-based arms can hinder the central boron cores from accepting electrons from the neighbor molecules. So, this study may provide a useful hint that when designing host materials containing triarylboron moieties, the triarylboron moiety should not be deeply besieged by bulky groups.

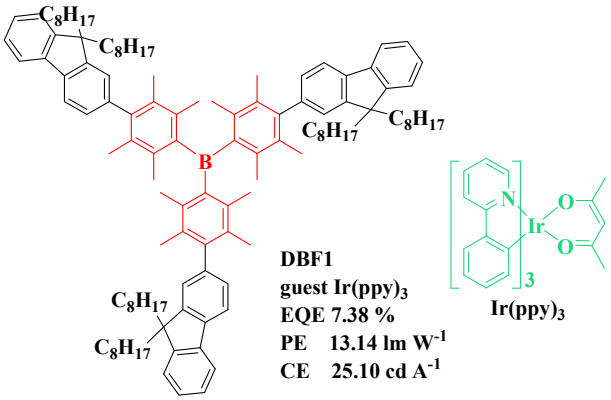

Fig. 2 Chemical structure of **DBF1** and peak efficiency data of related OLED.

3.2 Host materials containing aromatic silane moiety

Effective energy transfer from host materials to phosphorescent emitter guests and confinement of the excitons within the EMLs are two basic requirements for host materials to achieve high device performance, which demand the host materials to possess high enough triplet energies as well as low-lying HOMO levels and high-lying LUMO levels. For the well-known blue phosphorescent emitters **FIrpic** and **FIr6**, they have high E_T of 2.62 eV and 2.72 eV, respectively.[47] In addition, the phosphorescent emitters used for fabricating deep-blue OLEDs need to have E_T at least of 2.8 eV.[55] It is a big challenge to obtain host materials with such high E_T. One practical way to acquire ultrawide energy gap hosts is to interrupt the conjugation system of host molecules. It is well-known that the

silicon atom is usually bonded to four other atoms with sp^3 hybrid orbitals, leaving no lone pair electrons to participate in molecular conjugation system, which makes it to be a very suitable tool to interrupt the conjugation system of host molecules. In addition, the compounds containing aromatic silane moieties usually show high T_d and T_g, which will benefit the morphological stability and thus increase the device operational stability.[56, 57] Therefore, aromatic silane moieties have shown great potential for developing high performance host materials (Fig. 3 and Table 1).

Thomson *et al.* firstly reported several ultrahigh energy gap host materials **UGH1**, **UGH2** and **UGH3** for blue PHOLEDs (Fig. 3 and Table 1).[47, 58] Their HOMO and LUMO levels are estimated at 7.2 and 2.8 eV, respectively, which can not only effectively confine the excitons within the EML but also promote direct charge-trapping excitation of the phosphorescent dopants. Blue PHOLEDs based on **UGH1**, **UGH2** and **UGH3** doped with 10% **FIr6** show maximum EQEs of 7.0%, 9.1% and 8.8%, respectively, much higher than that with 1,3-bis(*N*-carbazolyl)benzene (**mCP**) as host, indicating the advantages of the aromatic silane moieties in developing host materials with high E_T. Compared with **UGH1–UGH3**, the host materials **BSB** (E_T = *ca.* 2.76 eV) and **BST** (E_T = *ca.* 2.58 eV) possess reduced E_T due to the longer conjugated spacers between the two aromatic silane moieties (Fig. 3).[59] The T_g for **UGH1** is *ca.* 26 ^oC, while **UGH3** possesses T_g of *ca.* 46 ^oC. The hosts **BSB** and **BST** with larger molecular weight can show even higher T_g at *ca.* 100 ^oC and 113 ^oC, respectively. These results have clearly indicated that molecular weight and molecular rigidity represent the key factors which should be considered in designing host materials with high T_g. With higher E_T to effectively block the reverse energy transfer process, **BSB** doped with FIrpic can afford blue PHOLEDs with noticeably higher EL efficiencies (14.7%, 30.4 cd A^{-1} and 7.4 lm W^{-1}) than **BST** (2.9%, 6.0 cd A^{-1} and 2.0 lm W^{-1}).

These EL results clearly indicate the critical role played by high E_T host materials in achieving high EL performance. In addition, it also clearly reveals that employing aromatic silane moieties to interrupt the conjugation is an effective strategy to develop host materials with high E_T and thereby enhance the blue phosphorescent device performance.

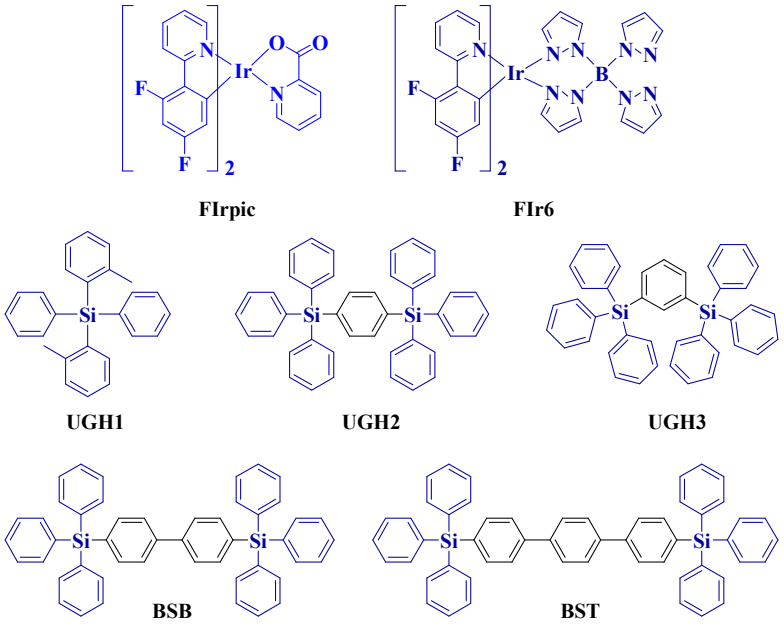

Fig. 3 Chemical structures of host materials containing aromatic silane moiety and peak efficiency data of related OLEDs.

Table 1. Host materials containing triarylboron or aromatic silane group and their properties

Main-group element unit	Host	E_T eV	T_g °C	Dopant	EQE %	CE cd A^{-1}	PE lm W^{-1}	Ref.
triarylboron	**DBF1**	2.76	62	**Ir(ppy)$_3$**	7.38	25.1	13.1	54
aromatic silane	**UGH1**	~ 3.5	26	**FIr6**	7.0	–	–	47
aromatic silane	**UGH2**	~ 3.5	–	**FIr6**	9.1	–	–	47
aromatic silane	**UGH3**	~ 3.5	46	**FIr6**	8.8	–	–	47
aromatic silane	**BSB**	2.76	100	**FIrpic**	14.7	30.4	7.4	59

aromatic silane	**BST**	2.58	113	**FIrpic**	2.9	6.0	2.0	59

3.3 Host materials bearing nitrogen-containing aromatic system

According to the aforementioned working mechanism of PHOLEDs (Fig. 1), the charge carrier injection/transporting ability is very crucial for a qualified host material, which will increase the charge carrier recombination efficiency, broaden recombination zone to relieve TTA effect, low device driving voltage and improve EL efficiency, *etc*. Aromatic systems containing nitrogen atoms can display electron-donating or electron-withdrawing properties depending on the nature of hybridized orbital adopted by the nitrogen atoms. Generally, aromatic systems containing nitrogen atoms with sp^3 hybrid mode tend to donate electrons, thus exhibiting good HI/HT abilities. On the contrary, aromatic systems containing nitrogen atoms with sp^2 hybrid pattern usually show electron-withdrawing properties and thereby possess good EI/ET abilities. Therefore, due to their versatile electronic properties, nitrogen-containing aromatic systems are suitable building blocks to construct novel host materials with diverse charge injection/transporting properties to furnish highly efficient PHOLEDs.

3.3.1 Host materials with hole injection/transporting (HI/HT) properties

3.3.1.1 Triphenylamine-based host materials

The lone electron pair on the sp^3 hybrid nitrogen atom in triphenylamine will participate in the π-conjugation of the phenyl rings, which makes the whole system rich of electrons and tend to donate electrons. Thus, triphenylamine moiety is a good electron-donor, indicating its good HI property. When one electron is taken from the lone electron pair on the nitrogen atom, the formed radical cation will be

stabilized by the three peripheral phenyl rings, leaving a relatively stable system containing a so-called "hole" charge carrier. So, introducing the triphenylamine moieties to host molecules can enhance the hole transporting (HT) properties.

In this kind of host materials, the triphenylamine moiety can be imbedded into the center of the molecular skeleton (Fig. 4).[60, 61] In **TFTPA**, the triphenylamine core is surrounded by three fluorene-based units. The sp^3-hybridized carbon atom at the C-9 position of the fluorene moiety effectively interrupts the conjugation length, resulting in a high E_T of 2.89 eV for **TFTPA** (Table 2). The reversible oxidation process with low oxidation potential of 0.46 V implies the good HI/HT property of **TFTPA**. Owing to it good HI/HT property and high E_T, **TFTPA** can even act as a universal host to fabricate highly efficient blue, green and red PHOLEDs, especially affording blue PHOLED with the peak EQE, CE and PE of 13.1%, 29.4 cd A^{-1} and 18.1 lm W^{-1}, respectively. In addition, the phenyl rings of the triphenylamine core can be bridged by two sp^3-hybridized carbon atoms to develop triphenylamine-based host materials **BTPAF**[62] and **FATPA**[63] (Fig. 4). By doing so, the enhanced rigidity of the host molecule can be achieved to benefit their thermal properties. Despite the fact that the improved coplanar configuration of the triphenylamine will have the risk to lower the E_T, **BTPAF** and **FATPA** can still show high E_T of 2.86 and 2.78 eV (Table 2), which are high enough to make them suitable hosts for the blue and green phosphorescent emitters. Different from **TFTPA** (T_g at *ca.* 186 ^oC), **BTPAF** possesses a more rigid molecular core which can furnish noticeably higher T_g at *ca.* 204 ^oC. Hence, enhancement of the molecular rigidity can be a very effective way to furnish high T_g to the host materials. Through doping FIrpic into **BTPAF**, the obtained blue PHOLED can show EL efficiencies of 9.4%, 20 cd A^{-1} and 14 lm W^{-1}. With **FATPA** as host material, the green PHOLED with

$Ir(ppy)_3$ as emitter can display very decent EL performance with the maximum EQE, CE and PE of 23.4%, 83.5 cd A^{-1} and 71.4 lm W^{-1}, respectively.

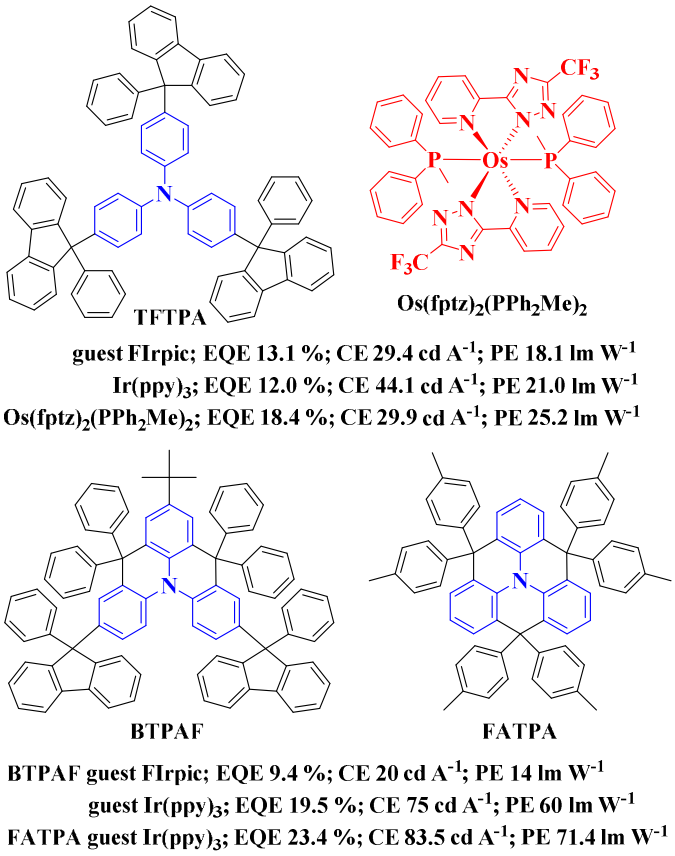

Fig. 4 Chemical structures of **TFTPA**, **BTPAF** and **FATPA** and peak efficiency data of related OLEDs.

Triphenylamine moieties can also be end-capped to a conjugated spacer to develop host materials (Fig. 5).[64] In **DTPAFB**, a twist fluorene-based spacer has been employed to block the conjugation extension and furnish high E_T of 2.79 eV for **DTPAFB**. The HOMO energy level of **DTPAFB** is calculated to be 5.39 eV, favoring its HI/HT ability. With optimized doping level of FIrpic, the blue PHOLED can show the maximum CE and PE of 24.3 cd A^{-1} and 13.0 lm W^{-1}, respectively. The thermal properties of this kind of host materials can be optimized by fixing the phenyl rings in the

triphenylamine moieties. Thus, **SAFDPA** and **SAFCz** (Fig. 5) possess high T_g (128 °C for **SAFDPA** and 150 °C for **SAFCz**) as well as high E_T (2.72 eV for **SAFDPA** and 2.84 eV for **SAFCz**) (Table 2).[65] The difference in T_g between **SAFDPA** and **SAFCz** also indicates the critical role played by the molecular rigidity in furnishing high T_g in the host materials. With FIrpic as blue phosphorescent emitter, the PHOLED with **SAFDPA** as host can achieve the maximum EQE, CE and PE of 17.9%, 39.0 cd A^{-1} and 36.5 lm W^{-1}, while the device with **SAFCz** as host exhibits EL efficiencies of 19.4%, 42.1 cd A^{-1} and 38.5 lm W^{-1}. Clearly, these results have provided important clues for improving the thermal properties of the triphenylamine-based host materials through enhancing the molecular rigidity while the high E_T could be maintained at the same time. Meanwhile, materials containing carbazole units can show comparable or even better electroluminescent properties than materials containing triphenylamie units as hosts for phosphorescent emitters (*vide infra*).

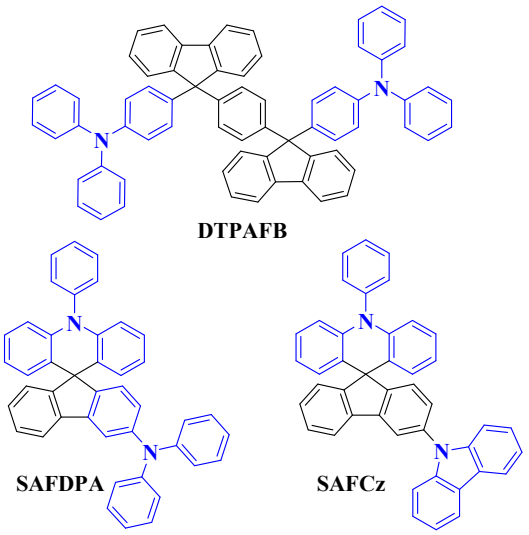

Fig. 5 Chemical structures of **DTPAFB**, **SAFDPA** and **SAFCz** and peak efficiency data of related OLEDs.

3.3.1.2 Carbazole-based host materials

Similar to triphenylamine moiety, carbazole-based group also has sp^3 hybridized nitrogen atom, indicating its HI/HT capacity. Different from triphenylamine moiety, carbazole unit shows more rigid molecular structure and poorer π-electron-donating ability than triphenylamie moiety,[66, 67] which makes molecules containing carbazole units usually showing higher T_g than their corresponding analogues bearing triphenylamine moieties.[64, 65, 68-70] Some carbazole compounds such as 4,4′-bis(9-carbazolyl)-biphenyl (**CBP**), 4,4′-bis(9-carbazolyl)-2,2′-dimethyl-biphenyl (**CDBP**) and 3,5-bis(9-carbazolyl)benzene (**mCP**) have been regarded as star host materials to fabricate efficient PHOLEDs (Fig. 6).[44, 71-73]

Despite its critical position as host material in PHOLEDs for its good HI/HT or even ambipolar ability, **CBP** exhibits vital drawbacks, such as low T_g of 62 °C and low E_T of 2.56 eV, which makes it unsuitable for blue phosphorescent emitters. Therefore, numerous efforts have been made to overcome these shortcomings of **CBP**.[74] By simply adjusting the spacers between the two carbazole units, two **CBP** isomers ***m*-CBP** and ***o*-CBP** have been obtained (Fig. 6).[75] Compared with **CBP**, the more twisted configurations of ***m*-CBP** and ***o*-CBP** effectively reduce the π-conjugation between the carbazole moieties and the central biphenyl units, resulting in higher E_T of 3.00 eV for ***o*-CBP** and 2.84 eV for ***m*-CBP** (Table 2). Furthermore, the T_g of ***m*-CBP** (97 °C) and ***o*-CBP** (82 °C) are also increased due to the higher steric hindrance effect of these molecules (Table 2). The FIrpic-doped PHOLEDs with ***m*-CBP** and ***o*-CBP** as host materials can outperform the ones with the famous **CBP** host. The highest efficiencies for the device based on ***o*-CBP** can show EL efficiencies of 14.2%, 29.9 cd A^{-1} and 25.3 lm W^{-1}, which are nearly 2 times higher than those using **CBP** host.

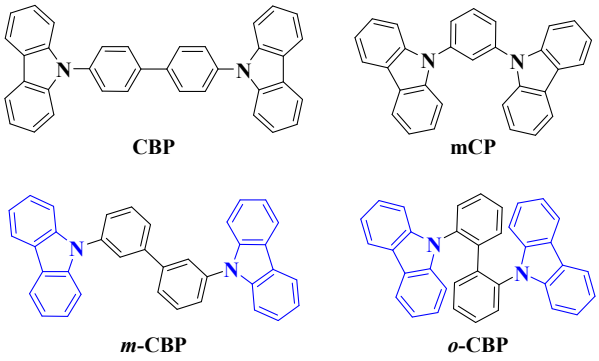

Fig. 6 Chemical structures for both the star hosts **CBP**, **mCP** and some **CBP** isomers with the peak efficiency data of related OLEDs.

Besides changing the substitution position of the carbazole group on the spacer, introduction of substituents, such as methyl or/and phenyl groups *etc.*, to twist the spacer represents another popular way to synthesize novel carbazole-based host materials with HI/HT ability and high E_T. Based on this idea, the well-known hosts 4,4′-bis(9-carbazolyl)-2,2′-dimethyl-biphenyl (**CDBP**)[72] and 1,4-bis-[4-(9-carbazolyl)-phenyl]-durene (**CPD**) [76] have been developed with high E_T of *ca.* 3.0 eV. Even carborane moieties have been employed to develop host for **FIr6** based on **CBP** skeleton.[77]

Recent results have shown that changing the spacer can also furnish qualified carbazole-based host materials. Jou *et al.* proposed a **CBP** analogue **Spiro-2CBP** (Fig. 7), in which the spacer is a *spiro*-bifluorene unit.[78] This rigid molecular configuration greatly improved the T_g of **Spiro-2CBP** up to 174 °C.[79] However, the low E_T of **Spiro-2CBP** can be expected since the biphenyl group becomes co-planar and the conjugation will be extended. Nevertheless, **Spiro-2CBP** can still serve as high performance host for the orange-red PHOLED which exhibits high EL performance with EQE, CE and PE of 20.3%, 46.2 cd A^{-1} and 34.9 lm W^{-1} at 100 cd m^{-2}, respectively. Triphenylbenzene can also act as

the core of carbazole-based host with high performance.[80] The host material **TCPB** (Fig. 7) bears three peripheral carbazole units around the triphenylbenzene core. The green PHOLED with $Ir(ppy)_3$-**TCPB** co-deposited EML can show excellent EQE and PE of 23.4% and 107 lm W^{-1}. Despite its relatively low E_T of 2.66 eV due to the delocalized π-conjugation between the carbazole moieties and triphenylbenzene core, **TCPB** can still help the blue PHOLED achieve high EQE and PE of 26.0% and 65.4 lm W^{-1}, respectively. Besides the aid from the host material, the high EL efficiencies should also be benefitted from the carefully optimized device architecture. Both **Spiro-2CBP** and **TCPB** have the disadvantage of relatively low E_T. However, the spacer in the host **DCPFB** shows the potential of coping with this problem.[64] The twisted phenyl-substituted fluorene dimeric spacer in **DCPFB** can afford high E_T of 2.77 eV (Table 2). This host possesses the HOMO level of 5.64 eV together with high E_T, favoring the HI/HT as well as exciton confinement for a FIrpic-based PHOLED. Thus, the solution-processed blue PHOLED with **DCPFB** as host can show fairly good EL efficiencies of 25.6 cd A^{-1} and 12.7 lm W^{-1} for maximum CE and PE, respectively.

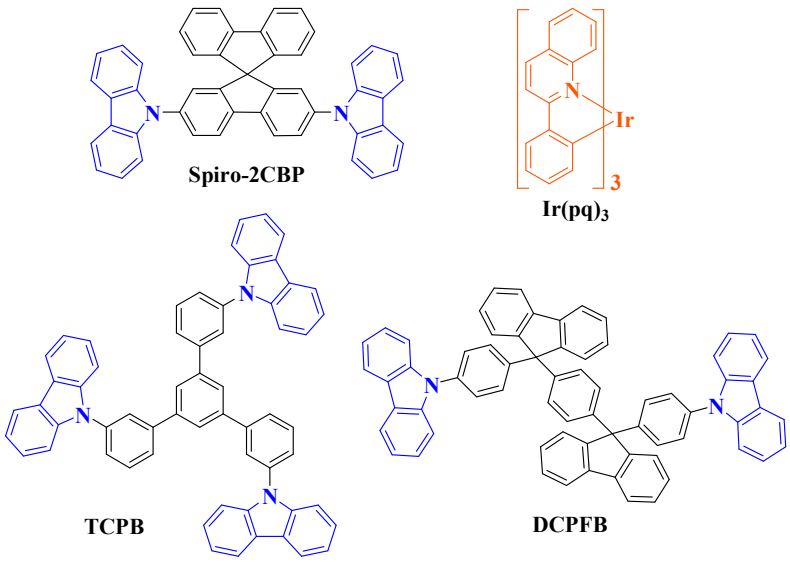

Fig. 7 Chemical structures of **Spiro-2CBP**, **TCPB** and **DCPFB** and peak efficiency data of related OLEDs.

Different from the host materials aforementioned with carbazole moiety attached to the spacer through the nitrogen atom of 9-position, some novel host materials have also been developed by employing *N*-phenylcarbazole unit (Fig. 8).[74] Compared with carbazole group, the *N*-phenylcarbazole possesses larger molecular weight, which will benefit the thermal property of the resultant host materials. In addition, the bonding style will block the conjugation between the nitrogen atoms in carbazole moieties and the spacer, which will increase the E_T. With a shorter spacer and more twisted configuration possessing higher steric hindrance, **PBCz** (Fig. 8) can show higher T_g of 115 °C and E_T of 2.76 eV[81] than **CTP-1** with T_g of 113 °C and E_T of 2.73 eV (Table 2). Hence, **PBCz** can afford FIrpic-based PHOLEDs with better EL performance (19.5%, 45.5 cd A^{-1} and 43.8 lm W^{-1}) than **CTP-1** (15.9%, 40.5 cd A^{-1} and 33.9 lm W^{-1}). In order to further increase E_T and T_g, much shorter spacers with

high steric hindrance effect have been employed to develop **TMCz** and **DMCz**.[82] Due to its higher steric hindrance effect involved, **TMCz** can show E_T of 2.99 eV and T_g of 165 °C, which are higher than those of **DMCz** (E_T of 2.71 eV and T_g of 127 °C) (Table 2). Unfortunately, the blue PHOLEDs based on **TMCz** show inferior EL results as compared with those based on **DMCz** (18.5%, 43.7 cd A^{-1} and 36.0 lm W^{-1}), which can be ascribed to that the over-twisted configuration of **TMCz** that has resulted in too short conjugation to maintain the required hole mobility. These results have clearly indicated that an optimized trade-off should be maintained among high E_T, T_g and charge carrier transporting ability when designing high performance hosts of PHOLEDs.

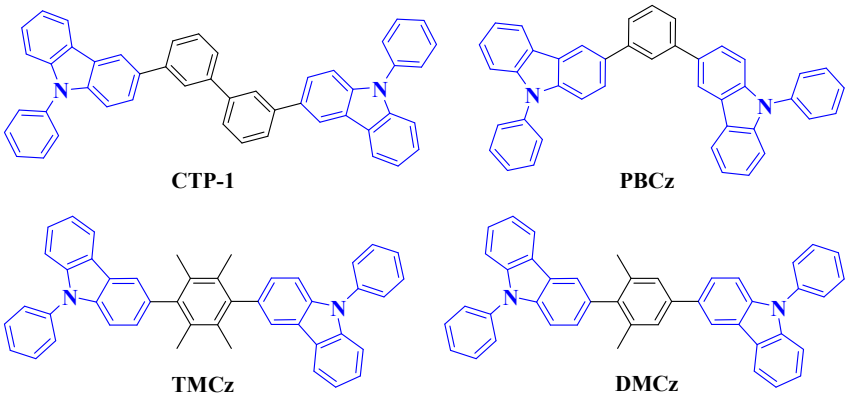

CTP-1; guest FIrpic; EQE 15.9 %; CE 40.5 cd A^{-1}; PE 33.9 lm W^{-1}
PBCz; guest FIrpic; EQE 19.5 %; CE 45.5 cd A^{-1}; PE 43.8 lm W^{-1}
TMCz; guest FIrpic; EQE 14.7 %; CE 35.9 cd A^{-1}; PE 25.1 lm W^{-1}
DMCz; guest FIrpic; EQE 18.5 %; CE 43.7 cd A^{-1}; PE 36.0 lm W^{-1}

Fig. 8 Chemical structures of **CTP-1**, **PBCz**, **TMCz** and **DMCz** and peak efficiency data of related OLEDs.

The *N*-phenylcarbazole-based host materials can also be obtained by bonding bulky substituents or fusing aromatic rings. Two bulky *m*-terphenyl units can be introduced to the *N*-phenylcarbazole core to obtain **CzTP** (Fig. 9) with high T_g of 135 °C due to the large molecular size.[83] With highly rigid molecular skeleton, **CmInF** (Fig. 9) can show very high T_g of 195 °C.[84] However, due to their large

conjugation, **CzTP** possesses E_T of 2.70 eV and the E_T for **CmInF** is 2.77 eV (Table 2), implying that they are unfavorable for blue phosphorescent emitters. Fortunately, their proper conjugation results in enhanced HI/HT ability. **CmInF** can exhibit hole mobility in the range from 2×10^{-3} to 5×10^{-3} cm^2 V^{-1} s^{-1} for electronic fields varying from 10^5 to 3.3×10^5 V cm^{-1} together with high-lying HOMO level of 5.4 eV. Both **CzTP** and **CmInF** can serve as suitable hosts for phosphorescent emitter with longer emission wavelength, in which **CzTP** can bring super higher EL efficiencies of 102 cd A^{-1} and 113 lm W^{-1} for green PHOLEDs. Once again, these results clearly indicate that an optimized compromise between high E_T and HI/HT should be a crucial issue to be addressed in developing host materials.

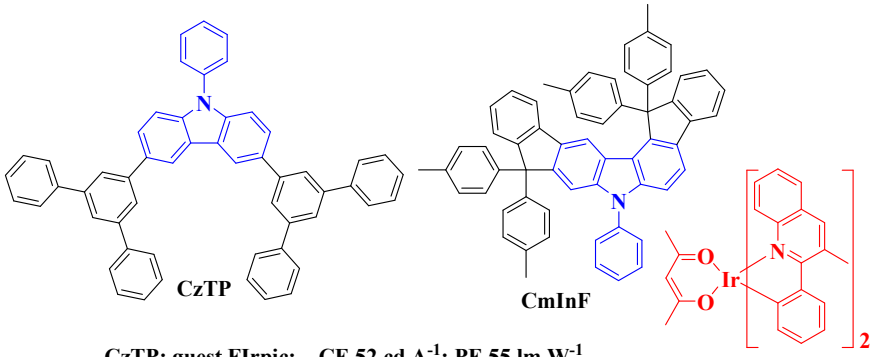

Fig. 9 Chemical structures of **CzTP** and **CmInF** and peak efficiency data of related OLEDs.

Wang *et al.* reported an interesting molecule **DNDT-ICZ** (Fig. 10) based on the indolo[3,2-*b*]carbazole unit which can be regarded as two fused carbazole units.[85] Due to the large π-conjugation of the core, **DNDT-ICZ** shows low E_T of 2.41 eV (Table 2), which is only suitable for yellow and red phosphorescent emitters. However, the extended π-conjugation also raises the HOMO level of **DNDT-ICZ** up to 5.00 eV, benefiting the HI process. Using **DNDT-ICZ** as host for yellow

emitter **(ppy)$_2$Ir(tipg)** and red emitter **(bt)$_2$Ir(dipba)**, the optimized devices can show decent performance, *i.e.*, the maximum EQE, CE and PE are 18.6%, 66.2 cd A^{-1}, 80.5 lm W^{-1} for the yellow-emitting device and 12%, 18.5 cd A^{-1}, 22.1 lm W^{-1} for the red device, respectively. In addition, devices using **DNDT-ICZ** as host show low efficiency roll-off at the brightness of 1000 cd m^{-2}, especially for the yellow device whose current efficiency reduces by only 1.3% at 1000 cd m^{-2}.

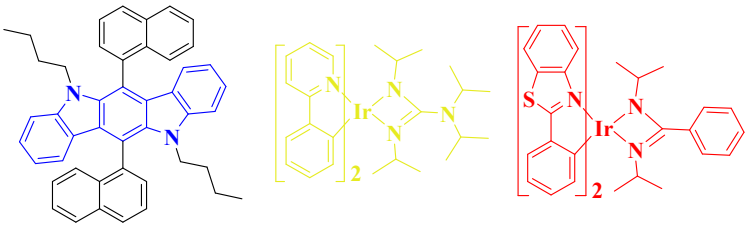

Fig. 10 Chemical structures of **DNDT-ICZ** and its guests and peak efficiency data of related OLEDs.

It has been shown that 3,9′-linked oligocarbazole can possess high E_T of *ca.* 3.0 eV, which is close to that of the carbazole monomer (3.03 eV).[86] The 3(6),9′-linked tricarbazoles also possess high triplet energies above 2.9 eV. Together with the three reaction active sites (*i.e.* 3, 6 and 9 positions), the above interesting properties of carbazole unit will provide a great opportunity to design and synthesize various oligocarbazole hosts or even carbazole-based dendritic hosts with high T_g as well as E_T suitable for blue phosphorescent emitters. Oligocarbazole-based hosts **TCz1** and **BTCC-36** have been prepared through 3(6),9′-linking pattern with high E_T (2.92 eV for **TCz1**[86] and 2.96 eV for **BTCC-36**[87]) (Fig. 11 and Table 2). Thus, the tricarbazole-based compounds can act as the hosts of blue phosphorescent emitters. For example, the FIrpic-doped PHOLEDs with **TCz1** as host can achieve good EL performance with maximum EQE, CE and PE of 14.7%, 31.1 cd A^{-1} and 28.4 lm W^{-1}, respectively.

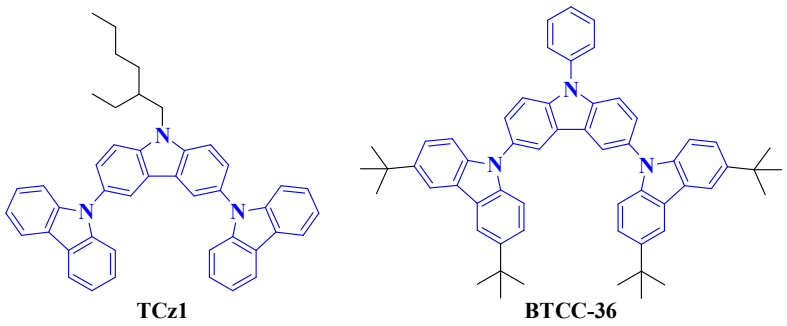

TCz1 **BTCC-36**

TCz1; guest FIrpic; EQE 14.7 %; CE 31.1 cd A^{-1}; PE 28.4 lm W^{-1}
BTCC-36; guest FIrpic; EQE 14.0 %; CE 27.2 cd A^{-1}; PE 11.8 lm W^{-1}

Fig. 11 Chemical structures of **TCz1** and **BTCC-36** and peak efficiency data of related OLEDs.

By incorporating more carbazole units into one single molecule, dendrimers are obtained with large molecular size and thereby high T_g, high solubility, good film-forming property as well as good HI/HT property. Due to the favorable linking mode at 3-, 6- and 9′- positions, the carbazole moieties are twisted from each other to some extent, thus the π-conjugation is effectively limited and the E_T of the whole dendritic molecule will remain at a very high level. Dendrimer **Cz-TCB** (Fig. 12) has the E_T of 2.86 eV (Table 2) and high-lying HOMO level of 5.24 eV, indicating the advantages of using **Cz-TCB** as host for blue phosphorescent emitters.[88] The solution-processed blue-emitting device based on **Cz-TCB** shows fair performance with maximum EQE, CE and PE of 13.0% and 25.7 cd A^{-1}, respectively. When the benzene core in **Cz-TCB** is replaced by an *N*-phenyl carbazole moiety, dendrimer **H2** (Fig. 12) still possesses the E_T as high as 2.89 eV (Table 2) and its HOMO level is slightly increased to 5.11 eV, indicating the enhanced HI ability as compared with **Cz-TCB**.[89] Using **H2** as host for FIrpic, the resulting solution-processed device gives the maximum EQE, CE and PE of 12.7%, 27.6 cd A^{-1} and 15.4 lm W^{-1}, respectively. In addition, when an orange triplet emitter **Ir(Flpy-CF_3)$_3$** and **FIrpic** were co-doped into **H2** to fabricate the solution-processed single emissive layer white-light OLEDs (WOLEDs), extremely high efficiencies of 26.0%, 70.6 cd A^{-1} and 47.6 lm W^{-1} can be achieved even at

a luminance of 100 cd m^{-2}.[90] This outstanding performance can be partly ascribed to the high E_T as well as high-lying HOMO level of **H2**, which can effectively confine the triplet excitons on the triplet emitters and enhance the HI.

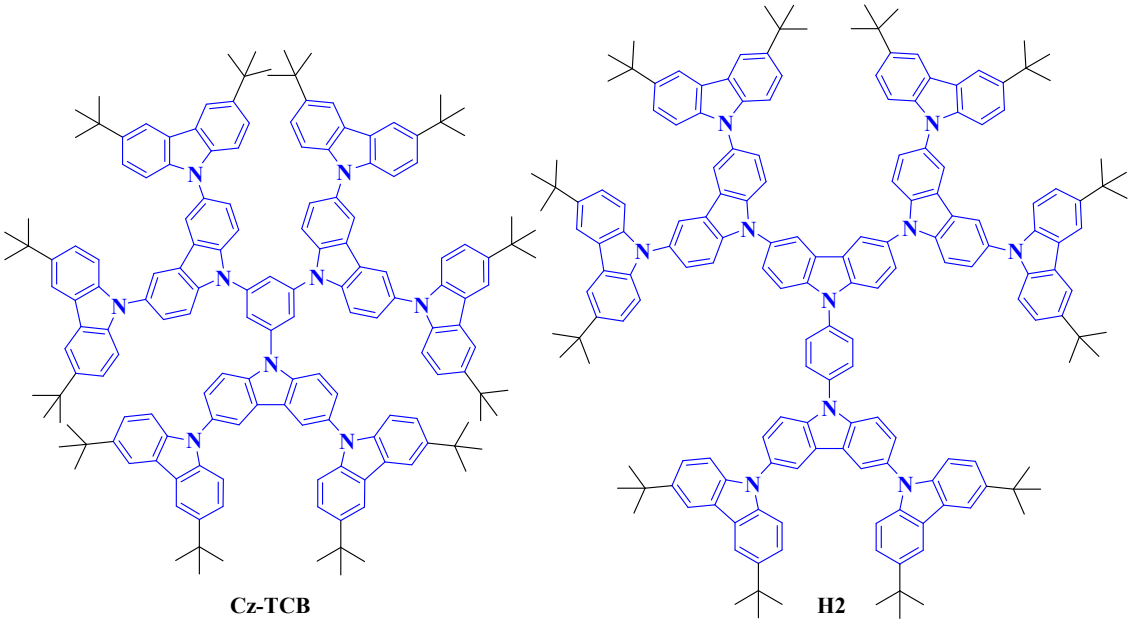

Fig. 12 Chemical structures of **Cz-TCB** and **H2** and peak efficiency data of related OLEDs.

Li *et al.* reported a larger carbazole-based dendrimer **G3** (Fig. 13) which can be regarded as a derivative of **CBP**.[30] The enlarged molecular size endows **G3** with extremely high T_g up to 376 °C, but the E_T (2.61 eV) of **G3** (Table 2) still remains very close to that of **CBP**, indicating that **G3** is a convenient host for green and other longer wavelength emissive phosphorescent guests. In addition, **G3** possesses a higher-lying HOMO level of 5.42 eV than that of **CPB**, suggesting its improved HI ability. Solution-processed devices using **Ir(ppy)$_3$** (green) and **(CF$_3$-bt)$_2$Ir(acac)** (orange) as emitters were fabricated. The green-emitting device gives the maximum EQE, CE and PE of 10.73%, 36.38 cd A^{-1} and

18.59 lm W^{-1}, respectively. The orange-emitting device shows the maximum EQE, CE and PE of 10.82%, 30.49 cd A^{-1} and 19.15 lm W^{-1}, respectively. When the biphenyl core of **G3** is replaced by the 2,2′-dimethyl-biphenyl group, a small change in molecular size but a big change in E_T is achieved.[91] The new carbazole-based dendrimer **G3MP** (Fig. 13) reported by Wang *et al.* also shows extremely high T_g of 368 °C, comparable to that of **G3**. However, **G3MP** possesses a higher HOMO level of 5.30 eV and higher E_T of 2.85 eV (Table 2), implying the enhanced HI ability. Owing to its proper E_T and good HI ability, **G3MP** can be used as a universal host to fabricate blue-, green- and red-emitting devices based on **FIrpic**, **G0** and **$(TPAPQ)_2Ir(acac)$**, respectively. The maximum EQEs, CEs and PEs are achieved with 12.8%, 28.2 cd A^{-1} and 14.1 lm W^{-1} for the blue PHOLED, 15.9%, 54.0 cd A^{-1} and 48.6 lm W^{-1} for the green-emitting device and 14.0%, 12.7 cd A^{-1} and 7.4 lm W^{-1} for the red-emitting device, respectively.

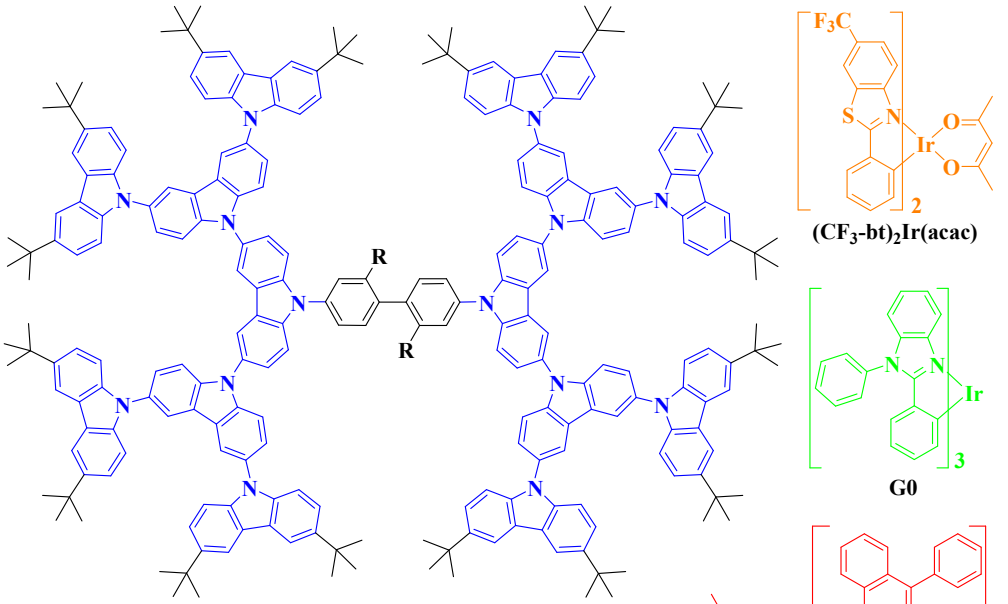

G3; guest $Ir(ppy)_3$; EQE 10.73 %; CE 36.38 cd A^{-1}; PE 18.59 lm W^{-1}
G3; guest $(CF_3\text{-bt})_2Ir(acac)$; EQE 10.82 %; CE 30.49 cd A^{-1}; PE 19.15 lm W^{-1}
G3MP; guest FIrpic; EQE 12.8 %; CE 28.2 cd A^{-1}; PE 14.1 lm W^{-1}
G3MP; guest G0; EQE 15.9 %; CE 54.0 cd A^{-1}; PE 48.6 lm W^{-1}
G3MP; guest $(TPAPQ)_2Ir(acac)$; EQE 14.0 %; CE 12.7 cd A^{-1}; PE 7.4 lm W^{-1}

Fig. 13 Chemical structures of **G3**, **G3MP** and the guests and peak efficiency data of related OLEDs.

These studies using carbazole-based dendrimers as host materials demonstrate that carbazole unit is a versatile building block which can be used to construct host materials with desirable properties, such as enhanced HI/HT ability and improved amorphous stability by increasing T_g due to both the large molecular size and high molecular rigidity afforded by the substantial steric hindrance effect. Most importantly, the E_T of the dendritic hosts will remain close to those of the core groups, which is convenient to predict and design materials with suitable E_T for various phosphorescent emitters. The outstanding performances of these devices show the promise of using carbazole-based dendritic host materials for highly efficient solution-processed PHOLEDs.

Table 2. Host materials with hole injection/transporting group and their properties

Main-group element unit	Host	E_T eV	T_g °C	Dopant	EQE %	CE cd A^{-1}	PE lm W^{-1}	Ref.
triphenylamine	**TFTPA**	2.89	186	**FIrpic**	13.1	29.4	18.1	60
triphenylamine	**TFTPA**	2.89	186	**Ir(ppy)$_3$**	12.0	44.1	21.0	60
triphenylamine	**TFTPA**	2.89	186	**Os(fptz)$_2$(PPh$_2$Me)$_2$**	18.4	29.9	25.2	61
triphenylamine	**BTPAF**	2.86	204	**FIrpic**	9.4	20	14	62
triphenylamine	**BTPAF**	2.86	204	**Ir(ppy)$_3$**	19.5	75	60	62
triphenylamine	**FATPA**	2.78	178	**Ir(ppy)$_3$**	23.4	83.5	71.4	63
triphenylamine	**DTPAFB**	2.79	147	**FIrpic**	–	24.3	13.0	64
triphenylamine	**SAFDPA**	2.72	128	**FIrpic**	17.9	39.0	36.5	65
Triphenylamine + carbazole	**SAFCz**	2.84	150	**FIrpic**	19.4	42.1	38.5	65
carbazole	**CBP**	2.56	62	**FIrpic**	5.2	10.7	8.5	75
carbazole	***m*-CBP**	2.84	97	**FIrpic**	8.7	18.6	11.3	75
carbazole	***o*-CBP**	3.00	82	**FIrpic**	14.2	29.9	25.3	75
carbazole	**Spiro-2CBP**	–	174	**Ir(pq)$_3$**	20.3	46.2	34.9	78, 79
carbazole	**TCPB**	2.66	146	**FIrpic**	26.0	–	65.4	80
carbazole	**TCPB**	2.66	146	**Ir(ppy)$_3$**	23.4	–	107	80
carbazole	**DCPFB**	2.77	–	**FIrpic**	–	25.6	12.7	64

carbazole	**CTP-1**	2.73	113	**FIrpic**	15.9	40.5	33.9	81
carbazole	**PBCz**	2.76	115	**FIrpic**	19.5	45.5	43.8	81
carbazole	**TMCz**	2.99	165	**FIrpic**	14.7	35.9	25.1	82
carbazole	**DMCz**	2.71	127	**FIrpic**	18.5	43.7	36.0	82
carbazole	**CzTP**	2.70	135	**FIrpic**	–	52	55	83
carbazole	**CzTP**	2.70	135	**$Ir(ppy)_3$**	–	102	113	83
carbazole	**CmInF**	2.77	195	**FIrpic**	9.2	20.2	11.8	84
carbazole	**CmInF**	2.77	195	**$(ppy)_2Ir(acac)$**	15.1	55.6	42.2	84
carbazole	**CmInF**	2.77	195	**$(mpq)_2Ir(acac)$**	13.3	14.1	9.7	84
carbazole	**DNDT-CIZ**	2.41	124	**$(ppy)_2Ir(tipg)$**	18.6	66.2	80.5	85
carbazole	**TCz1**	2.92	88	**FIrpic**	14.7	31.1	28.4	86
carbazole	**BTCC-36**	2.96	210	**FIrpic**	14.0	27.2	11.8	87
carbazole	**Cz-TCB**	2.86	–	**FIrpic**	13.0	25.7	-	88
carbazole	**H2**	2.89	466	**FIrpic**	12.7	27.6	15.4	89
carbazole	**G3**	2.61	376	**$Ir(ppy)_3$**	10.7	36.4	18.59	30
carbazole	**G3MP**	2.85	368	**FIrpic**	12.8	28.2	14.1	91
carbazole	**G3MP**	2.85	368	**G0**	15.9	54.0	48.6	91
carbazole	**G3MP**	2.85	368	**$(TPAPQ)_2Ir(acac)$**	14.0	12.7	7.4	91

3.3.2 Host materials with electron injection/transporting (EI/ET) properties

In this category of host materials, the compounds possess aromatic systems containing nitrogen atoms with sp^2 hybrid mode. Owing to the lone electron-pair on the nitrogen atom which cannot participate in conjugation and the high electronegativity of nitrogen atom, the conjugated *N*-heterocycles, such pyridine, oxadiazole and triazine, exhibit electron-deficient characters, which can afford EI/ET ability to the related host materials. It is well known that organic semiconductors typically exhibit much better HI/HT ability than EI/ET ability. Hence, the host materials with EI/ET features should be more desirable in PHOLEDs.

3.3.2.1 Oxadiazole-based host materials

Oxadiazole (OXD) derivatives have been widely used as ET materials for OLEDs.[92-94] Their high

electron mobility as well as thermal stability could dramatically increase the device performance.[95, 96] Therefore, oxadiazole moieties can be incorporated into host materials to improve the ET abilities.[97-99] A green-emitting device based on **OXD1** (Fig. 14) and $Ir(ppy)_3$ co-doped film was fabricated and gave a CE of 26 cd A^{-1} at a brightness of 200 cd m^{-2}.[98] Lee *et al.* demonstrated that by replacing **mCP** with **OXD2** as host for **FIrpic**, the CE and PE of the resultant device can be improved from 11.7 cd A^{-1} to 13.0 cd A^{-1} and 4.60 lm W^{-1} to 6.29 lm W^{-1}, respectively, indicating the advantage of using materials with good EI/ET properties as host for phosphorescent emitters.[100] In order to improve the thermal property and morphological stability, the OXD-based hosts **SBF-*m*-OXD** and **SBF-*o*-OXD** have been by Yang and coworkers.[101] Compounds **SBF-*m*-OXD** and **SBF-*o*-OXD** show E_T of *ca.* 2.50 eV (Table 3) due to the π-conjugation between oxadiazole and spirobifluorene moieties, which implies that they can be used as host for red triplet emitters. The EL results show that **SBF-*o*-OXD** can be a better host than **SBF-*m*-OXD** due to the lower-lying LUMO level of **SBF-*o*-OXD** (2.48 eV) than that of **SBF-*m*-OXD** (2.33 eV), which is beneficial for EI into the emissive layer. Besides, the seriously twisted conformation of *ortho*-linked **SBF-*o*-OXD** could more effectively separate the guest molecules to suppress the exciton quenching. In addition, a PHOLED using **SBF-*m*-OXD** as host for **$Ir(ppy)_3$** was also fabricated to show the maximum EQE, CE and PE of 11.7%, 41.1 cd A^{-1} and 38.1 lm W^{-1}, respectively.

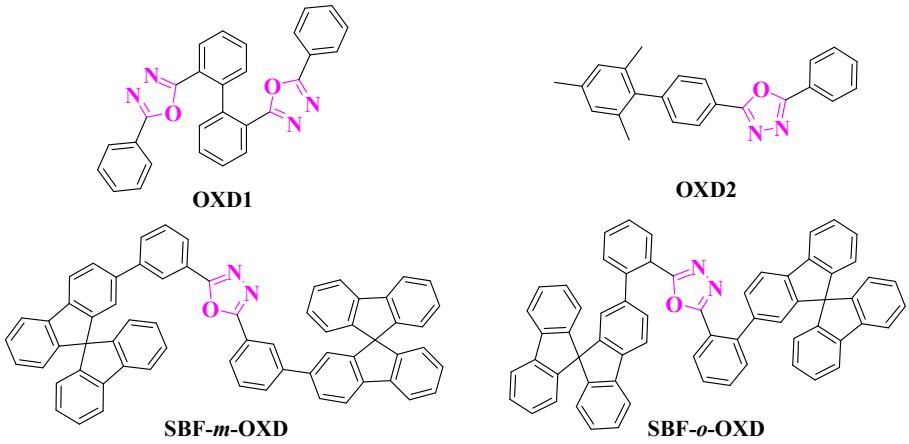

OXD1; guest $Ir(ppy)_3$; CE 26 cd A^{-1}
OXD2; guest FIrpic; EQE 4.01 %; CE 13.0 cd A^{-1}; PE 6.29 lm W^{-1}
SBF-*m*-OXD; guest $Ir(ppy)_3$; EQE 11.7 %; CE 41.1 cd A^{-1}; PE 38.1 lm W^{-1}
SBF-*m*-OXD; guest $(piq)_2Ir(acac)$; EQE 7.1 %; CE 5.0 cd A^{-1}; PE 3.6 lm W^{-1}
SBF-*o*-OXD; guest $(piq)_2Ir(acac)$; EQE 9.8 %; CE 7.6 cd A^{-1}; PE 5.4 lm W^{-1}

Fig. 14 Chemical structures of oxadiazole-based host materials and peak efficiency data of related OLEDs.

3.3.2.2 Triazine-based host materials

Triazine unit contains three sp^2 hybridized nitrogen atoms, which make it to show larger electron affinity (EA) than other typical electron-deficient heteroaromatic rings, such as pyridine and pyrimidine.[92] Hence, triazine derivatives, particularly 1,3,5-triazine with proper substituents, have been widely used as ET materials for OLEDs.[102-105] The 1,3,5-triazine derivative exhibits an electron mobility of *ca.* 7.2×10^{-4} cm^2 V^{-1} s^{-1} at a field of 8.00×10^5 V cm^{-1}, which is 10-fold larger than that of the widely used ET material tris(8-hydroxyquinoline) aluminum (Alq_3).[103] These studies clearly reveal the great potential of using 1,3,5-triazine unit for developing host materials with enhanced EI/ET abilities.

Wong *et al.* reported a series of 1,3,5-triazine-based host materials with good EI/ET ability.[106, 107] Among them, the star-shaped hosts consisting of 1,3,5-triazine cores and biphenyl arms can show good ET mobility above 10^{-4} cm^2 V^{-1} s^{-1} at the electrical field of 3.6×10^5 V cm^{-1}. They also exhibit good

thermal stability and sufficiently high E_T for green triplet emitters. The best EL performance is achieved by **T2T** (Fig. 15) in the green PHOLED doped with **(ppy)$_2$Ir(acac)**, showing the maximum EQE, CE and PE of 17.5%, 56 cd A^{-1} and 59 lm W^{-1}, respectively. The decent device performance can be attributed to the **T2T** host which possesses high thermal stability, good ET ability and the E_T value large enough for confining the excitons on the guest molecules (Table 3). By replacing the peripheral phenyl ring with 1-pyrazolyl, the host **3P-T2T** (Fig. 15) has been developed with high E_T of *ca.* 2.80 eV (Table 3) and LUMO level of *ca.* 2.33 eV. The electron-only device indicates that **3P-T2T** shows higher EI/ET ability than **T2T** due to the electron-withdrawing pyrazolyl moiety. Owing to its good EI/ET property and high E_T, **3P-T2T** can not only furnish highly efficient blue FIrpic-doped PHOLED with 8.0%, 21.0 cd A^{-1} and 19.1 lm W^{-1}, but also act as suitable host for green [**(ppy)$_2$Ir(acac)**], yellow [**(bt)$_2$Ir(acac)**] and red [**(mpq)$_2$Ir(acac)**] phosphorescent emitters. These studies demonstrate that triazine-based hosts with high thermal stability as well as good EI/ET ability are promising candidates to enhance the performance of PHOLEDs.

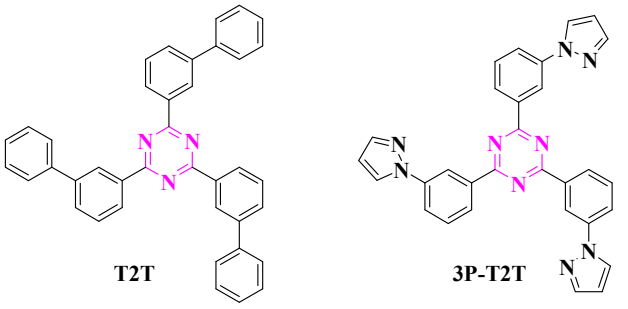

T2T; guest (ppy)$_2$Ir(acac); EQE 17.5 %; CE 56 cd A^{-1}; PE 59 lm W^{-1}
3P-T2T; guest FIrpic; EQE 8.0 %; CE 21.0 cd A^{-1}; PE 19.1 lm W^{-1}
3P-T2T; guest (ppy)$_2$Ir(acac); EQE 15.7 %; CE 56.6 cd A^{-1}; PE 71.6 lm W^{-1}
3P-T2T; guest (bt)$_2$Ir(acac); EQE 16.9 %; CE 41.6 cd A^{-1}; PE 45.8 lm W^{-1}
3P-T2T; guest (mpq)$_2$Ir(acac); EQE 16.4 %; CE 11.5 cd A^{-1}; PE 20.0 lm W^{-1}

Fig. 15 Chemical structures of **T2T** and **3P-T2T** and peak efficiency data of related OLEDs.

3.3.2.3 Carboline-based host materials

When a pyridine ring is fused to an indole skeleton, the carboline unit is formed. Due to the EI/ET ability of the pyridine segment, carboline unit can show good EI/ET capacity. In order to evaluate the potential carboline unit for developing hosts with EI/ET ability, a series of carboline-based compound have been prepared (Fig. 16). The carboline-based compound **Ad-Pd** with two carboline units linked to an adamantane spacer can show very high E_T of 2.97 eV (Table 3).[35] The electron-only device indicates its higher ET ability than the famous **UGH2** host. The optimized device based on **Ad-Pd** using **FIr6** as emitter can achieve a maximum EQE of 19% corresponding to a maximum PE of 33 lm W^{-1}, which is higher than those of the device based on **UGH2**. In addition, the operation voltages at certain current densities are much lower for device based on **Ad-Pd** due to the enhanced ET ability of the EML. This study demonstrates that carboline unit is very promising for developing EI/ET hosts with high E_T to enhance the device performance.

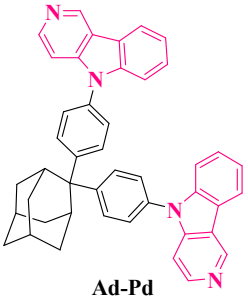

Ad-Pd

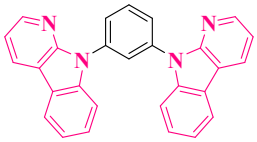

mCaP

Ad-Pd; guest FIr6; EQE 19 %; PE 33 lm W^{-1}
mCaP; guest FIrpic; EQE 17 %; CE 36 cd A^{-1}; PE 37 lm W^{-1}
mCaP; guest $Ir(ppy)_3$; EQE 24 %; CE 85 cd A^{-1}; PE 94 lm W^{-1}

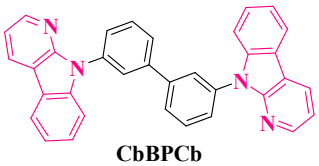

CbBPCb

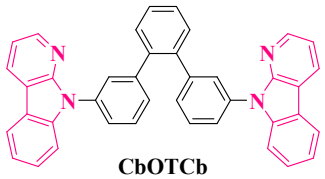

CbOTCb

CbBPCb; guest FIrpic; EQE 30.1 %; CE 53.6 cd A^{-1}; PE 50.6 lm W^{-1}
CbOTCb; guest FIrpic; EQE 28.8 %; CE 47.4 cd A^{-1}; PE 44.0 lm W^{-1}

Fig. 16 Chemical structures of carboline-based hosts and peak efficiency data of related OLEDs.

The carboline-based host **mCaP**[108] (Fig. 16) is quite similar to the famous host **mCP**. Compared with **mCP**, **mCaP** shows higher thermal stability and lower E_T. However, the E_T of 2.81 eV for **mCaP** (Table 3) still makes it a suitable host for blue phosphorescent emitters. Both FIrpic-doped blue PHOLED (17%, 36 cd A^{-1} and 37 lm W^{-1} at 100 cd m^{-2}) and $Ir(ppy)_3$-doped green PHOLED (24%, 85 cd A^{-1} and 94 lm W^{-1} at 100 cd m^{-2}) based on **mCaP** show obviously higher EL efficiencies than the corresponding devices based on **mCP**. In addition, devices based on **mCaP** show lower driving voltages as compared to the ones based on **mCP**, indicating the critical role played by the good EI/ET properties of **mCaP** in improving the EL efficiencies of PHOLEDs. The carboline-based hosts with oligophenyl spacers have also been developed (Fig. 16). The twisted configuration affords high E_T to **CbBPCb** (2.77 eV)[109] and **CbOTCb** (2.90 eV) (Table 3).[110] Besides, **CbBPCb** can show higher electron mobility of 3.83×10^{-6} cm^2 V^{-1} s^{-1} than hole mobility of 6.33×10^{-7} cm^2 V^{-1} s^{-1}. Given the high ET ability and suitable E_T, **CbBPCb** can endow the FIrpic-doped blue PHOLED with extremely high EL efficiencies (EQE of 30.1%, CE of 53.6 cd A^{-1} and PE of 50.6 lm W^{-1}). The exceptional device performance can be attributed to the efficient host-guest energy transfer, balanced charge injection/transporting and effective exciton confinement within the emitting layer. With high E_T of 2.90 eV, **CbOTCb** can also serve as a host for blue phosphorescent **FIrpic** to achieve very high efficiencies with maximum EQE, CE and PE of 28.8%, 47.4 cd A^{-1} and 44.0 lm W^{-1}. These studies clearly demonstrate the great potential of using carboline derivatives as host materials showing good EI/ET ability to fabricate highly efficient PHOLEDs.

3.4 Diphenylphosphoryl-based host materials

Aromatic phosphonic compounds with lone pair electrons on phosphor atom are usually very sensitive to oxidant and can be easily converted into phosphoryl units containing highly polarized P=O group, thereby showing strong electron-deficient character. Therefore, compounds containing P=O group have been widely used as ET materials[111-115] and host materials in OLEDs to balance the charge carrier flux within the devices.[116, 117] In addition, the tetrahedral configuration of the phosphoryl unit can effectively interrupt conjugation and thereby maintain the high E_T of the corresponding compounds, which is of great importance to obtain high E_T hosts with good EI/ET abilities. Besides, the bulky size of the diphenylphosphoryl can enlarge the molecular size and thus increase the molecular thermal stability.

PO1 (Fig. 17) with E_T of 2.72 eV (Table 3) should represent the first diphenylphosphoryl-based host to be used for the FIrpic-doped blue PHOLEDs which show the maximum EQE and CE of 7.8% and 20.8 cd A^{-1}, respectively.[116] By replacing the biphenyl spacer in **PO1** with a fluorene moiety, **PO6** (Fig. 17) has been obtained with similar E_T and EL performance to **PO1**. The higher T_g of **PO6** (*ca.* 105 °C) than that of **PO1** (*ca.* 90 °C) can be ascribed to its rigid spacer. Despite the common EL efficiencies associated with these blue PHOLEDs based on **PO1** and **PO6**, the driving voltages are significantly reduced as compared to that of the device using inert host materials, which can be attributed to the efficient EI/ET properties of the diphenylphosphoryl hosts. However, the moderate T_g of **PO1** (*ca.* 90 °C) and **PO6** (*ca.* 105 °C) cannot keep the good amorphous stability due to the crystallization in both **PO1** and **PO6**, which has been assigned to the high crystallization propensity induced by the presence of highly polar P=O groups coupled with the small rotational barrier about

the P-C bond.[118]

To reduce the crystallization propensity of **PO1** and **PO6**, introduction of bulky spacers between the two diphenylphosphoryl units is a feasible way.[119] Thus, **SPPO13** (Fig. 17) has been prepared with a *spiro*bifluorene core,[120] which can not only effectively enlarge the molecular size to increase the thermal stability but also enhance the ET ability. Besides, the E_T of 2.73 eV for **SPPO13** can be maintained (Table 3). In addtion, the low-lying LUMO level of 2.91 eV for **SPPO13** helps to enhance the EI ability. The blue PHOLED using **SPPO13** as host gives decent performance with the maximum EQE of 19.6% and PE of 48.5 lm W^{-1}. Two host materials consisting of a diphenylphosphine oxide unit and a spirofluorene core have also been prepared. The host **SPPO11**[121] with diphenylphosphoryl group at the 4-position can show obvious advantages over **SPPO1**[117] having diphenylphosphoryl group at the 2-position: significantly higher T_g (127 °C for **SPPO11** vs 96 °C for **SPPO1**) due to the higher steric hindrance in **SPPO11** (Table 3), lower LUMO level (2.82 eV for **SPPO11** vs 2.73 eV for **SPPO1**) which will benefit EI process, and higher electron mobility (7×10^{-4} cm^2 V^{-1} s^{-1} for **SPPO11** vs 5×10^{-4} cm^2 V^{-1} s^{-1} for **SPPO1**).[117] In spite of their similar E_T of 2.78 eV, **SPPO11** can furnish the blue PHOLED (EQE of 17.2%) with higher EL efficiency than **SPPO1** (EQE of 15.6%). Expanding the conjugation of the *spiro*bifluorene unit can effectively lower the E_T (2.40 eV for **SPPO2**[122] vs 2.77 eV for **SPPO1**) (Table 3). However, the ET ability of **SPPO2** is still higher than that of the famous Alq_3. A red-emitting device using $(pq)_2Ir(acac)$ as emitter and **SPPO2** as host displays high performance with EQE of 14.3% and CE of 20.4 cd A^{-1}. By linking diphenylphosphoryl group to the 3-position of *spiro*bifluorene, **SF3PO**[123] has a medium T_g of 119 °C, which is in good accordance with the steric hindrance of the three isomers **SF3PO**, **SPPO1** and **SPPO11**. However, **SF3PO** shows the

highest E_T of 2.87 eV among these isomers (Table 3), rendering **SF3PO** a good host for blue phosphorescent emitters. Thus, with **FIr6** as emitter, the device based on **SF3PO** shows much better performance (EQE, CE and PE of 13.6%, 28.5 cd A^{-1} and 23.7 lm W^{-1}, respectively) than the device based on **SPPO1** (4.5%, 10.5 cd A^{-1} and 8.8 lm W^{-1}). These impressive results not only show the great potential of the diphenylphosphoryl-based hosts in achieveing high EL performance but also draw a clear picture of the structure-property relationship for these novel hosts, which provides valuable clues for designing high-performance diphenylphosphoryl-based hosts.

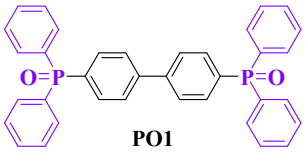

PO1

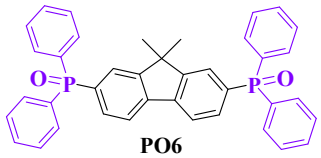

PO6

PO1; guest FIrpic; EQE 7.8 %; CE 20.8 cd A^{-1}
PO6; guest FIrpic; EQE 8.1 %; CE 21.5 cd A^{-1}

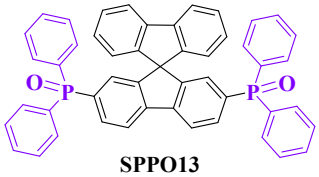

SPPO13

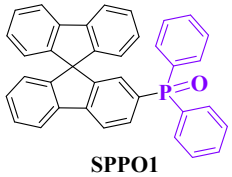

SPPO1

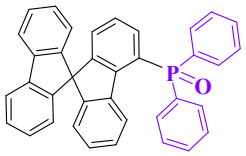

SPPO11

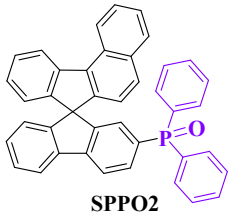

SPPO2

SPPO13; guest FIrpic; EQE 19.6 %; PE 48.5 lm W^{-1}
SPPO1; guest FIrpic; EQE 15.6 %
SPPO11; guest FIrpic; EQE 17.2 %; CE 35.3 cd A^{-1}
SPPO2; guest $(pq)_2Ir(acac)$; EQE 14.3 %; CE 20.4 cd A^{-1}

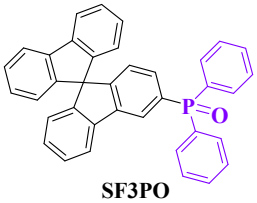

SF3PO

SF3PO; guest FIr6; EQE 13.6 %; CE 28.5 cd A^{-1}; PE 23.8 lm W^{-1}
SPPO1; guest FIr6; EQE 4.50 %; CE 10.5 cd A^{-1}; PE 8.80 lm W^{-1}

Fig. 17 Chemical structures of diphenylphosphoryl-based hosts and peak efficiency data of related OLEDs.

Table 3. Host materials with electron injection/transporting group and their properties

Main-group element unit	Host	E_T eV	T_g °C	Dopant	EQE %	CE cd A^{-1}	PE lm W^{-1}	Ref.
oxadiazole	**OXD1**	–	44.6	**Ir(ppy)$_3$**	–	26	–	98
oxadiazole	**OXD2**	–	–	**FIrpic**	4.01	13.0	6.29	100
oxadiazole	**SBF-*m*-OXD**	2.55	178	**Ir(ppy)$_3$**	11.7	41.1	38.1	101
oxadiazole	**SBF-*m*-OXD**	2.55	178	**(piq)$_2$Ir(acac)**	7.1	5.0	3.6	101
oxadiazole	**SBF-*o*-OXD**	2.5	136	**(piq)$_2$Ir(acac)**	9.8	7.6	5.4	101
triazine	**T2T**	2.8	95	**(ppy)$_2$Ir(acac)**	17.5	56	59	106
triazine	**3P-T2T**	2.8	–	**FIrpic**	8.0	21.0	19.1	107
triazine	**3P-T2T**	2.8	–	**(ppy)$_2$Ir(acac)**	15.7	56.6	71.6	107
carboline	**Ad-Pd**	2.97	181	**FIr6**	19	–	33	35
carboline	**mCaP**	2.81	–	**FIrpic**	17	36	37	108
carboline	**CbBPCb**	2.77	–	**FIrpic**	30.1	53.6	50.6	109
carboline	**CbOTCb**	2.90	–	**FIrpic**	28.8	47.4	44.0	110
diphenylphosphine oxide	**PO1**	2.72	90	**FIrpic**	7.8	20.8	–	116
diphenylphosphine oxide	**PO6**	2.72	105	**FIrpic**	8.1	21.5	–	118
diphenylphosphine oxide	**SPPO13**	2.73	–	**FIrpic**	19.6	–	48.5	120
diphenylphosphine oxide	**SPPO11**	2.78	127	**FIrpic**	17.2	35.3	–	121
diphenylphosphine oxide	**SPPO1**	2.77	96	**FIrpic**	15.6	–	–	117
diphenylphosphine oxide	**SPPO2**	2.4	119	**(pq)$_2$Ir(acac)**	14.3	20.4	–	122
diphenylphosphine oxide	**SF3PO**	2.87	119	**FIr6**	13.6	28.5	23.8	123

3.5 Dibenzothiophene- and sulfone-based host materials

Dibenzothiophene unit has been widely incorporated into host materials due to its high E_T of 3.04 eV as well as the weak ET property.[124, 125] Liao *et al.* reported two dibenzothiophene-based host materials in which the dibenzothiophene unit is linked to a spirofluorene at the 2-position (**DBTSF2**) or 4-position (**DBTSF4**) (Fig. 18).[126] Similar to the cases in isomers **SPPO1** and **SPPO11**, the

4-position linkage makes larger steric hindrance in **DBTSF4**, leading to the higher T_g and E_T of 131 °C and 2.82 eV (Table 4), respectively, for **DBTSF4**, relative to those of 122 °C and 2.49 eV for **DBTSF2**, indicating that **DBTSF4** is a suitable host for blue phosphors. The device using FIrpic-doped **DBTSF4** as EML gives peak EQE, CE and PE of 10.3%, 23.5 cd A^{-1} and 16.6 lm W^{-1}, respectively. However, when using **DBTSF4** as host for a blue-yellow two-color based WOLED, the device displays better performance. The optimized WOLED gives high efficiencies of peak EQE, CE and PE of 16.9%, 52.3 cd A^{-1} and 33.1 lm W^{-1}, respectively, with stable electroluminescent spectra and very low efficiency roll-off at 1000 cd m^{-2}.

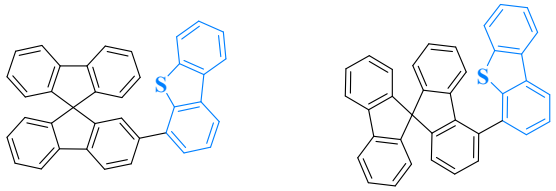

DBTSF2 **DBTSF4**

DBTSF4; guest FIrpic; EQE 10.3 %; CE 23.5 cd A^{-1}; PE 16.6 lm W^{-1}
DBTSF4; guest FIrpic and PO-01; EQE 16.9 %; CE 52.3 cd A^{-1}; PE 33.1 lm W^{-1}

Fig. 18 Chemical structures of **DBTSF2** and **DBTSF4** and peak efficiency data of related OLEDs.

Liao *et al.* also synthesized a series of host materials containing two dibenzothiophene units and investigated the structure-property correlations.[127] Two dibenzothiophene units are connected by biphenyl or terphenyl spacer with *para*-, *meta*- or *ortho*-linkages (Fig. 19). The different linkages result in obvious differences in terms of thermal stability, E_T as well as MO levels. With extended phenyl spacers, the T_g gradually increases from 79 °C to 102 °C for *meta*-linked materials due to the increased molecular weight and steric effect. ***o*-BPDBT** and ***p*-BPDBT** have the tendency to crystallization, indicating their low T_g, although their glass transition process on their DSC traces were not observed. Due to the extended conjugation length, ***p*-BPDBT** shows the lowest E_T of 2.46 eV (Table 4), which

fails to be used as a host for blue phosphors. The E_T of *meta*- and *ortho*-linked materials are higher in the range from 2.64 eV to 2.73 eV result from the restrained conjugation length by *meta*- or *ortho*-linkages. The HOMO and LUMO levels of these materials are quite different from each other, but the frontier orbitals, especially the LUMO, of all these materials are significantly lower as compared to those of the traditional carbazole-basaed host materials, which may facilitate the EI process. Therefore, FIrpic-based devices using *meta*- and *ortho*-linked materials as host were fabricated and gave comparable performance. The slightly higher efficiencies obtained by the device based on ***m*-TPDBT** may come from the effective EI due to its low-lying LUMO level of 2.80 eV. In addition, a blue-yellow two-color based WOLED with optimized configuration exhibits improved efficiencies with peak EQE, CE and PE of 14.1%, 41.0 cd A^{-1} and 37.3 lm W^{-1}, respectively. These results demonstrate that the dibenzothiophene unit is a useful block to design and synthesize host materials possessing properties different from carbazole-based materials. The low-lying LUMO levels induced by dibenzothiophene unit may facilitate EI and enhance ET in the EML, resulting in good device performance.

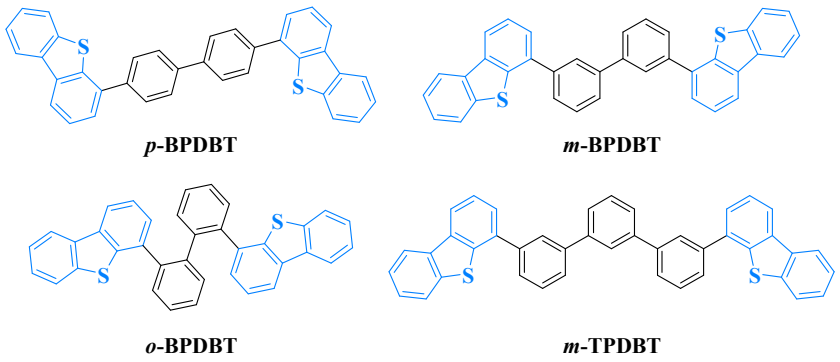

Fig. 19 Chemical structures of **B(T)PDBT**s and peak efficiency data of related OLEDs.

The sulfone unit has also drawn an increased attention due to its strong electron-withdrawing ability, which can be applied to enhance the EI/ET properties of host materials. The sulfone-based host **SO1** (Fig. 20 and Table 4) can endow FIrpic-doped blue PHOLED with EL efficiency (EQE of 6.9%) very similar to that of the similar device with **PO1** as host for FIrpic.[128] The sulfone-based host **SF-DPSO** (Fig. 20) with larger size and twisted configuration has also been obtained to furnish blue PHOLED with EQE of 6.8%.[129] To further tap the potential of sulfone-containing hosts for PHOLEDs, a *m*-terphenyl-modifed sulfone derivative **BTPS** (Fig. 20) has been prepared with E_T of 2.79 eV (Table 4) that can be used as the host material for FIrpic.[130] The blue PHOLED using 15 wt% FIrpic-doped **BTPS** film as EML gives impressive efficiencies with EQE, CE and PE of 21.8%, 48.6 cd A^{-1} and 46.0 lm W^{-1}, respectively, at a brightness of 100 cd m^{-2}. The green PHOLED with 10 wt% $Ir(ppy)_3$-doped **BTPS** film as EML displays remarkably high efficiencies with EQE, CE and PE of 28.0%, 100 cd A^{-1} and 105 lm W^{-1}, respectively, at a brightness of 100 cd m^{-2}. Furthermore, devices based on **BTPS** exhibit reduced driving voltages. All these attractive EL results can be attributed to the high E_T of **BTPS** as well as the impoved EI/ET property induced by the strong electron accepting character of the sulfone unit. This study shows that exquisite designed sulfone-containing materials can be regarded as an attractive host applied for highly efficient PHOLEDs.

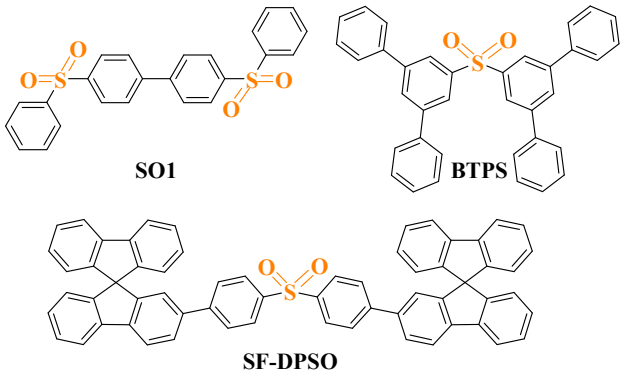

SO1; guest FIrpic; EQE 6.9 %; CE 12.9 cd A^{-1}
SF-DPSO; guest FIrpic; EQE 6.8 %; CE 13.7 cd A^{-1}
BTPS; guest FIrpic; EQE 21.8 %; CE 48.6 cd A^{-1}; PE 46.0 lm W^{-1}
BTPS; guest Ir(ppy)$_3$; EQE 28.0 %; CE 100 cd A^{-1}; PE 105 lm W^{-1}

Fig. 20 Chemical structures of sulfone-containing host materials and peak efficiency data of related OLEDs.

Table 4. Host materials containing dibenzothiophene or sulfone group and their properties

Main-group element unit	Host	E_T eV	T_g °C	Dopant	EQE %	CE cd A^{-1}	PE lm W^{-1}	Ref.
dibenzothiophene	**DBTSF4**	2.82	131	**FIrpic**	10.3	23.5	16.6	126
dibenzothiophene	***o*-BPDBT**	2.64	–	**FIrpic**	12.2	26.5	23.4	127
dibenzothiophene	***m*-BPDBT**	2.72	92	**FIrpic**	12.5	29.0	26.5	127
dibenzothiophene	***m*-TPDBT**	2.71	102	**FIrpic**	12.9	30.0	27.4	127
sulfone	**SO1**	2.72	–	**FIrpic**	6.9	12.9	–	128
sulfone	**SF-DPSO**	2.85	211	**FIrpic**	6.8	13.7	–	129
sulfone	**BTPS**	2.79	–	**FIrpic**	21.8	48.6	46.0	130
sulfone	**BTPS**	2.79	–	**Ir(ppy)$_3$**	28.0	100	105	130

3.6 Host materials containing hybrid main-group moieties with one predominant charge carrier transporting feature

From the EL results aforementioned, high E_T, T_g and charge carrier injection/transporting ability are very important features for high-performance host materials. However, some well-known hosts, such as

UGH1, **UGH2** and **UGH3**, with high E_T show relatively poor charge carrier injection/transporting feature, while some host materials such as **BCP** and **mCP** with high charge carrier injection/transporting properties possess too low T_g to maintain stable amorphous characters. To solve this problem, incorporation of different main-group moieties into a single host molecule is a feasible way.

By combining carbazole and aromatic silane moieties, some high-performance hosts have been developed with high E_T, T_g and good HI/HT abilities. The host **SimCP** (Fig. 21) can be regarded as a derivative of **mCP** by introducing the aromatic silane moiety.[131] The T_g of **SimCP** (101 °C) almost doubles that of **mCP** (55 °C), while the E_T of **SimCP** is still as high as 2.9 eV (Table 5). The triphenylsilyl substituent in **SimCP** does not reduce the E_T but increases the morphological stability. Furthermore, the bulky triphenylsilyl substituent will lead to the loose packing of **SimCP** in the condensed phase, resulting in a slightly lower HT ability to achieve charge carrier balance in EML.[132] As a result, **SimCP** can bring about blue-emitting PHOLEDs with higher EL efficiencies (14.4% and 11.9 lm W^{-1}) than the famous **mCP**. Another new carbazole/tetraphenylsilane hybrid host **SimCP2** (Fig. 21) was also reported with even higher T_g of 148 °C and E_T of 3.01 eV (Table 5).[133] Owing to the good HI/HT ability of the carbazole moiety, **SimCP2** can cope with the charge carrier injection/transporting problem of the high E_T host aforementioned. The blue PHOLEDs based on **SimCP2** shows an EQE of 17.7% at 100 cd m^{-2} with a PE of 24.4 lm W^{-1}. The PE of **SimCP2**-based device is much higher than those of **mCP**- and **SimCP**-based devices. Other carbazole/phenylsilane hybrid host materials have also been reported with improved thermal stability, high E_T and enhanced HI/HT ability.[134-136] For example, both **CzSi** and **CzCSi** (Fig. 21) display high T_g above 130 °C and high E_T of *ca.* 3.0 eV (Table 5), which are very close to that of the unsubstituted carbazole (3.02 eV). Using **FIrpic** as the emitter, the

PHOLEDs based on **CzSi** and **CzCSi** can also furnish decent EL performance. These examples show that combination of the unique characters of different main-group moieties to a single material can realize an enhancement of material properties in a more comprehensive way.

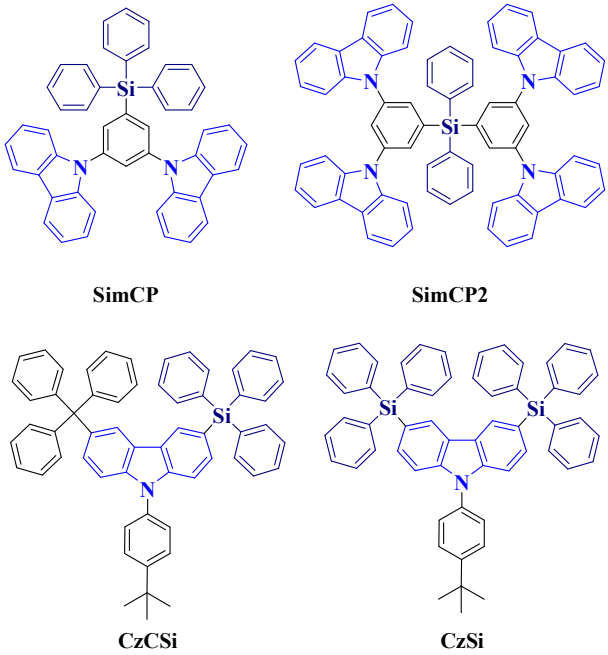

Fig. 21 Chemical structures of carbazole/phenylsilane hybrids and peak efficiency data of related OLEDs.

Triphenylamine/phenylsilane hybrids have also been developed as host materials for PHOLEDs with good performance. Owing to its larger size, **BTPASi** (Fig. 22) shows a very high T_g of 168 °C and E_T of 2.95 eV,[137] while **BTPAF** gives a lower E_T of 2.86 eV (Table 5), indicating the role of triphenylsilane moiety in increasing the E_T. The blue PHOLED based on FIrpic-doped **BTPASi** displays improved efficiencies with the EQE, CE and PE of 15.4%, 44 cd A^{-1} and 55 lm W^{-1}, respectively, in compasion to the device based on **BTPAF** (9.4%, 20 cd A^{-1} and 14 lm W^{-1}). Compared with **BTPASi**,

SiBSTPA and **SSTF** possess less rigid molecular skeleton and smaller size, and hence they show lower T_g (133 °C for **SiBSTPA**[138] and 109 °C for **SSTF**[139]) (Table 5). The E_T for **SSTF** is 2.81 eV, which is higher than that for **SiBSTPA** (2.75 eV) (Table 5). Accordingly, the blue PHOLED with **SSTF** as host can show improved EL performance, as compared with that employing **SiBSTPA** as host due to the higher E_T of **SSTF**.

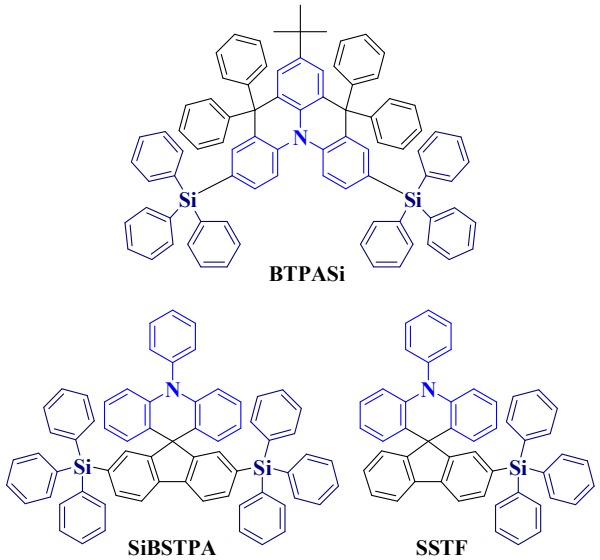

BTPASi; guest FIrpic; EQE 15.4 %; CE 44.0 cd A^{-1}; PE 55.0 lm W^{-1}
SiBSTPA; guest FIrpic; EQE 17.4 %; CE 41.0 cd A^{-1}; PE 35.2 lm W^{-1}
SSTF; guest FIrpic; EQE 18.7 %; CE 44.0 cd A^{-1}; PE 41.5 lm W^{-1}

Fig. 22 Chemical structures of triphenylamine/triphenylsilane hybrids and the peak efficiency data of related OLEDs.

Combining the high E_T property of tetraphenylsilane with the good ET ability of 1,3,4-oxadiazole, a series of oxadiazole/tetraphenylsilane hybrids have been synthesized.[140] All of these hosts show very high E_T above 3.0 eV (Table 5). Using FIrpic as emitter, the blue PHOLED based on **OXDSi** (Fig. 23) displays good EL performance with the peak EQE, CE and PE of 12.9%, 36.6 cd A^{-1} and 23.0 lm W^{-1}, respectively. However, the T_g of **OXDSi** is only 57 °C, which may be detrimental to the device stability.

So, the second tetraphenylsilane moiety can be attached to the oxadiazole core to obtain **OXDBSi** with acceptable T_g of 98 °C. Furthermore, the device based on **OXDBSi** exhibits improved performance with the EQE, CE and PE of 13.1%, 39.9 cd A^{-1} and 31.4 lm W^{-1}, respectively. These results indicate that merging phenylsilane moieties with ET groups is a promising strategy to obtain host materials with high E_T as well as good ET abilities. However, this kind of host materials is relatively rare and hence there are many opportunities to develop using this kind of host materials.

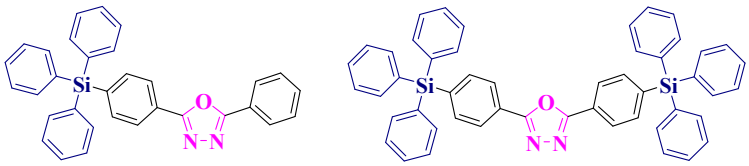

OXDSi **OXDBSi**

OXDSi; guest FIrpic; EQE 12.9 %; CE 36.6 cd A^{-1}; PE 23.0 lm W^{-1}
OXDBSi; guest FIrpic; EQE 13.1 %; CE 39.9 cd A^{-1}; PE 31.4 lm W^{-1}

Fig. 23 Chemical structures of **OXDSi** and **OXDBSi** and peak efficiency data of related OLEDs.

Due to their electron-deficient character and high E_T above 3.0 eV,[124] dibenzofuran and dibenzothiophene moieties have been employed to develop other types of hosts. However, their ET abilities are relatively weak, and therefore, other ET groups, such as diphenylphosphine oxide moiety and oxadiazole can be introduced to improve their EI/ET abilities. Tuning the substitution position of the diphenylphosphine oxide moiety can effectivly influence the T_g (105 °C for ***p*-DBFDPO**[141] vs 190 °C for ***o*-DBFDPO**[142]; 100 °C for **DBT3**[143] vs 232 °C for **DBTDPO**[144]), but show negligible impact on E_T (3.14 eV for ***p*-DBFDPO**[141] vs 3.16 eV for ***o*-DBFDPO**[142]; 2.90 eV for **DBT3**[143] vs 2.90 eV for **DBTDPO**[144]) (Fig. 24 and Table 5). The E_T of these materials are quite close to that of their cores, indicating the trivial effect of the diphenylphosphine oxide moiety on changing the E_T. In addition, the E_T of these materials are also high enough to avoid the reverse energy transfer process when used

as host for most blue phosphorescent emitters. The device based on ***o*-DBFDPO** using FIrpic as emitter shows lower efficiencies as compared to that based on ***p*-DBFDPO** at low current densities. However, the EQE and PE of the ***o*-DBFDPO** based device are higher than those of the ***p*-DBFDPO** based device at high current densities. Furthermore, the driving voltage of the ***o*-DBFDPO** based device is much lower than that of the ***p*-DBFDPO** based device. These results may be attributed to the more twisted molecular configuration of ***o*-DBFDPO**, leading to improved morphological stability and the uniform dispersion of the FIrpic in ***o*-DBFDPO** to suppress the exciton quenching at high current densities.

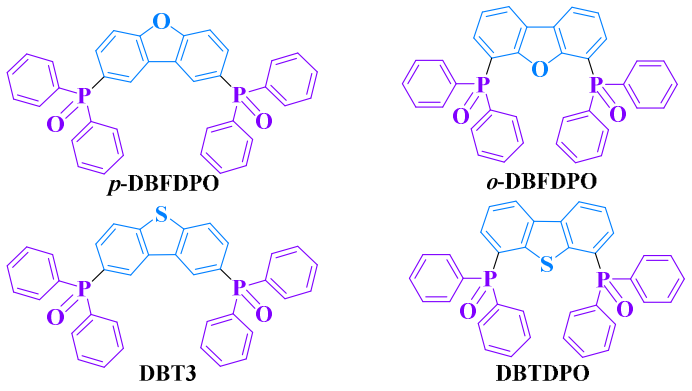

Fig. 24 Chemical structures of **DBFDPO**s, **DBT3** and **DBTDPO** and peak efficiency data of related OLEDs.

Compared with dibenzofuran, dibenzothiophene shows weaker ET ability due to the lower electronegativity of S atom. Therefore, incorporating strong electron-withdrawing groups into dibenzothiophene unit can greatly improve the ET properties of the dibenzothiophene-based host materials. The electron only device shows that **DBT3** is a predominant ET material. Besides, the

low-lying LUMO level of **DBT3** (2.99 eV) can effectively facilitate the EI process. The device using bis((3,5-difluoro-4-cyanophenyl)pyridine)iridium picolinate (**FCNIrpic**) as emitter and **DBT3** as host gives high performance with the maximum EQE, CE and PE of 19.0%, 29.9 cd A^{-1} and 17.8 lm W^{-1}, respectively. The blue PHOLED with **DBTDPO** as host shows very low driving voltages (10800 cd m^{-2} at 4.4 V), indicating its outstanding EI/ET ability. Undoubtedly, these studies show that introducting ET groups to the proper positions of a dibenzothiophene core is a practical way to obtain host materials of high E_T with good ET properties for high performance phosphorescent OLEDs. Therefore, there are a lot of opportunities for developing dibenzothiophene/ET-group hybrids since other ET groups such as pyridine, triazine, triazole, organoborane and sulfone *etc.* almost have not been used in this kind of host materials.

Table 5. Host materials containing hybrid main-group moieties and their properties

Main-group element unit	Host	E_T eV	T_g °C	Dopant	EQE %	CE cd A^{-1}	PE lm W^{-1}	Ref.
aromatic silane + carbazole	**SimCP**	2.9	101	**FIrpic**	14.4	–	11.9	132
aromatic silane + carbazole	**SimCP2**	3.01	148	**FIrpic**	17.7	–	24.4	133
aromatic silane + carbazole	**CzSi**	3.02	131	**FIrpic**	14.2	–	25.0	136
aromatic silane + carbazole	**CzCSi**	2.98	146	**FIrpic**	16.0	–	26.7	136
aromatic silane + triphenylamine	**BTPASi**	2.95	168	**FIrpic**	15.4	44.0	55.0	137
aromatic silane + triphenylamine	**SiBSTPA**	2.75	133	**FIrpic**	17.4	41.0	35.2	138
aromatic silane + triphenylamine	**SSTF**	2.81	109	**FIrpic**	18.7	44.0	41.5	139
aromatic silane + oxadiazole	**OXDSi**	3.00	57	**FIrpic**	12.9	36.6	23.0	140
aromatic silane + oxadiazole	**OXDBSi**	3.01	98	**FIrpic**	13.1	39.9	21.4	140
dibenzofuran + diphenylphosphine oxide	***p*-DBFDPO**	3.14	105	**FIrpic**	10.1	26.9	25.9	141
dibenzofuran + diphenylphosphine oxide	***o*-DBFDPO**	3.16	190	**FIrpic**	10.0	19.5	15.3	142
dibenzothiophene +	**DBT3**	2.90	100	**FIrpic**	14.3	28.8	33.1	143

diphenylphosphine oxide								
dibenzothiophene + diphenylphosphine oxide	**DBTDPO**	2.90	232	**FCNIrpic**	19.0	29.9	17.8	144

3.7 Bipolar host materials

Besides the E_T and thermal stability, the high charge carrier injection/transporting abilities of the host materials is very crucial in PHOLEDs. Host materials with preference for HT or ET ability have been widely used for triplet emitters. The "unipolar" transporting type host materials might not be preferable for PHOLEDs, which typically require balanced injeciton/transport for both kinds of charge carriers to achieve high EL efficiency. Although some devices can achieve high EL performance at low current densities, their efficiencies roll-off may be serious at high current densities. The ordinary device performance and efficiency roll-off can be largely ascribed to the unbalanced charge carrier injection/transporting in the device using unipolar host materials. Since the unbalanced charge carrier injection/transporting will narrow and shift the hole-electron recombination zone closer to the interface between the EML and the electron-transporting layer (ETL) or hole-transporting layer (HTL) (Fig. 25), resulting in the enhanced triplet–triplet annihilation and efficiency roll-off at high current density.[145] Besides, the shifted recombination zone is harmful for the emission color purity.[146] In addition, the severely unbalanced charge transport may result in charge leakage and reduce the device operation lifetime.[147] To solve these charge transporting imbalance induced detrimental effects, inserting a hole blocking layer (HBL) between the EML and ETL[148] or a electron blocking layer (EBL) between the EML and HTL[149] or using mixed host systems in a single emissive layer with both HT and ET hosts have been reported.[150] Obviously, these solutions will make device fabrication more complicated, and

the device lifetime may suffer from the unstable charge blocking or the phase separation of mixed host systems. Hence, the preferable solution is to design host materials possessing balanced injection/transporting properties for both kinds of charge carriers, *i.e.* bipolar host materials. Bipolar host materials showing both decent HT and ET abilities have drawn increased attention due to their successful application in high performance PHOLEDs.[151-154]

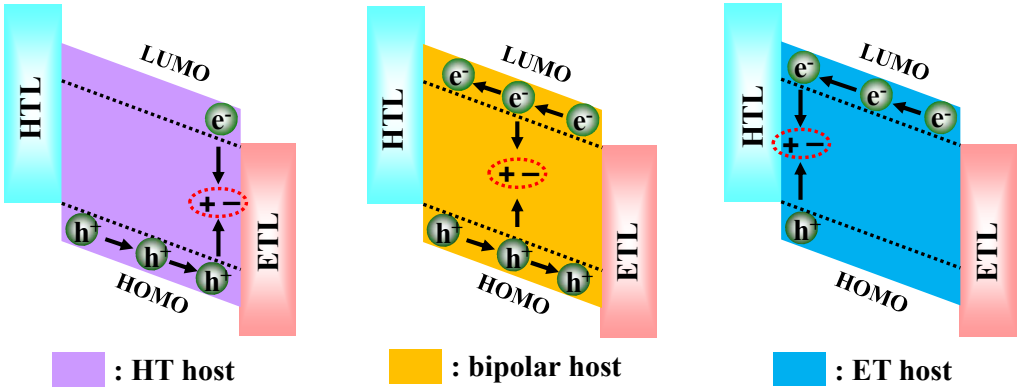

Fig. 25 Recombination zones in devices based on HT host, bipolar host and ET host.

The typical bipolar host materials usually contain electron-rich groups or electron donors to improve the HI/ET property and electron-deficient groups or electron acceptors to enhance the EI/ET ability. However, the electron donors and acceptors in a single bipolar host molecule will have a great chance to decrease the E_g of the material if the intramolecular charge transfer happens. Hence, the design of bipolar host materials with proper E_T should be crafted so as to minimize the interaction between the the electron donors and acceptors. To date, the effective strategies of weakening electron donor-acceptor interaction and thus increasing the E_T of host material include: a) connecting the electron donors and acceptors with π-conjugated spacer via *meta*- and/or *ortho*-linkages instead of *para*-linkages to form highly twisted molecular configurations, which will suppress the π-conjugation between electron donors and acceptors; b) linking the electron donors and acceptors with units containing sp^3-C

or Si atoms to interrupt the π-conjugation between electron donors and acceptors. Besides the requirments of a) sufficiently high E_T for bipolar host materials to confine the excitons on guest molecules and avoid reverse energy transfer; and b) proper HT and ET abilities for bipolar host materials to achieve balanced charge flux in devices, there are some other qualities that good bipolar host materials should possess: a) suitable HOMO and LUMO levels that match the neighboring functional layers to facilitate the charge injection process; and b) high thermal stability and T_g to enhance the device stability.

After years of development of bipolar host materials, electron donors are basically carbazole units and triphenylamine/diphenylamine units, while the electron acceptors are more diverse, such as nitrogen-containing heterocycles, phosphine oxide groups, phenylsulfonyl moieties, *etc.* Thus, there are a lot of combinations between different electron donors and electron acceptors through various linkage patterns.

3.7.1 Triphenylamine-based bipolar host materials

In this kind of bipolar host materials, the triphenylamine moiety acts as the electron donor, while the electron acceptor can be azole-based moieties, carboline, triazine, diphenylphosphoryl unit, sulfones *etc.* to afford different kinds of bipolar host materials with different characters.

3.7.1.1 Triphenylamine-azole type bipolar host materials

Inspired by the high electron mobility ($3.3\text{-}8\times10^{-5}$ cm^2 V^{-1} s^{-1} under the electrical field of $4.7\text{-}7\times10^5$ V cm^{-1}) of 1,3,5-tris(phenyl-2-benzimidazolyl)benzene (TPBI),[155] phenylbenzimidazole has been widely

used as the ET unit in tri(di)phenylamine-containing bipolar host materials.[156-159] By replacing the phenyl ring attached to the phenylbenzimidazole moiety with triphenylamine group, a TPBI analogue **TPBI-Da** has been developed (Fig. 26).[160] The E_T of **TPBI-Da** (2.70 eV) is comparable to that of TPBI (2.67 eV) (Table 6), and the LUMO level of **TPBI-Da** is also barely changed to maintain its EI ability. However, the HOMO level of **TPBI-Da** is significantly increased from 6.03 eV for TPBI up to 5.40 eV, indicating the greatly enhanced HI property of **TPBI-Da**. Using **$(ppy)_2$Ir(acac)** as emitter, the device based on **TPBI-Da** shows notably improved EL performance with the maximum EQE, CE and PE of 15.0%, 59.2 cd A^{-1} and 70.0 lm W^{-1}, respectively, as compared to the device based on TPBI (maximum EQE, CE and PE of 4.7%, 18.8 cd A^{-1} and 21.0 lm W^{-1}, respectively.) The significant enhancement of the EL performance shows the advantages of using bipolar host materials to balance the charge injection/transporting properties and broaden the exciton recombination zone and thereby increase the device efficiencies. Other bipolar hosts **TPAPBA1** and **TPAPBA2** have also been obtained by employing phenylbenzimidazole.[161] Due to their stronger conjugation, they show low E_T which makes them suitable host for green phosphorescent emitters. Owing to its more twisted configuration, **TPAPBA1** shows higher E_T of 2.55 eV than that of **TPAPBA2** (2.41 eV) (Table 6). Because of its similar E_T to that of $Ir(ppy)_3$ (2.42 eV), **TPAPBA2** furnishes inferior EL efficiencies for the $Ir(ppy)_3$-doped PHOLED as compared to **TPAPBA1**.

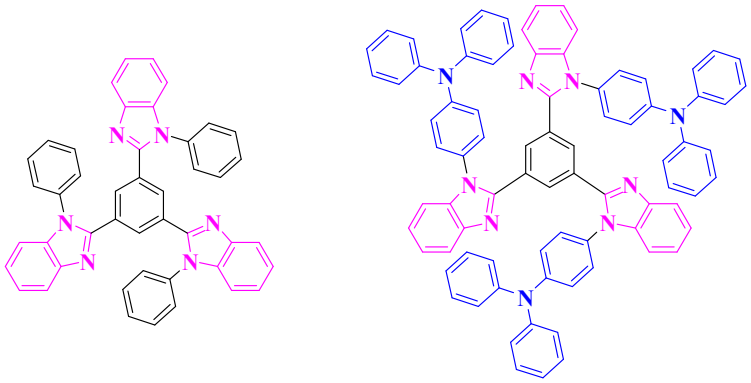

TPBI **TPBI-Da**

TPBI; guest $(ppy)_2Ir(acac)$; EQE 4.70 %; CE 18.8 cd A^{-1}; PE 21.0 lm W^{-1}
TPBI-Da; guest $(ppy)_2Ir(acac)$; EQE 15.0 %; CE 59.2 cd A^{-1}; PE 70.0 lm W^{-1}

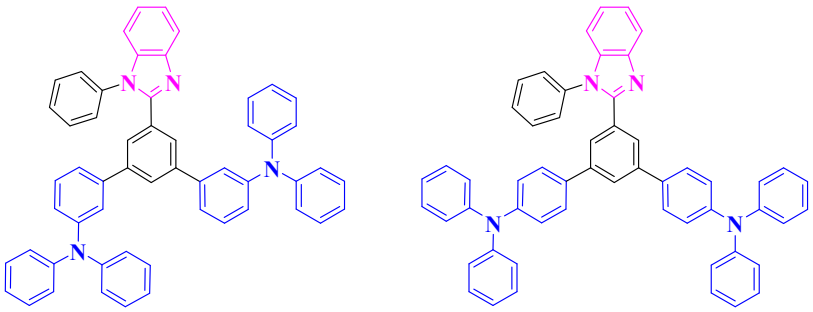

TPAPBA1 **TPAPBA2**

TPAPBA1; guest $Ir(ppy)_3$; EQE 17.0 %; CE 64.3 cd A^{-1}; PE 68.3 lm W^{-1}
TPAPBA2; guest $Ir(ppy)_3$; EQE 15.5 %; CE 59.0 cd A^{-1}; PE 48.7 lm W^{-1}

Fig. 26 Chemical structures of some benzimidazole-based bipolar hosts and peak efficiency data of related OLEDs.

The relatively low E_T associated with the benzimidazole/triphenylamine bipolar hosts makes them unsuitable as the hosts for blue phosphorescent emitters, such as the famous FIrpic (E_T = 2.62 eV). In order to obtain benzimidazole/triphenylamine bipolar hosts with high E_T, the aromatic silane moiety has been introduced to connect the triphenylamine unit and benzimidazole block.[162] The resulting bipolar host ***p*-BISiTPA** (Fig. 27) shows good thermal stability with T_g of 102 °C. More importantly, ***p*-BISiTPA** possesses a high E_T of 2.69 eV (Table 6) due to the sp^3-Si bridge which effectively interrupts the electronic interactions between triphenylamine and benzimidazole units. Owing to its

appropriate E_T, ***p*-BISiTPA** can help FIrpic-doped blue PHOLED achieve satisfactory efficiencies (EQE, CE and PE of 16.1%, 35.1 cd A^{-1} and 26.1 lm W^{-1}, respectively). The orange PHOLED using **$(fbi)_2Ir(acac)$** as emitter shows even better performance with EQE above 20.0%. In view of the high efficiency for both blue and orange PHOLEDs based on ***p*-BISiTPA**, the two-color based WOLED using FIrpic and $(fbi)_2Ir(acac)$ co-doped ***p*-BISiTPA** in single EML was fabricated and could exhibit very high maximum EQE, CE and PE of 19.1%, 51.8 cd A^{-1} and 42.7 lm W^{-1}, respectively. Furthermore, the efficiency roll-offs of these devices are quite low at high brightness, indicating the advantages of using bipolar host material to fabricate high efficiency devices with stable performance in a wide range of operation voltages.

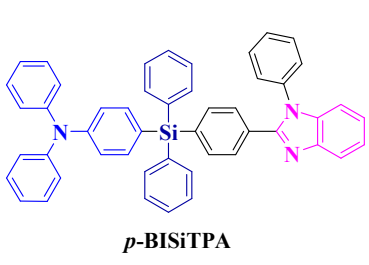

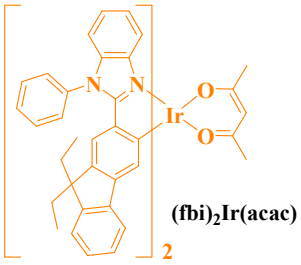

guest FIrpic; EQE 16.1 %; CE 35.1 cd A^{-1}; PE 26.1 lm W^{-1}
guest $(fbi)_2Ir(acac)$; EQE 20.5 %; CE 57.8 cd A^{-1}; PE 51.9 lm W^{-1}
guest FIrpic and $(fbi)_2Ir(acac)$; EQE 19.1 %; CE 51.8 cd A^{-1}; PE 41.7 lm W^{-1}

Fig. 27 Chemical structures of ***p*-BISiTPA** and $(fbi)_2Ir(acac)$ and peak efficiency data of related OLEDs.

1,3,4-Oxadiazole (OXD) unit is also a high-performance ET building block for triphenylamine-containing bipolar host materials.[159, 163-165] Among the numerous 1,3,4-oxadiazole/triphenylamine hybrids, attaching two triphenylamine units to an oxadiazole core through phenyl bridges with different linking topologies is commonly used, and the resultant materials also show decent EL performance when used as bipolar hosts (Fig. 28). Except for **TPA-*p*-OXD** (E_T of 2.35 eV) with longer conjugation, all the other 1,3,4-oxadiazole/triphenylamine bipolar hosts with more

twisted configuration exhibit E_T of *ca.* 2.50 eV (2.46 eV for ***p*-TPA-*o*-OXD**, 2.54 eV for ***o*-TPA-*m*-OXD** and 2.51 eV for ***m*-TPA-*o*-OXD**) (Table 6), which makes them as the perferable hosts for green, orange and red phosphorescent emitters.[163, 166] Using **$(ppy)_2$Ir(acac)** as green emitter, the optimized device based on ***p*-TPA-*o*-OXD** can give impressively high CE and PE of 90.0 cd A^{-1} and 97.7 lm W^{-1}, respectively.[167] The optimized device using **$(fbi)_2$Ir(acac)** doped ***p*-TPA-*o*-OXD** as the EML also displays decent performance with maximum EQE, CE and PE of 19.0%, 55.2 cd A^{-1} and 64.2 lm W^{-1}, respectively. When ***o*-TPA-*m*-OXD** is applied to fabricate a deep-red PHOLED using bis(1-phenylisoquinolinato)(acetylacetonate)iridium [**$(piq)_2$Ir(acac)**] as the guest, very high EQE of 21.6% has been achieved, which is much higher than that of the **CBP** hosted control device (EQE = 4.3%). An optimized green PHOLED using **$(ppy)_2$Ir(acac)** doped ***m*-TPA-*o*-OXD** as EML can fulfill a peak PE of 105 lm W^{-1} together with EQE of 23.7%.[168] Using ***m*-TPA-*o*-OXD** as the host for the orange emitter **$(fbi)_2$Ir(acac)**, the resultant device shows outstanding performance with the PE of 61.7 lm W^{-1} and CE of 62.1 cd A^{-1}. As presented above, the triphenylamine/oxadiazole hybrid bipolar host materials (**TPA-XOD**s) reported by Yang *et al.* show very impressive EL performance when used for green-to-red phosphorescent emitters, however, their relatively low E_T have restricted their application in blue PHOLEDs.

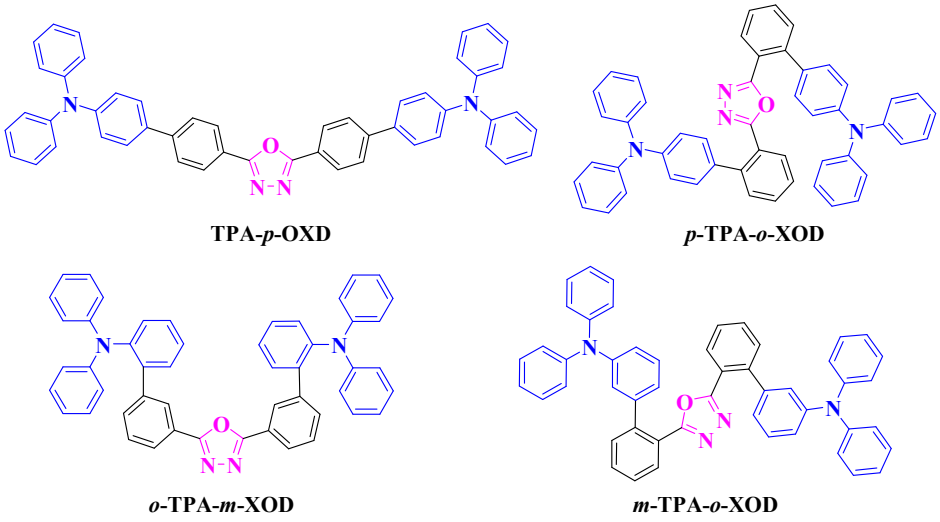

p-TPA-o-XOD; guest $(ppy)_2Ir(acac)$; EQE 23.5 %; CE 90.0 cd A^{-1}; PE 97.7 lm W^{-1}
p-TPA-o-XOD; guest $(fbi)_2Ir(acac)$; EQE 19.0 %; CE 55.2 cd A^{-1}; PE 64.2 lm W^{-1}
p-TPA-o-XOD; guest $(piq)_2Ir(acac)$; EQE 14.8 %; CE 11.4 cd A^{-1}; PE 11.8 lm W^{-1}
o-TPA-m-XOD; guest $(piq)_2Ir(acac)$; EQE 21.6 %; CE 15.9 cd A^{-1}; PE 16.1 lm W^{-1}
o-TPA-m-XOD; guest $Ir(ppy)_3$; EQE 19.6 %; CE 70.8 cd A^{-1}; PE 66.5 lm W^{-1}
m-TPA-o-XOD; guest $(ppy)_2Ir(acac)$; EQE 23.7 %; CE 91.6 cd A^{-1}; PE 105 lm W^{-1}
m-TPA-o-XOD; guest $(fbi)_2Ir(acac)$; EQE 20.6 %; CE 62.1 cd A^{-1}; PE 61.7 lm W^{-1}

Fig. 28 Chemical structures of **TPA-XOD**s and peak efficiency data of related OLEDs.

In order to increase the E_T of triphenylamine/oxadiazole hybrid host material, a similar strategy to the case of ***p*-BISiTPA** was adopted, *i.e.* by incorporating a sp^3-Si atom to prevent the π-conjugation extension between the triphenylamine and oxadiazole moieties.[169] Accordingly, the E_T of the resulting host ***p*-OXDSiTPA** (Fig. 29) is increased to 2.70 eV (Table 6), which is capable of hosting blue emitter FIrpic. The blue-emitting device based on ***p*-OXDSiTPA** shows a peak CE of 36.9 cd A^{-1} and PE of 31.4 lm W^{-1}, which are slightly higher than those of the ***p*-BISiTPA**-based device and much higher than the **mCP**-based control device. In addition, ***p*-OXDSiTPA** can also be employed to fabricate green and orange PHOLEDs with high efficiencies. If the OXD unit in ***p*-OXDSiTPA** is replaced by 1,2,4-triazole group, the resultant compound ***p*-TAZSiTPA** (Fig. 29) can show a much higher E_T of 2.93 eV (Table 6),[170] which is even sufficient for hosting the blue emitter **FIr6** (E_T = 2.72 eV). The PHOLED based on

***p*-TAZSiTPA** gives a maximum EQE of 6.3% and a CE of 12.5 cd A^{-1}. These efficiencies are very impressive as compared to those of the solution-processed FIr6-based device using traditional poly(9-vinylcarbazole) (PVK) as host. Furthermore, improved EL performance can be achieved by ***p*-TAZSiTPA** in FIrpic-doped device. Importantly, all these PHOLEDs only show slight efficiency roll-off effect. These results once again demonstrate the advantage of using the sp^3-Si containing bipolar host with high E_T and balanced charge injection/transporting properties to enhance the device performance.

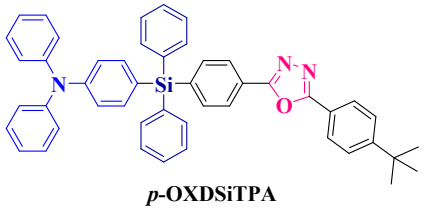

***p*-OXDSiTPA**

guest FIrpic; EQE 14.5 %; CE 36.9 cd A^{-1}; PE 31.4 lm W^{-1}
guest $(ppy)_2Ir(acac)$; EQE 19.7 %; CE 75.5 cd A^{-1}; PE 77.8 lm W^{-1}
guest $(fbi)_2Ir(acac)$; EQE 17.9 %; CE 52.4 cd A^{-1}; PE 48.7 lm W^{-1}

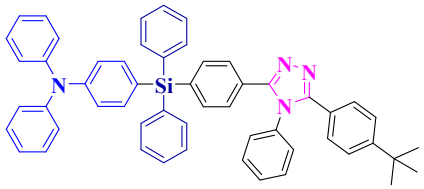

***p*-TAZSiTPA**

guest FIr6; EQE 6.3 %; CE 12.5 cd A^{-1}; PE 6.2 lm W^{-1}
guest FIrpic; EQE 11.2 %; CE 23.7 cd A^{-1}; PE 11.8 lm W^{-1}

Fig. 29 Chemical structures of ***p*-OXDSiTPA** and ***p*-TAZSiTPA** and peak efficiency data of related OLEDs.

3.7.1.2 Triphenylamine-carboline type bipolar host materials

As discussed in the previous section, carboline unit can show ET character and its derivatives possess high E_T above 2.7 eV. All these features also indicate the potential of using carboline unit as a suitable building block to design bipolar host materials. The triphenylamine/carboline bipolar hosts

TATA and **DACTA** (Fig. 30) have been developed with similar T_g as high as 164 °C and E_T of 2.86 eV (Table 6),[171] suggesting their suitability for blue triplet emitters. Using 6% FIrpic doped **TATA** as emissive layer, the blue PHOLED gives remarkably high efficiencies of 24.2%, 43.9 cd A^{-1} and 50.3 lm W^{-1}, which are much better than the **mCP**-based control device. In addition, the voltages for turn-on and at 1000 cd m^{-2} for **TATA**-based device are only 2.42 V and 4.08 V, respectively, which are also greatly reduced as compared to those of the **mCP**-based device. The **FIrpic** doped PHOLED based on **DACTA** can even show elevated efficiencies of 25.8%, 46.2 cd A^{-1} and 45.4% lm W^{-1} with reduced driving voltages. More importantly, the efficiencies of the device based on **DACTA** at a luminance of 1000 cd m^{-2} are still as high as 25.7%, 46.1 cd A^{-1} and 41.5 lm W^{-1}. The very low efficiency roll-off suggests that **DACTA** with two carboline units and a carbazole unit possesses more balanced charge transporting property than **TATA** with three carboline units, showing that the charge transporting properties of bipolar host materials can be fine-tuned by stoichiometric ratio control between HT and ET units. All these encouraging results show the great potential of the triphenylamine/carboline bipolar hosts in fulfulling high E_T as well as balanced charge carrier flux in the device and thus broadening the recombination zone to enhance the device efficiencies.

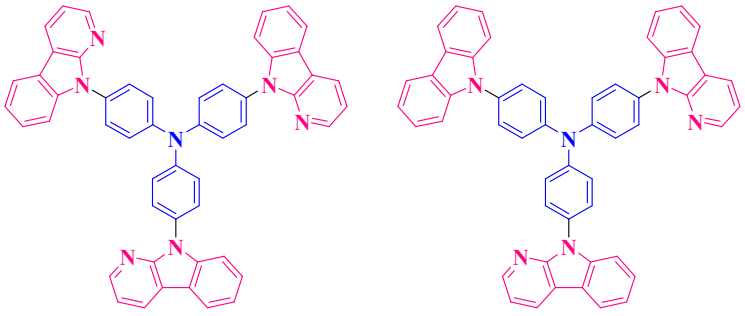

TATA **DACTA**

TATA; guest FIrpic; EQE 24.2 %; CE 43.9 cd A^{-1}; PE 50.3 lm W^{-1}
DACTA; guest FIrpic; EQE 25.8 %; CE 46.2 cd A^{-1}; PE 45.4 lm W^{-1}

Fig. 30 Chemical structures of **TATA** and **DACTA** and peak efficiency data of related OLEDs.

3.7.1.3 Triphenylamine-pyridine/triazine type bipolar host materials

Nitrogen-containing six-membered heterocyclic groups such as pyridine, pyrimidine and triazine are electron-deficient structures and have been used to develop ET materials for OLEDs.[105, 172-174] Connecting these electron-withdrawing groups with electorn-donating units will result in bipolar materials with good HT and ET properties. Lee *et al.* prepared a bridged triphenylamine-based compound containing two pyridyl moieties, named **PBPPA** (Fig. 31).[175] The E_T of **PBPPA** is 2.76 eV (Table 6). A green-emitting device using **Ir(ppy)$_3$** as emitter gives a moderate maximum EQE of 13.5% at low luminance and 13.2% at the luminance of 1000 cd m^{-2}, which are higher than those of the **CBP**-based control device. However, the electron-only device and hole-only device show that **PBPPA** possesses lower ET ability than the HT ability due to the weak ET pyridine unit. In order to improve the ET ability of triphenylamine-based materials and thereby achieve better charge transporting balance, the strongly electron-deficient 1,3,5-triazine unit has been incorporated to obtain a triphenylamine/triazine bipolar material **POTA** showing a E_T of 2.44 eV (Table 6).[176] A green-emitting device using **Ir(ppy)$_3$** as emitter and an orange-red device using tris(2-phenylquinoline)iridium [**Ir(pq)$_3$**] as emitter were fabricated to test for the practicability of using **POTA** as a host. The resulting devices give high maximum EQEs of 17.1% for the green-emitting device and 18.8% for the orange-red-emitting device. Besides, given the high fluorescent quantum yield of **POTA** (PLQY of 0.75) and good performance of the PHOLED using **POTA** as host, a single-EML RGB fluorescence and phosphorescence hybrid WOLED was fabricated. This device using **POTA** as the blue fluorophor as well as host for **Ir(ppy)$_3$** and **Ir(pq)$_3$** at the same time can show impressive performance with the peak EQE, CE and PE of 24.7%, 57.2 cd A^{-1} and 59.8 lm W^{-1}, respectively.

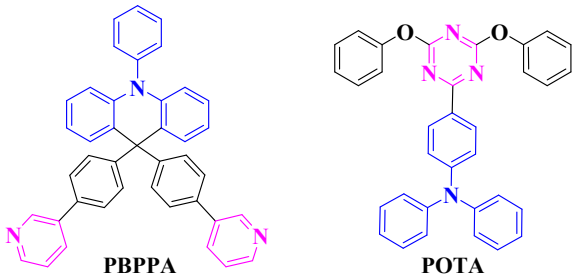

PBPPA; guest Ir(ppy)$_3$; EQE 13.5 %
POTA; guest Ir(ppy)$_3$; EQE 17.1 %; CE 57.6 cd A^{-1}; PE 52.3 lm W^{-1}
POTA; guest Ir(pq)$_3$; EQE 18.8 %; CE 36.7 cd A^{-1}; PE 28.1 lm W^{-1}
POTA; guest Ir(ppy)$_3$ and Ir(pq)$_3$; EQE 24.7 %; CE 57.2 cd A^{-1}; PE 59.8 lm W^{-1}

Fig. 31 Chemical structures of **PBPPA** and **POTA** and peak efficiency data of related OLEDs.

3.7.1.4 Triphenylamine-diphenylphosphoryl type bipolar host materials

Phosphine oxide is a well-recognized group with strongly electron-withdrawing structure and can be very conveniently combined with electron-donating groups to form bipolar charge transporting materials. The simple host **HM-A1** (Fig. 32) with high E_T of 2.84 eV (Table 6) can furnish a FIrpic-doped blue-emitting device with EQE above 17% and a highly efficient bluish green device (PE of 61.2 lm W^{-1}) doped with platinum(II) complex bis[3,5-bis(2-pyridyl)-1,2,4-triazolato]platinum(II) [**Pt(ptp)$_2$**].[177, 178] Zheng *et al.* has modified **HM-A1** by inserting a phenyl ring between the triphenylamine group and diphenylphosphoryl unit to obtain the bipolar host **POA**.[179] Due to the extended conjugation, the E_T of **POA** is as low as 2.50 eV (Table 6). Thus, a green-emitting device based on **Ir(ppy)$_3$** was fabricated showing high EL efficiencies of 18.1% and 61.2 cd A^{-1}. Besides, only slight efficiency roll-off at 1000 cd m^{-2} was observed, indicating the balanced charge carrier flux in the device at high luminance. Owing to its effective π-conjugation interruption, the sp^3-C spacer has been employed to afford high E_T of 2.93 eV for the triphenylamine/diphenylphosphoryl hybrid host material **POPCPA** (Table 6).[180] The device using **FIr6** doped **POPCPA** as the EML leads to a record PE of 45.3

lm W^{-1} with a maximum EQE above 20%. This outstanding EL performance not only highlights the merits of the high E_T bipolar host **POPCPA**, but also indicates the great potential of applying triphenylamine/diphenylphosphoryl bipolar hosts to high performance PHOLEDs.

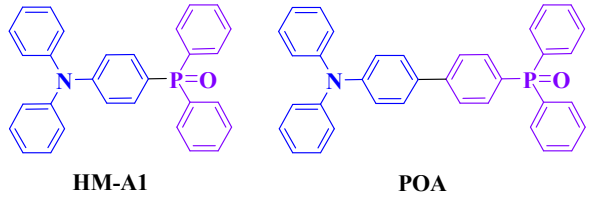

HM-A1 **POA**

HM-A1; guest FIrpic; EQE 16.7 %; PE 40.8 lm W^{-1}
HM-A1; guest $Pt(ptp)_2$; EQE 11.8 %; PE 61.2 lm W^{-1}
POA; guest $Ir(ppy)_3$; EQE 18.1 %; CE 61.2 cd A^{-1}

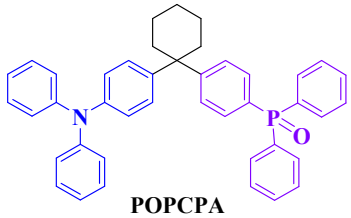

POPCPA

guest FIr6; EQE 20.8 %; CE 37.5 cd A^{-1}; PE 45.8 lm W^{-1}

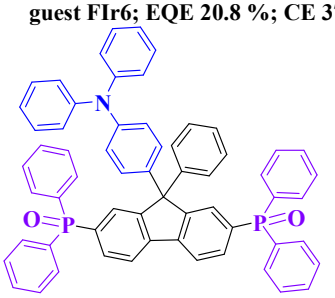

POAPF

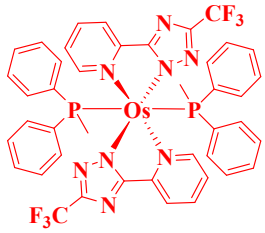

$Os(fptz)_2(PPh_2Me)_2$

guest FIrpic; EQE 20.6 %; CE 35.4 cd A^{-1}; PE 36.7 lm W^{-1}
guest $Os(fptz)_2(PPh_2Me)_2$; EQE 19.9 %; CE 32.8 cd A^{-1}; PE 34.5 lm W^{-1}
guest FIrpic and $Os(fptz)_2(PPh_2Me)_2$; EQE 18.4 %; PE 43.9 lm W^{-1}

Fig. 32 Chemical structures of triphenylamine/diphenylphosphoryl bipolar hosts and peak efficiency data of related OLEDs.

In order to improve the thermal property of this kind of bipolar hosts, **POAPF** has been obtained.[181] Owing to its twist configuration and bulky size, **POAPF** can show E_T of 2.75 eV and T_g of 129 °C (Table 6). The proper E_T makes **POAPF** not only suitable for highly efficient FIrpic-doped blue

PHOLED with EQE over 20%, but also preferable for high-performance red PHOLEDs doped by **Os(fptz)$_2$(PPh$_2$Me)$_2$** (fptz = 3-trifluoromethyl-5-pyridyl-1,2,4-triazole)[182] with efficiencies much higher than those of the **CBP**-based device. Furthermore, the bipolar host **POAPF** can fulfill highly efficient WOLEDs (EQE, CE and PE of 18.4%, 34.5 cd A^{-1} and 43.9 lm W^{-1}, respectively) using **FIrpic** and **Os(fptz)$_2$(PPh$_2$Me)$_2$** as emitters.

3.7.1.5 Triphenylamine-dibenzothiophene/sulfone type bipolar host materials

Dibenzothiophene (DBT) unit is a good building block for designing high E_T bipolar host materials due to its high E_T of 3.04 eV aforementioned. Liao *et al.* synthesized three *spiro*-annulated triphenylamine/dibenzothiophene bipolar host materials (Fig. 33).[183] As expected, the C2-substituted isomer **ST2DBT4** shows a low E_T of 2.48 eV because of the extended π-conjugation between the DBT unit and fluorene core via the *para*-linkage, while the *meta*-linking analogues **STDBT4** and **STDBT2** show high E_T above 2.8 eV (Table 6). The high T_g of *ca.* 150 °C renders **STDBT4** and **STDBT2** good morphological stability. Devices using **STDBT4** and **STDBT2** as host materials for FIrpic were fabricated to give EQEs above 18.0% and CE above 44.0 cd A^{-1}, indicating the high feasibility of **STDBT4** and **STDBT2** as host materials for blue phosphors. In addition, **STDBT4** and **STDBT2** were also applied to fabricate two-color WOLEDs using **FIrpic** (blue) and iridium(III) bis(4-phenylthieno[3,2-c]pyridinato-N,$C^{2'}$)acetylacetonate (**PO-01**, yellow) as emitters. The double-emission-layer (dEML) white device based on **STDBT4** shows a slightly better performance with the peak EQE of 23.7% and PE of 65.0 lm W^{-1}. When co-doping **FIrpic** and **PO-01** into **STDBT4** as a single-emission-layer (sEML), impressive efficiencies can be achieved with the maximum EQE of 24.0%, CE of 77.0 cd A^{-1} and PE of 63.2 lm W^{-1}, although the Commission Internationale de

L'Eclairage (CIE) coordinates of (0.38, 0.49) are located in the warm white region. However, it should be noted that both the blue-emitting devices and WOLEDs using **STDBT4** and **STDBT2** as host materials suffer from relatively high efficiency roll-offs at high luminance. This can be assigned to the fact that the much weaker ET ability of DBT cannot match the high HT ability associated with the triphenylamine unit, leading to the unbalanced charge carrier flux in the device at high luminance.

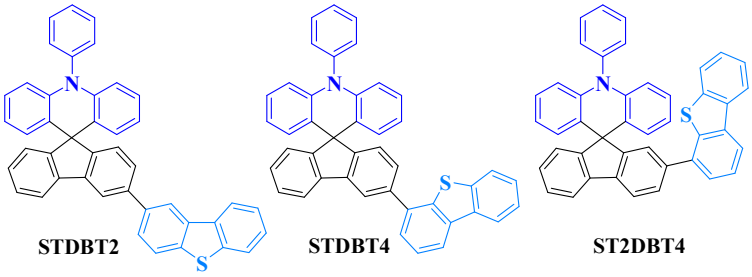

STDBT2; guest FIrpic; EQE 18.4 %; CE 44.5 cd A^{-1}; PE 37.8 lm W^{-1}
STDBT4; guest FIrpic; EQE 19.6 %; CE 47.0 cd A^{-1}; PE 38.7 lm W^{-1}
STDBT2; guest FIrpic and PO-01; EQE 22.2 %; CE 67.7 cd A^{-1}; PE 57.5 lm W^{-1} (dEML)
STDBT4; guest FIrpic and PO-01; EQE 23.7 %; CE 75.0 cd A^{-1}; PE 65.0 lm W^{-1} (dEML)
STDBT4; guest FIrpic and PO-01; EQE 24.0 %; CE 77.0 cd A^{-1}; PE 63.2 lm W^{-1} (sEML)

Fig. 33 Chemical structures of triphenylamine/DBT hybrids and peak efficiencies of related OLEDs.

In order to deal with the problem associated with DBT in developing bipolar hosts, sulfone group has been employed. The triphenylamine/sulfonyl bipolar host **SAF**[184] (Fig. 34) shows similar molecular configuration to **POAPF** aforementioned except for the ET moieties. The E_T (2.71 eV), T_g (127 °C) as well as the HOMO level (5.29 eV) of **SAF** are all close to those of **POAPF** (Table 6). However, the LUMO level of **SAF** is significantly lower than that of **POAPF** (2.88 eV for **SAF** vs 2.40 eV for **POAPF**), indicating the stronger electron-withdrawing character of sulfonyl group than that of diphenylphosphoryl group to facilitate the EI process. Using time-of-flight (TOF) transient photocurrent techniques, the hole and electron mobilities in the **SAF** film were measured to be 3.5×10^{-5} cm^2 V^{-1} s^{-1}

and 3.4×10^{-5} cm^2 V^{-1} s^{-1} under the electric field of 4.1×10^5 V cm^{-1}, indicating the balanced bipolar charge transporting character of **SAF**. The red PHOLED using tris(1-phenylisoquinolinato-C^2,N)iridium(III) [**Ir(piq)$_3$**] doped **SAF** as EML achieves very high efficiencies of 15.8% and 22.0 lm W^{-1}. The driving voltages at 1 cd m^{-2} and 1000 cd m^{-2} are as low as 2.4 V and 3.6 V, respectively. The efficiency roll-off at high luminance of **SAF**-based device is also relieved as compared to the devices based on triphenylamine/DBT hosts. These great achievements can be attributed to the enhanced EI/ET ability of the sulfonyl group and well balanced charge carrier flux in the EML. The bipolar host **DSTPA** (Fig. 34) bearing dibenzothiophene-S,S-dioxide unit has also been prepared to enhance the EI/ET ability.[185] Owing to the strong conjugation and intramolecular charge-transfer (ICT), **DSTPA** possesses very low E_T of 2.39 eV (Table 6). Therefore, **DSTPA** was used as a host for an orange-red emitter **(pq)$_2$Ir(acac)** and the related device shows very high efficiencies of 16.4%, 26.4 cd A^{-1} and 26.3 lm W^{-1}, respectively. To further test the bipolar charge carrier transporting character of **DSTPA**, a very simple single layer device was fabricated with the configuration of ITO/MoO_3(2 nm)/**DSTPA**: 5 wt% $(pq)_2Ir(acac)$ (90 nm)/LiF (1.5 nm)/Al, in which the hole and electron charge transporting layers have been omitted. Encouragingly, this device still shows the peak EQE, CE and PE as high as 7.3%, 11.7 cd A^{-1} and 12.6 lm W^{-1}, respectively, indicating the excellent bipolar ability of **DSTPA**. All these results show that the sulfonyl unit is an outstanding ET building block for designing bipolar host materials.

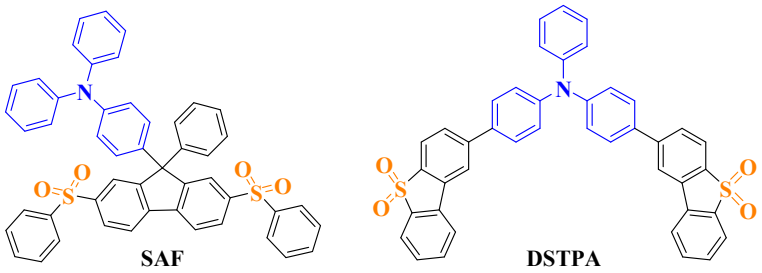

SAF DSTPA

SAF; guest Ir(piq)$_3$; EQE 15.8 %; CE 19.6 cd A^{-1}; PE 22.0 lm W^{-1}
DSTPA; guest (pq)$_2$Ir(acac); EQE 16.4 %; CE 26.4 cd A^{-1}; PE 26.3 lm W^{-1}

Fig. 34 Chemical structures of **SAF** and **DSTPA** and peak efficiency data of related OLEDs.

Table 6. Triphenylamine-based bipolar host materials and their properties

Main-group element unit	Host	E_T eV	T_g °C	Dopant	EQE %	CE cd A^{-1}	PE lm W^{-1}	Ref.
triphenylamine + phenylbenzimidazole	**TPBI-Da**	2.70	–	**(ppy)$_2$Ir(acac)**	15.0	59.2	70	160
triphenylamine + phenylbenzimidazole	**TPAPBA1**	2.55	109	**Ir(ppy)$_3$**	17.0	64.3	68.3	161
triphenylamine + phenylbenzimidazole	**TPAPBA2**	2.41	129	**Ir(ppy)$_3$**	15.5	59.0	48.7	161
triphenylamine + aromatic silane + phenylbenzimidazole	***p*-BISiTPA**	2.69	102	**FIrpic**	16.1	35.1	26.1	162
triphenylamine + aromatic silane + phenylbenzimidazole	***p*-BISiTPA**	2.69	102	**(fbi)$_2$Ir(acac)**	20.5	57.8	51.9	162
triphenylamine + oxadiazole	***p*-TPA-*o*-OXD**	2.46	–	**(ppy)$_2$Ir(acac)**	23.5	90.0	97.7	167
triphenylamine + oxadiazole	***o*-TPA-*m*-OXD**	2.54	92	**(piq)$_2$Ir(acac)**	21.6	15.9	16.1	168
triphenylamine + oxadiazole	***m*-TPA-*o*-OXD**	2.51	84	**(ppy)$_2$Ir(acac)**	23.7	91.6	105	168
triphenylamine + aromatic silane + oxadiazole	***p*-OXDSiTPA**	2.7	100	**FIrpic**	14.5	36.9	31.4	169
triphenylamine + aromatic silane + triazole	***p*-TAZSiTPA**	2.93	119	**FIrpic**	11.2	23.7	11.8	170
triphenylamine + carboline	**TATA**	2.86	164	**FIrpic**	24.2	43.9	50.3	171
triphenylamine + carboline	**DACTA**	2.86	164	**FIrpic**	25.8	46.2	45.5	171
triphenylamine + pyridine	**PBPPA**	2.76	–	**Ir(ppy)$_3$**	13.5	–	–	175
triphenylamine + triazine	**POTA**	2.44	–	**Ir(ppy)$_3$**	17.1	57.6	52.3	176
triphenylamine + diphenylphosphine oxide	**HM-A1**	2.84	–	**FIrpic**	16.1		40.8	177
triphenylamine + diphenylphosphine oxide	**POA**	2.50	75	**Ir(ppy)$_3$**	18.1	61.2		179
triphenylamine +	**POPCPA**	2.93	90	**FIr6**	20.8	37.5	45.8	180

diphenylphosphine oxide								
triphenylamine + diphenylphosphine oxide	**POAPF**	2.75	129	**FIrpic**	20.6	35.4	36.7	181
triphenylamine + dibenzothiophene	**STDBT2**	2.82	151	**FIrpic**	18.4	44.5	37.8	183
triphenylamine + dibenzothiophene	**STDBT4**	2.83	149	**FIrpic**	19.6	47.0	38.7	183
triphenylamine + sulfone	**SAF**	2.71	127	**Ir(piq)$_3$**	15.8	19.6	22.0	184
triphenylamine + sulfone	**DSTPA**	2.39	–	**(pq)$_2$Ir(acac)**	16.4	26.4	26.3	185

3.7.2 Carbazole-based bipolar host materials

3.7.2.1 Carbazole-dimesitylborane type bipolar host materials

Carbazole unit is the most widely used electron-donating building block for designing bipolar host materials due to its high E_T and rigid molecular structure. Dimesitylborane group can show strong electron-accepting ability due to the vacant *p*-orbital of the boron atom.[186] Combination of the electron-donating carbazole unit and electron-accepting dimesitylborane group is a natural proposal to obtain bipolar materials. Several carbazole/dimesitylborane bipolar hosts with different substituion positions and number of dimesitylborane group have been developed (Fig. 35). From the E_T of **CzB1** (2.88 eV) and **CzB2** (2.72 eV) (Table 7),[187] it can be seen that the substituent position of the dimesitylborane group can show an obvious effect on the E_T of the carbazole/dimesitylborane bipolar hosts. Furthermore, the substituent position of the dimesitylborane group also exerts a great influence on the charge carrier transporting properties. The single charge carrier devices reveal that both holes and electrons migrate easier in **CzB2** than **CzB1**. As a result, the **Ir(ppy)$_3$**-based devices using **CzB2** as host gives a peak EQE of 23.8%, which is much higher than that of **CzB1**-based device (peak EQE of 6.5%), and this indicates the critical role of the substitution position of the dimesitylborane group in deciding

the host performance. The carbazole/dimesitylborane bipolar host **BDDPC** composing of one *N*-phenylcarbazole core and three dimesitylborane arms exhibits the E_T of 2.83 eV (Table 7), comparable to that of **CzB1** and **CzB2**.[188] The single charge carrier devices indicate that the ET ability of **BDDPC** is better than its HT ability, which can be ascribed to the presence of three dimesitylborane groups. When **BDDPC** was employed as host for **FIrpic** (blue), **$(ppy)_2Ir(acac)$** (green) and **$Os(bpftz)_2(PPh_2Me)_2$** (red), the CEs of these devices are common (7.39 cd A^{-1} for blue-emitting device, 38.6 cd A^{-1} for green-emitting device and 11.04 cd A^{-1} for red-emitting device), which may be caused by the unbalanced charge fluxes within these devices. Therefore, in order to obain well-balanced charge transporting properties and good device performance, the carbazole/dimesitylborane hybrid host materials need to be further polished by adjusting the ratio between the carbazole unit and dimesitylborane unit as well as the substitution pattern.

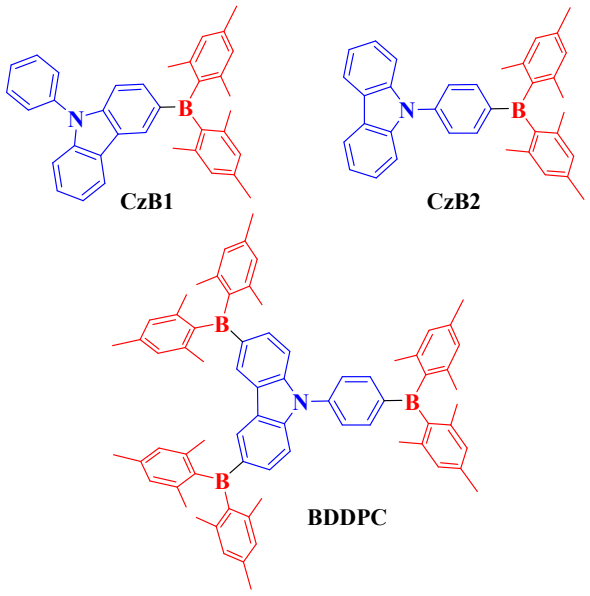

Fig. 35 Chemical structures of carbazole/dimesitylborane hybrids and peak efficiency data of related OLEDs.

3.7.2.2 Carbazole-azole type bipolar host materials

Benzimidazole-modified carbazole is a simple approach to develop bipolar host materials.[189-191] By attaching both carbazole and benzimidazole units to proper spacers, several bipolar hosts have been successfully synthesized (Fig. 36). The spacers can be phenyl, terphenyl and fluorene-based unit with twisted configuration to maintain desirable E_T. In the bipolar hosts **mBICP**,[192] **mPhBINCP**[193] and **PhBIDmpCP**[194], the phenyl spacer is adopted. With a larger size than **mBICP** (T_g of 84 °C), **mPhBINCP** possesses higher T_g of 113 °C. For **CzFCBI** and **CzFNBI**, the large bulky fluorene-based spacer can afford them with an even higher T_g > 170 °C.[195] Despite its low T_g, **mBICP** can show the E_T as high as 3.0 eV (Table 7). Owing to the extended conjugation of the benzimidazole segment, **mPhBINCP** and **PhBIDmpCP** possess relatively lower E_T of 2.61 eV and 2.59 eV, respectively (Table 7). For the bipolar hosts **PhCzNBI** and **PhCzCBI**[196] together with **CzFNBI** and **CzFCBI**, they are isomers with the benzimidazole unit attached to the spacer with different atoms in the imidazole segment. With the benzimidazole unit bounded to the nitrogen atom of the spacer, **PhCzNBI** (2.71 eV) and **CzFNBI** (2.72 eV) show higher E_T than their corresponding isomer **PhCzCBI** (2.55 eV) and **CzFCBI** (2.52 eV) with the benzimidazole unit bounded to carbon atom on the spacer (Table 7). This might be due to the fact that the connecting mode in **PhCzCBI** and **CzFCBI** will be favorable for conjugation extension and thereby lead to lower E_T. Hence, these results have provided very important information for tuning the E_T of this kind of bipolar hosts.

Benefiting from the high E_T of 3.0 eV for **mBICP**, the related blue PHOLED with FIrpic as emitter can show attractive EL performance with peak EQE of 18.7% and PE of 33.6 lm W^{-1}. For their proper E_T, other carbazole/benzimidazole bipolar hosts can furnish highly efficient PHOLEDs with longer

emission wavelength as well. The **mPhBINCP**-based green PHOLED doped with **Ir(ppy)$_3$** can achieve very high maximum CE of 77.6 cd A^{-1} and PE of 80.3 lm W^{-1}. Using **CzFCBI** and **CzFNBI** as hosts for red emitter **Os(bpftz)$_2$(PPhMe$_2$)$_2$**, both devices show comparable performance with peak EQEs over 18.0%. Furthermore, these two bipolar materials can serve well as common hosts for green-to-red PHOLEDs with high efficiencies. The yellow PHOLEDs using **(bt)$_2$Ir(acac)** as emitter and **PhCzNBI** and **PhCzCBI** as hosts can show good EL performance with PE over 40 lm W^{-1}.

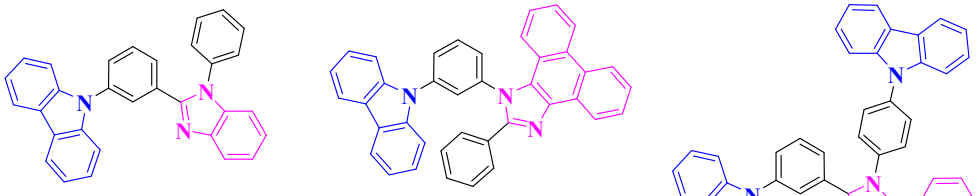

mBICP; guest FIrpic; EQE 18.7 %; CE 36.4 cd A^{-1}; PE 33.6 lm W^{-1}
mPhBINCP; guest Ir(ppy)$_3$; EQE 21.0 %; CE 77.6 cd A^{-1}; PE 80.3 lm W^{-1}
PhBIDmpCP; guest Ir(ppy)$_3$; EQE 20.2 %; CE 74.3 cd A^{-1}; PE 74.4 lm W^{-1}

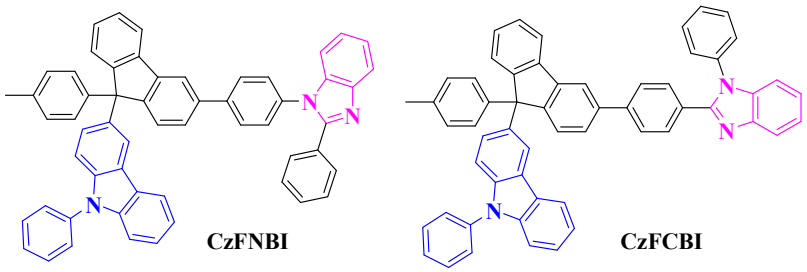

CzFNBI; guest (ppy)$_2$Ir(acac); EQE 17.8 %; CE 64.1 cd A^{-1}; PE 46.0 lm W^{-1}
CzFNBI; guest (bt)$_2$Ir(acac); EQE 19.5 %; CE 48.1 cd A^{-1}; PE 36.5 lm W^{-1}
CzFNBI; guest Os(bpftz)$_2$(PPhMe$_2$)$_2$; EQE 18.6 %; CE 18.6 cd A^{-1}; PE 13.0 lm W^{-1}
CzFCBI; guest Os(bpftz)$_2$(PPhMe$_2$)$_2$; EQE 18.1 %; CE 18.2 cd A^{-1}; PE 17.0 lm W^{-1}
CzFCBI; guest (ppy)$_2$Ir(acac); EQE 20.0 %; CE 74.4 cd A^{-1}; PE 75.0 lm W^{-1}
CzFCBI; guest (bt)$_2$Ir(acac); EQE 19.4 %; CE 48.7 cd A^{-1}; PE 47.6 lm W^{-1}

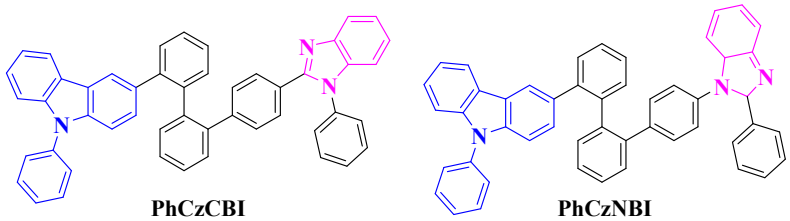

PhCzCBI; guest (bt)$_2$Ir(acac); EQE 18.7 %; CE 47 cd A^{-1}; PE 42.2 lm W^{-1}
PhCzNBI; guest (bt)$_2$Ir(acac); EQE 19.6 %; CE 51 cd A^{-1}; PE 43.1 lm W^{-1}

Fig. 36 Chemical structures of carbazole/benzimidazole bipolar hosts and peak efficiency data of

related OLEDs.

Yang *et al.* designed a 1,8-disubstituted carbazole/benzimidazole hybrid **1,8-mBICz** (Fig. 37) with a carbazole-based spacer to link up two benzimidazole units. The bipolar host **1,8-mBICz** can show relatively high E_T of 2.70 eV (Table 7).[197] Owing to its comparable E_T to that of FIrpic, **1,8-mBICz** can furnish the FIrpic-doped PHOLED with moderate EL performance (CE of 27.6 cd A^{-1} and PE of 27.0 lm W^{-1}), while the $Ir(ppy)_3$-doped green PHOLED based on **1,8-mBICz** exhibits better performance with the peak CE of 64.0 cd A^{-1} and PE of 70.0 lm W^{-1}. By employing fused carbazole moiety, *i.e.*, indolo[3,2-*b*]carbazole group, as the spacer, the bipolar hosts **TICCBI** and **TICNBI** show lower E_T of 2.61 eV because of the extended conjugation of the fused carbazole spacer (Table 7).[198] Owing to their more rigid molecular skeleton and larger size, **TICCBI** and **TICNBI** have high T_g of 174 °C and 168 °C, respectively. Red PHOLEDs using **$Os(bpftz)_2(PPhMe_2)_2$** as emitter and **TICCBI** and **TICNBI** as hosts can achieve very high EL efficiencies with EQEs exceeding 20% even at a luminance of 1000 cd m^{-2}, indicating the well-balanced charge carrier fluxes and broadened recombination region within the EMLs.

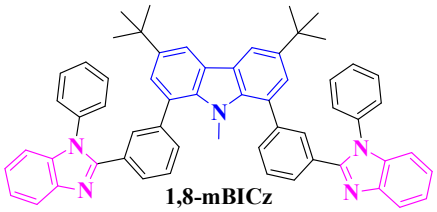

1,8-mBICz

1,8-mBICz; guest FIrpic; EQE 11.6 %; CE 27.6 cd A^{-1}; PE 27.0 lm W^{-1}
1,8-mBICz; guest $Ir(ppy)_3$; EQE 17.5 %; CE 64.0 cd A^{-1}; PE 70.0 lm W^{-1}

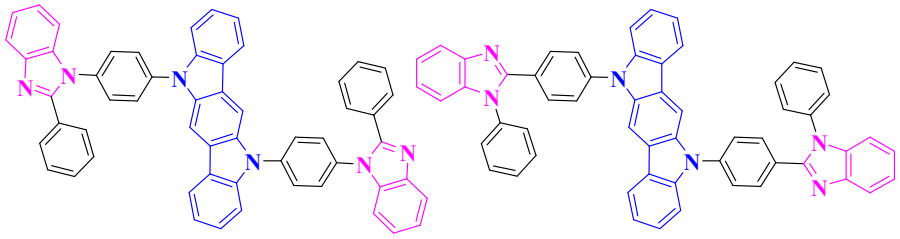

TICNBI **TICCBI**

TICNBI; guest $Os(bpftz)_2(PPhMe_2)_2$; EQE 22 %; CE 28.0 cd A^{-1}; PE 22.1 lm W^{-1}
TICCBI; guest $Os(bpftz)_2(PPhMe_2)_2$; EQE 21 %; CE 26.6 cd A^{-1}; PE 25.0 lm W^{-1}

Fig. 37 Chemical structures of **1,8-mBICz**, **TICCBI** and **TICNBI** and peak efficiency data of related OLEDs.

Besides the benzimidazole units, the oxadiazole moiety has also been employed to couple it with carbaozle to construct other bipolar hosts. Yang *et al.* synthesized a series of simple carbazole/oxadiazole hybrid bipolar materials in which two *N*-phenylcarbazole units were connected to an oxadiazole core though *para*-, *meta*- and *ortho*-linkages (Fig. 38).[199, 200] These bipolar materials show T_g in the range from 97 to 133 °C and E_T above 2.60 eV (Table 7). Green-emitting devices using these carbazole/oxadiazole hybrid bipolar materials as hosts were fabricated. Among these bipolar hosts, the *ortho*-linked isomer ***o*-CzOXD** can endow the **$Ir(ppy)_3$**-doped green PHOLED with the highest efficiencies at EQE of 20.2% and PE of 59.3 lm W^{-1}. The fact that ***o*-CzOXD**-based device shows better performance may be due to the reduced HI barrier because the HOMO level of ***o*-CzOXD** is higher than that of other isomers. In addition, using ***o*-CzOXD** as host for red emitter **$(piq)_2Ir(acac)$**, the PE is greatly increased from 1.2 lm W^{-1} for a **CBP**-based device up to 11.5 lm W^{-1}, which can be attributed to

the well-matched HOMO levels and LUMO levels between the ***o*-CzOXD** and **(piq)$_2$Ir(acac)** as well as a more balanced charge flux within ***o*-CzOXD** layer induced by its bipolar charge transporting character. Different from the other hosts aforementioned with oxadiazole cores, the bipolar host **1,8-OXDCz** (Fig. 38) employs carbaozle moiety as the core.[197] Although **1,8-OXDCz** possesses relatively low E_T of 2.60 eV which is unsuitable for hosting blue emitters (Table 7), the green device using **Ir(ppy)$_3$** doped **1,8-OXDCz** film as EML exhibits very impressive PE of 89.7 lm W^{-1}. These encouraging results show that 1,3,4-oxadiazole group also has great potential to excel in developing high-performance bipolar hosts.

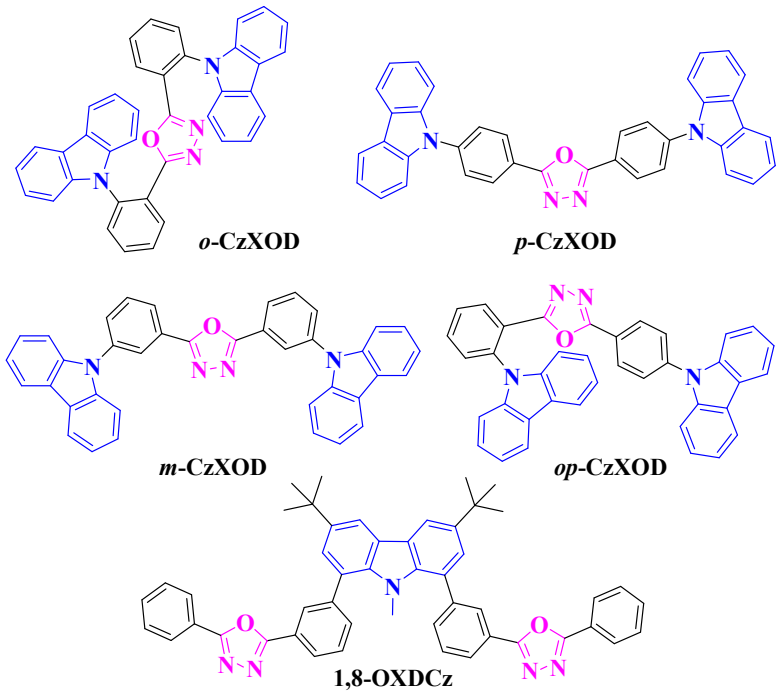

1,8-OXDCz; guest Ir(ppy)$_3$; EQE 20.3 %; CE 73.9 cd A^{-1}; PE 89.7 lm W^{-1}
***o*-CzXOD; guest Ir(ppy)$_3$; EQE 20.2 %; CE 77.9 cd A^{-1}; PE 59.3 lm W^{-1}**
***o*-CzXOD; guest (piq)$_2$Ir(acac); EQE 18.5 %; CE 13.6 cd A^{-1}; PE 11.5 lm W^{-1}**

Fig. 38 Chemical structures of **1,8-OXDCz** and **CzXOD**s and peak efficiency data of related OLEDs.

The abovementioned carbazole/oxadiazole hybrids usually have symmetric molecular structures and show T_g below 140 °C. As inspired by the asymmetric fluorene-bridged carbazole/benzimidazole hybrids **CzFCBI** and **CzFNBI** showing very high T_g above 170 °C, the similar asymmetric molecular structures can also be adopted by carbazole/oxadiazole hybrid to realize the high T_g.[201] As expected, **CzFOxa** (Fig. 39) has a high T_g of 170 °C and E_T of 2.70 eV. The single charge carrier devices reveal that both hole and electron mobilities of **CzFOxa** can be maintained at the level of 10^{-6} cm^2 V^{-1} s^{-1} with electrical fields varying from 2.9×10^5 to 5.8×10^5 V cm^{-1}, indicating the good bipolar charge transporting character of **CzFOxa**. The red-emitting device using **Os(bpftz)$_2$(PPhMe$_2$)$_2$** as guest and **CzFOxa** as host achieves the peak PE of 22.3 lm W^{-1} and CE of 21.3 cd A^{-1}, much higher than those of **CzFCBI**- and **CzFNBI**-based red PHOLED, indicating the good potential of using **CzFOxa** as bipolar host for red phosphorescent emitters.

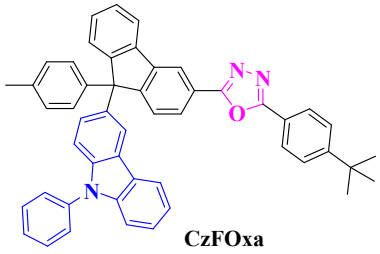

CzFOxa

guest Os(bpftz)$_2$(PPhMe$_2$)$_2$; EQE 19.4 %; CE 21.3 cd A^{-1}; PE 22.3 lm W^{-1}

Fig. 39 Chemical structure of **CzFOxa** and peak efficiency data of the related OLED.

While carbazole/oxadiazole hybrids can be used as bipolar host materials for green-to-red phosphorescent OLEDs with high performance, most of them, however, cannot be used as host for blue triplet emitters due to their relatively low E_T. In order to increase the E_T of carbazole/oxadiazole hybrids, the widely used symmetric 1,3,4-oxadiazole unit can be replaced by the asymmetric 1,2,4-oxadiazole

unit. Liao *et al.* designed several novel carbazole-based bipolar materials containing the asymmetric 1,2,4-oxadiazole unit as ET component (Fig. 40).[202, 203] These asymmetric bipolar materials have high T_g above 100 °C. More importantly, the E_T of these materials have been greatly increased. For example, the E_T of the *para*-linked hybrid **pCzmOXD** is 2.71 eV, which is the lowest among these 1,2,4-oxadiazole-based bipolar hosts, but still higher than that of 1,3,4-oxadiazole-based isomer ***p*-CzOXD** (E_T of 2.60 eV). The *meta*-linked hybrid **mCzmOXD** shows even higher E_T of 2.81 eV (Table 7). Although blue PHOLED using **mCzmOXD** as host shows typical performance (EQE of 5.8% and PE of 9.8 lm W^{-1}), the attempt of increasing the E_T by using 1,2,4-oxadiazole is successful. Inspired by this example, another two 1,2,4-oxadiazole-based bipolar hosts **DCzmOXD-1** and **DCzmOXD-2** were prepared. Importantly, **DCzmOXD-1** and **DCzmOXD-2** show even higher E_T up to 2.85 eV and 2.88 eV, respectively (Table 7). The blue PHOLEDs using **DCzmOXD-1** and **DCzmOXD-2** as hosts achieve much higher efficiencies than the device based on **mCzmOXD**. The maximum EQE, CE and PE of the device based on **DCzmOXD-1** are 11.2%, 23.0 cd A^{-1} and 20.5 lm W^{-1}, respectively. The maximum EQE, CE and PE of device based on **DCzmOXD-2** are 9.7%, 20.5 cd A^{-1} and 17.2 lm W^{-1}, respectively. The efficiency enhancement for the devices based on **DCzmOXD-1** and **DCzmOXD-2** may be related to the increased E_T of **DCzmOXD-1** and **DCzmOXD-2**, which can more effectively confine the excitons on the guest molecules and avoid reverse energy transfer. Besides, the higher HOMO levels of **DCzmOXD-1** (5.64 eV) and **DCzmOXD-2** (5.80 eV) than that of **mCzmOXD** (5.99 eV) can promote HI in the devices based on **DCzmOXD-1** and **DCzmOXD-2** to enhance the EL performance as well. This study demonstrates that the 1,2,4-oxadiazole unit is a very promising ET moiety for designing bipolar hosts with high E_T, and the different substitution position on

1,2,4-oxadiazole unit can show a large impact on the properties of the final bipolar hosts.

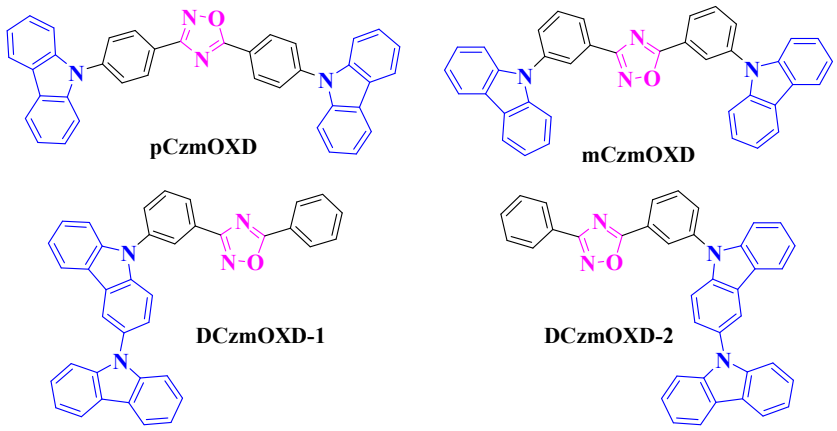

mCzmOXD; guest FIrpic; EQE 5.80 %; CE 12.0 cd A^{-1}; PE 9.80 lm W^{-1}
DCzmOXD-1; guest FIrpic; EQE 11.2 %; CE 23.0 cd A^{-1}; PE 20.5 lm W^{-1}
DCzmOXD-2; guest FIrpic; EQE 9.70 %; CE 20.5 cd A^{-1}; PE 17.2 lm W^{-1}

Fig. 40 Chemical structures of 1,2,4-oxadiazole/carbazole hybrids and peak efficiency data of related OLEDs.

1,2,4-Thiadiazole is a relative of 1,2,4-oxadiazole and also shows good electron-transporting property. Wang *et al.* firstly incorporated 1,2,4-thiadiazole with carbazole via *para*-, *meta*- and *ortho*-linkages to obtain three bipolar materials ***o*-CzTHZ**, ***m*-CzTHZ** and ***p*-CzTHZ** (Fig. 41) exhibiting high T_g close to 170 °C.[204] Similar to the cases of carbazole/oxadiazole analogues, ***p*-CzTHZ** containing *para*-linkage has the lowest E_T of 2.48 eV, while the ones adopting *meta*- and *ortho*-linkages show higher E_T (*ca.* 2.60 eV for ***m*-CzTHZ** and ***o*-CzTHZ**) (Table 7). The time-of-flight (TOF) technique reveals that all these 1,2,4-thiadiazole/carbazole hosts exhibit bipolar charge transporting characters. Especially, the hole and electron mobilities of ***o*-CzTHZ** are almost indentical (3.72×10^{-4} to 4.47×10^{-4} cm^2 V^{-1} s^{-1} for hole mobility under the electrical field from 3.6×10^5 to 5.6×10^5 V cm^{-1} and 3.41×10^{-4} to 3.91×10^{-4} cm^2 V^{-1} s^{-1} for electron mobility under the electric field from 3.3×10^5 to 4.7×10^5 V cm^{-1}). The $Ir(ppy)_3$-based green devices using these 1,2,4-thiadiazole/carbazole hybrids as hosts show

very impressive performance with EQEs exceeding 20.0% even at extremely high luminance of 10000 cd m^{-2}. The highest EQE of 26.1% with CE of 92.3 cd A^{-1} come from the ***o*-CzTHZ**-based device due to its highest E_T of 2.62 eV which can more effectively confine the excitons together with the higher and more balanced charge carrier transporting abilities of ***o*-CzTHZ** than that of ***m*-CzTHZ** and ***p*-CzTHZ**. These results have successfully provided a new design strategy for bipolar host materials in which 1,2,4-thiadiazole unit serves as the ET conponent. Besides, efforts are also needed to be made to increase the E_T of 1,2,4-thiadiazole-based bipolar materials in order to apply this kind of bipolar materials to the blue PHOLEDs.

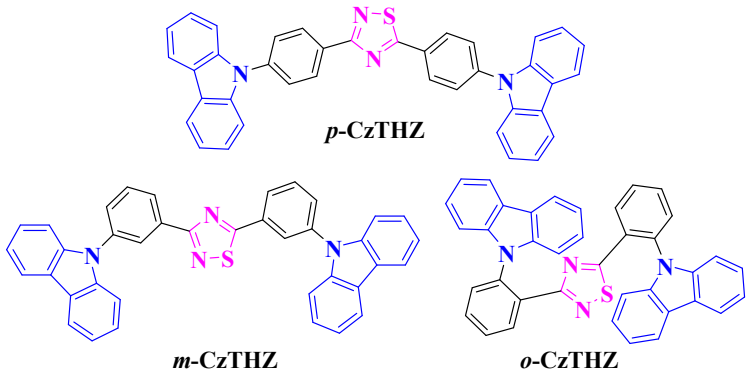

***o*-CzXOD; guest Ir(ppy)$_3$; EQE 26.1 %; CE 92.3 cd A^{-1}; PE 78.8 lm W^{-1}**
***m*-CzXOD; guest Ir(ppy)$_3$; EQE 24.0 %; CE 86.4 cd A^{-1}; PE 61.8 lm W^{-1}**
***p*-CzXOD; guest Ir(ppy)$_3$; EQE 22.9 %; CE 80.2 cd A^{-1}; PE 56.7 lm W^{-1}**

Fig. 41 Chemical structures of 1,2,4-thiadiazole/carbazole hybrids and peak efficiency data of related OLEDs.

Aromatic 1,2,4-triazole is an electron-deficient structure and has been incorporated with the HT groups to synthesize bipolar materials.[205-208] With different linking modes, carbazole/triazole hybrids can realize high E_T in the range of 2.8 to 3.0 eV, and **CzTAZ** (Fig. 42) shows better performance than **CBP** when used as the host for FIrpic-based blue device.[208] Zhuang *et al.* synthesized several triazole/carbazole hybrids with T_g from 116 to 156 °C.[209] The single charge

carrier devices show that these materials have slightly higher ET abilities than HT abilities, indicating the bipolar charge carrier transporting characters of these hosts. As expected, the fully *meta*-linked isomer **CzTAZ4** with the most twisted configuration shows the highest E_T of 2.76 eV (Table 7). Importantly, it also shows the highest charge carrier transporting ability. Therefore, the blue PHOLED using FIrpic-doped **CzTAZ4** as EML shows the best device performance with peak CE of 21.1 cd A^{-1} and PE of 18.7 lmW^{-1}, which are much higher than that of the blue-emitting device with **mCP** as host.

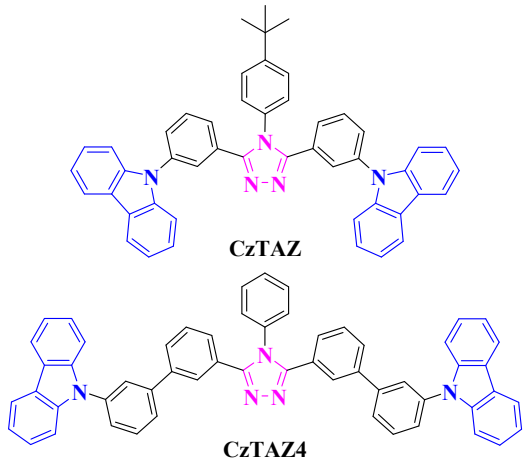

Fig. 42 Chemical structures of **CzTAZ**s and peak efficiency data of related OLEDs.

In order the increase the E_T of carbazole/trizole bipolar hosts, some hosts with highly twisted configuration have been obtained as well. In the bipolar host **CTPO** (Fig. 43), the carbazole is attached to the triazole through *meta*-linkage.[210] **CTPO** also contains a diphenylphosphoryl moiety to enhance the EI/ET ability. As expected, **CTPO** possesses very high E_T of 3.06 eV, far enough to host a blue phosphorescent emitters. The blue PHOLED using **CTPO** as host and a sky-blue emitter tris[1-(2,4-diisopropyldibenzo[*b,d*]furan-3-yl)-2-phenyl-1*H*-imidazole]iridium(III) [**Ir(dbi)$_3$**] as guest

has been fabricated to bring about very high EL efficiencies with CE of 41.6 cd A^{-1} and PE of 43.0 lm W^{-1}. With the *ortho*-linking pattern, the bipolar hosts ***o*-CzTAZ1**, ***o*-CzTAZ2** and ***o*-CzTAZ3** possess even higher steric hindrance effect than **CTPO**, which leads to higher E_T of *ca.* 3.10 eV (Table 7).[211] The blue PHOLEDs using these hosts for **FIrpic** achieve very attractive EL efficiencies, *e.g.*, the device based on ***o*-CzTAZ1** can show the EQE of 20.2% and PE of 41.2 lm W^{-1}. All these results show that it is feasible to adopt *meta*- and *ortho*-linkage to increase the E_T of host materials.

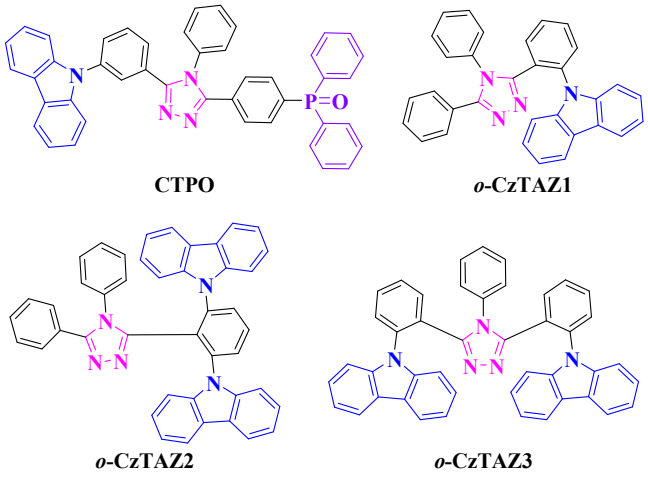

CTPO; guest $Ir(dbi)_3$; CE 41.6 cd A^{-1}; PE 43.0 lm W^{-1}
***o*-CzTAZ1; guest FIrpic; EQE 20.2 %; CE 47.1 cd A^{-1}; PE 41.2 lm W^{-1}**
***o*-CzTAZ2; guest FIrpic; EQE 17.9 %; CE 43.3 cd A^{-1}; PE 38.6 lm W^{-1}**
***o*-CzTAZ2; guest FIrpic; EQE 17.1 %; CE 40.2 cd A^{-1}; PE 36.1 lm W^{-1}**

Fig. 43 Chemical structures of **CTPO** and ***o*-CzTAZ**s and peak efficiency data of related OLEDs.

3.7.2.3 Carbazole-pyridine/pyrimidine (pyrazine)/triazine type bipolar host materials

As discussed in section **3.7.1.3**, nitrogen-containing six-membered heterocyclic groups such as pyridine, pyrimidine and triazine are electron-deficient structures and can be combined with triphenylamine moiety to synthesize bipolar host materials and show good performance in PHOLEDs. Incorporating these nitrogen-containing heterocyclic groups with carbazole moiety to obtain bipolar host

materials has also been widely studied.[151, 212-216]

Modification of the host **CBP** by replacing one phenyl ring in the biphenyl unit with a pyridine or pyrimidine ring, **CPPY** and **CPHP** (Fig. 44) has been made with significantly reduced LUMO levels (2.74 eV for **CPPY** and 2.88 eV for **CPHP**) than **CBP** (2.55 eV) (Table 7),[217] indicating their enhanced EI ability. However, the E_T of **CPPY** (2.62 eV) and **CPHP** (2.61 eV) are slightly lower than that of **CBP** (2.67 eV). The green-emitting device based on **CPPY** shows greatly improved efficiencies as compared to **CBP**-based device in terms of maximum EQE, CE and PE because of the reduced EI barrier induced by the low-lying LUMO of **CPPY**. However, the **CPPY**-based device suffers from severe efficiency roll-off and the device performance is inferior to the **CBP**-based device at luminance above 200 cd m^{-2}. The efficiency roll-off of **CPPY**-based device was attributed to the intrinsic property of **CPPY** that the transverse dipole moment of **CPPY** is perpendicular to the molecular long axis, which can significantly increase the barrier for HI at the anode.[217] However, this phenomenon was not observed for **CPHP**. The device based on **CPHP** exhibits the best performance with peak EQE of 26.8% and CE of 92.2 cd A^{-1}, and higher efficiencies than that of **CBP**-based device at high luminances. This study demostrates that the introduction of electron-deficient unit to **CBP** can effectively reduce the LUMO level while keeping the HOMO level unchanged, leading to improved EI/ET property.

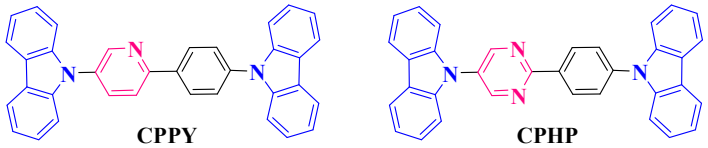

CBP; guest $(ppy)_2Ir(acac)$; EQE 13.3 %; CE 54.3 cd A^{-1}; PE 36.0 lm W^{-1}
CPPY; guest $(ppy)_2Ir(acac)$; EQE 21.5 %; CE 74.9 cd A^{-1}; PE 56.3 lm W^{-1}
CPHP; guest $(ppy)_2Ir(acac)$; EQE 26.8 %; CE 92.2 cd A^{-1}; PE 106 lm W^{-1}

Fig. 44 Chemical structures of **CPPY** and **CPHP** and peak efficiency data of related OLEDs.

Kido *et al.* also modified **CBP** by inserting a six-membered aromatic ring via *meta*-linkages into the center of the **CBP** skeleton to optimize the T_g, charge mobility, MO level and E_T, *etc.* of the obtained bipolar hosts (Fig. 45).[218] The middle six-membered ring containing one or two nitrogen atoms with different orientations greatly influences the above parameters. Most of them have E_T close to 2.7 eV except for **CzP7**. Regardless of the nitrogen orientation, introducing pyridine ring instead of benzene ring has a slight influence on the electron mobility but also reduces the hole mobility, and thus **CzP2-4** shows bipolar character with similar hole and ET abilities. The electron mobilities in **CzP5** and **CzP7** are higher than hole mobilities. The two outer nitrogen atoms at the heterocyclic core endow **CzP6** with stronger molecular polarity which leads to the higher HT ability of **CzP6** than ET ability, yet **CzP6** still shows bipolar transporting property. Blue-to-red PHOLEDs were fabricated using these materials as hosts. As a result, the blue PHOLED based on **CzP2** shows the best performance with EQE of 24.3% and PE of 46.1 lm W^{-1} at 100 cd m^{-2}. All green-emitting devices can show very high efficiencies with EQEs above 22.0% and PEs close to 98 lm W^{-1} at 100 cd m^{-2}. The best performance is achieved by the green PHOLED based on **CzP2** with EQE of 26.9% and PE of 102 lm W^{-1} at 100 cd m^{-2}. The red PHOLED also affords high EQEs in the range of 15% to 19% at 10 cd m^{-2}. The red emitting device based on **CzP6** gives the EQE of 18.4% and PE of 20.3 lm W^{-1} at 10 cd m^{-2}. It appears that the host **CzP2** with central pyridine substituted at 2,6 position is most suitable for blue, green, and even red PHOLEDs.

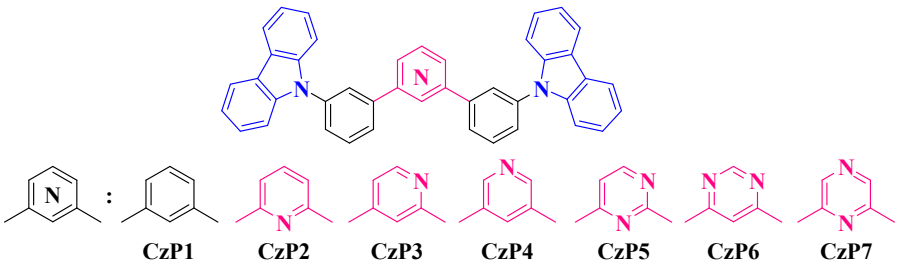

CzP2; guest FIrpic; EQE 24.3 %; PE 46.1 lm W^{-1} @ 100 cd m^{-2}
CzP2; guest $Ir(ppy)_3$; EQE 26.9 %; PE 102 lm W^{-1} @ 100 cd m^{-2}
CzP2; guest $Ir(piq)_3$; EQE 15.8 %; PE 15.5 lm W^{-1} @ 10 cd m^{-2}
CzP6; guest $Ir(piq)_3$; EQE 18.4 %; PE 20.3 lm W^{-1} @ 10 cd m^{-2}

Fig. 45 Chemical structures of **CzP**s and the peak efficiency data of related OLEDs.

Through modifying **CzP1**, **CzP2** and **CzP6** by adding one more *meta*-linked *N*-phenylcarbazole to the central six-membered aromatic ring, **TCPB**, **TCPY** and **TCPM** (Fig. 46) have been obtained by Kido's group as well.[80] Due to the electron-deficient cores, **TCPY** and **TCPM** exhibit lower-lying LUMO levels and much more balanced charge transporting properties than **TCPB**. The E_T values are 2.66, 2.63 and 2.64 eV for **TCPB**, **TCPY** and **TCPM**, respectively (Table 7). The three materials were used as the universal host for blue, green and red PHOLEDs. Although device based on **TCPB** shows much better peak efficiencies, which may result from the higher E_T of **TCPB** and better charge balance at low current densities, the differences of efficiencies between **TCPB**-based device and **TCPY**-/**TCPM**-based devices are smaller at high luminances. The best performance of green-emitting devices comes from the **TCPY**-based device which gives peak EQE of 26.0% and PE of 119 lm W^{-1}. The **TCPM**-based green PHOLED shows slightly inferior peak EQE of 25.6% and PE of 116 lm W^{-1}. However, the **TCPM**-based green-emitting device exhibits the best performance at 1000 cd m^{-2} with EQE of 24.9% and PE of 89.1 lm W^{-1}, which are slightly higher than that of **TCPY**-based device and much higher than that of **TCPB**-based device. The red-emitting devices based on these three hosts display similar peak efficiencies, but those based on bipolar **TCPY** and **TCPM** exhibit efficiencies

almost two times higher than the red-emitting device based on **TCPB** at 1000 cd m^{-2}. These results imply that by introducing heterocyclic cores of pyridine and pyrimidine instead of benzene into the carbazole-based materials, the lower-lying LUMO levels and much more balanced charge transporting properties can be realized, which are crucial for reducing the charge injection barrier, improving device efficiencies and suppresing the efficicncy roll-off at high luminances. On the whole, the high efficiencies with reduced driving voltages and low efficiency roll-off at practically useful conditions achieved by devices based on bipolar host materials are the essential advantages over devices based on unipolar host materials.

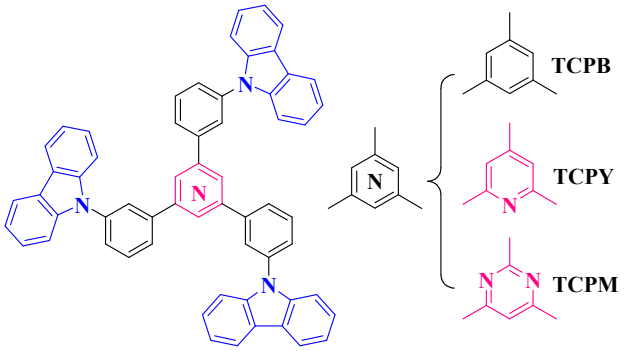

TCPB; guest FIrpic; EQE 17.3 %; PE 27.1 lm W^{-1}
TCPY; guest FIrpic; EQE 17.5 %; PE 26.5 lm W^{-1}
TCPM; guest FIrpic; EQE 15.2 %; PE 24.9 lm W^{-1}
TCPB; guest $Ir(ppy)_3$; EQE 19.4 %; PE 68.2 lm W^{-1}
TCPY; guest $Ir(ppy)_3$; EQE 23.7 %; PE 84.8 lm W^{-1}
TCPM; guest $Ir(ppy)_3$; EQE 24.9 %; PE 89.1 lm W^{-1}
TCPB; guest $Ir(piq)_3$; EQE 7.93 %; PE 3.83 lm W^{-1}
TCPY; guest $Ir(piq)_3$; EQE 13.8 %; PE 6.72 lm W^{-1}
TCPM; guest $Ir(piq)_3$; EQE 15.4 %; PE 9.80 lm W^{-1}

@ 1000 cd m^{-2}

Fig. 46 Chemical structures of **TCPB**, **TCPY** and **TCPM** and peak efficiency data of related OLEDs.

Lee *et al.* reported several carbazole/pyridine-based bipolar host materials showing good applicability for blue and green PHOLEDs.[219-221] A pyridine unit directly linked to the nitrogen atom of

a carbazole moiety will lead to the significantly decreased electron density of carbazole and thus improve the ET property of the 9-pyridylcarbazole moiety. Therefore, in **PyCz1** (E_T = 2.74 eV) (Fig. 47 and Table 7), the 9-pyridylcarbazole moiety is responsible for transporting electron while the two outer carbazole units declare the HT. The green-emitting device using **Ir(ppy)$_3$** as emitter shows the maximum EQE of 21.3% and CE of 68.1 cd A^{-1}, and displays no EQE and CE roll-off at the luminance of 1000 cd m^{-2}, *i.e.*, the EQE and CE are still as high as 21.3% and 68.1 cd A^{-1} at 1000 cd m^{-2}. This phenomenon may result from the small difference of HT and ET properties of **PyCz1** and well-balanced charge flux in the emissive layer. However, the FIrpic-based blue PHOLED using **PyCz1** as host exhibits poor performance, which may be caused by the shifted recombination zone close to the ET layer inducing exciplex formation at the surface. Bipolar material **PPBC** is evolved from the common unipolar host **mCP**. The presence of the pyridine ring in **PPBC** can improve the ET ability, evidenced by the electron-only device. As the E_T of **PPBC** is as high as 2.99 eV (Table 7), a blue-emitting device using **PPBC** as host shows the peak EQE of 19.8%, suggesting the good charge balance within the EML at low current densities. However, the efficiency roll-off is quite severe at high current densities. A two-color type white-emitting device based on **FIrpic** and **(pq)$_2$Ir(acac)** achieves high EQE of 17.1% and good color stability with 0.01 change of color coordinates between 100 cd m^{-2} and 10000 cd m^{-2}, showing the promising ability of **PPBC** as host for color-stable WOLEDs.

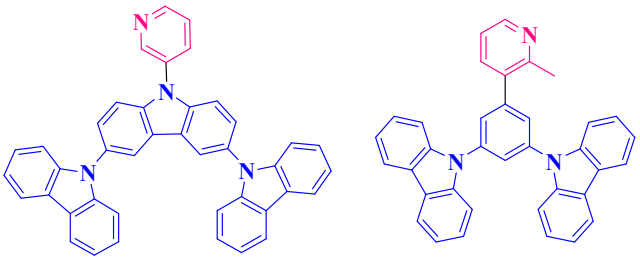

PyCz1 **PPBC**

PyCz1; guest FIrpic; EQE 9.60 %; CE 19.9 cd A^{-1}; PE 10.6 lm W^{-1}
PyCz1; guest $Ir(ppy)_3$; EQE 21.3 %; CE 68.1 cd A^{-1}; PE 46.2 lm W^{-1}
PPBC; guest FIrpic; EQE 19.8 %
PPBC; guest FIrpic and $(pq)_2Ir(acac)$; EQE 17.1 %

Fig. 47 Chemical structures of **PyCz1** and **PPBC** and peak efficiency data of related OLEDs.

Deduced from pyridine unit, quinoline moiety also has an electron-deficient structure and can be used as ET component for bipolar materials. Cheng *et al.* synthesized several quinoline/carbazole hybrid bipolar materials (Fig. 48) showing high T_g in the range of 90−145 °C and E_T of 2.51−2.95 eV.[222] The number and position of carbazole units attached to the quinoline core have great influences on the thermal stability and E_T, *etc.* With the molecular size enlarged, the T_g is also raised in the order of **CzPPQ** (90 °C) < **CzPPQCz** (138 °C) < **CzPPCzQ** (145 °C). Introducing one more carbazole unit at the 4-position of quinoline results in an increased E_T, while that at the 6-position leads to a reduced E_T, *i.e.*, the order for E_T follows the sequence **CzPPCzQ** (2.95 eV) > **CzPPQ** (2.61 eV) > **CzPPQCz** (2.51 eV) (Table 7). Using these quinoline/carbazole hybrids as host, the orange-emitting device based on **$Ir(pq)_3$** and deep-red emitting device based on **$Ir(piq)_3$** were fabricated. All orange devices show very high EQEs above 17.0% with PEs exceeding 50.0 lm W^{-1}. Especially for the **CzPPQ**-based device, it shows the peak EQE of 25.6% with PE of 68.1 lm W^{-1}, which are among the highest efficiencies reported for the orange-emitting devices so far. The red PHOLEDs also exhibit very high peak EQEs above 19.0% with PEs exceeding 20.0 lm W^{-1}. The **CzPPQCz**-based device shows the peak EQE of

21.4% and PE of 24.1 lm W^{-1}. In addition, the operational lifetime of both the orange and deep-red PHOLEDs based on **CzPPQ** at an initial luminance of 500 cd m^{-2} could be dramatically extended long up to the T_{50} of more than 26 412 and 11 450 h, respectively, which are 12 times (orange) and 6 times (red) longer than those of the corresponding devices based on **CBP**. These outstanding performance including high efficiencies, low efficiency roll-off and long device stability for devices based on quinoline/carbazole hybrid host provide a good illustration for using quinoline as ET building block to develop high performance bipolar host materials.

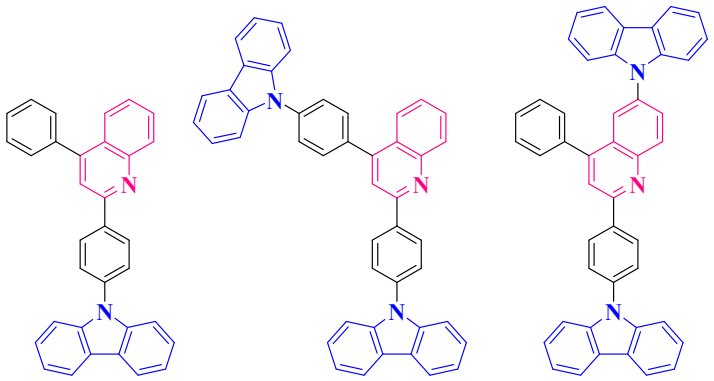

Fig. 48 Chemical structures of quinoline/carbazole hybrids and peak efficiency data of related OLEDs.

For its strong electron-deficient character, triazine unit has been widely incorporated with carbazole unit to obtain bipolar hosts.[213-215, 223] However, it seems that the carbazole/triazine bipolar hosts with direct linkages between the triazine and the nitrogen atom in carbazole cannot bring about high efficiencies to the related blue PHOLEDs, which can be ascribed to the fact that the strong

electron-deficient character will significantly decrease the electron density on carbazole to weaken the HI/HT ability,[221] and thereby fail to show bipolar character. In order to cope with the problem, **CzT**[224] (Fig. 49) with the second carbazole moiety far away from the triazine unit and **DPTPCz**[225] with triazine group connected to the carbon atom in carbazole have been prepared. Compared with **CBP**, **CzT** shows better ET and HT ability. The blue PHOLED using **CzT** as host gives nice maximum CE of 27.4 cd A^{-1} and PE of 30.5 lm W^{-1}, which are much better than those from the devices based on other *N*-triazinylcarbazole type host materials.[214, 215] A yellowish-green PHOLED using bis(o-tolylpyrimidinato-*N*,$C^{2'}$)Ir(III)acetylacetonate [**$(TPm)_2Ir(acac)$**] as emitter and **CzT** as host achieves very high CE of 76.3 cd A^{-1} and PE of 72.7 lm W^{-1} with quite low efficiency roll-off at 1000 cd m^{-2}. With a high E_T of 2.78 eV (Table 7), **DPTPCz** was used to fabricate a blue PHOLED showing peak EQE of 14.4%. The green-emitting device using **DPTPCz** as host can give the maximum EQE of 21.2% and CE of 65.7 cd A^{-1}. Furthermore, this device can still maintain high efficiencies of 20.0% and 61.8 cd A^{-1} at an extremely high luminance of 10000 cd m^{-2}. These two studies give good examples that high EL performance can be realized by the device using the carbazole/triazine bipolar hosts.

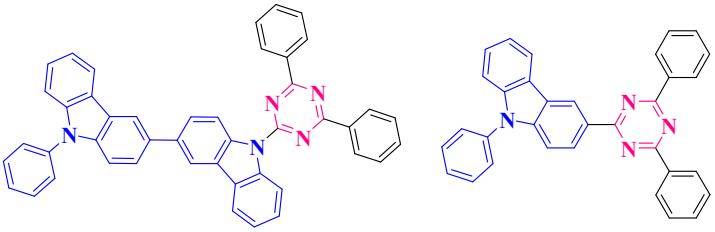

CzT **DPTPCz**

CzT; guest FIrpic; EQE 9.9 %; CE 27.4 cd A^{-1}; PE 30.5 lm W^{-1}
CzT; guest $(TPm)_2Ir(acac)$; EQE 20.1 %; CE 76.3 cd A^{-1}; PE 72.7 lm W^{-1}
DPTPCz; guest FIrpic; EQE 14.4 %; CE 27.4 cd A^{-1}
DPTPCz; guest $(ppy)_2Ir(acac)$; EQE 21.2 %; CE 65.7 cd A^{-1}

Fig. 49 Chemical structures of **CzT** and **DPTPCz** and peak efficiency data of related OLEDs.

3.7.2.4 Carbazole-carboline type bipolar host materials

Due to the electron-deficient pyridine moiety, carboline unit showing ET property has been employed to couple with carbazole moiety for developing carbazole/carboline bipolar hosts. Taking **mCP** as a template, several carbazole/carboline bipolar hosts have been obtained to show high E_T. **CzCb1** (Fig. 50) shows E_T of 2.88 eV, while **CzCb2** and **CzCb3** possess even higher E_T of 2.96 eV and 2.98 eV, respectively (Table 7).[226] In addition, these three hosts also show quite different LUMO levels of 2.55 eV for **CzCb1**, 2.62 eV for **CzCb2** and 2.49 eV for **CzCb3**, which are lower than the LUMO level of **mCP** (2.40 eV). These results indicate that nitrogen positions in carboline unit can show an obvious influence on both E_T and LUMO level. Despite their low electron mobility (1.8×10^{-7} cm^2 V^{-1} s^{-1} for **CzCb1**, 1.0×10^{-7} cm^2 V^{-1} s^{-1} for **CzCb2**, 1.4×10^{-8} cm^2 V^{-1} s^{-1} for **CzCb3**), they can still furnish FCNIrpic-doped blue PHOLEDs with impressive EQEs (24.3% for **CzCb1**, 21.9% for **CzCb2** and 17.0% **CzCb3**).

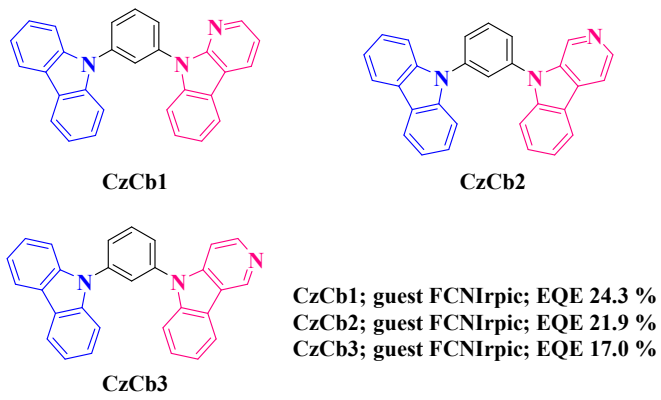

Fig. 50 Chemical structures of **CzCb**s and peak efficiency data of related OLEDs.

In order to further explore the potential of the carbazole/carboline bipolar hosts, other systems have

been developed as well to optimize the properties of this kind of hosts. With larger molecular size and 3,9-position connected to bicarbazole unit, **pBCb2Cz** (Fig. 51) can show both high T_g of 146 °C and E_T of 2.93 eV (Table 7),[227] rendering **pBCb2Cz** good qualities for hosting blue triplet emitters. The FIrpic-based device using **pBCb2Cz** as host gives higher peak EQE of 23.0% and reduced efficiency roll-off with respect to the **mCP**-based controlled device. With properly extended conjugation, **PCb-PCz** can show high hole mobility of 1.3×10^{-4} cm^2 V^{-1} s^{-1} and electron mobility of 4.1×10^{-5} cm^2 V^{-1} s^{-1} as well as E_T of 2.74 eV (Table 7).[228] The blue-emitting device using FIrpic-doped **PCb-PCz** as emissive layer achieves outstanding performance with peak EQE of 29.7% and PE of 44.2 lm W^{-1}. At 1000 cd m^{-2}, the EQE is still as high as 27.1%. Another carbazole/carboline hybrid **2CbCzT** is also suitable for hosting blue emitters due to its high E_T (2.73 eV) and bipolar charge transporting properties (Table 7).[229] The low doping (3%) FIrpic-based device can give nice peak EQE of 22.1%. Using high E_T bipolar materials **CzBPCb** (E_T = 2.75 eV)[109] and **CzOTCb** (E_T = 2.90 eV)[110] as hosts for **FIrpic** (Table 7), both devices achieve remarkable high peak EQEs exceeding 27.0% with low efficiency roll-off at high luminances. These examples clearly demonstrate that combining the good ET carboline unit with HT carbazole group by proper linkage has great opportunities to obtain good bipolar host materials with good thermal property, suitable MO level, high E_T and balanced charge carrier transporting properties, which all favor high device performance.

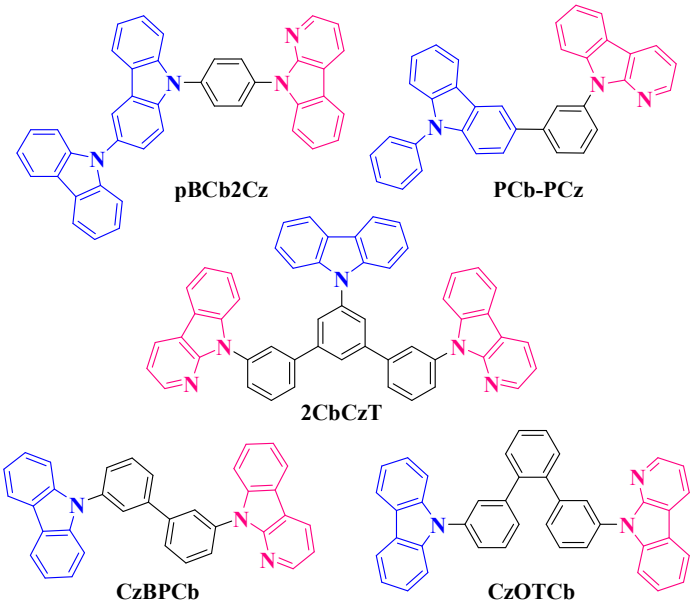

pBCb2Cz; guest FIrpic; EQE 23.0 %; CE 38.3 cd A^{-1}; PE 34.6 lm W^{-1}
pBCb2Cz; guest FCNIrpic; EQE 16.2 %; CE 21.5 cd A^{-1}; PE 10.7 lm W^{-1}
PCb-PCz; guest FIrpic; EQE 29.7 %; PE 44.2 lm W^{-1}
2CbCzT; guest FIrpic; EQE 22.1 %
CzBPCb; guest FIrpic; EQE 27.6 %
CzOTCb; guest FIrpic; EQE 27.4 %; CE 45.8 cd A^{-1}; PE 36.6 lm W^{-1}

Fig. 51 Chemical structures of carbazole/carboline hybrids and peak efficiency data of related OLEDs.

3.7.2.5 Carbazole-cyano group type bipolar host materials

Cyano (CN) group is a strong electron-accepting unit which can improve the ET properties of the corresponding materials.[230, 231] By introducing cyano group into the well-known **mCP** and **CBP**, bipolar hosts **mCPCN**[232] and **CBPCN**[233] (Fig. 52) can be obtained. Importantly, introducing the CN group can be a very effective strategy to improve the thermal property of these bipolar host (97 °C for **mCPCN** vs 60 °C for **mCP** and 162 °C for **CBPCN** vs 62 °C for **CBP**) and maintain high E_T (3.03 eV for **mCPCN** and 2.69 eV for **CBPCN**) at the same time (Table 7). Using **mCPCN** as host for FIrpic, the resulting device shows remarkably high peak EQE of 26.4%, CE of 58.7 cd A^{-1} and PE of 57.6 lm W^{-1}, which are much higher than those of the **mCP**-based control device. At the luminance of 1000 cd m^{-2}, this device

still maintains a high EQE of 25.0%. Furthermore, a two-color type white-emitting device using FIrpic and **Os(bpftz)$_2$(PPh$_2$Me)$_2$** doped **mCPCN** as the EML exhibits outstanding device performance with maximum EQE, CE and PE of 23.3%, 50.7 cd A^{-1} and 49.7 lm W^{-1}, respectively. At 1000 cd m^{-2}, the efficiencies only decrease to 21%, 46 cd A^{-1} and 25 lm W^{-1}. **CBPCN** can properly host both green emitter **Ir(ppy)$_3$** and red emitter **Ir(piq)$_3$** to fulfill much improved EL performance as compared with **CBP**. These important results clearly indicate the advantages of utilizing cyano unit to develop high performance bipolar hosts.

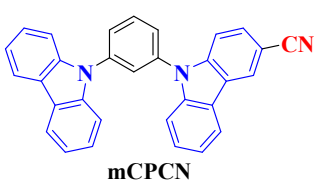

mCPCN

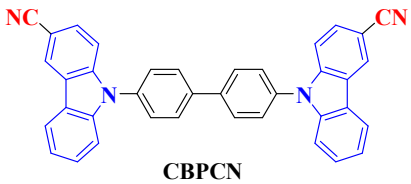

CBPCN

mCPCN; guest FIrpic; EQE 26.4 %; CE 58.7 cd A^{-1}; PE 57.6 lm W^{-1}
mCPCN; guest FIrpic and Os(bpftz)$_2$(PPh$_2$Me)$_2$; EQE 23.3 %; PE 49.7 lm W^{-1}
CBPCN; guest Ir(ppy)$_3$; EQE 23.1 %; CE 80.6 cd A^{-1}; PE 48.9 lm W^{-1}
CBPCN; guest Ir(piq)$_3$; EQE 15.5 %; CE 10.7 cd A^{-1}; PE 5.58 lm W^{-1}

Fig. 52 Chemical structures of **mCPCN** and **CBPCN** and peak efficiency data of related OLEDs.

Other carbazole/cyano hybrid bipolar host materials have also been synthesized to show high thermal stability and E_T suitable for hosting blue-to-red triplet emitters.[234-237] For instance, the bipolar **ACDCN** (Fig. 53) with E_T of 2.57 eV (Table 7) is quite suitable for hosting yellow triplet emitters.[236] A device based on **PO-01** shows very high peak EQE of 25.7% and low efficiency roll-off (EQE of 21.9% at 1000 cd m^{-2}). Lee *et al.* reported tricyano-modified bicarbazole compounds **3CN33BCz**, **3CN34BCz** and **3CN44BCz** (Fig. 53) with different connecting styles.[237] The 3,3′-, 3,4′- and 4,4′-linkages in **3CN33BCz**, **3CN34BCz** and **3CN44BCz**, respectively, endow these three hosts with different charge carrier mobility. Due to the facile molecular packing mode induced by the smaller dihedral angle

between two carbazole units, the 3-position linkage facilitates the charge transporting properties, *i.e.*, the charge carrier transporting abilities of **3CN33BCz** and **3CN34BCz** are higher than that of **3CN44BCz**. Furthermore, all the three hosts show high T_g (128 °C for **3CN33BCz**, 132 °C for both **3CN34BCz** and **3CN44BCz**) and E_T (2.95 eV for **3CN33BCz**, 2.98 eV for **3CN34BCz**, 3.00 eV for **3CN44BCz**) (Table 7). Nevertheless, these three materials show bipolar transporting characters. Both blue (**FIrpic**) and green (**Ir(ppy)$_3$**) PHOLEDs based on these bipolar hosts exhibit dramatically highly efficiencies with EQEs exceeding 25.0%. Especially, the blue PHOLED based on **3CN33BCz** achieves a peak EQE of 28.2%, while the green-emitting devices based on **3CN34BCz** and **3CN44BCz** give extremely high EQEs above 30.0% with CEs above 93 cd A^{-1}. These outstanding device performance reveal that 3,3′-connection can increase the charge carrier transporting ability and 4,4′-connection will lead to high E_T.

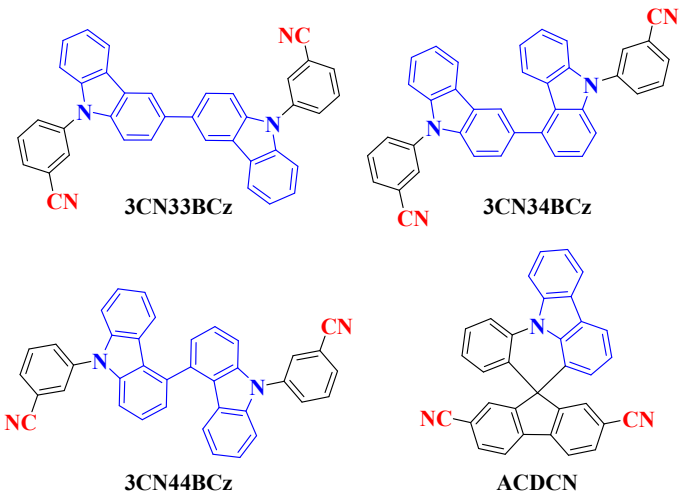

3CN33BCz; guest FIrpic; EQE 28.2 %; CE 49.6 cd A^{-1}; PE 26.5 lm W^{-1}
3CN34BCz; guest FIrpic; EQE 25.9 %; CE 44.7 cd A^{-1}; PE 23.9 lm W^{-1}
3CN44BCz; guest FIrpic; EQE 27.7 %; CE 47.5 cd A^{-1}; PE 23.6 lm W^{-1}
3CN33BCz; guest Ir(ppy)$_3$; EQE 26.0 %; CE 80.2 cd A^{-1}; PE 46.4 lm W^{-1}
3CN34BCz; guest Ir(ppy)$_3$; EQE 30.4 %; CE 93.6 cd A^{-1}; PE 50.0 lm W^{-1}
3CN44BCz; guest Ir(ppy)$_3$; EQE 30.4 %; CE 93.2 cd A^{-1}; PE 46.2 lm W^{-1}
ACDCN; guest PO-01; EQE 25.7 % for peak, 21.9 % @1000 cd m^{-2}

Fig. 53 Chemical structures of carzabole/CN hybrids and peak efficiency data of related OLEDs.

3.7.2.6 Carbazole-diphenylphosphoryl type bipolar host materials

Diphenylphosphoryl unit is a very popular ET building block for synthesizing bipolar host materials, because its strong electron-deficient properties can afford the ET properties and its tetrahedral molecular configuration can effectively block conjugation extension to achieve high E_T. Hence, it is a wise idea to obtain bipolar hosts with high E_T by incorporating the rigid carbazole unit with diphenylphosphoryl unit into a single molecule. PHOLEDs with various emission wavelength using carbazole/diphenylphosphoryl bipolar hosts have been reported to show very high efficiencies.[114, 125, 238, 239]

A simple way to develop this kind of bipolar hosts is to introduce the diphenylphosphoryl unit to the popular carbazole-based hosts, such as **mCP**. Lee *et al.* developed several bipolar hosts derived from the **mCP** skeleton: **DCPPO**, **mCPPO1**, **CPBDC** and **mCPmPO** (Fig. 54). It appears that introduction of the diphenylphosphoryl unit can further raise the E_T of the obtained bipolar hosts, since **DCPPO**, **mCPPO1** and **CPBDC** all show higher E_T (*ca.* 3.0 eV) than that of the **mCP** (E_T = 2.90 eV) skeleton (Table 7).[240-242] The substitution position and number of the diphenylphosphoryl unit will show trivial influence on the E_T of the concerned bipolar hosts. The lower E_T of **mCPmPO** should be induced by the extended conjugation by the phenyl ring between the carbazole and diphenylphosphoryl units.[243] Owing to their high E_T (Table 7), PHOLEDs using **DCPPO**, **mCPPO1** and **CPBDC** as hosts for **FCNIrpic** show very high peak EQEs exceeding 22.0%. Especially, the optimized **mCPPO1**-based device can achieve the peak EQE as high as 25.1%. The better device performance realized by the **mCPPO1**-based device may result from the lower-lying LUMO level of **mCPPO1** (2.64 eV), which facilitates the EI process and results in more balanced charge flux within

the **mCPPO1**-based device. Bearing two diphenylphosphoryl units, the electron mobility of **CPBDC** is greatly improved to give very good EL performance in blue PHOLED as well.[251] Despite its relatively lower E_T of 2.75 eV (Table 7), **mCPmPO** still can furnish a blue PHOLED with decent EL performance (EQE of 20.3% and PE of 39.7 lm W^{-1}). These works show that the simple modification of **mCP** with diphenylphosphoryl unit through proper linkages can furnish good bipolar host materials with high E_T for high performance blue PHOLEDs.

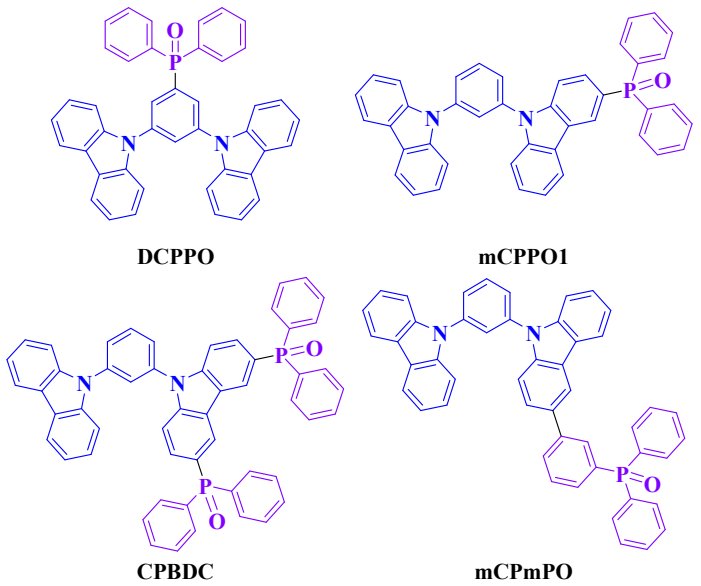

Fig. 54 Chemical structures of some carbazole/diphenylphosphine oxide hybrids and peak efficiency data of related OLEDs.

In the simple bipolar host **NPO** (Fig. 55) developed by Adachi *et al.*, the diphenylphosphoryl unit is directly linked to the carbazole moiety through the P-N bond.[244] The direct connection between the

electorn-donating and electron-accepting moieties shows no harm to the E_T of **NPO** (2.99 eV) (Table 7), and therefore **NPO** can host blue-emitter FIr6 (E_T of 2.72 eV) to cause very high EQE of 19.7%, which is higher than that of the device using **MPO12** (14.3%) as host. Although **MPO12** possesses very high E_T of 3.02 eV (Table 7), its HOMO level (6.04 eV)[253] is higher than that of **FIr6** (6.1 eV), indicating that **FIr6** deped in **MPO12** should be excited by host-to-guest energy transfer, which may suffer from energy losses. However, the HOMO level of **NPO** (6.20 eV) is lower than that of **FIr6** (6.1 eV), indicating the direct charge-trapping excitation of **FIr6** in **NPO** host to benefit the device efficiencies. By incorporating the diphenylphosphine oxide into the 3-position of an *N*-phenylcarbazole moiety, Lee *et al.* synthesized the bipolar compound **PPO1** showing a high E_T of 3.02 eV (Table 7),[238] which can be employed to fabricate the blue PHOLED with tris((3,5-difluoro-4-cyanophenyl)pyridine)iridium (**FCNIr**) as emitter. With highly twisted configration, **POBPCz** can also show a high E_T of 3.01 eV (Table 7),[245] which is high enough for the blue emitter **FIr6** to furnish high EL performance with peak EQE, CE and PE of 19.5%, 40 cd A^{-1} and 36 lm W^{-1}, respectively.

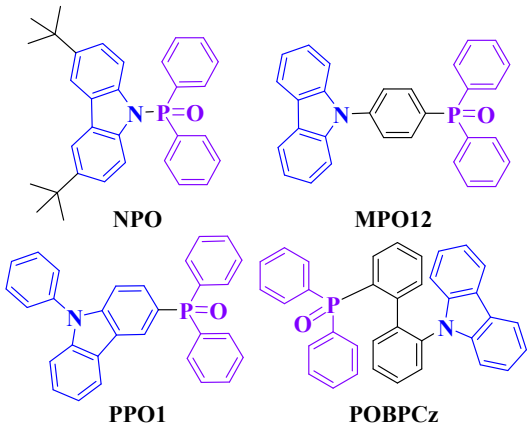

NPO; guest FIr6; EQE 19.7 %
MPO12; guest FIr6, EQE 14.3 %; guest FIrpic; EQE 9.1 %
PPO1; guest FCNIr; EQE 17.1 %; CE 20.5 cd A^{-1}; PE 14.3 lm W^{-1}
POBPCz; guest FIr6; EQE 19.5 %; CE 40 cd A^{-1}; PE 36 lm W^{-1}

Fig. 55 Chemical structures of some carbazole/diphenylphosphine oxide hybrids and peak efficiency

data of related OLEDs.

Although the above carbazole/diphenylphosphoryl hosts bearing one carbazole unit and one diphenylphosphoryl unit can show bipolar behavior, these materials still show higher hole mobility than electron mobility.[238] To further increase the ET ability, some novel hosts with more diphenylphosphoryl units have been obtained. Due to the one more diphenylphosphine oxide group, the electron mobility of **PPO2** (Fig. 56) is 2×10^{-6} cm^2 V^{-1} s^{-1}, which is much higher than that of **PPO1** (1×10^{-7} cm^2 V^{-1} s^{-1}).[238] As a result, although **PPO2** and **PPO1** possess the same E_T of 3.02 eV (Table 7), the device using FCNIr-doped **PPO2** as EML shows higher efficiencies (18.4%, 21.1 cd $A^{-1}$and 16.6 lm W^{-1}) as compared to those of **PPO1**-based device (17.1%, 20.5 cd A^{-1} and 14.3 lm W^{-1}), indicating the improved charge carrier transporting balance in **PPO2**-based device. Interestingly, the relative position of the two diphenylphosphoryl units can influence greatly the properties of these hosts. In **PPO21**, the diphenylphosphine oxide unit attached to the 3-position of carbazole is used to adjust the HOMO level and charge transporting property, the other diphenylphosphine oxide unit attached to the phenyl ring of the *N*-phenylcarbazole is expected to improve the ET ability.[246] As a result, **PPO21** shows elevated HOMO level (6.25 eV) and higher electron mobility of 3×10^{-6} cm^2 V^{-1} with respect to **PPO2**. The 2,7-position substituted isomer **PPO27** shows much lower-lying LUMO level (3.00 eV) as compared to those of **PPO2** (2.77 eV) and **PPO21** (2.68 eV) (Table 7), while its HOMO level (6.25 eV) is similar to that of **PPO2** and **PPO21**.[247] Besides the MO level, the substitution pattern of the two diphenylphosphoryl units also affects the E_T of these bipolar hosts. For **PPO2** and **PPO21**, they possess the same E_T (*ca.* 3.0 eV). Using **PPO21** as host for **FCNIr**, the device gives EL efficiencies of 19.2%, 22.5 cd $A^{-1}$and 19.0 lm W^{-1}, which are comparable to those of **PPO2**-based device. With **PPO27** as host,

the blue emitter FCNIr furnishes lower efficiencies of 16.2% and 15.1 lm W^{-1} due to the lower E_T of **PPO27** (E_T = 2.81 eV) (Table 7). However, highly efficient blue PHOLED doped with **FIrpic** can be fulfilled by **PPO27** with impressively high peak EQE of 23.9% and PE of 37.6 lm W^{-1}. The high performance of FIrpic/**PPO27**-based device benefits from the low-lying LUMO level of **PPO27**, which improves the EI/ET properties and thereby balances the charge flux within the device. By changing the subsititution position on **PPO27**, the MO levels (6.17 eV for HOMO and 2.90 eV for LUMO) and E_T (2.8 eV) of **PPO25** are similar to those of **PPO27**.[248] However, the blue-emitting device using **FIrpic** doped **PPO25** film as EML achieves extremely high EQE of 31.4% and PE of 53.1 lm W^{-1}, which are the highest efficiency values for blue phosphorecent devices to date. Additionally, the device still shows dramatically high EQE of 28.6% at the luminance of 1000 cd m^{-2}. The extraordinary device performance improvement can be attributed to the efficient energy transfer from host to guest, charge balance and effective exciton confinement on the guest molecules. Besides, the substitution of diphenylphosphine oxide at 5-position will increase the steric hindrance and restrict the molecular aggregation, which leads to improved morphological stability and suppressed triplet-triplet annihilation of **FIrpic**, resulting in high device efficiencies.

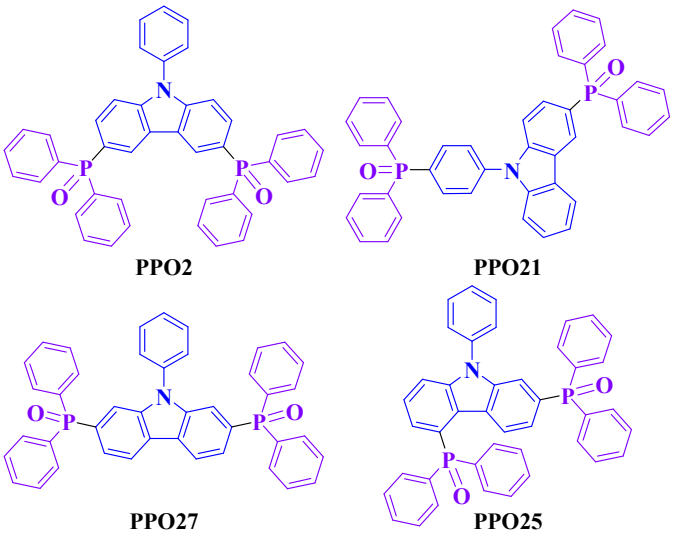

PPO2; guest FCNIr; EQE 18.4 %; CE 21.1 cd A-1; PE 18.6 lm W^{-1}
PPO21; guest FCNIr; EQE 19.2 %; CE 22.5 cd A-1; PE 19.0 lm W^{-1}
PPO27; guest FCNIr; EQE 16.2 %; PE 15.1 lm W^{-1}
PPO27; guest FIrpic; EQE 23.9 %; PE 37.5 lm W^{-1}
PPO25; guest FIrpic; EQE 31.4 %; PE 53.1 lm W^{-1}

Fig. 56 Chemical structures of some carbazole/diphenylphosphine oxide hybrids and peak efficiency data of related OLEDs.

Unfortunately, it seems that introduction of the third diphenylphosphoryl unit cannot further enhance the EL performance of this kind of hosts. Despite its high T_g of 143 °C and E_T of 3.07 eV (Table 7), the host **TPCz** (Fig. 57) bearing three diphenylphosphoryl unit can just show moderate EL ability in blue PHOLEDs without electron-blocking layer (EBL).[249] However, after inserting EBL in the device, **TPCz** can bring about much higher EL performance. Hence, it can be concluded that too many diphenylphosphoryl units make **TPCz** to show predominated ET ability to weaken its bipolar character. Hence, number balance between carbazole and diphenylphosphoryl units need to be carefully considered in developing high-performance carbazole/diphenylphosphoryl bipolar hosts. This conclusion has been supported by the EL performance of the following two hosts **TCTP**[249] and **BCPO**[250]. These two hosts possess similar E_T (3.03 eV for **TCTP** and 3.01 eV for **BCPO**) (Table 7).

However, the FIrpic-doped PHOLED with **BCPO** can show much better EL performance (23.5%, 45.1 cd A^{-1} and 40.6 lm W^{-1}) than the device using **TCTP** as host (16.7% and 36.4 cd A^{-1}). This result can also be ascribed to the weakened bipolar character of **TCTP** due to the improper carbazole/diphenylphosphoryl ratio.

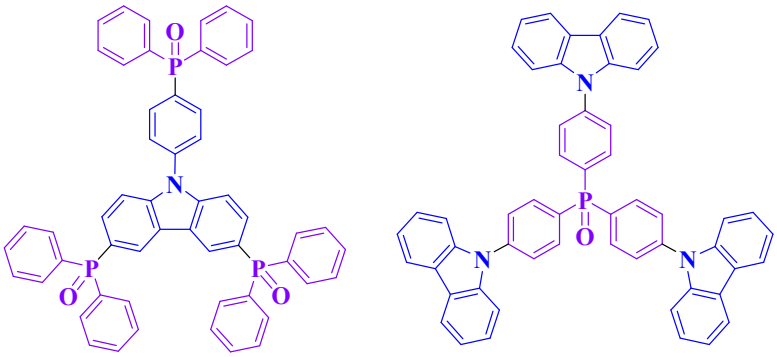

TPCz **TCTP**

TPCz; guest FIrpic; EQE 0.30 %; CE 0.75 cd A^{-1} without EBL
TPCz; guest FIrpic; EQE 16.7 %; CE 36.4 cd A^{-1} with EBL
TCTP; guest FIrpic; EQE 15.9 %; CE 35.0 cd A^{-1}

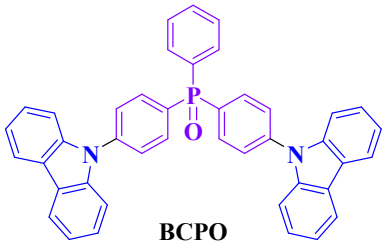

BCPO

guest FIrpic; EQE 23.5 %; CE 45.1 cd A^{-1}; PE 40.6 lm W^{-1}
guest FIr6; EQE 19.8 %; CE 36.8 cd A^{-1}; PE 33.1 lm W^{-1}
guest $Ir(ppy)_3$; EQE 21.6 %; CE 83.4 cd A^{-1}; PE 87.5 lm W^{-1}
guest $Ir(piq)_3$; EQE 17.0 %; CE 19.4 cd A^{-1}; PE 20.4 lm W^{-1}

Fig. 57 Chemical structures of **TPCz**, **TCTP** and **BCPO** and peak efficiency data of related OLEDs.

Chi *et al.* synthesized a simple carbazole-based bipolar host material **CzPhO** (Fig. 58) in which the dibenzophosphole oxide moiety was expected to increase the ET ability.[251] The novel **CzPhO** possesses a E_T of 2.71 eV (Table 7) and good bipolar transporting property as indicated by the single charge carrier devices. An orange-red PHOLED using **$Os(fppz)_2(pp2b)$** as guest doped into **CzPhO** gives very high CE of 34.8 cd A^{-1} and PE of 45.2 lm W^{-1}, which are much higher than those of the **CBP**-based device.

This efficiency enhancement could be attributed to the more balanced charge injection/transporting property of **CzPhO** as compared to that of **CBP**, indicating that dibenzophosphole oxide moiety could also be an attractive ET component in the design of bipolar materials.

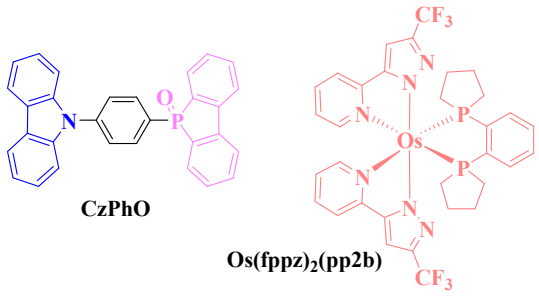

CzPhO; guest Os(fppz)$_2$(pp2b); EQE 14.3 %; CE 34.8 cd A-1; PE 45.2 lm W^{-1}
CBP; guest Os(fppz)$_2$(pp2b); EQE 10.9 %; CE 21.7 cd A-1; PE 11.9 lm W^{-1}

Fig. 58 Chemical structures of **CzPhO** and **Os(fppz)$_2$(pp2b)** and peak efficiency data of related OLEDs.

As discussed above, the properties of carbazole/diphenylphosphine oxide hybrid bipolar host materials can be tuned by changing the number of carbazole or/and diphenylphosphine oxide units or by altering the substitution position. Besides, the properties of carbazole/diphenylphosphine oxide hybrid can be adjusted by incorporating other functional moieties, such as the ET dibenzofuran[252-254] and dibenzothiophene.[143] Lee *et al.* designed two carbazole/diphenylphosphine oxide hybrids **DFCzPO** and **DBT2** (Fig. 59) in which the carbazole and diphenylphosphine oxide units were bridged by a dibenzofuran and dibenzothiophene, respectively.[143, 253] The two bipolar hosts show very similar MO levels and high E_T (> 2.90 eV) due to the similar molecular configuration (Table 7). The theoretical calculation results imply that the HOMOs of **DFCzPO** and **DBT2** are localized mostly over the electron-donating carbazole units while the LUMOs are localized on the dibenzofuran (**DFCzPO**) and dibenzothiophene (**DBT2**) unit instead of diphenylphosphine oxide unit, indicating the adjustment

effects of dibenzofuran and dibenzothiophene. Due to their high E_T and bipolar charge carrier transporting properties, **DFCzPO** and **DBT2** were used as hosts for FCNIrpic to fabricate blue PHOLEDs. Both blue-emitting devices give very high EQEs exceeding 20.0% with CEs above 26.0 cd A^{-1}. The performance of **DFCzPO**-based device is even better than a FCNIrpic-based device using mixed-host (20.3%). This result shows that the dibenzofuran and dibenzothiophene units can be employed to further adjust the properties of carbazole/diphenylphosphoryl bipolar hosts, leading to better charge injection/transporting balance in the devices.

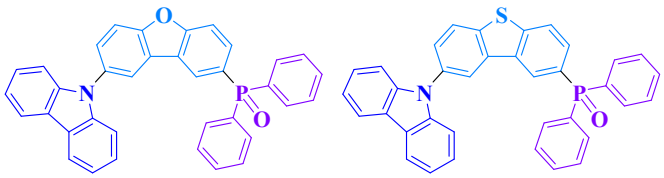

DFCzPO **DBT2**

DFCzPO; guest FCNIrpic; EQE 21.4 %; CE 26.4 cd A-1; PE 22.6 lm W^{-1}
DBT2; guest FCNIrpic; EQE 20.2 %; CE 28.9 cd A-1; PE 28.9 lm W^{-1}

Fig. 59 Chemical structures of **DFCzPO** and **DBT2** and peak efficiency data of related OLEDs.

3.7.2.7 Carbazole-dibenzofuran/dibenzothiophene type bipolar host materials

The ET dibenzofuran and dibenzothiophene units can also be used directly to synthesize carbazole/dibenzofuran and carbazole/dibenzothiophene hybrid bipolar host materials.[255, 256] Lee *et al.* reported several carbazole/dibenzofuran hybrids in which the dibenzofuran units were substituted at 2-, 3- and 4-positions by *N*-phenylcarbazole unit (Fig. 60).[257, 258] Due to the different linking positions, the E_T and LUMO distributions of these materials are different. The *meta*-linked **2-DFPCz** gives the highest E_T of 2.89 eV, while the *ortho*-linked **4-DFPCz** shows E_T of 2.79 eV and the *para*-linked **3-DFPCz** possesses the lowest E_T of 2.59 eV as expected (Table 7). The HOMO distributions are similar for these hosts while the LUMO distributions of **3-DFPCz** and **4-DFPCz** are more expanded than that of

2-DFPCz. As a result, the HT abilities of these materials are similar while the ET abilities of **3-DFPCz** and **4-DFPCz** is higher than that of **2-DFPCz**, which is supported by the single charge carrier devices. Using these materials as host for **$(ppy)_2$Ir(acac)**-based green PHOLEDs and **FIrpic**-based blue PHOLEDs, both green- and blue-emitting devices using **2-DFPCz** as host show the highest EQEs (21.2% for green device and 19.6% for blue device) due to the better charge balance in the EML. Besides, the high E_T of **2-DFPCz** is also beneficial for increasing the blue device efficiency. A carbazole/dibenzothiophene bipolar host **CzDBS** with E_T of 2.77 eV has also been developed (Table 7).[259] The time of flight (TOF) measurements reveal that **CzDBS** possesses bipolar transporting character with same hole and electron mobilities of 7×10^{-5} cm^2 V^{-1} s^{-1}. The solution-processed FIrpic/**CzDBS**-based device shows high peak EQE, CE and PE of 13.9%, 29.7 cd A^{-1} and 18.6 lm W^{-1}, respectively. At high luminance of 1000 cd m^{-2}, the device also gives satisfactory EQE, CE and PE of 12.5%, 27.2 cd A^{-1} and 14.7 lm W^{-1}, respectively, indicating the low efficiency roll-off due to the balanced charge flux within the device at high luminance. Besides, a solution-processed white-emitting device using **FIrpic** and **Os(btfp)$_2$(dppb)**[260] co-doped **CzDBS** as EML exhibits high peak EQE, CE and PE of 16.3%, 35.0 cd A^{-1} and 22.0 lm W^{-1} with a slight efficiency roll-off at high luminance.

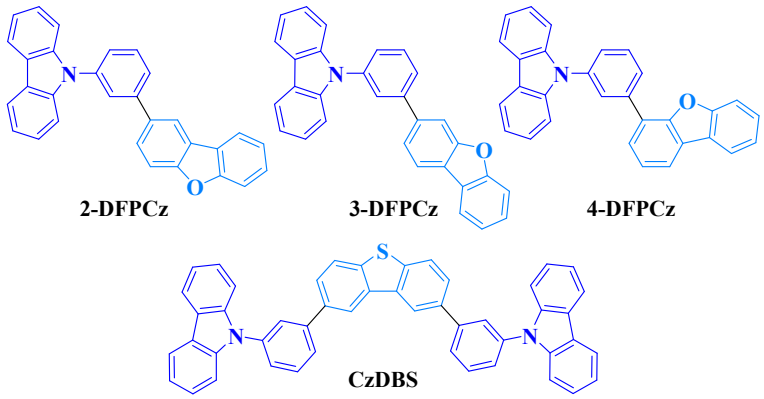

2-DFPCz; guest $(ppy)_2$Ir(acac), EQE 21.2 %; guest FIrpic, EQE 19.6 %
CzDBS; guest FIrpic; EQE 13.9 %; CE 29.7 cd A-1; PE 18.6 lm W^{-1}
CzDBS; guest FIrpic and Os(btfp)$_2$(dppb); EQE 16.3 %; 35.0 cd A-1; PE 22.0 lm W^{-1}

Fig. 60 Chemical structures of **DFPCz**s and **CzDBS** and peak efficiency data of related OLEDs.

Hong *et al.* synthesized two bipolar host materials **B2tCz** and **DB2tCz** (Fig. 61) in which benzo[*b*]thiophene (**B2tCz**) and dibenzothiophene (**DB2tCz**) have been attached to oligocarbazole with 3(6),9′-linking pattern.[256] As aforementioned, the oligocarbazole with 3(6),9′-linking pattern has the potential of achieving high E_T. Hence, these two bipolar hosts show high E_T (2.84 eV for **B2tCz** and 2.94 eV for **DB2tCz**) (Table 7). Higher EL efficiencies can be achieved by blue PHOLEDs using **B2tCz** and **DB2tCz** as hosts than that of the **mCP**-based device. Especially, the **B2tCz**-based device gives very high peak EQE of 24.6% with low efficiency roll-off, indicating the good potential of benzothiophene unit for developing new bipolar hosts.

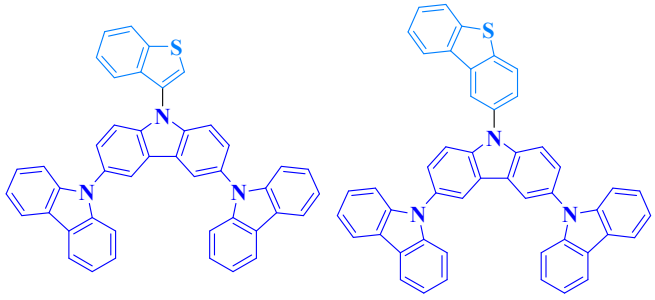

B2tCz **DB2tCz**

mCP; guest FIrpic; EQE 18.1 %; CE 33.1 cd A^{-1}; PE 23.1 lm W^{-1}
B2tCz; guest FIrpic; EQE 24.6 %; CE 43.3 cd A^{-1}; PE 34.0 lm W^{-1}
DB2tCz; guest FIrpic; EQE 20.0 %; CE 35.6 cd A^{-1}; PE 29.4 lm W^{-1}

Fig. 61 Chemical structures of **B2tCz** and **DB2tCz** and peak efficiency data of related OLEDs.

3.7.2.8 Carbazole-benzofuropyridine/benzothienopyridine type bipolar host materials

By fusing benzofuran or benzothiophene group with pyridine ring, Lee *et al.* synthesized some new ET structures, *i.e.*, benzofuropyridine and benzothienopyridine.[152, 261] Incorporating these newly prepared ET structures with HT carbazole unit will result in bipolar host materials with high E_T. **PCzBFP** (Fig. 62) possesses the E_T of 2.89 eV (Table 7) with suitable MO levels (6.10 eV for HOMO

and 2.52 eV for LUMO) for charge injection process. A vacuum deposited blue PHOLED based on FIrpic/**PCzBFP** exhibits very high peak EQE of 23.0% and an efficiency roll-off up to 20.0 % at a luminance of 1000 cd m^{-2}. Besides, the solution-processed device also gives high peak EQE of 18.0%. The high efficiencies for both vacuum- and solution-processed blue PHOLEDs can be attributed to the balanced charge transporting property of **PCzBFP** as supported by hole-only and electron-only devices, indicating the good ET ability of benzofuropyridine group. Bearing a higher ET moiety, **CzPFP** was synthesized with lower LUMO level (2.58 eV) as compared to **PCzBFP**,[262] indicating the enhanced EI/ET property. The E_T of **CzPFP** (E_T = 2.82 eV) is slightly lower than that of **PCzBFP** (2.89 eV) (Table 7). A green-emitting device based on **Ir(ppy)$_3$** using **CzPFP** as host displays very high peak EQE of 27.7% with PE of 86.8 lm W^{-1}. Besides, the EQE is still as high as 27.0% at 1000 cd m^{-2}, indicating the low efficiency roll-off due to the improved bipolar character of **CzPFP**.

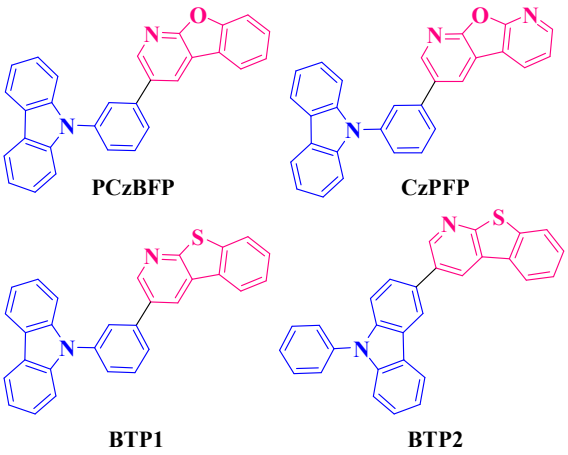

Fig. 62 Chemical structures of **PCzBFP**, **CzPFP** and **BTP**s and peak efficiency data of related OLEDs.

Lee *et al.* also reported two benzothienopyridine-based bipolar material **BTP**s (Fig. 62) in which

the ET benzothienopyridine structure was linked to a different position of the *N*-phenylcarbazole group.[261] The HOMO levels of **BTP1** (6.11 eV) and **BTP2** (6.04 eV) are comparable to that of **PCzBFP** (6.10 eV) due to the same HT component, however, the LUMO levels of **BTP1** (2.71 eV) and **BTP2** (2.80 eV) are much lower than that of **PCzBFP** (2.52 eV) (Table 7), indicating the different electron deficiency of the benzofuropyridine and benzothienopyridine. Due to the higher E_T of **BTP1** (E_T = 2.73 eV) than that of **BTP2** (E_T = 2.65 eV), the blue-emitting device based on **BTP1** shows much higher EQE than that of **BTP2**-based blue device. However, both green-emitting devices based on **BTP1** and **BTP2** exhibit outstanding EQEs over 23.0% even at 1000 cd m^{-2}. These results imply that benzothienopyridine unit has great potential to serve as ET building block for designing good bipolar host materials, and efforts can also be made to develop more benzothienopyridine- and benzofuropyridine-based bipolar host materials in view of the rare reports on this kind of host materials.

Table 7. Carbazole-based bipolar host materials and their properties

Main-group element unit	Host	E_T eV	T_g °C	Dopant	EQE %	CE cd A^{-1}	PE lm W^{-1}	Ref.
carbazole + dimesitylborane	**CzB1**	2.88	105	**Ir(ppy)$_3$**	6.50	–	–	187
carbazole + dimesitylborane	**CzB2**	2.72	89	**Ir(ppy)$_3$**	23.8	–	–	187
carbazole + dimesitylborane	**BDDPC**	2.83	110	**(ppy)$_2$Ir(acac)**	–	38.6	–	188
carbazole + benzimidazole	**mBICP**	3.0	84	**FIrpic**	18.7	36.4	33.6	192
carbazole + benzimidazole	**mPhBINCP**	2.61	113	**Ir(ppy)$_3$**	21.0	77.6	80.3	193
carbazole + benzimidazole	**PhBIDmpCP**	2.59	147	**Ir(ppy)$_3$**	20.2	74.3	74.4	194
carbazole + benzimidazole	**CzFNBI**	2.72	181	**Os(bpftz)$_2$(PPhMe$_2$)$_2$**	18.6	18.6	13.0	195
carbazole + benzimidazole	**CzFCBI**	2.52	175	**Os(bpftz)$_2$(PPhMe$_2$)$_2$**	18.1	18.2	17.0	195
carbazole + benzimidazole	**PhCzNBI**	2.71	124	**(bt)$_2$Ir(acac)**	18.7	47	42.2	196
carbazole + benzimidazole	**PhCzCBI**	2.55	130	**(bt)$_2$Ir(acac)**	19.6	51	43.1	196
carbazole + benzimidazole	**1,8-mBICz**	2.70	154	**Ir(ppy)$_3$**	17.5	64.0	70.0	197
carbazole + benzimidazole	**TICCBI**	2.61	174	**Os(bpftz)$_2$(PPhMe$_2$)$_2$**	22.0	28.0	22.1	198
carbazole + benzimidazole	**TICNBI**	2.61	168	**Os(bpftz)$_2$(PPhMe$_2$)$_2$**	21.0	26.6	25.0	198
carbazole + oxadiazole	**1,8-OXDCz**	2.60	138	**Ir(ppy)$_3$**	20.3	73.9	89.7	197
carbazole + oxadiazole	***o*-CzOXD**	2.68	97	**Ir(ppy)$_3$**	20.2	77.9	59.3	200

carbazole + oxadiazole	**CzFOxa**	2.70	170	**$Os(bpftz)_2(PPhMe_2)_2$**	19.4	21.3	22.3	201
carbazole + oxadiazole	**mCzmOXD**	2.81	100	**FIrpic**	5.80	12.0	9.80	203
carbazole + oxadiazole	**DCzmOXD-1**	2.85	110	**FIrpic**	11.2	23.0	20.5	203
carbazole + oxadiazole	**DCzmOXD-2**	2.88	114	**FIrpic**	9.70	20.5	17.2	203
carbazole + thiadiazole	***o*-CzTHZ**	2.62	167	**$Ir(ppy)_3$**	26.1	92.3	78.8	204
carbazole + thiadiazole	**m-CzTHZ**	2.58	170	**$Ir(ppy)_3$**	24.0	86.4	61.8	204
carbazole + thiadiazole	***p*-CzTHZ**	2.48	168	**$Ir(ppy)_3$**	22.9	80.2	56.7	204
carbazole + triazole	**CzTAZ4**	2.76	137	**FIrpic**	–	21.1	18.7	209
carbazole + triazole	***o*-CzTAZ1**	3.09	87	**FIrpic**	20.2	47.1	41.2	211
carbazole + triazole	***o*-CzTAZ2**	3.07	–	**FIrpic**	17.9	43.3	38.6	211
carbazole + triazole	***o*-CzTAZ3**	3.09	–	**FIrpic**	17.1	40.2	36.1	211
carbazole + pyridine	**CPPY**	2.62	–	**$Ir(ppy)_3$**	21.5	74.9	56.3	217
carbazole + pyrimidine	**CPHP**	2.61	–	**$Ir(ppy)_3$**	26.8	92.2	106	217
carbazole + pyridine	**CzP2**	2.71	102	**$Ir(piq)_3$**	15.8	–	15.5	218
carbazole + pyrimidine	**CzP6**	2.64	107	**$Ir(piq)_3$**	18.4	–	20.3	218
carbazole + pyridine	**TCPY**	2.63	149	**$Ir(piq)_3$**	13.8	–	6.72	80
carbazole + pyrimidine	**TCPM**	2.64	155	**$Ir(piq)_3$**	15.4	–	9.80	80
carbazole + pyridine	**PyCz1**	2.74	–	**FIrpic**	9.60	19.9	10.6	221
carbazole + pyridine	**PPBC**	2.99	–	**FIrpic**	19.8	–	–	220
carbazole + quinoline	**CzPPQ**	2.61	90	**$Ir(pq)_3$**	25.6	75.8	68.1	222
carbazole + quinoline	**CzPPQCz**	2.51	138	**$Ir(pq)_3$**	17.2	51.2	50.1	222
carbazole + quinoline	**CzPPCzQ**	2.95	145	**$Ir(pq)_3$**	21.6	59.4	53.4	222
carbazole + triazine	**CzT**	2.67	134	**FIrpic**	9.9	27.4	30.5	224
carbazole + triazine	**DPTPCz**	2.78	86	**FIrpic**	14.4	27.4	–	225
carbazole + carboline	**CzCb1**	2.88	–	**FCNIrpic**	24.3	–	–	226
carbazole + carboline	**CzCb2**	2.96	–	**FCNIrpic**	21.9	–	–	226
carbazole + carboline	**CzCb3**	2.98	–	**FCNIrpic**	17.0	–	–	226
carbazole + carboline	**pBCb2Cz**	2.93	146	**FIrpic**	23.0	38.3	34.6	227
carbazole + carboline	**PCb-PCz**	2.74	97	**FIrpic**	29.7	–	44.2	228
carbazole + carboline	**2CbCzT**	2.73	149	**FIrpic**	22.1	–	–	229
carbazole + carboline	**CzBPCb**	2.75	–	**FIrpic**	27.6	–	–	109
carbazole + carboline	**CzOTCb**	2.90	108	**FIrpic**	27.4	45.8	36.6	110
carbazole + cyano	**mCPCN**	3.03	97	**FIrpic**	26.4	58.7	57.6	232
carbazole + cyano	**CBPCN**	2.69	162	**$Ir(ppy)_3$**	23.1	80.6	48.9	233
carbazole + cyano	**ACDCN**	2.57	–	**PO-01**	25.7	–	–	236
carbazole + cyano	**3CN33BCz**	2.95	128	**$Ir(ppy)_3$**	26.0	80.2	46.4	237
carbazole + cyano	**3CN34BCz**	2.98	132	**$Ir(ppy)_3$**	30.4	93.6	50.0	237
carbazole + cyano	**3CN44BCz**	3.00	132	**$Ir(ppy)_3$**	30.4	93.2	46.2	237
carbazole + diphenylphosphine oxide	**DCPPO**	2.99	107	**FCNIrpic**	22.4	27.1	–	240
carbazole + diphenylphosphine oxide	**mCPPO1**	3.00	–	**FCNIrpic**	25.1	28.9	29.8	241

carbazole + diphenylphosphine oxide	**CPBDC**	3.01	–	**FCNIrpic**	24.5	–	31.0	242
carbazole + diphenylphosphine oxide	**mCPmPO**	2.75	130	**FIrpic**	20.3	40.0	39.7	243
carbazole + diphenylphosphine oxide	**NPO**	2.99	68	**FIr6**	19.7	–	–	244
carbazole + diphenylphosphine oxide	**MPO12**	3.02	–	**FIr6**	14.3	–	–	253
carbazole + diphenylphosphine oxide	**PPO1**	3.02	74	**FCNIr**	17.1	20.5	14.3	238
carbazole + diphenylphosphine oxide	**POBPCz**	3.01	170	**FIr6**	19.5	40	36	245
carbazole + diphenylphosphine oxide	**PPO2**	3.02	123	**FCNIrpic**	18.4	21.1	18.6	238
carbazole + diphenylphosphine oxide	**PPO21**	3.01	111	**FCNIrpic**	19.2	22.5	19.0	246
carbazole + diphenylphosphine oxide	**PPO27**	2.81	–	**FIrpic**	23.9	–	37.5	247
carbazole + diphenylphosphine oxide	**PPO25**	2.80	140	**FIrpic**	31.4	–	53.1	248
carbazole + diphenylphosphine oxide	**TPCz**	3.07	143	**FIrpic**	16.7	36.4	–	249
carbazole + diphenylphosphine oxide	**TCTP**	3.03	163	**FIrpic**	15.9	35.0	–	249
carbazole + diphenylphosphine oxide	**BCPO**	3.01	–	**FIrpic**	23.5	45.1	40.6	250
carbazole + diphenylphosphine oxide	**CzPhO**	2.71	105	**Os(fppz)$_2$ (pp2b)**	14.3	34.8	45.2	251
carbazole + dibenzofuran + diphenylphosphine oxide	**DFCzPO**	3.00	–	**FCNIrpic**	21.4	26.4	22.6	143
carbazole + dibenzothiophene + diphenylphosphine oxide	**DBT2**	2.92	115	**FCNIrpic**	20.2	28.9	28.9	253
carbazole + dibenzofuran	**2-DFPCz**	2.89	–	**(ppy)$_2$Ir(acac)**	21.2	–	–	257
carbazole + dibenzothiophene	**CzDBS**	2.77	133	**FIrpic**	13.9	29.7	18.6	259
carbazole + benzo[*b*]thiophene	**B2tCz**	2.84	179	**FIrpic**	24.6	43.3	34.0	256
carbazole + dibenzothiophene	**DB2tCz**	2.94	185	**FIrpic**	20.0	35.6	29.4	256
carbazole + benzofuropyridine	**PCzBFP**	2.89	–	**FIrpic**	23.0	–	–	152
carbazole + benzothienopyridine	**CzPFP**	2.82	–	**Ir(ppy)$_3$**	27.7	–	86.8	262
carbazole + benzothienopyridine	**BTP1**	2.73	–	**Ir(ppy)$_3$**	25.4	–	–	261
carbazole + benzothienopyridine	**BTP2**	2.65	–	**Ir(ppy)$_3$**	24.7	–	–	261

4. Main-group moiety functionalized phosphorescent emitters in OLEDs

As one of the two components of the EML in PHOLEDs, phosphorescent emitters hold the irreplaceable position in fabricating higly efficient PHOLEDs, since these emitters can make the 100% internal quantum efficency of PHOLEDs possible. Furthermore, the emission wavelengthes of the phosphorescent emitters can be easily tuned to fulfill application in full-color displays and WOLEDs. More importantly, the phosphorescent emitters also possess unipolar or bipolar charge injection/transporting properties through functionalization, which can optimize the charge recombination and balance in the devices. To date, most phosphorescent emitters are organometallic complexes containing Pt(II), Ir(III), Os(II), Ru(II), Au(III), *etc.*, and the properties (quantum efficiency, emission color, charge injection/transporting property and stability) of phosphorescent emitters mostly depend on the organic ligands of these metal complexes. Therefore, modifying organic ligands with proper main-group moieties is a very practical way to obtain phosphorescent emitters with desirable properties for achieving high-performance PHOLEDs.

4.1 Phosphorescent emitters bearing triarylborane moiety

Due to the intriguing electronic and photophysical properties, triarylborane moiety, e.g., $B(Mes)_2$ group, has been widely used to synthesize organic ligands for Pt(II) and Ir(III) phosphorescent emitters.[25, 31, 263-267] Triarylborane moiety has many merits for functionalizing Pt(II) and Ir(III) complexes, such as improving the ET properties, increasing the phosphorescent quantum yields (Φ_P), tuning the emission colors and suppressing the intermolecular aggregations, *etc.*

Pt(II) phosphorescent emitters

Introducing triarylborane moiety into the different position of 2-phenylpyridine (ppy) is a common way to obtain functionalized *N*,*C*-cyclometalating ligands.[25, 266, 267] The resulting Pt(II) complexes (Fig. 63) can exhibit emission colors from bluish-green to orange with Φ_P up to 0.98 (using **Ir(ppy)$_3$** Φ_P = 1.0 as reference). Compared with the non-borylated parent complex **(ppy)Pt(acac)**, the high Φ_P of some triarylborane-containing Pt(II) complexes result from the increased mixing of the singlet metal-to-ligand charge transfer (^{1}MLCT) and triplet ligand-centered (^{3}LC) states promoted by triarylborane moiety.[25] In addtion, introducing the B(Mes)$_2$ group into the 4-position of the phenyl ring or 5-position of the pyridyl ring will cause a red-shift effect in emission (542 nm for **Pt-PPY-B1**, 527 nm for **Pt-PPY-B5**) (Table 8), but introducing the B(Mes)$_2$ group into the 5-position of the phenyl ring leads to a blue-shift effect in emission (481 nm for **Pt-PPY-B2**). When some of these B(Mes)$_2$ group functionalized Pt(II) complexes are used as emitters to fabricate PHOLEDs, the devices based on **Pt-PPY-B1** and **Pt-PPY-B5** show good device performance. The **Pt-PPY-B1**-based device gives a peak EQE of 9.52% with CE of 30.0 cd A^{-1}.[267] With higher Φ_P, the device based on **Pt-PPY-B5** shows improved CE and PE.[25] After careful optimization, the device with a structure of ITO/MoO_3/**CBP** (35 nm)/**CBP**:**Pt-PPY-B5** (15 nm)/TPBI:**Pt-PPY-B5** (10 nm)/TPBI (65 nm)/LiF/Al leads to outstanding performance with EQE exceeding 20.0% and PE close to 80 lm W^{-1}, which is comparable to the device based on **Ir(ppy)$_3$**.[268] The high performance of the device based on **Pt-PPY-B5** could be partly attributed to the high Φ_P of the emitter. However, the high efficiencies should also give the credit to the improved ET property of Pt(II) emitter due to the strong electron-deficient character of B(Mes)$_2$ group, which will facilitate the charge balance in the

device. Besides, due to the bulky triarylboron group, the intermolecular aggregation which is a very common phenomenon in the device based on planar Pt(II) complexes[10] will be suppressed to some extent, which may improve the device efficiency.

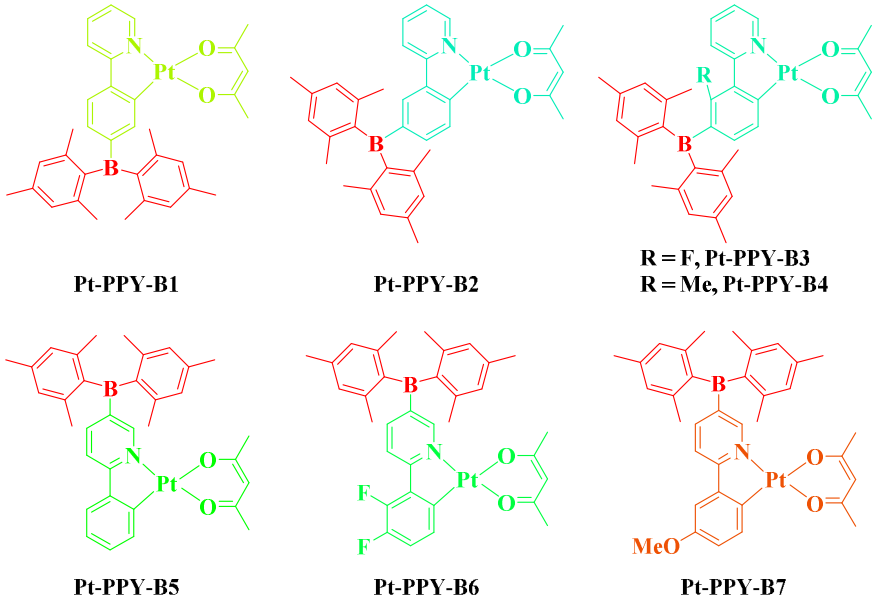

Fig. 63 Chemical structures of some triarylborane functionalized Pt(II) complexes and peak efficiency data of related OLEDs.

Besides the ppy ligands, Pt(II) ions can easily coordinate with various other ligands.[10] Therefore, triarylborane functionalized Pt(II) complexes can be obtained by attaching other ligand types with $B(Mes)_2$ group. For example, **Pt-NCN-B** possesses $B(Mes)_2$-functionalized 3,5-dipyridylbenzene ligand while **Pt-NCb-B1** and **Pt-NCb-B2** have $B(Mes)_2$-functionalized *N*-heterocyclic carbene ligands (Fig. 64) (Table 8).[266, 269] The $B(Mes)_2$ groups in these complexes also greatly increase the Φ_P as well as improve the EI/ET properties. A device using **Pt-NCN-B** (Φ_P = 0.70) as emitter gives the maximum CE of 30.1 cd A^{-1} and PE of 33.8 lm W^{-1} with the emission peak in the bluish-green region.

The **Pt-NCb-B1**-based device also shows bluish-green emission, but exhibits much higher EL efficiencies. The peak EQE of 17.9% achieved by the **Pt-NCb-B1**-based device is among the highest reported for devices using carbene-based Pt(II) complexes as emitters. However, the device based on **Pt-NCb-B2** gives inferior efficiencies due to the relatively low Φ_P (0.87 for **Pt-NCb-B1** vs 0.41 for **Pt-NCb-B2**) (Table 8).

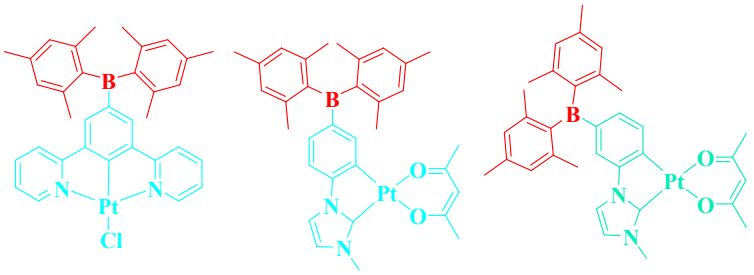

Pt-NCN-B **Pt-NCb-B1** **Pt-NCb-B2**

Pt-NCN-B; EQE 15.3 %; CE 30.1 cd A^{-1}; PE 33.8 lm W^{-1}
Pt-NCb-B1; EQE 17.9 %; CE 53.0 cd A^{-1}; PE 41.6 lm W^{-1}
Pt-NCb-B2; EQE 9.80 %; CE 25.8 cd A^{-1}; PE 22.5 lm W^{-1}

Fig. 64 Chemical structures of some triarylborane functionalized Pt(II) complexes and peak efficiency data of related OLEDs.

It should be noted that all the property changes of triarylborane functionalized Pt(II) complexes as compared to the non-borylated parent Pt(II) complexes may result from the changes of molecular orbital distributions, especially the changes of LUMOs induced by the $B(Mes)_2$ groups. For non-borylated parent Pt(II) complexes, the theoretical calculation results have shown that the HOMOs are mainly distributed on the Pt(II) centers and phenyl rings of the ligands, while the LUMOs are centered at the *N*-heterocyclic moieties of the ligands.[270] However, when the $B(Mes)_2$ groups are incorporated into the Pt(II) complexes, the HOMO distributions are barely affected, but the LUMOs (except for **Pt-PPY-B2**) show large or even predominated contributions from the empty *p*-orbital on boron centers instead of the *N*-heterocyclic moieties of the ligands. The LUMO of

Pt-PPY-B2 is still mainly located on the pyridyl ring, similar to the non-borylated parent Pt(II) complex.[266] With similar HOMOs but different LUMOs, these Pt(II) complexes show different Φ_P, charge injection/transporting properties and emission colors.

Ir(III) phosphorescent emitters

$B(Mes)_2$-functionalized Ir(III) complexes have also been reported.[31, 264, 265, 271, 272] However, except for **Ir-PPY-B3** which is a green triplet emitter, all Ir(III) complexes in Fig. 65 exhibit red or even near-infrared (NIR) phosphorescent emissions (Table 8). Although the HOMO distribution patterns of **Ir-PPY-B1**, **Ir-PPY-B2** and **Ir-PPY-B3** are very similar, *i.e.*, the HOMOs are dominated by the electron density on the Ir(III) centers, the LUMOs show large contributions from the boron centers in **Ir-PPY-B1** and **Ir-PPY-B2** but from pyridyl ring in **Ir-PPY-B3**. Obviously, this great difference of the LUMO distribution patterns for these three complexes is caused by the different substitution position of $B(Mes)_2$ group in the ligand. The 4-position of the phenyl ring and 5-position of the pyridyl ring make apparent contributions to the LUMO of the non-borylated **$(ppy)_2$Ir(acac)**, indicating that these two positions are electron-deficient. Therefore, when the $B(Mes)_2$ group is incorporated into the ligand, these two positions will enhance the electron-deficient property of $B(Mes)_2$ group so that the boron centers make great contributions to the LUMOs of **Ir-PPY-B1** and **Ir-PPY-B2**. On the contrary, the HOMO of **$(ppy)_2$Ir(acac)** has a significant electron density on the 5-position of the phenyl ring, so the electron-deficient property of $B(Mes)_2$ group will be retarded, leading to negligible contribution to the LUMO from the boron center. The different LUMO distributions result in as least two major outcomes. First, in **Ir-PPY-B1** and **Ir-PPY-B2**, it appears that the electrons in the MLCT process have been hosted by the $B(Mes)_2$ group rather than the

pyridyl moiety. Owing to the strong electron-accepting ability of $B(Mes)_2$, it will stabilize the MLCT states of **Ir-PPY-B1** and **Ir-PPY-B2**. Hence, red-shift effects have been observed both in their MLCT absorption and phosphorescent emission. With the HOMO and LUMO distribution patterns similar to **$(ppy)_2$Ir(acac)**, **Ir-PPY-B3** shows green phosphorecent emission similar to **$(ppy)_2$Ir(acac)**. Second, the ET abilities of **Ir-PPY-B1** and **Ir-PPY-B2** are higher than that of **Ir-PPY-B3** due to the enhanced electron-deficient property of $B(Mes)_2$ group in **Ir-PPY-B1** and **Ir-PPY-B2**. As a result, a red device using **Ir-PPY-B1** as emitter achieves peak CE of 21.4 cd A^{-1} and PE of 22.2 lm W^{-1}, which are two times higher than that of a reference device based on a well-known high-performance red phosphorescent emitter bis(2-methyldibenzo[*f,h*]-quinoxaline)Ir(III)(acetylacetonate) [**$(MDQ)_2$Ir(acac)**].[264] This great enhancement can be attributed to the high quantum efficiency as well as good ET property of **Ir-PPY-B1** (Φ_P = 0.95) (Table 8). When $B(Mes)_2$ groups are introduced to the 2-phenylthiophene-based Ir(III) complexes, even deeper red phosphorescent emitters **Ir-PPY-B4** and **Ir-PPY-B5** were obtained with high Φ_P above 0.3.[272] Further extending the π-conjugation, the phosphorescent emission peaks of **Ir-PPY-B6** and **Ir-PPY-B7** could be shifted to the NIR region (λ_{em} = *ca.* 745 nm). Although devices based on these four Ir(III) complexes containing thiophene units display rather poor efficiencies with EQEs less than 1.0%, these examples show the possibility of using electron-deficient $B(Mes)_2$ groups to develop NIR-emitting Ir(III) complexes.

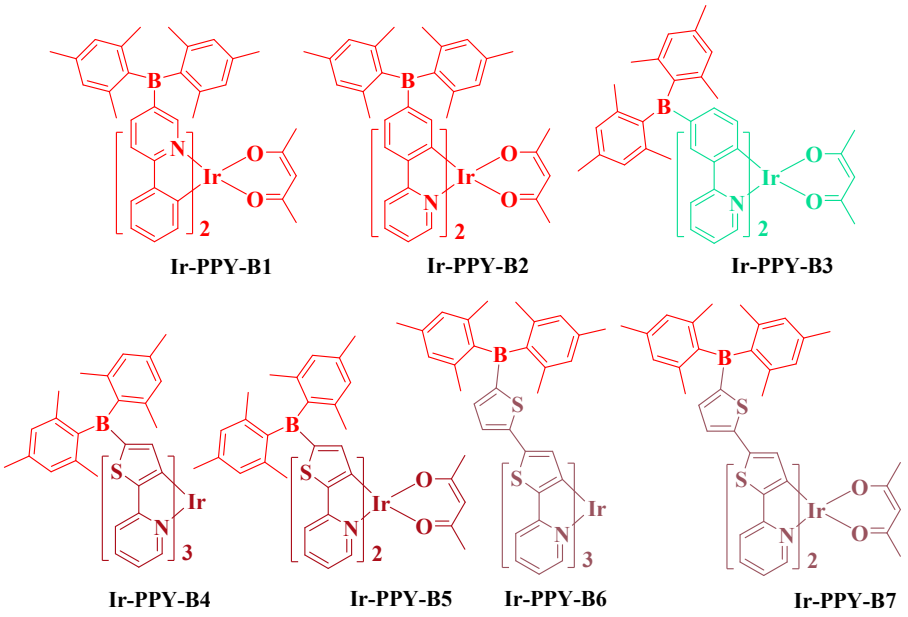

$(MDQ)_2Ir(acac)$; EQE 6.00 %; CE 10.4 cd A^{-1}; PE 9.50 lm W^{-1}
Ir-PPY-B1; EQE 14.7 %; CE 21.4 cd A^{-1}; PE 22.2 lm W^{-1}; 612 nm
Ir-PPY-B2; EQE 9.31 %; CE 10.3 cd A^{-1}; PE 5.04 lm W^{-1}; 609 nm
Ir-PPY-B3; EQE 6.10 %; CE 20.1 cd A^{-1}; PE 21.0 lm W^{-1}; 508 nm

Fig. 65 Chemical structures of some triarylborane functionalized Ir(III) complexes and peak efficiency data of related OLEDs.

Due to the strong electron-withdrawing property, triarylborane moiety shows very good potential to functionalize Pt(II) and Ir(III) complexes with desirable properties, *e.g.*, specific emission color and good EI/ET ability, by simply altering the substitution position on the ligands. These functionalization effects induced by triarylborane moiety may also be realized by other transition metal complexes.

4.2 Phosphorescent emitters bearing aromatic Si/Ge moiety

The sp^3-Si/Ge atoms show poor electron-donating as well as electron-accepting properties. As a result, the triphenylsilane and triphenylgermane substituents can show trivial influence on both charge carrier injection/transporting and emission color of **Pt-PPY-Si** and **Pt-PPY-Ge** (Fig. 66) (Table 8).[267, 273]

However, the bulky triphenylsilane and triphenylgermane groups will make the molecules more rigid with enlarged molecular size, which facilitates radiative pathways and result in high Φ_P (> 0.6). Devices based on **Pt-PPY-Si** and **Pt-PPY-Ge** show EL performance with CE exceeding 8.0 cd A^{-1}. The relatively low efficiencies result from the leaking of electrons from the EML, which is supported by the observation of emission from the HTL. The LUMO levels of **Pt-PPY-Si** and **Pt-PPY-Ge** are *ca.* 2.4 eV, close to that of the HT material 4,4′-Bis[*N*-(1-naphthyl)-*N*-phenylamino]biphenyl (NPB) (2.45 eV), and so the electrons could leak into the NPB layer and recombine with holes, leading to emission from the NPB layer. However, the electron-leaking can be employed to achieve high quality white light with simple device structure. The device with configuration of ITO/NPB/10% **Pt-PPY-Ge**:**CBP**/BCP/Alq_3/LiF/Al displays very high quality white light with color rendering index (CRI) of 97, which is even higher than that of sunlight (ca. 90 at CIE Standard Illuminant D_{65}). The deliberately leaked electrons into NPB cause the blue emission, the intrinsic emission of **Pt-PPY-Ge** is responsible for the green emission and the excimer emission of **Pt-PPY-Ge** contributes to the red emission. Thus, the R-G-B three color white light is generated with high quality. The high CRI of 97 achieved by **Pt-PPY-Ge**-based single-guest WOLED represents the best white light quality in terms of CRI for this kind of WOLEDs to date. Although the triphenylsilane and triphenylgermane substituents show trivial influence on both charge carrier injection/transporting and emission color of the related complexes, they can greatly increase the steric hindrance effect to effectively control the intermolecular interactions as indicated by the long Pt···Pt distances in the crystal structures of **Pt-PVSi** and **Pt-PVGe** (6.7669(5) Å and 6.7859(3) Å, respectively).[274]

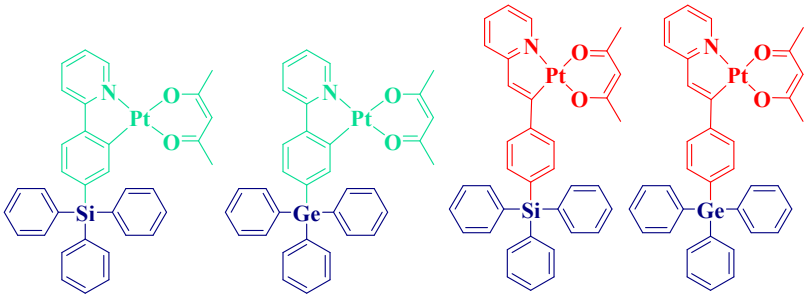

Pt-PPY-Si; EQE 3.51 %; CE 8.47 cd A^{-1}; PE 4.79 lm W^{-1}
Pt-PPY-Ge; EQE 4.02 %; CE 8.49 cd A^{-1}; PE 5.23 lm W^{-1}

Fig. 66 Chemical structures of Pt(II) complexes bearing aromatic Si/Ge moieties and peak efficiency data of related OLEDs.

Similar to the situation in their Pt(II) analogues, the ppy-type Ir(III) phosphorescent emitters are also developed with aromatic Si/Ge moieties (Fig. 67).[31, 275, 276] As expected, the enlarged molecular size and enhanced molecular rigidity could successfully increase the Φ_P of aromatic Si/Ge moiety functionalized Ir(III) complexes as compared to their parent Ir(III) complexes **Ir(ppy)$_3$** and **(ppy)$_2$Ir(acac)**. The Φ_P of **Ir-PPY-Si1** (0.38) and **Ir-PPY-Ge1** (0.42) are slightly higher than that of **(ppy)$_2$Ir(acac)** (Φ_P = *ca.* 0.34), and the Φ_P of **Ir-PPY-Si2** (0.48), **Ir-PPY-Ge2** (0.53) and **Ir-PPY-Si3** (0.63) are higher than that of **Ir(ppy)$_3$** (Φ_P = 0.4) (Table 8). Devices using these aromatic Si/Ge moiety functionalized Ir(III) complexes show electrophosphorescent emission peaks in the range of 524 nm to 535 nm with high efficiencies. For example, the green-emitting devices based on **Ir-PPY-Si2** and **Ir-PPY-Ge2** furnish peak EQE over 10.0% and CE exceeding 44.0 cd A^{-1}.[276] The device using **Ir-PPY-Si3**/PVK as the emitting layer also gives high CE of 32.8 cd A^{-1}, which excels that of Ir(ppy)$_3$-based device.[275] The tetraphenylsilane modified Ir(III) dendrimer complex **Ir-PPY-Si4** shows almost identical photoluminescence spectra with **Ir(ppy)$_3$**, indicating the negligible effects on the

emission color by the tetraphenylsilane dendron.[277] However, the bulky branched non-conjugated tetrahedral tetraphenylsilane dendrons can effectively suppress the interactions between the Ir(III) cores, and render the dendrimer good solubility and film-forming ability. Thus, a non-doped solution-processed green device could be fabricated using **Ir-PPY-Si4** as the self-hosted emitter.

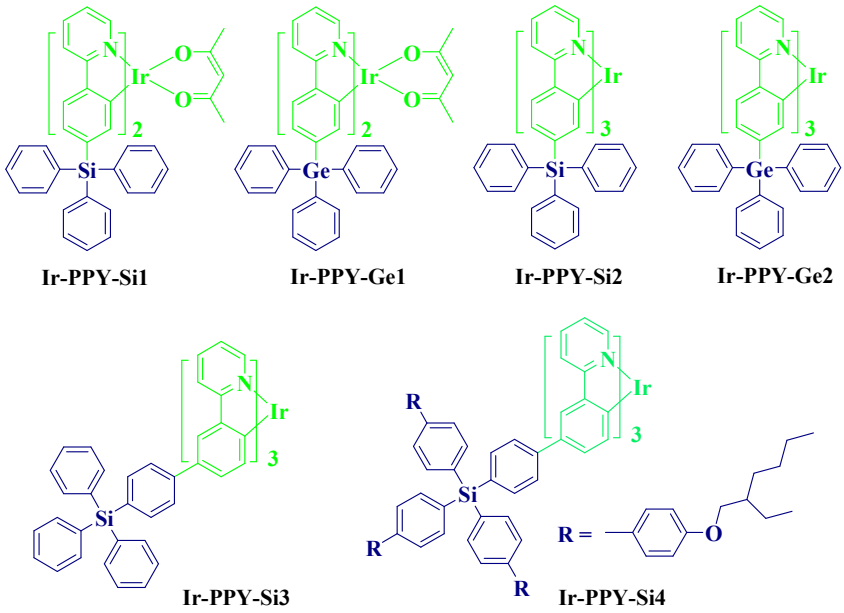

Fig. 67 Chemical structures of **Ir-PPY-Si/Ge**s and peak efficiency data of related OLEDs.

Table 8. Phosphosrent emitters containing borane/silane/germanium elements and their properties

Main-group element unit	Metal center	Emitter	Φ_P	$\lambda_{max,em}$ nm	EQE %	CE cd A^{-1}	PE lm W^{-1}	Ref.
triarylborane	**Pt**	**Pt-PPY-B1**	0.42	542	9.52	30.0	8.36	267
triarylborane	**Pt**	**Pt-PPY-B5**	0.98	527	20.9	64.8	79.3	25, 268
triarylborane	**Pt**	**Pt-NCN-B**	0.70	485	15.3	30.1	33.8	266
triarylborane	**Pt**	**Pt-NCb-B1**	0.87	478	17.9	53.0	41.6	269
triarylborane	**Pt**	**Pt-NCb-B2**	0.41	462	9.80	25.8	22.5	269
triarylborane	**Ir**	**Ir- PPY-B1**	0.95	607	14.7	21.4	22.2	264
triarylborane	**Ir**	**Ir- PPY-B2**	0.18	605	9.31	10.3	5.04	31
triarylborane	**Ir**	**Ir- PPY-B3**	0.71	504	6.10	20.1	21.0	264

triphenylsilane	**Pt**	**Pt-PPY-Si**	0.84	534	3.51	8.47	4.79	267
triphenylgermane	**Pt**	**Pt-PPY-Ge**	0.63	528	4.02	8.49	5.23	267
triphenylsilane	**Ir**	**Ir-PPY-Si2**	0.48	530	10.8	44.6	29.9	276
triphenylsilane	**Ir**	**Ir-PPY-Si3**	0.63	531	–	32.8	18.7	275
triphenylgermane	**Ir**	**Ir-PPY-Ge2**	0.53	525	13.4	48.4	32.6	276

4.3 Phosphorescent emitters bearing nitrogen-containing functional moieties

4.3.1 Triphenylamine-based phosphorescent emitters

Due to the strong electron-donating properties aforementioned, triphenylamine moieties are widely incorporated into phosphorescent emitters to enhance the HI/HT abilities to enhance the EL performance. Triphenylamine unit can also be used to fine-tune the HOMO and LUMO levels of the corresponding complexes to achieve different emitting colors.

A series of ppy-type Pt(II) phosphorescent emitters bearing triphenylamine/diphenylamine moiety have been developed. For **Pt-Am1** to **Pt-Am5** (Fig. 68) (Table 9), the triphenylamine-based moieties can show conjugation with the chelated sections in their organic ligands. Hence, all of them show red-shifted phosphorescent emission maxima (540 nm for **Pt-Am1**[267], 561 nm for **Pt-Am2**[278], 573 nm for **Pt-Am3**[279], 593 nm for **Pt-Am4**[289] and 639 nm for **Pt-Am5**[288]) as compared to their parent complex **(ppy)Pt(acac)** (λ_{em} = 486 nm) (Table 9). However, for **Pt-Am2** to **Pt-Am5**, the larger conjugation of their ligands can also contribute to their red-shifted phosphorescence wavelength. Due to the small contributions to the HOMOs from the Pt(II) cores, which indicates the weak spin–orbital coupling effect of the Pt(II) metal, these complexes (except for **Pt-Am4**) show relatively low Φ_P (< 0.07). Owing to the strong electron-donating ability of the triphenylamine/diphenylamine moiety, these complexes possess elevated HOMO levels. For example, **Pt-Am1** can show the first oxidation

potential as low as 0.33 eV which could be attributed to the oxidation of the electron-rich triphenylamine-based moiety. These results clearly indicate their greatly enhanced HI ability by the triphenylamine/diphenylamine moiety to benefit their EL performance.

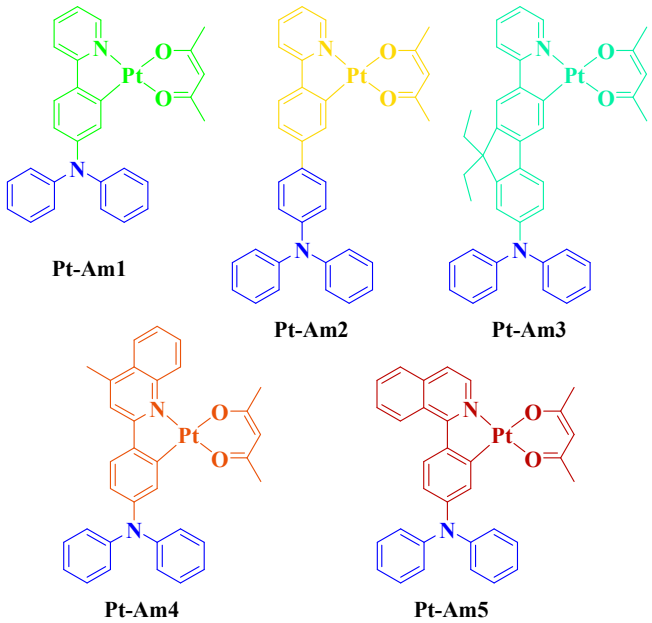

Fig. 68 Chemical structures of some triphenylamine functionalized Pt(II) complexes and peak efficiency data of related OLEDs.

If the triphenylamine moiety is linked to the ligand via sp^3-C atom to eliminate the conjugation effect, it may show little impact on the emission color. Complex **Pt-Fl** (Fig. 69) shows an emission peak at 538 nm,[279] and **Pt-Am6** displays an intense emission maximum at 540 nm.[280] In addition, the quantum efficiencies are also similar for **Pt-Fl** (Φ_P = 0.17) and **Pt-Am6** (Φ_P = 0.18) (Table 9), indicating the trivial influence of triphenylamine moieties on the phosphorescent transitions. However, introducing triphenylamine moieties on the C9-position of the ligand could effectively suppress the

intermolecular aggregation due to the large steric hindrance induced by the triphenylamine moieties. Using **Pt-Am6** as the emitter, the efficiencies of the devices are enhanced with increasing dopant concentration from 3% to 10%. Even at a high dopant concentration of 15%, no excimer emission is observed for the related device. It has been reported that the device based on (2-(4′,6′-difluorophenyl)pyridinato-N,$C^{2'}$)Pt(2,4-pentanedionato) shows a strong excimer emission at the dopant concentration of *ca.* 7%.[281] Therefore, the bulky triphenylamine moieties linked to the proper positions of the ligands can be used to increase the steric hindrance effect to block the excimer formation and relieve the triplet-triplet annihilation effect at the same time.

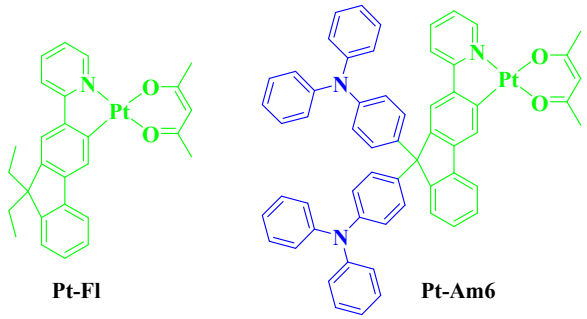

Fig. 69 Chemical structures of **Pt-Fl** and **Pt-Am6** and peak efficiency data of the related OLED.

By replacing a *tert*-butyl group with a triphenylamine moiety, the emission peak can be slightly red-shifted from 560 nm for phosphorescent Pt(II) Schiff base complex **Pt-SF** (Fig. 70) to 568 nm for **Pt-Am7** (Table 9).[282] In addition, the Φ_P and MO levels of **Pt-Am7** are also very similar to those of **Pt-SF**. However, the device based on **Pt-Am7** gives a higher EQE of 8.3% than that of the **Pt-SF**-based device, resulting from the improved HI/HT ability of **Pt-Am7** afforded by the triphenylamine moiety.

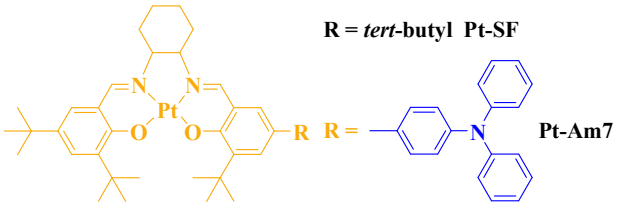

Fig. 70 Chemical structures of **Pt-SF** and **Pt-Am7** and peak efficiency data of the related OLED.

It is generally accepted that the rigidity of the molecular skeletons of the luminescent materials can benefit their emitting ability by reducing the nonradiative decay pathway. Rather than being linked to the ligands with free rotation, novel triphenylamine-based ligands have been obtained to prepare Pt(C^N)$_2$-type phosphorescent emitter with highly rigid skeketons (Fig. 71). **Pt-Am8** is a novel Pt(II) complex with very rigid molecular structure and displays an intense red phosphorescence at 613 nm in solution.[283] The structures of **Pt-Am9** and **Pt-Am10** are quite similar to that of **Pt-Am8**.[284] The 6 wt% doped **Pt-Am9**/Bebq$_2$ (bis(benzo*[h]*quinolin-10-olato-N′,O′)beryllium(II), Bebq$_2$) film displays a strong red emission at 621 nm with a Φ_P of 0.58 (Table 9). The optimized red-emitting device using **Pt-Am9** shows an impressive performance with peak EQE of 19.5% and PE of 25.5 lm W^{-1}. At 100 cd m^{-2}, this device also gives high EQE of 17.2% and PE of 10.7 lm W^{-1}, which are even higher than those of the referecne device using **Ir(piq)$_3$** as the emitter. The optimized device using **Pt-Am10** as the emitter can achieve even higher PE over 30.0 lm W^{-1} and over 10000 h half-life (LT$_{50}$) at an initial luminance of 1000 cd m^{-2}. These results show that exquisite designed Pt(II) complexes bearing triphenylamine-based moieties are very promising candidates for fabricating high performance PHOLEDs.

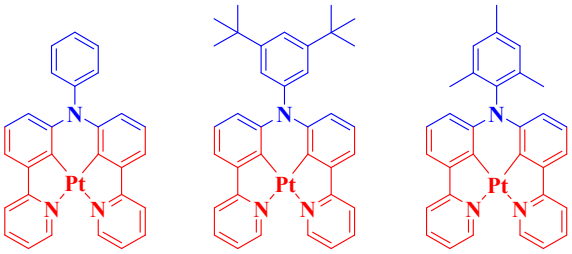

Fig. 71 Chemical structures of **Pt-Am8 – Pt-Am10** and peak efficiency data of related OLEDs.

Attaching triphenylamine/diphenylamine moieties to Ir(III) complexes has been an attractive tactic to synthesize phosphorescent emitters with desirable properties.[32, 285-287] Compared with **(ppy)$_2$Ir(acac)** and **Ir(ppy)$_3$**, diphenylamine functionalized complexes **Ir-Am1** and **Ir-Am2** (Fig. 72) display red-shifted emissions at *ca.* 530 nm due to the elevated HOMO levels (Table 9).[31, 276] The electron-rich diphenylamine moieties also shift the first oxidation potentials of **Ir-Am1** and **Ir-Am2** to less positive positions in the cyclic voltammograms, indicating the enhanced HI/HT properties of **Ir-Am1** and **Ir-Am2**. Green-emitting devices using **Ir-Am1** and **Ir-Am2** show good performance. For example, the device based on **Ir-Am2** displays peak PE close to 50 lm W^{-1} and CE exceeding 60 cd A^{-1}, much higher than those of the Ir(ppy)$_3$-based devices with similar device structures. By replacing the pyridyl ring in **Ir-Am1** and **Ir-Am2** with thiazole moiety, the emission colors of **Ir-Am3** and **Ir-Am4** can be shifted to the orange region, but the oxidation properties of **Ir-Am3** and **Ir-Am4** are almost unchanged as compared to that of **Ir-Am1** and **Ir-Am2**.[288] The device based on **Ir-Am4** exhibits a peak EQE of 14.8% and a PE of ca. 35 lm W^{-1}. In addition, by co-doping **Ir-Am4** and **FIrpic** into the host 4,4′,4″-tri(*N*-carbazolyl)triphenylamine (TCTA) to form a single EML, the two-color WOLEDs have been fabricated to give a nice PE close to 20 lm W^{-1}, indicating the good EL potential of **Ir-Am4**.

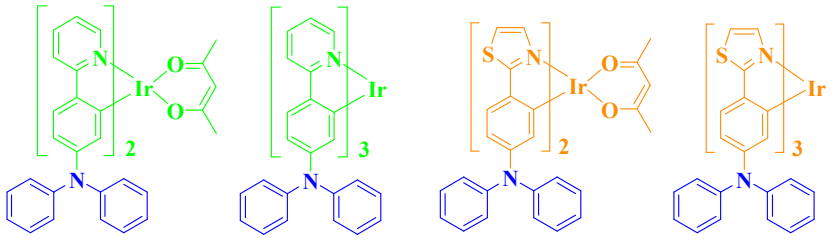

Fig. 72 Chemical structures of **Ir-Am1 – Ir-Am4** and peak efficiency data of related OLEDs.

Although diphenylamine moieties are connected to the fluorene fragments, the Ir(III) complexes **Ir-Am5** and **Ir-Am6** (Fig. 73) show similar MO levels and quantum yields to **Ir-Am1** and **Ir-Am2** (Table 9).[289] The yellow-emitting device based on **Ir-Am6** shows nice performance in terms of peak CE of 29.8 cd A^{-1} and PE of 20.8 lm W^{-1}. However, these devices exhibit severe efficiency roll-off due to the TTA effects. In order to minimize the TTA effects at high current densities, triphenylamine units were linked to the C-9 position on the fluorene fragments.[280] The resulting Ir(III) complexes **Ir-Am7** and **Ir-Am8** show much larger molecular sizes with more rigid configurations. The solution-processed device based on **Ir-Am7** can afford peak EQE over 7.0% and CE exceeding 21.0 cd A^{-1} (Table 9). Most importantly, instead of dropping the efficiency at high current densities, the EQE even slightly increases with increasing current densities within the operating range of 0-150 mA cm^{-2}. This result indicates that the peripheral triphenylamine units with suitable substitution position can efficiently prevent the adverse TTA effects besides enhancing the HI/HT ability of the related phosphorescent emitters.

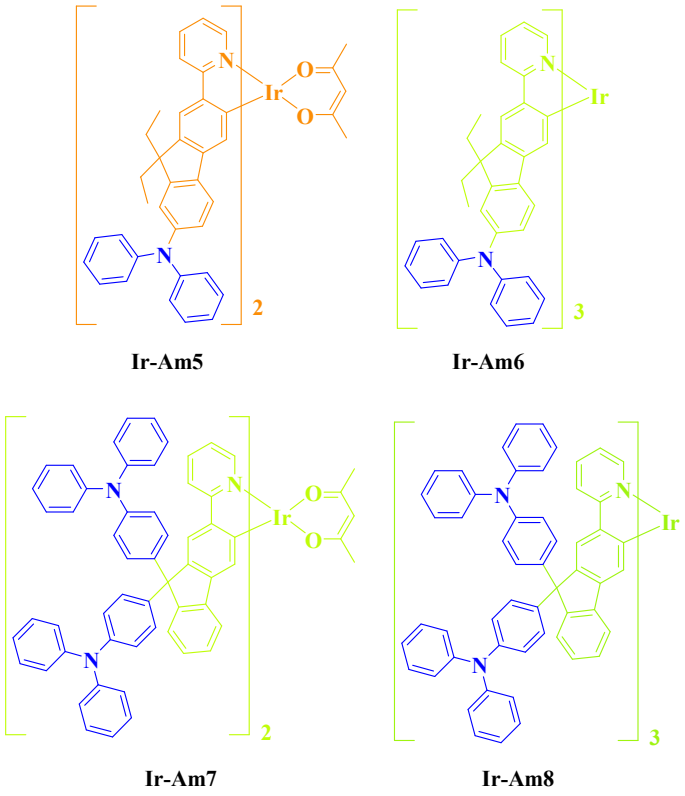

Fig. 73 Chemical structures of **Ir-Am5 – Ir-Am8** and peak efficiency data of related OLEDs.

By attaching a triphenylamine unit on the 4-position of the pyridyl ring in **Ir-Am2**, a yellow emitter **Ir-Am9** (λ_{em} = 561 nm) was obtained (Fig. 74 and Table 9).[286] Through altering the triphenylamine/diphenylamine substitution position on the ppy ligand, the emission color could be changed to red (**Ir-Am10**, λ_{em} = 608 nm)[290] and green (**Ir-Am11**, λ_{em} = 537 nm) (Table 9).[291] The theoretical calculation results reveal that the HOMOs of **Ir-Am9** and **Ir-Am10** are distributed on the central Ir(III) cores and diphenylamine moieties linked to the phenyl rings of 2-phenylpyridyl ligands, while the HOMO of **Ir-Am11** is mainly distributed over the triphenylamine moieties attached on the pyridyl rings of 2-phenylpyridyl ligands with small contribution from the metal *d* orbital. Thus, the

diphenylamine moieties linked to the electron-rich 5-position on the phenyl rings of 2-phenylpyridyl ligands will greatly destabilize the metal *d* orbital of **Ir-Am10**, leading to the highest HOMO of 4.68 eV. However, the electron-deficient 4-position on the phenyl rings of 2-phenylpyridyl ligands will relieve the HOMO destabilization induced by the diphenylamine moieties in **Ir-Am9**, resulting in a slightly lower HOMO level of 4.72 eV. For **Ir-Am11**, the HOMO destabilization caused by the triphenylamine moieties will be greatly retarded by the electron-deficient pyridyl ring, and so **Ir-Am11** shows the deepest HOMO level of 4.96 eV. On the other hand, the LUMO distributions of these three complexes are much similar, *i.e.*, the LUMOs are mainly contributed from the 2-phenylpyridine fragment, and their LUMO levels are slightly affected by the different substitution patterns (2.39 eV for **Ir-Am9**, 2.45 eV for **Ir-Am10** and 2.46 eV for **Ir-Am11**). Clearly, the different MO levels lead to the emission color changes in these three complexes. The device based on **Ir-Am11** gives peak EQE of 15.1% at a dopant concentration of 15 wt%, and the device based on **Ir-Am10** can show peak EQE of 15.3% at a much higher dopant concentration of 30 wt%, indicating the greatly suppressed TTA due to the strong steric hindrance induced by the peripheral triphenylamine/diphenylamine moieties. For **Ir-Am9**, it can even be used to fabricate non-doped PHOLED with high EQE of 14.6% and 31.6 lm W^{-1} even at 1000 cd m^{-2}. Enlarging the molecular size by attaching more triphenylamine units to **Ir-Am9**, phosphorescent dendrimer **Ir-Am12** was obtained with emission color (λ_{em} of 562 nm) similar to **Ir-Am9**.[286] The non-doped device based on **Ir-Am12** shows high efficiencies of 15.6% and 38.3 lm W^{-1} for EQE and PE, respectively, which are comparable to those of **Ir-Am9**-based non-doped device. Based on **Ir-Am10**, dendrimer **Ir-Am13** displays an intense red phosphorescence at 608 nm with a high Φ_P of 0.43 (Table 9), similar to **Ir-Am10** (Φ_P = 0.42), which indicates that the more peripheral triphenylamine units have

negligible influence on the emission color and Φ_P.[290] The high performance of these devices could be attributed to the good HI/HT properties and suppressed TTA effect, which are both afforded by the triphenylamine-based moieties. These results demostrate that the emission colors of Ir(III) complexes can be effectively tuned by tuning the substitution patterns of the triphenylamine-based moieties on the 2-phenylpyridyl ligands. Besides, the triphenylamine-based moieties can be used as a bulky building block to encapsulate the Ir(III) cores so that the undesired TTA effect can be minimized.

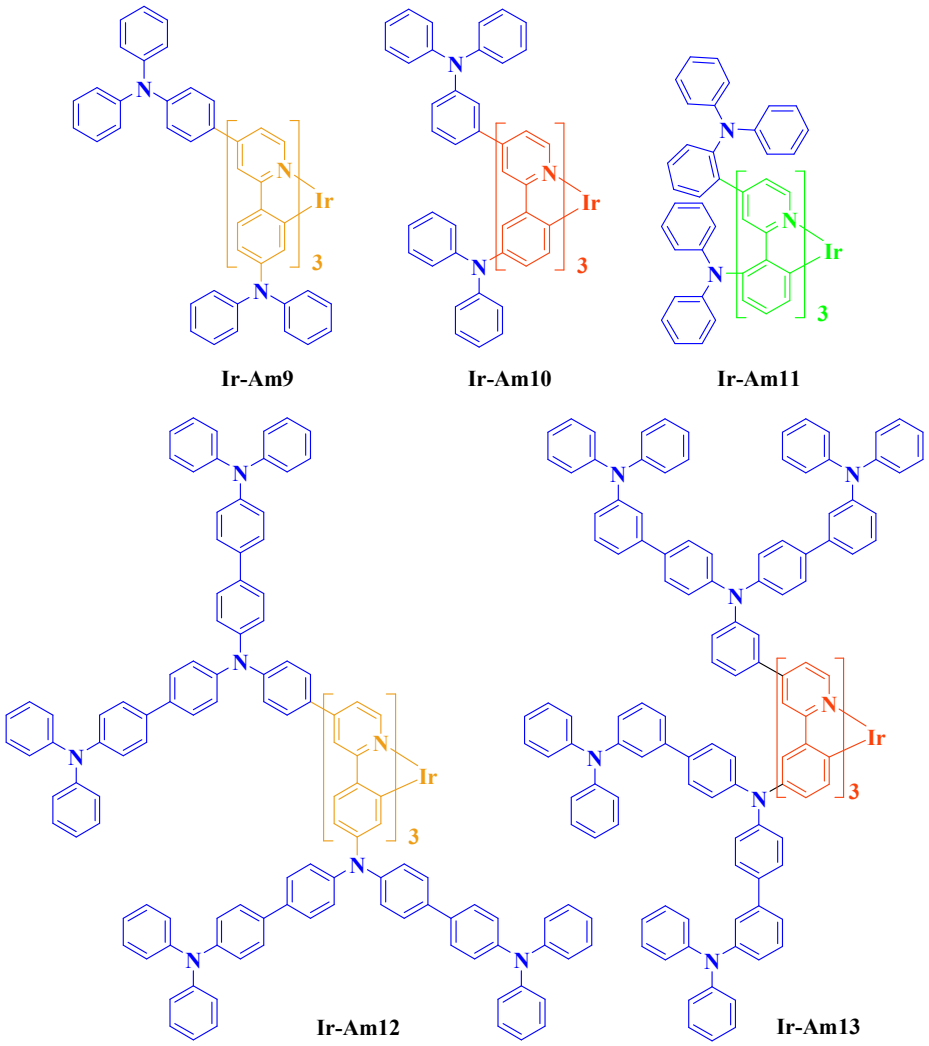

Ir-Am9; EQE 16.4 %; CE 40.9 cd A^{-1}; PE 39.5 lm W^{-1}
Ir-Am10; EQE 15.3 %
Ir-Am11; EQE 15.1 %; CE 43.8 cd A^{-1}; PE 20.5 lm W^{-1}
Ir-Am12; EQE 15.6 %; CE 38.9 cd A^{-1}; PE 38.3 lm W^{-1}

Fig. 74 Chemical structures of **Ir-Am9 – Ir-Am13** and peak efficiency data of related OLEDs.

Besides being linked to 2-phenylpyridine type (ppy-type) ligands, triphenylamine/diphenylamine units can also be introduced to other *N*-heterocyclic ligands. Complexes **Ir-Am14** and **Ir-Am15** (Fig. 75) display an intense deep-red phosphorescence at *ca.* 640 nm, red-shifted by *ca.* 20 nm as compared to their core complex **Ir(piq)$_3$** (λ_{em} = 620 nm) (Table 9), which can be attributed to the raised HOMO levels of **Ir-Am14** and **Ir-Am15** as induced by the triphenylamine-based units.[32] The solution-processed

pure red PHOLED based on **Ir-Am14** can give high peak EQE of 11.65%, which even outperforms the vacuum-deposited device based on the well-known **Ir(piq)$_3$**. However, the peak EQE is 5.43% for the **Ir-Am14**-based device at a doping level of 12 wt%. In contrast, the red-emitting device based on **Ir-Am15** shows a higher peak EQE of 6.42% at the same doping level due to the suppressed interactions among the Ir(III) emissive cores induced by the more surrounding triphenylamine moieties. Complex **Ir-Am16** is also as a red emitter with a high Φ_P of 0.62 (Table 9).[285] The vacuum-processed device using **Ir-Am16** as emitter shows high peak EQE of 15.2% with CE of 14.9 cd A^{-1}. These results show that triphenylamine/diphenylamine units can improve the performance of red Ir(III) complexes by increasing the charge injection/transporting properties and suppressing the TTA effect.

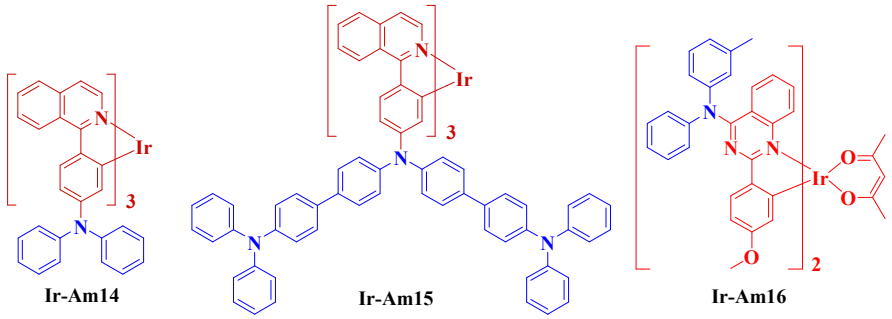

Fig. 75 Chemical structures of **Ir-Am14 – Ir-Am16** and peak efficiency data of related OLEDs.

Au(III) cmplexes with properly designed structures can also show phosphorescent emissions at room temperature, and therefore, they can be used as emitters for phosphorescent OLEDs.[12, 292, 293] Complex **Au-Am0** (Fig. 76) shows blue emission with the peak at around 480 nm, which is assigned to the intraligand (IL) charge transfer from the phenyl ring to the pyridyl unit.[293] When the phenyl ring is replaced by a triphenylamine unit, the emission color is greatly red-shifted to the red with a structureless

band at 620 nm for **Au-Am1** (Table 9). Because of the higher-lying π[C≡C–$C_6H_4N(C_6H_5)_2$-*p*] orbital energy raised by the strong electron-donating triphenylamine unit, this huge red-shift may be caused by the ligand-to-ligand charge transfer (LLCT) (^{3}{π[C≡C–$C_6H_4N(C_6H_5)_2$-*p*] → π*(C^N^C)}) excited state. Devices using **Au-Am1** as emitter can show emission peaks from 500 nm to 580 nm upon increasing the dopant concentration. This phenomenon indicates that **Au-Am1** with planar molecular structure tends to form aggregation at high concentrations. The optimized device with 6 wt% doping concentration gives an attractive performance with peak EQE of 5.5% and PE of 14.5 lm W^{-1}. Complex **Au-Am2** can show even deeper red emission at 669 nm which is assigned to ^{3}LLCT ^{3}{π[C≡C–$C_6H_4N(C_6H_5)_2$-*p*] → π* (2,5-$F_2C_6H_3$-C^N^C)] excited state (Table 9).[294] The π-π stacking behavior of **Au-Am2** at high concentration is also observed due to the slightly distorted square planar structure. At the optimized dopant concentration of 4 wt%, the device using **Au-Am2** as emitter leads to very high efficiencies of 11.5%, 37.4 cd A^{-1} and 26.2 lm W^{-1} for peak EQE, CE and PE, respectively. However, severe efficiency roll-off at high luminances is observed.

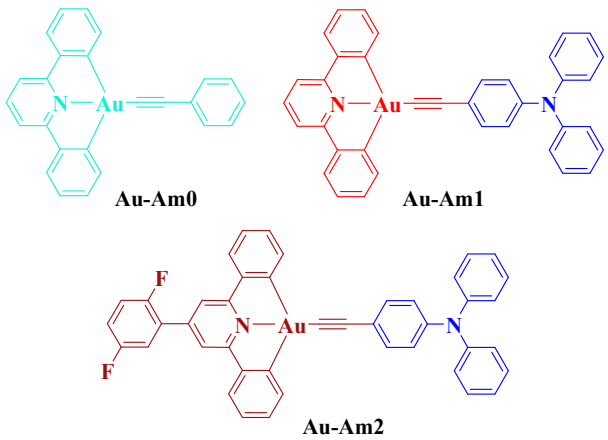

Au-Am1; EQE 5.50 %; CE 17.6 cd A^{-1}; PE 14.5 lm W^{-1}
Au-Am2; EQE 11.5 %; CE 37.4 cd A^{-1}; PE 26.2 lm W^{-1}

Fig. 76 Chemical structures of **Au-Am0** – **Au-Am2** and peak efficiency data of related OLEDs.

To further tap the potential of using Au(III) complexes as emitters for OLEDs, **Au-Am3** to **Au-Am5** (Fig. 77) were synthesized with triphenylamine moiety.[295] In toluene at 298 K, **Au-Am3** shows red emission with a peak at 612 nm and a second peak at 662 nm, while dendrimers **Au-Am4** and **Au-Am5** display structureless broad emission bands with peak at around 685 nm (Table 9). With more electron-donating triphenylamine units in higher-generation dendrimers, the first oxidations of **Au-Am4** and **Au-Am5** ($E_{1/2}^{ox}$ = 0.73 V) are less possitive than that of **Au-Am3** ($E_{1/2}^{ox}$ = 0.90 V), indicating the higher HOMO levels of **Au-Am4** and **Au-Am5** (5.33 eV) than that of **Au-Am3** (5.70 eV). Considering the same LUMO level of **Au-Am3** to **Au-Am5**, the higher HOMO levels lead to narrower energy gaps and thereby longer wavelength emissions of **Au-Am4** and **Au-Am5**. Besides, the higher HOMO levels also result in improved HI/HT properties of **Au-Am4** and **Au-Am5**. Solution-processed devices using **Au-Am3-5** as emitters show red emission bands. The best performance is achieved by the **Au-Am4**-based device which shows peak EQE of 3.62% and PE of 3.47 lm W^{-1}. In addition, compared with the device based on **Au-Am3**, the device based on **Au-Am4** also shows a reduced efficiency roll-off at the high luminance of 100 cd m^{-2} because of the short excited-state lifetime of **Au-Am4** as well as the suppressed intermolecular interaction due to the presence of more triphenylamine units. Although the device based on **Au-Am5** gives a lower efficency of 2.33%, its turn-on voltage is 0.3 V which is lower than that of the device based on **Au-Am4**, indicating the enhanced HI/HT ability of higher-generation dendrimer **Au-Am5**. Anyway, this study provides a new choice of fabricating solution-processed red OLEDs.

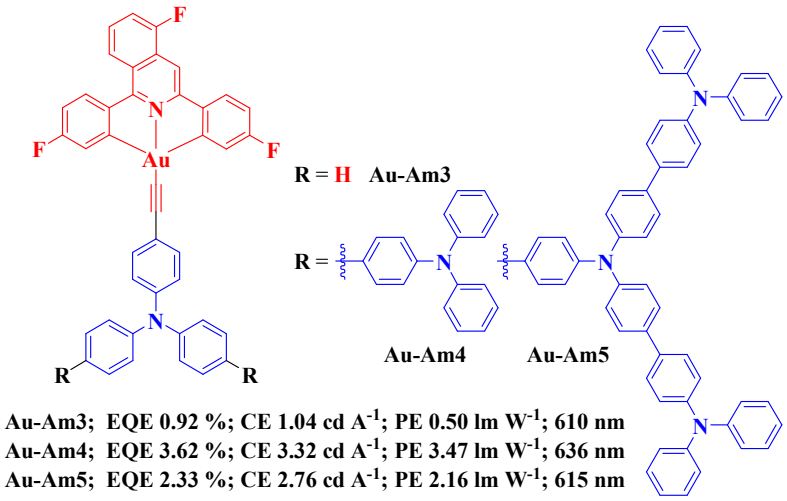

Fig. 77 Chemical structures of **Au-Am3 – Au-Am5** and peak efficiency data of related OLEDs.

Au(III) complexes bearing triphenylamine/carbazole hybrid dendrons (Fig. 78) were reported to show broad structureless emission bands in the range of 620–695 nm in dichloromethane at 298 K.[296] It should be noted that introducing more carbazole units causes blue-shifts in λ (695 nm for **Au-Am6**, 646 nm for **Au-Am7** and 620 nm for **Au-Am8**) (Table 9) because the relatively electron-withdrawing nature of the carbazole dendron will lower the HOMO levels through a negative inductive effect of the electronegative nitrogen atom.[297] However, the intermolecular interactions could be controlled effectively in higher-generation dendrimers due to the rigid and highly twisted structure. The device based on **Au-Am6** displays good performance with peak EQE of 7.8% at 0.1 mA cm^{-2}. Devices based on **Au-Am7** and **Au-Am8** give lower EQE of 7.0% and 3.8%, respectively, which are still higher than those for the devices based on **Au-Am4** and **Au-Am5** bearing triphenylamine dendrons. This indicates that carbazole moieties may be more suitable for developing Au(III) dendritic complexes for high performance solution-processable phosphorescent OLEDs.

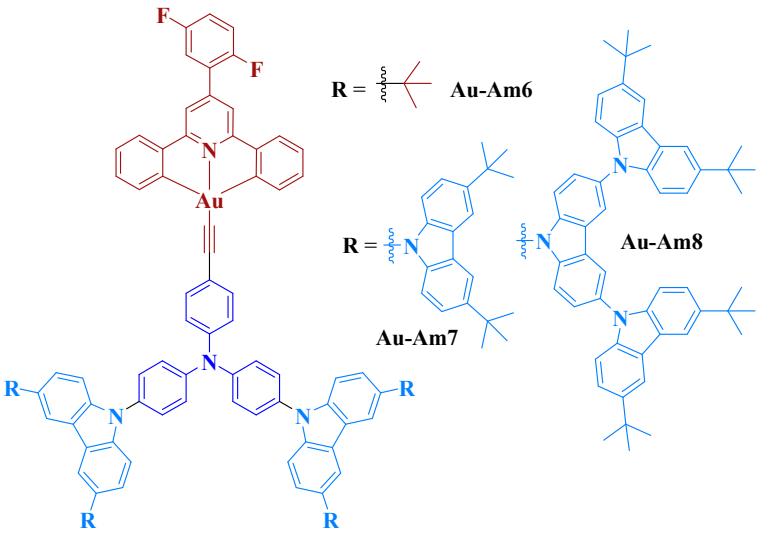

Au-Am6; EQE 7.8 %; CE 24.0 cd A^{-1}; PE 14.5 lm W^{-1}
Au-Am7; EQE 7.0 %; CE 21.9 cd A^{-1}; PE 16.4 lm W^{-1}
Au-Am8; EQE 3.8 %; CE 11.4 cd A^{-1}; PE 9.60 lm W^{-1}

Fig. 78 Chemical structures of **Au-Am6 – Au-Am8** and peak efficiency data of related OLEDs.

4.3.2 Carbazole-based phosphorescent emitters

Carbazole unit has several highly reactive sites, which can be conveniently incorporated into organic ligands to synthesize versatile carbazole-functionalized phosphorescent emitters. Complexes bearing carbazole units usually show high HT abilities due to the electron-donating character of the carbazole units. Besides, the electron-donating ability at different positions on a carbazole unit is diverse, and therefore, by altering the substitution position, the MO level or emission color of the complexes can be fine-tuned.

Generally, the carbazole moiety can be either directly chelated with the metal center or attached to the organic ligands. For the phosphorescent emitters **Pt-Cz1** and **Pt-Cz2** (Fig. 79), the Pt(II) center is chelated with different position of the carbazole moiety.[298] Interestingly, **PtCz1** displays a yellow-orange phosphorescence at *ca.* 560 nm, while **PtCz2** shows a bluish-green phosphorescent signal at 493 nm (Table 9). The significantly red-shifted emission of **Pt-Cz1** can be attributed to its higher HOMO level

and lower LUMO level than those of **Pt-Cz2**. In **Pt-Cz1**, the Pt(II) core is ligated to the more electron-donating carbon of carbazole at the 3-position which will destabilize the metal *d* orbital, resulting in a higher HOMO than that of **Pt-Cz2** whose metal is connected to the less electron-donating carbon at the 2-position. On the other hand, in **Pt-Cz1**, the pyridyl ring is linked to the carbon at the less electron-rich 2-position of the carbazole unit, which can stabilize the LUMO more than that at the 3-position. Therefore, **Pt-Cz1** has a narrower energy gap and thus a lower energy emission. Regardless of the emission color, the device based on **Pt-Cz1** shows a high performance with peak EQE of 13.1% and PE of 25.0 lm W^{-1}, while the peak EQE of the device based on **Pt-Cz2** is only 1.99%. The conspicuous superiority of the **Pt-Cz1**-based device may result from the more suitable MO levels which facilitate the charge injection/transporting process. In addition, **Pt-Cz2** shows a tendency to form molecular aggregation at high doping levels, which leads to the excimer emissions and thereby reduces the efficiencies of the **Pt-Cz2**-based device. When the metal is connected to the phenyl ring of the *N*-phenylcarbazole, the resulting complex **Pt-Cz3** gives a green phosphorescence at 502 nm (Table 9).[299] With extended π-conjugation, **Pt-Cz4** exhibits a peak emission at 547 nm (Table 9). Compared with **Pt-Fl** (λ_{em} = 538 nm) and **Pt-Cz3**, the notable red-shift of **Pt-Cz4** can be attributed to the higher HOMO level as induced by both the electron-donating character of the carbazole unit and the extended conjugation of the organic ligand. On the whole, these studies show that both the emission color and MO level of carbazole-functionalized Pt(II) complexes can be conveniently tuned simply through alteration of the chelating positions connected to the central metal.

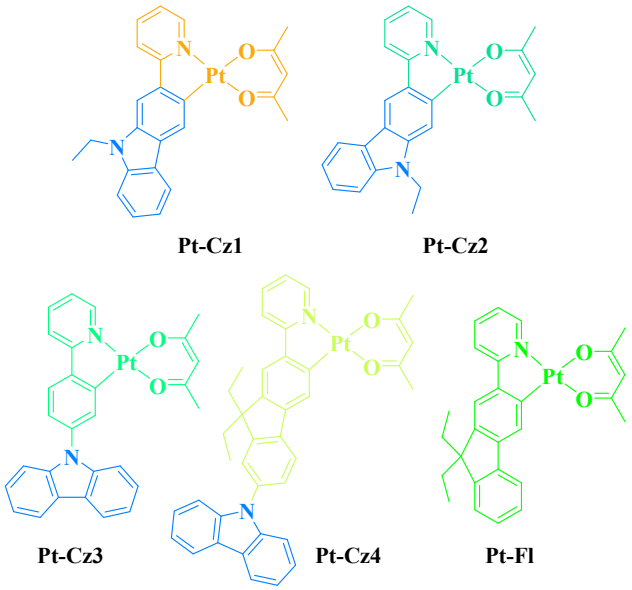

Fig. 79 Chemical structures of some carbazole functionalized Pt(II) complexes and peak efficiency data of related OLEDs.

As aforementioned, introducing carbazole moiety to the main-ligand of the Pt(II) phosphorescent complexes typically will change the emission color of the concerned complexes. However, when a carbazole unit is connected to the auxiliary ligand acetylacetonate (acac), the emission color of the corresponding Pt(II) phosphorescent complexes can be maintained.[300] Hence, **Pt-Cz5** and **Pt-Cz6** (Fig. 80) can exhibit similar phosphorescence maxima to that of **Pt-F1** (*ca.* 470 nm) (Table 9). However, the carbazole moiety attached to the acac ligand can effectively tune the molecular interaction of **Pt-Cz5** and **Pt-Cz6**. In crystal, **Pt-Cz6** can show similar packing mode to that of **Pt-F1** with a dimeric structure in a head-to-tail fashion to show strong molecular interaction. However, **Pt-Cz5** shows a head-to-head packing pattern in crystal with much weaker molecular interaction as compared to **Pt-Cz6** and **Pt-F1**. Devices using these complexes as emitters show different behaviors

at different doping level. At a low dopant concentration of 12 wt%, devices based on **Pt-F1** and **Pt-Cz5** display comparable efficiencies with EQEs of around 8%. However, the EL band arising from excimer is much weaker in the EL spectrum of the **Pt-Cz5**-based device. At a high doping level of 50 wt%, the device based on **Pt-Cz5** gives improved efficiencies with peak EQE of 9.33% and PE of 26.4 lm W^{-1}, while the device based on **Pt-F1** displays slumped efficiencies with peak EQE of 3.42%. When **Pt-F1** and **Pt-Cz5** are used to fabricate non-doped device, the device based on **Pt-Cz5** shows the PE nine times higher than that of the device based on **Pt-F1**. In addition, all devices based on **Pt-Cz5** show reduced turn-on voltages than devices based on **Pt-F1**. These results indicate that the intermolecular aggregation can be suppressed by the *para*-linked carbazole unit in **Pt-Cz5** and thereby high device efficiencies can be achieved at high doping levels. Besides, the enhanced EL performance for **Pt-Cz5** may also be benefited from the improved HI/HT abilities induced by the carbazole unit. However, due to the strong intermolecular Pt···Pt bimetallic interaction induced self-quenching effects, the non-doped device based on **Pt-Cz6** shows a relatively poor performance. All these results show the diverse roles of the carbazole moieties in controlling the intermolecular aggregation characters of the Pt(II) phosphorescent complexes as well as furnishing the HI/HT abilities to bring about improved EL performance.

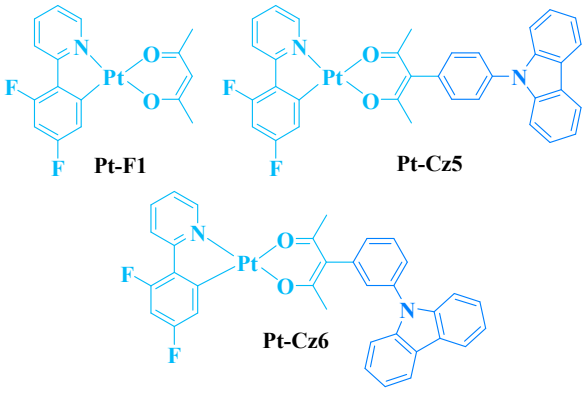

Pt-F1; EQE 7.96 %; CE 21.6 cd A^{-1}; PE 8.71 lm W^{-1} @ 12 wt% doped
Pt-Cz5; EQE 7.24 %; CE 18.2 cd A^{-1}; PE 9.27 lm W^{-1} @ 12 wt% doped
Pt-F1; EQE 3.24 %; CE 7.52 cd A^{-1}; PE 2.25 lm W^{-1} @ 50 wt% doped
Pt-Cz5; EQE 9.33 %; CE 26.4 cd A^{-1}; PE 11.8 lm W^{-1} @ 50 wt% doped
Pt-F1; EQE 2.01 %; CE 3.02 cd A^{-1}; PE 1.03 lm W^{-1} @ nondoped
Pt-Cz5; EQE 9.76 %; CE 28.1 cd A^{-1}; PE 9.91 lm W^{-1} @ nondoped
Pt-Cz6; EQE 6.63 %; CE 17.1 cd A^{-1}; PE 5.11 lm W^{-1} @ nondoped

Fig. 80 Chemical structures of **Pt-F1**, **Pt-Cz5** and **Pt-Cz6** and peak efficiency data of related OLEDs.

Owing to its unique chemical feature and rigid structure, carbazole unit has also been used to synthesize the rigid tetradentate ligands for Pt(II) complexes in which the carbazole is bonded with the Pt(II) center to form a rigid molecular skeleton and enhance the phosphorescent ability. Hence, the rigid Pt(II) complex **Pt-Cz7** (Fig. 81) developed by Che *et al.* shows an intense yellow emission with remarkably high Φ_P of 0.86 in solution (Table 9).[301] Li *et al.* also designed several rigid tetradentate ligands containing carbazole units.[302, 303] The resultant complexes **Pt-Cz8** and **Pt-Cz9** show very high Φ_P of over 0.85 in doped polymethyl methacrylate (PMMA) films and **Pt-Cz10** shows Φ_P of 0.4 in doped PMMA film (Table 9). As a result, the device based on **Pt-Cz7** shows an outstanding performance in terms of peak PE of 52.1 lm W^{-1} and CE of 74.9 cd A^{-1}, which are among the best efficiencies achieved by phosphorescent emitters in yellow OLEDs. An optimized two-color white emitting device using **Pt-Cz7** and FIrpic as emitters with the device structure of ITO/MoO_x (5 nm)/NPB (40 nm)/4% **Pt-Cz7**:TCTA (20 nm)/8% **FIrpic**:**mCP**(10 nm)/8% FIrpic:UGH2 (10

nm)/BAlq (40 nm)/LiF (0.5 nm)/Al (100 nm) gives a total PE of over 60.0 lm W^{-1} with peak CE exceeding 45.0 cd A^{-1}. The **Pt-Cz10**-based device shows a red emission with the peak EQE of 12.5% while the **Pt-Cz9**-based device displays a blue emission with much higher peak EQE of 23.7% and EQE of 20.4% at 100 cd m^{-2}. The highest peak EQE of 25.2% is achieved by the device based on **Pt-Cz8**, which is among the highest efficiency of the devices based on Pt(II) complexes. Considering the narrow EL spectrum with a peak at about 450 nm, the performance of the **Pt-Cz8**-based device is among the best blue-emitting devices based on Pt(II) complexes and comparable or superior to the best reported Ir(III) complex-based blue-emitting devices to date. These examples demonstrate that carbazole-based rigid tetradentate ligands hold great promise for synthesizing Pt(II) complexes with high Φ_P and tunable color to fabricate PHOLEDs showing outstanding EL performance.

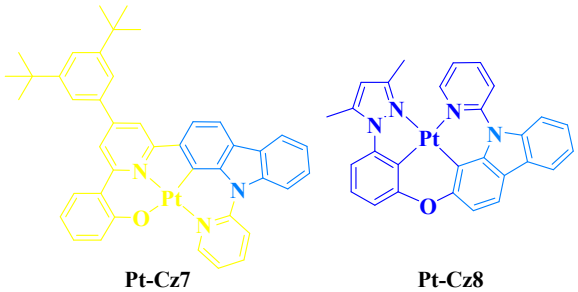

Pt-Cz7 **Pt-Cz8**

Pt-Cz9 **Pt-Cz10**

Pt-Cz7; CE 74.9 cd A^{-1}; PE 52.1 lm W^{-1}; 568 nm
Pt-Cz8; EQE 23.3 %; PE 20.6 lm W^{-1} @ 100 cd m^{-2}
Pt-Cz9; EQE 20.4 %; PE 16.8 lm W^{-1} @ 100 cd m^{-2}
Pt-Cz10; EQE 12.5 %

Fig. 81 Chemical structures of **Pt-Cz7 – Pt-Cz10** and peak efficiency data of related OLEDs.

Carbazole unit also shows versatile effects on the properties of Ir(III) complexes due to its

electron-donating character and rigid chemical structure.[304-307] Similar to the case of **Pt-Cz1** and **PtCz2**, the complex **Ir-Cz1** (Fig. 82) with the central metal ligated to the 3-position of the carbazole moiety shows red-shifted emission color as compared to **Ir-Cz2** with the central metal ligated to the 2-position of the carbazole moiety (594 nm for **Ir-Cz1** vs 511 nm for **Ir-Cz2**) (Table 9).[298] In the ligand of **Ir-Cz1**, the more electron-donating carbon at the 3-position linked to Ir(III) ion will destabilize the metal *d* orbital so as to raise the HOMO level, while the less electron-rich carbon at the 2-position connected to pyridine will stabilize the LUMO level. Therefore, **Ir-Cz1** has a narrower energy gap and thus emits at lower energy. The device using **Ir-Cz1** as emitter displays a red emission with peak EQE of 7.35% and PE of 4.63 lm W^{-1} and the device based on **Ir-Cz2** gives much higher efficiencies of 11.02% and 19.03 lm W^{-1} for maximum EQE and PE, respectively. The improved device performance could be attributed to the higher quantum yield of **Ir-Cz2** (Φ_P = 0.22) than that of **Ir-Cz1** (Φ_P = 0.02). The emission colors of complexes **Ir-Cz3** and **Ir-Cz4** (both at *ca.* 515 nm) are similar to that of **Ir-Cz2**, but the quantum yields of complexes **Ir-Cz3** and **Ir-Cz4** (both at Φ_P = 0.43) are higher than that of **Ir-Cz2** (Table 9).[308, 309] Devices based on **Ir-Cz3** and **Ir-Cz4** also show satisfactory performance with EQE above 11.5% and CE around 40 cd A^{-1}. These efficiencies are much higher than that of $Ir(ppy)_3$-based device with similar device structure, indicating the improved HI/HT properties of **Ir-Cz3** and **Ir-Cz4** and thereby the enhanced device performance. Complexes **Ir-Cz5** to **Ir-Cz9** have similar molecular skeletons to **Ir-Cz3** and **Ir-Cz4**, and their emission peaks are located in the range from 500 nm to 544 nm depending on the substituents and substitution positions (Table 9).[310] Hosted by the PVK polymer, **Ir-Cz5** to **Ir-Cz9** could be used as emitters to fabricate devices showing good performance with CE up to 40.0 cd A^{-1} and EQE up to 12.0%. Form all these results, it can be clearly seen that both the chemical features and electronic

characters of the carbazole moiety can provide a good means to manipulate the properties of Ir(III) phosphorescent emitters.

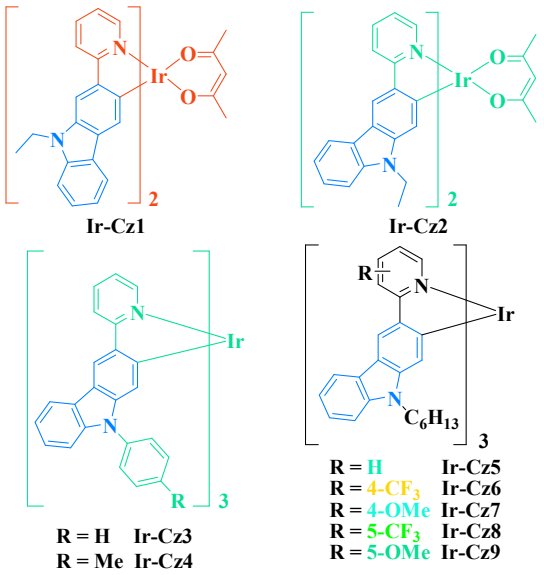

Fig. 82 Chemical structures of **Ir-Cz1 – Ir-Cz9** and peak efficiency data of related OLEDs.

Because the 3,6-positions on carbazole unit are highly active sites, carbazole unit is a very suitable candidate to synthesize Ir(III) dendrimers. Wang *et al.* had synthesized Ir(III) dendrimers up to the third generation with carbazole dendrons (Fig. 83).[311] The emission peak of the third generation dendrimer **Ir-Cz10** appears at 622 nm (Table 9), which is only 11 nm red-shifted as compared to that of the parent Ir(III) complex **Ir-Q** bearing no carbazole units. The quantum efficiency of **Ir-Cz10** is almost unchanged. However, the solution-processed device based on **Ir-Cz10** shows much better performance relative to the device based on **Ir-Q**. At 100 cd m^{-2}, the EQE of the device based on **Ir-Cz10** is 11.8%, which is almost two times higher than that of the device based on **Ir-Q** and also much better than those

of the dendritic systems based on phenylene (5.4% at 100 cd m^{-2})[312] and triphenylamine dendrons (**Ir-Am14**, 7.0%, 3.5 cd A^{-1}, 1.4 lm W^{-1} at 100 cd m^{-2}).[32] Besides, the non-doped device based on **Ir-Cz10** gives peak EQE of 6.3%, which is over 30 times higher than that of the non-doped device based on **Ir-Q**, indicating the greatly improved device efficiency. This significant efficiency enhancement can be attributed to the introduction of the oligocarbazole functional dendrons which effectively improves the charge transporting properties and reduces the intermolecular interaction between the emissive Ir(III) cores. Kido *et al.* also reported a Ir(III) dendrimer **Ir-Cz11** in which the Ir(III) core was completely surrounded by carbazole units.[313] The neat film of **Ir-Cz11** gives a bright orange emission at 580 nm with a high Φ_P of 0.66. The solution-processed non-doped device using the neat film of **Ir-Cz11** as the emissive layer affords the decent EQE of 12.0% with PE of 19.0 lm W^{-1} at 100 cd m^{-2}, which are much higher than those of the device based on a triphenylamine dendritic congener (0.075% and 0.057 lm W^{-1} at 100 cd m^{-2}), indicating that the carbazole dendron shows better charge injection/transporting property than triphenylamine dendron to improve the charge balance. More importantly, at a practically high luminance of 1000 cd m^{-2}, the device based on **Ir-Cz11** still shows a low efficiency roll-off with the EQE still as high as 9.1%, indicating the efficiently suppressed intermolecular interaction between emissive Ir(III) centers and hence reduced self-quenching effects. Highly efficient blue-emitting (λ_{em} = 467 nm, Φ_P = 0.69) dendrimer **Ir-Cz12** (Table 9) is also a suitable candidate for developing non-doped PHOLED because the intermolecular interaction is almost completely suppressed by the carbazole dendrons.[314] Surprisingly, the non-doped device based on dendrimer **Ir-Cz12** even shows a better performance than the corresponding devices at different doping concentrations. Accordingly, this non-doped device can show an impressive performance with the peak

EQE of 15.3% and PE of 28.9 lm W^{-1}, which are among the highest efficiencies obtained by solution-processed non-doped devices based on phosphorescent dendrimers. The carbazole-based dendrimers with Ir(III) metal completely embedded in the center have better charge injection/transporting properties than the triphenylamine dendritic congeners and can effectively suppress the intermolecular interaction between emissive Ir(III) centers in the fabrication of high performance non-doped PHOLEDs.

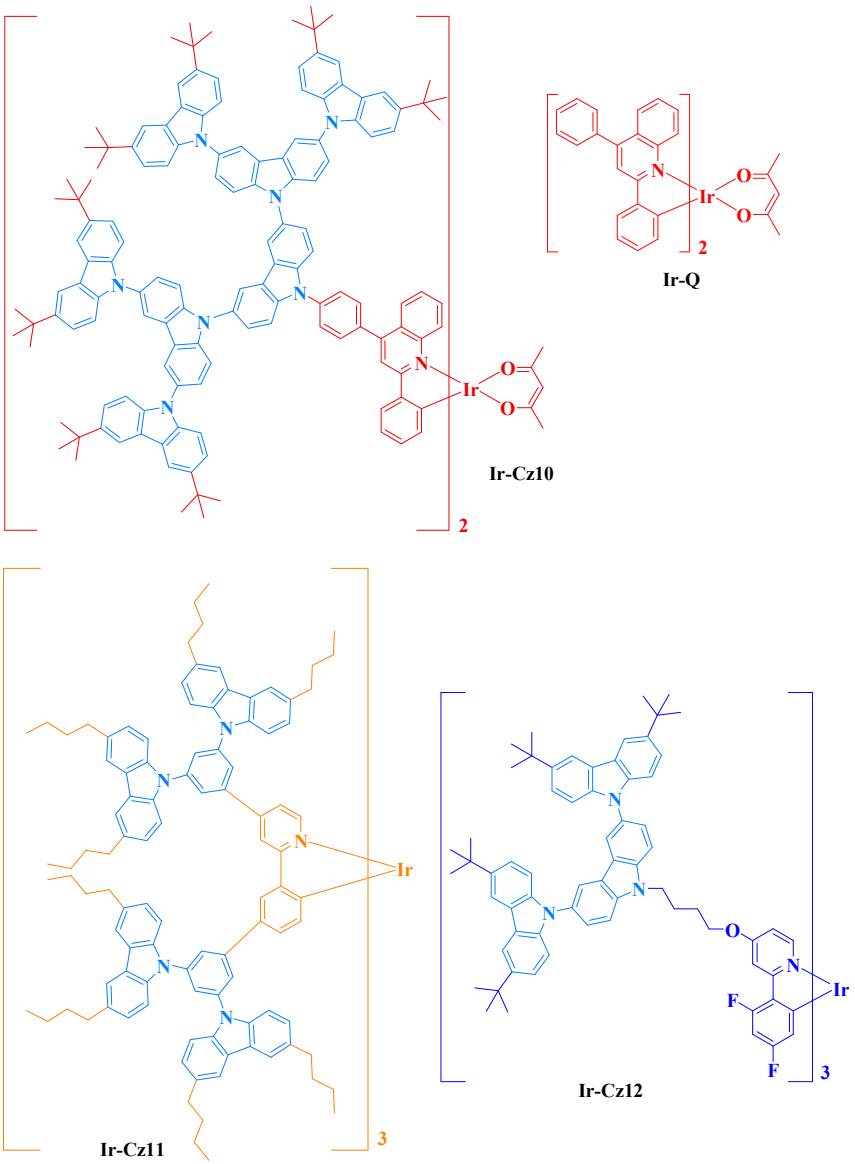

Ir-Q; EQE 0.19 %; CE 0.15 cd A^{-1}; PE 0.04 lm W^{-1} @ 100 cd m^{-2} non-doped
Ir-Cz10; EQE 5.00 %; CE 3.30 cd A^{-1}; PE 1.30 lm W^{-1} @ 100 cd m^{-2} non-doped
Ir-Cz11; EQE 12.0 %; CE 31.0 cd A^{-1}; PE 19.0 lm W^{-1} @ 100 cd m^{-2} non-doped
Ir-Cz12; EQE 15.3 %; CE 31.3 cd A^{-1}; PE 28.9 lm W^{-1} maximum data non-doped

Fig. 83 Chemical structures of **Ir-Q**, **Ir-Cz10 – Ir-Cz12** and peak efficiency data of related OLEDs.

4.3.3 Azole-based phosphorescent emitters

For the complexes mentioned above, almost all the central metals are ligated to the nitrogen atoms on the pyridyl moieties, however, the central metals can also be coordinated with the nitrogen atoms on some azole groups, such as pyrazole,[315-317] imidazole,[318-320] triazole,[321-323] *etc*. These azole

groups containing more than one nitrogen atom usually display strong electon-withdrawing characters, which may facilitate the EI/ET properties of the corresponding complexes.

By introducing a pyrazole unit into 2,2′-bipyridine, Chi *et al.* synthesized a N^N^N terdentate cyclometalling ligand which can be used to prepare a rigid Pt(II) complex (**Pt-Az1**) with distorted square-planar molecular structure (Fig. 84).[315] In **Pt-Az1** crystal, the molecules pack with a head-to-tail fashion and the shortest Pt···Pt distance is 3.385 Å, indicating the strong Pt···Pt interaction. As a result, **Pt-Az1** shows a notable concentration-dependent emission feature, which is supported by the gradually increased low energy emission peak at *ca.* 660 nm and the slightly decreased high energy emission peak at 520 nm with the increase of the concentration of **Pt-Az1** solution (Table 9). Given the short Pt···Pt distance of 3.385 Å, the low energy emission may be attributed to either metal-metal-to-ligand charge transfer (MMLCT) or excimeric ligand-to-ligand charge transfer emission.[315] Devices based on **Pt-Az1** also show dopant concentration dependent red-shifted emission. At a doping level of 28 wt%, the device shows the highest efficiencies with 8.5% for peak EQE and 18.5 cd A^{-1} for peak CE. When the dopant concentration is increased to 100%, the device still gives peak EQE of 6.5% and CE of 10.1 cd A^{-1}, which can be attributed to the fact that **Pt-Az1** possesses a moderate quantum yield (Φ_P = 0.2) in the solid-state and a short lifetime of about 113 ns. The short lifetime is important for reducing the triplet–triplet annihilation. Recently, another pyrazole-based Pt(II) complex **Pt-Az2** was also reported to show concentration-dependent emission feature.[20] In addition, the lifetime decreases from 903 ns at 10% doping level to 326 ns for neat film. The spectral red-shift and reduction of lifetime can be ascribed to the intermolecular aggregation. However, the intermolecular aggregation almost does no harm to the quantum yields of

Pt-Az2 at all doping levels because the excimer and/or MMLCT related emissions are strengthened with increasing doping levels. The neat film of **Pt-Az2** shows a high Φ_P up to 96 ± 3% (Table 9). As a result, a non-doped device with the configuration of ITO/TAPC/**mCP**/**Pt-Az2**/3TPYMB/LiF/Al furnishes an extremely high EQE of 31.1%, which is the highest EQE among those obtained by non-doped devices to date and is comparable to the highest EQE (32.3%) reported for a doped green OLED.[324] The PE of this non-doped red-emitting device are 50.0 ± 0.2 lm W^{-1} (peak value) at 47.1 cd m^{-2} and 35.0 ± 0.8 lm W^{-1} at 1000 cd m^{-2}, which are also higher than those of the most advanced red OLED reported so far.[325] Besides the carefully optimized device structure, the extraordinary performance of this non-doped device can be attributed to the near unity quantum yield in the neat form of **Pt-Az2** due to the reduced triplet–triplet annihilation. These studies demostrate that the square-planar Pt(II) complexes bearing proper ligands can give high Φ_P at high concentration due to the excimer and/or MMLCT related emissions, *e.g.*, **Pt-Az1** shows Φ_P of 0.013 in dilute solution and 0.2 in vacuum-deposited thin film,[315] and thus the high device efficiencies can be achieved by using high-dopant-concentration emissive layers or even neat films of the emissive complexes.

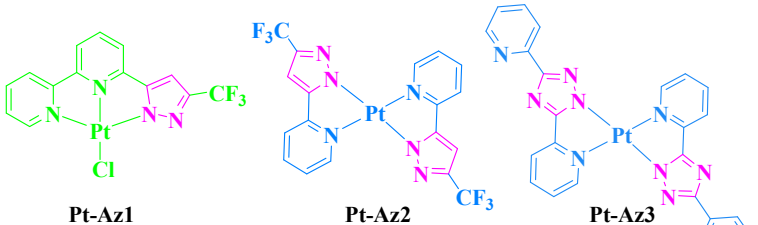

Fig. 84 Chemical structures of **Pt-Az1 – Pt-Az3** and peak efficiency data of related non-doped OLEDs.

Triazole-based Pt(II) complex **Pt-Az3** exhibits columnar packing style with strong intermolecular

Pt···Pt interactions (3.289 Å) in crystal form.[326] The emission colors of **Pt-Az3** doped films can be blue-green (structured monomer emission at *ca.* 480 nm) to yellow (unstructured excimer emission at *ca.* 550 nm) and orange–red (rather broad unstructured excimer and/or MMLCT emission at *ca.* 600 nm) depending on its doping level. The Φ_P of the neat **Pt-Az3** film is recorded as high as 98 ± 2% (Table 9), indicating the greatly reduced triplet–triplet quenching.[327] Due to the electron-deficient pyridyl and triazolyl moieties, **Pt-Az3** shows a high electron mobility in the order of 10^{-5} – 10^{-4} cm^2 V^{-1} s^{-1}.[328] As a result, the non-doped device based on **Pt-Az3** can show extremely high PE of 79.2 lm W^{-1} with EQE of over 20.0%. Besides, this non-doped device shows an extremely low turn-on voltage ($V_{turn-on}$ = 2.2 V) and high PE of 50.1 lm W^{-1} even at a practical luminance of 1000 cd m^{-2}. The high efficiency, low $V_{turn-on}$ and low efficiency roll-off characters render this device among the best OLEDs showing similar yellow/orange/red wavelength so far reported. **Pt-Az3** was also used to fabricate non-doped WOLED with the device configuration of ITO/TAPC/**mCP**/FIrpic/**Pt-Az3**/LiF/Al. The resulting device provides high peak PE of 49.5 lm W^{-1} and PE of 30.0 lm W^{-1} at 1000 cd m^{-2} with unchanged CIE coordinates in the luminance range of 1−10000 cd m^{-2}, which are very attractive in terms of the trade-off among efficiency/color-stability/simplicity aspects. From these results, we can clearly see the advantage of molecular interaction in these Pt(II) complexes to achieve highly emissive MMLCT states and guarantee high EL efficiencies in non-doped PHOLEDs with simple fabrication process.

However, the excimer and/or MMLCT related emissions are always in the yellow to red regions. To obtain high energy emissions in the green and blue regions, the intermolecular aggregations of Pt(II) complexes should be controlled. Strassert *et al.* designed several symmetric Pt(II) complexes

bearing tridentate N^N^N ligands (Fig. 85).[329] To control the intermolecular interactions of these Pt(II) complexes, bulky groups such as tolyl and adamantyl groups were connected to the flanks of the ligands. As a result, the adamantyl-substituted **Pt-Az4** in neat and 10 wt% doped PMMA films display structured monomeric spectra, similar to the solution emission, while the tolyl-substituted **Pt-Az5** in neat and 10 wt% doped PMMA films show structureless and broadened emissions, indicating that adamantyl group can better control the intermolecular aggregation of the related complex. A green-emitting device based on **Pt-Az4** at a doping level of 6% gives maximum CE of 15.2 cd A^{-1} and PE of 7.01 lm W^{-1}, which are comparable to those of the controlled device based on **Ir(ppy)$_3$** (16.4 cd A^{-1} and 7.54 lm W^{-1}), however, the color purity of the **Pt-Az4**-based device is improved due to the slightly blue-shifted spectrum. Strassert *et al.* also reported two asymmetric Pt(II) complexes bearing tridentate N^N^N ligands.[330] Although only one adamantyl group is attached to the triazolyl flank in **Pt-Az6** and **Pt-Az7**, the intermolecular interactions in **Pt-Az6** and **Pt-Az7** can still be controlled. Especially for **Pt-Az7**, the bulky triphenylphosphine ancillary ligand further prevents the Pt···Pt interactions. Solution-processed devices using **Pt-Az6** and **Pt-Az7** as emitters give good performance with PE up to 16.4 lm W^{-1} and CE up to 15.5 cd A^{-1} and electroluminescent peaks appear in the green region (Table 9), indicating the absence of notable Pt···Pt interactions in the device active layer.

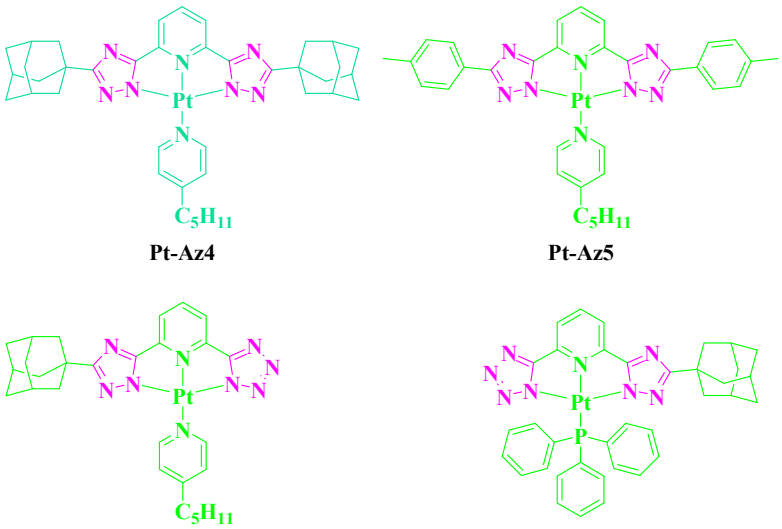

Fig. 85 Chemical structures of **Pt-Az4** – **Pt-Az7** and peak efficiency data of related OLEDs.

Imidazole group is also a suitable *N*-heterocycle which can be used to synthesize emissive Pt(II) complexes.[318, 320, 331-333] Li *et al.* reported a simple imidazole-based N^C^N Pt(II) complex **Pt-Az8** (Fig. 86) which can show an intense blue emission in a degassed solution with a peak at 470 nm and a tail extended to the green region (Table 9).[332] A device using **Pt-Az8** as emitter with a low dopant concentration of 2 wt% gives very high EQE of 18.1% and PE of 23.3 lm W^{-1}, revealing the advantage of using imidazole-based Pt(II) complex as emitter to fabricate high performance OLEDs. With extended π-conjugations, a series of benzimidazole-based Pt(II) complexes were synthesized by Yam *et al*. which displayed main emission peaks in the green region with long tails extended to the orange and even the red regions depending on the ancillary ligands.[318, 320] Complexes **Pt-Az9** to **Pt-Az11** show Φ_P around 0.2 (Table 9) in dichloromethane solution and even much higher Φ_P up to 0.78 in doped thin films (5 wt% in **mCP**). As a result, all the green PHOLEDs based on **Pt-Az9** to

Pt-Az11 exhibit EQE of over 10% with PE exceeding 26 lm W^{-1}, indicating that **Pt-Az9** to **Pt-Az11** are superior candidates as triplet emitters for green-emitting PHOLEDs.

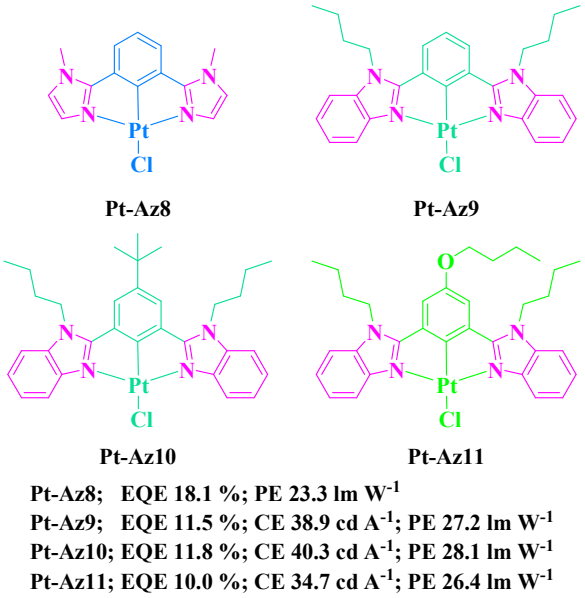

Fig. 86 Chemical structures of **Pt-Az8** – **Pt-Az11** and peak efficiency data of related OLEDs.

Li *et al.* designed a series of novel tetradentate Pt(II) complexes containing imidazole moieties.[333, 334] Blue emitter **Pt-Az12** (Fig. 87) possesses a very high quantum yield of 0.64 in solution and 0.81 in doped PMMA film (Table 9). Due to the significant distortion from planarity induced by the linking oxygen atoms, the intermolecular interactions between **Pt-Az12** molecules are greatly surpressed and hence the excimer emissions are absent regardless of the concentration. The device using **Pt-Az12** as emitter displays bluish-green light with impressively high EQE of 23.1% and PE of 48.8 lm W^{-1}.[335] Replacing the pyridine ring and the bridging oxygen atom in **Pt-Az12** with pyrazole or imidazole unit, the emission peaks are red-shifted from 470 nm for **Pt-Az12** to 490 nm for **Pt-Az13**, 480 nm for **Pt-Az14** and 476 nm for **Pt-Az15** (Table 9).[333] At a low doping level of 2%, the device based on **Pt-Az13** shows primarily green emission (λ_{em} = 496 nm) with remarkably high

EQE of 25.7%, CE of 70.6 cd A^{-1} and PE of 57.1 lm W^{-1}. Although the devices based on **Pt-Az13** can show excimeric EL bands at high doping levels, they can still exhibit very attractive EL performance with maximum EQE all above 24.0% and CE over 59.0 cd A^{-1}. Especially, at the doping level of 12%, the device based on **Pt-Az13** shows an outstanding performance with peak EQE of 26.5% and PE of 61.4 lm W^{-1}. As for **Pt-Az14**, at the dopant concentration from 2% to 16%, devices give very high peak EQE in the range of 22.6% to 24.1% and PE in the range of 47.6 to 53.5 lm W^{-1}. By adding two methyl groups to the pyrazole moiety in **Pt-Az14**, the primarily monomeric emission of **Pt-Az15** is only 4 nm blue-shifted as compared to that of **Pt-Az14**, but the excimer emission of **Pt-Az15** (556 nm) is significantly blue-shifted by 36 nm relative to that of **Pt-Az14** (592 nm), which may result from the modified stacking orientation or increased intermolecular spacing between the two **Pt-Az15** molecules due to the two methyl groups. Nevertheless, the efficiencies of **Pt-Az15**-based devices are higher than those of **Pt-Az14**-based devices at all doping levels (from 2% to 16%). The dramatically high performance is achieved by the 4% **Pt-Az15** doped device which gives peak EQE as high as 26.7% and PE up to 68.3 lm W^{-1}. The superior performance of these devices partly arise from the high Φ_P of both monomers and excimers of the concerned Pt(II) phosphorescent emitters. The contribution from their unique electronic features afforded by the imidazole and/or pyrazole moieties cannot be ignored. These impressive results demonstrate that tetradentate Pt(II) complexes containing imidazole and/or pyrazole moieties have great potential in developing PHOLEDs with outstanding performance which can even compete with the best performance achieved by the efficient Ir(III) complexes.

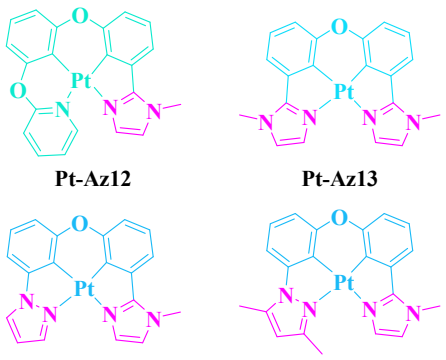

Fig. 87 Chemical structures of **Pt-Az12** – **Pt-Az15** and peak efficiency data of related OLEDs.

Ir(III) complexes bearing five-membered nitrogen-containing heterocyclic moieties such as pyrazole, imidazole and triazole units have also been developed. The phenylpyrazolyl-based Ir(III) complex **Ir-Az1** (Irppz) (Fig. 88) displays deep-blue light due to the high triplet energies of the phenylpyrazolyl ligand, which strongly affects the triplet intraligand $^3(\pi\rightarrow\pi^*)$ and ^{3}MLCT states.[336] The phosphorescence of **Ir-Az1** is extremely weak ($\Phi_P < 0.01$) at room temperature because of the thermally activated non-radiative pathways. However, when the temperature is lowered to 77 K, the strong phosphorescence of **Ir-Az1** can be observed.[337] The phenylimidazole-based Ir(III) complex **Ir-Az2** is a rather interesting triplet emitter, because **Ir-Az2** displays a broad and almost unstructured emission covering the broad spectral range from 440 to 800 nm with a maximum intensity at 570 nm, which is independent of the excitation wavelength, solution concentration and the presence or absence of oxygen in the dichloromethane solution.[338] The broad emission may result from the degenerate emitting states involving the lowest cyclometallated- and acac-based excited states as the theoretical calculation results reveal. When **Ir-Az2** is used as the emitter to fabricate a simple device,

a very broad white EL spectrum is observed. Although the efficiency of this device is low, it might represent a new avenue to generate white EL from a single emitter, which has great potential to excel in simplifying the WOLED fabrication. Introduction of aromatic moieties with large steric hindrance to the nitrogen atom at 1-position of the imidazole moiety can effectively enhance the phosphorescent ability of the phenylimidazole-based Ir(III) complexes. The complex **Ir-Az3** can show high Φ_P of 0.52 in acetonitrile,[339] while **Ir-Az4** possesses high Φ_P of 0.57 in CH_2Cl_2 (Table 9).[340] The blue phosphorescent **Ir-Az5** can exhibit Φ_P of 0.62 in doped thin film (Table 9).[341] Despite the different substituents at 1-position of phenylimidazole-based ligand, **Ir-Az3**, **Ir-Az4** and **Ir-Az5** show similar phosphorescent wavelengths and MO levels, indicating the trival influence from these substituents on these properties. A sky-blue-emitting device using **Ir-Az3** as emitter gives EQE of 23.1% (peak value) and 20.1% at 1000 cd m^{-2}, which are much higher than those of the reference device based on FIrpic (13.5% for peak and 12.6% at 1000 cd m^{-2}). The optimized device using **Ir-Az4** as emitter can give the EQE up to 23.0% as well. The device based on **Ir-Az5** with the configuration of ITO (90 nm)/HATCN (5 nm)/TAPC(35 nm)/10 wt% **Ir-Az5**-doped 26DCzPPy (10 nm)/Tm4PyPB (50 nm)/Liq (2 nm)/Al (80 nm) shows an extremely high EQE of 33.2%, PE of 71.9 lm W^{-1} and CE of 73.6 cd A^{-1} at 100 cd m^{-2} with a very low driving voltage of 3.22 V and efficiency roll-off. With further optimization, **Ir-Az5** can even bring about a higher PE of 75.6 lm W^{-1} at 100 cd m^{-2} with a lower driving voltage of 3.04 V. These EL perfromances are the best for blue PHOLEDs ever reported. The extremely good device performance should benefit from the superior electronic properties of **Ir-Az5** afforded by the phenylimidazole moiety besides the well-designed device configuration. These encouraging achievements show that introducing proper substituent to the

1-position nitrogen atom of the imidazole moiety can dramatically improve the Φ_P, while keeping suitable MO levels to facilitate the charge injection and short lifetimes to avoid T-T annihilation. Given the high E_T of these phenylimidazole-based Ir(III) complexes, proper modification on the phenyl moiety of the phenylimidazole ligand may further increase the E_T of the resulting Ir(III) complex and thus give high performance deep-blue PHOLEDs.

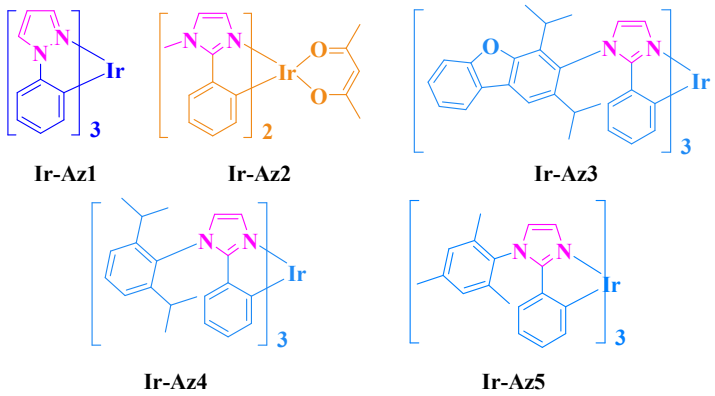

Fig. 88 Chemical structures of **Ir-Az1** – **Ir-Az5** and peak efficiency data of related OLEDs.

Benzoimidazole-based Ir(III) complexes usually display emission peaks above 500 nm with Φ_P decided by the substituents linked to the carbon at 2-position of the benzoimidazole moiety.[319] Complex **Ir-Az6** (Fig. 89) exhibits intense an green phosphoresccent emission (λ_{em} = 523 nm) in CH_2Cl_2 solution with a high Φ_P of 0.73 (Table 9). When *tert*-butyl groups are introduced into the benzoimidazole-based ligands, the λ_{em} (= 524 nm) and Φ_P (= 0.72) of the complex **Ir-Az7** are almost unchanged as compared to those of **Ir-Az6** (Table 9), because of the weak electron-donating property of *tert*-butyl group.[342] By replacing the auxiliary ligand acac in **Ir-Az6** with another benzoimidazole-based N^N bidentate ligand, *i.e.*, 2-benzo[*d*]imidazol-2-yl-quinoline, the resulting complex **Ir-Az8** shows a strong orange emission (λ_{em} = 573 nm) in CH_2Cl_2 with a Φ_P of 0.45 (Table

9), indicating that the N^N ligand is greatly involved in the transition process.[343] **Ir-Az9** is also an efficient orange emitter with the emission peak at 563 nm in CH_2Cl_2 with a Φ_P of 0.51 (Table 9).[319] The PHOLED based on **Ir-Az6** can give high EQE of 16.7% and CE of 61 cd A^{-1} with a serious efficiency roll-off due to TTA, which can be relieved by introducing *tert*-butyl groups (**Ir-Az7**). Owing to the involvement of the N^N bidentate ligand in the photo-induced transition process, the emissive excited states of **Ir-Az8** consist of an admixture of ^{3}MLCT, ^{3}LLCT and ^{3}LC transitions, which lead to a broad EL spectrum. This character will make **Ir-Az8** favorable for fabricating two-color WOLEDs. Accordingly, the device using **Ir-Az8** as an orange emitter and **FIr6** as a blue emitter shows good EL performance with peak PE of 25.5 lm W^{-1} and CE of 22.1 cd A^{-1}. The monochromic PHOLED based on **Ir-Az9** also displays an attractive EQE of 10.4%.[319] Thus, **Ir-Az9** has a great potential in fabricating two-color WOLEDs. The device with a structure of ITO/NPB (40 nm)/TCTA (5 nm)/**mCP**:6.5 wt% **FIrpic**:0.75 wt% **Ir-Az9** (20 nm)/TAZ (40 nm)/LiF/Al displays excellent performance with peak EQE of 19.3% and PE of 42.5 lm W^{-1}.[344] This impressive performance is partly attributed to the unique role played by **Ir-Az9** in the device. **Ir-Az9** can trap the holes in the emissive layer and transport electons at the same time, resulting in the direct charge-carrier recombination on the **Ir-Az9** molecules, and thereby improve the efficiency. On the whole, benzoimidazole-based Ir(III) complexes usually show lower energy emissions as compared to imidazole-based Ir(III) complexes. Especially, the orange-emitting benzoimidazole-based Ir(III) complexes with high PL quantum yields have great potential for developing two-color WOLEDs due to suitable emission colors and broad emission spectra.

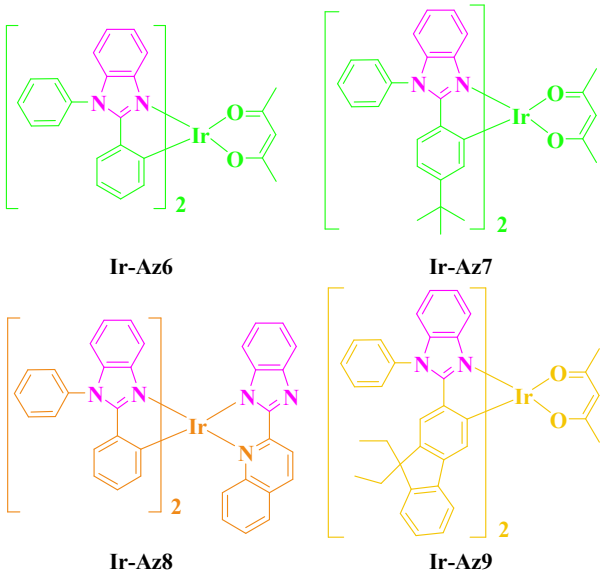

Fig. 89 Chemical structures of **Ir-Az6** – **Ir-Az9** and peak efficiency data of related OLEDs.

Lo *et al.* prepared a series of triazole-based Ir(III) complexes which could display strong blue emissions because of the high LUMO energies induced by the triazole moiety and high Φ_P up to 0.66 in toluene.[345] By introducing biphenyl units into the phenyltriazole ligands, several dendrimers were also synthesized.[321, 346] The mono- and doubly dendronized Ir(III) complexes **Ir-Az11** to **Ir-Az13** (Fig. 90) show similar emission colors to the non-dendronized **Ir-Az10**. However, **Ir-Az11** to **Ir-Az13** give higher Φ_P up to 0.94 as compared to **Ir-Az10** (Φ_P = 0.66) in toluene (Table 9). Besides, the attachment of the dendrons greatly improves the solid-state Φ_P from 0.09 for **Ir-Az10** up to above 0.6 for **Ir-Az11** to **Ir-Az13**, which is attributed to the effectively suppressed intermolecular interactions between the emissive Ir cores in **Ir-Az11** to **Ir-Az13** due to the bulky dendrons. Very simple bilayer blue-emitting devices with the structure of ITO/**Ir-Az11** or **Ir-Az12**/TPBI/LiF/Al show attractive performance. The mono-dendronized **Ir-Az11**-based device give a EQE of 4.6% at 138 cd m^{-2}, and the

doubly dendronized **Ir-Az12**-based device affords a much higher EQE of 7.9% at 142 cd m^{-2}. More importantly, at the high luminance of 1552 cd m^{-2}, **Ir-Az12**-based device still exhibits a EQE as high as 6.7%, indicating the greatly reduced intermolecular interactions between the **Ir-Az12** molecules. Using **Ir-Az13** as emitter, the bilayer device (ITO/**Ir-Az13**/PBD/LiF/Al) gives a lower EQE of 2.1% at 100 cd m^{-2} than that of the **Ir-Az12**-based device, but the emission CIE coordinates of (0.16, 0.17) obtained by the **Ir-Az13**-based device is much better than those of (0.18, 0.35) as shown by the **Ir-Az12**-based device. For the above results, the triazole moiety can show great promise in developing blue-emitting Ir(III) phosphorescent emitters due to its electronic characters. Furthermore, the phosphorescent ability can be effectively improved by employing dendritic structures.

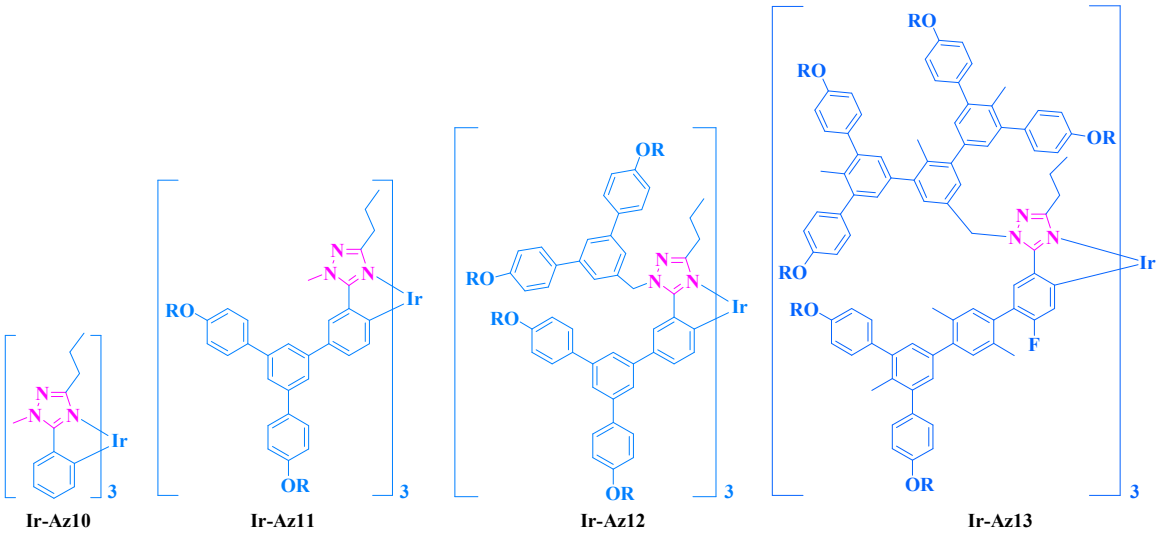

Fig. 90 Chemical structures of **Ir-Az10** – **Ir-Az13** and peak efficiency data of related OLEDs.

4.3.4 *N*-Heterocyclic carbene-based phosphorescent emitters

Due to the weak π-accepting and strong π-donating properties, the *N*-heterocyclic carbene

(NHC) ligands show very strong ligand field strength, resulting in a) the stable NHC-based cyclometallated Pt(II) and Ir(III) complexes as evidenced by the shorter metal–carbene bond length of the NHC-based complex as compared to that of the metal–nitrogen bond distance in the conventional complex in which the neutral nitrogen atom is ligated to the metal ion, b) high-energy emissions due to the elevated LUMO energy level and c) increased Φ_P because of the raised d−d level of the excited state and thus effectively suppressed thermally activated non-radiative decay.[36, 347, 348] Therefore, NHC-based cyclometallated Pt(II) and Ir(III) complexes are very suitable for developing efficient blue and deep-blue OLEDs, respresenting very important research direction in PHOLEDs.

Strassner *et al.* synthesized a series of NHC-based cyclometallated Pt(II) complexes which can show emission peaks in the range from deep-blue to bluish-green regions with high Φ_P in PMMA films.[348] Especially, complex **Pt-NHC1** (Fig. 91) shows an exceptionally high Φ_P of 0.9 in 2 wt% doped PMMA film (Table 9). However, the device based on **Pt-NHC1** displays green–blue color with CIE cooodinates of (0.162, 0.314) because of the large emission tail extended to the long wavelegth region. Li *et al.* reported that **Pt-NHC2** displayed strong blue emission with a peak at 448 nm in the degassed solution at room temperature (Table 9).[332] The device based on **Pt-NHC2** at low doping level of 2 wt% gives a high peak EQE of 15.7% and an attractive blue color purity with CIE of (0.16, 0.13). When the dopant concentration is increased to 10 wt%, a pronounced broad excimer emission band appears in the orange region, leading to a white emission with CIE coordinates of (0.33, 0.33) and a CRI of 80.[349] Besides the high quality white emission, this device also shows very high peak EQE of 20.1% and PE of 51.0 lm W^{-1}. These outcomes make **Pt-NHC2** a very promising

blue emitter for efficient pure blue OLEDs as well as OLEDs emitting high quality white light. Furthermore, this suggests the potential of using NHC-based cyclometallated Pt(II) complexes to realize saturated blue-emitting PHOLEDs. Most importantly, the successful fabrication of the single-doped WOLED with high efficiencies as well as high color quality holds a promise of using efficient blue-emitting square planar Pt(II) complex as single emitter to realize the high performance WOLED for practical solid-state lighting.

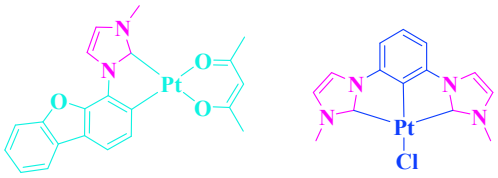

Pt-NHC1 **Pt-NHC2**

Pt-NHC1; EQE 6.2 %; CIE (0.162, 0.314)
Pt-NHC2; EQE 15.7 %; PE 22.0 lm W^{-1}; CIE (0.16, 0.13)
Pt-NHC2; EQE 20.1 %; PE 51.0 lm W^{-1}; CIE (0.33, 0.33)

Fig. 91 Chemical structures of **Pt-NHC1** and **Pt-NHC2** and peak efficiency data of related OLEDs.

Besides the reported bidentate carbene-type ligands,[348, 350] tetradentate ligand containing carbene moieties are also suitable for synthesizing efficient Pt(II) complexes.[302, 347, 351, 352] Che *et al.* synthesized a series of symmetric bis(carbene)-based Pt(II) complexes which are efficient blue triplet emitters.[347, 351] The doped PMMA films with 1 wt% doping level of **Pt-NHC3** and **Pt-NHC4** (Fig. 92) show similar phosphorescent peak at *ca.* 449 nm as well as Φ_P of *ca.* 0.25 (Table 9). At a doping level of 4 wt%, the device using **Pt-NHC4** as emitter gives peak EQE of *ca.* 15 % and PE of 16.6 lm W^{-1}. The emission color is beyond the deep-blue region as evidenced by the CIE coordinates of (0.191, 0.217). However, a two-color WOLED based on **Pt-NHC4** and a yellow triplet emitter leads to a remarkable high PE of 55.2 lm W^{-1} and CE of 87.8 cd A^{-1} under the optimized condition.

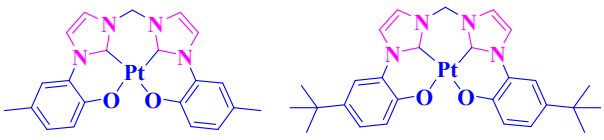

Pt-NHC3 **Pt-NHC4**

Pt-NHC4; EQE 15.0 %; PE 16.6 lm W^{-1}; CIE (0.191, 0.217)
Pt-NHC4; CE 87.8 cd A^{-1}; PE 55.2 lm W^{-1}; CIE (0.350, 0.458)

Fig. 92 Chemical structures of **Pt-NHC3** and **Pt-NHC4** and peak efficiency data of related OLEDs.

Li *et al.* also designed several tetradentate Pt(II) complexes bearing carbene moiety.[302, 352] The carbene-based Pt(II) complex **Pt-Cz9** is a very efficient blue emitter with an emission peak at 452 nm when doped into PMMA film. The blue-emitting device based on **Pt-Cz9** is very attractive in performance with peak EQE of 23.7% and PE of 26.9 lm W^{-1}, and satisfactory CIE coordinates of (0.14, 0.15). When the carbazolyl pyridine in **Pt-Cz9** is replaced with the phenoxy pyridine, a blue-shift of 10 nm is noted for **Pt-NHC5**.[302] As a result, the device based on **Pt-NHC5** (Fig. 93) shows better CIE coordinates of (0.15, 0.10). Although the device efficiencies are relatively low (4.1% and 3.7 lm W^{-1} at 100 cd m^{-2}), the small *y*-coordinate close to 0.08 is highly desirable for meeting the standard blue CIE coordinates of (0.14, 0.08) recommended by National Television System Committee (NTSC).[353] Further modifying **Pt-NHC5** by replacing the phenoxy pyridine with the imidazolyl benzene results in a symmetric carbene-based tetradentate Pt(II) complex **Pt-NHC6** which shows a red-shifted primary emission peak at 472 nm as compared to **Pt-NHC5**.[352] The bathochromic effect is attributed to the elevated HOMO level which is destabilized by the weakened bond strength of the Pt-C_{Ph} bond due to the Pt-C_{Cb} bond at the *trans* position (C_{Ph} and C_{Cb} refer to the carbon atom on the phenyl ring and carbene moiety, respectively). Therrefore, the device with a low doping level of 2 wt% **Pt-NHC6** gives the CIE coordinates of (0.12, 0.24), away from the standard blue point (0.14, 0.08). However, the performance of this device is remakably high in terms of the peak EQE of 26.3% and PE

of 32.4 lm W^{-1}. Similar to the case of **Pt-NHC2**-based devices, when the dopant concentration is increased, the devices based on **Pt-NHC6** show strong excimer emissions in the orange region, thus the single-dopant WOLED is expected. The device with the dopant concentration of 14 wt% shows white light with a CRI of 70 and CIE of (0.37, 0.42). Besides, this single-dopant excimer-based WOLED results in a high peak EQE of 24.5% and PE of 55.7 lm W^{-1}.

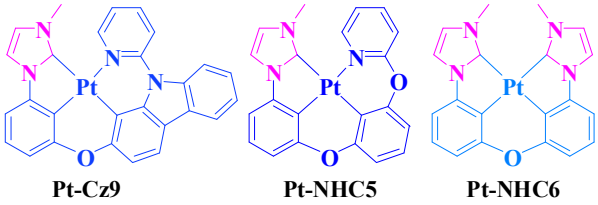

Pt-Cz9; EQE 23.7 %; PE 26.9 lm W^{-1}; CIE (0.15, 0.14)
Pt-NHC5; EQE 4.10 %; PE 3.70 lm W^{-1}; CIE (0.15, 0.10)
Pt-NHC6; EQE 26.3 %; PE 32.4 lm W^{-1}; CIE (0.12, 0.24)
Pt-NHC6; EQE 24.5 %; PE 55.7 lm W^{-1}; CIE (0.37, 0.43)

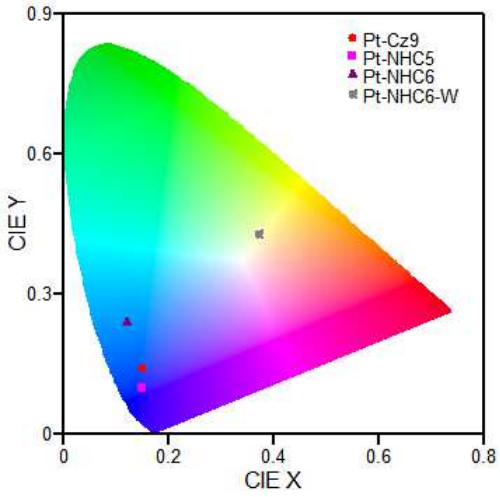

Fig. 93 Chemical structures of **Pt-Cz9**, **Pt-NHC5** and **Pt-NHC6** and peak efficiency data of related OLEDs, and the CIE diagram for these blue phosphorescent emitters.

It has been reported that carbene-based ligand can effectively increase the LUMO levels of the corresponding Ir(III) complexes, and thereby shift the emission color of the related Ir(III) complexes to the deep blue region.[36, 354] A deep-blue PHOLED derived from carbene-based Ir(III) complex **Ir-NHC1** (Fig. 94) has also been reoprted to show deep-blue emission with a EQE of 5.8% and CIE coordinates of (0.17, 0.08), very close to the highly desired point (0.14, 0.08) in the diagram.[355] However, the Φ_P of the tris(cyclometallated) iridium-carbene complex is very low ($\Phi_P < 0.05$).[354] Kido *et al.* reported that a meridional homoleptic Ir(III) complex **Ir-NHC2** bearing benzofuran-based

carbene ligands showed blue emission with high Φ_P of 0.7 in 10 wt% doped **PPO2** film.[356] The blue-emitting device based on **Ir-NHC2** affords an outstanding performance with a peak EQE of 18.6% and PE of 35.9 lm W^{-1}. However, the CIE coordinates of **Ir-NHC2**-based blue-emitting device red-shift to (0.15, 0.19). In order to obtain deep-blue emitter with high Φ_P, design of heteroleptic Ir(III) complexes with proper auxiliary ligands is a practical way. However, carbene ligands usually possess very large π–π* energy gaps, and thus the lowest one-electron excitation will occur solely on the auxiliary ligands with insufficient π–π* gaps, leading to undesired red-shifted emission. It has been reported that 2-pyridyl azole ligands have large π–π* gaps and have been widely used to synthesize blue emitters.[29, 357] Therefore, carbene ligands and 2-pyridyl azole ligands can be good collaborator to increase the Φ_P as well as keep the high emission energies of Ir(III) complexes. For example, Che *et al*. designed a heteroleptic carbene-based Ir(III) complex **Ir-NHC3** which showed an emission peak at 458 nm with the Φ_P as high as 0.73 (Table 9).[358] As a result, the device based on **Ir-NHC3** exhibits a blue emission with CIE coordinates of (0.158, 0.128), peak EQE of 6.0% and PE of 4.0 lm W^{-1}. Carbene-based complexes **Ir-NHC4** and **Ir-NHC5** also display an intense blue light in solution with relatively high Φ_P up to 0.18 (Table 9).[359] Compared to **Ir-NHC5** (λ_{em} = 471 nm), **Ir-NHC4** exhibits a bluer light (λ_{em} = 456 nm) due to the electron-withdrawing F substituent which greatly stabilizes the HOMO level and thus increase the energy gap of **Ir-NHC4**. As a result, the device based on **Ir-NHC4** displays a deep-blue emission with excellent CIE coordinates of (0.14, 0.10). Besides, this device shows higher efficiencies (peak EQE of 7.6% and PE of 4.1 lm W^{-1}) than the devices based on **Ir-NHC1** and **Ir-NHC3**. Although the device based on **Ir-NHC5** gives red-shifted emission with CIE coordinates of (0.14, 0.27), it displays

greatly improved efficiencies of 15.2% and 19.6 lm W^{-1} for the peak EQE and PE, respectively. These results clearly show the critical role played by the carbene-based moiety in achieving deep-blue Ir(III) phosphorescent emitters with high Φ_P.

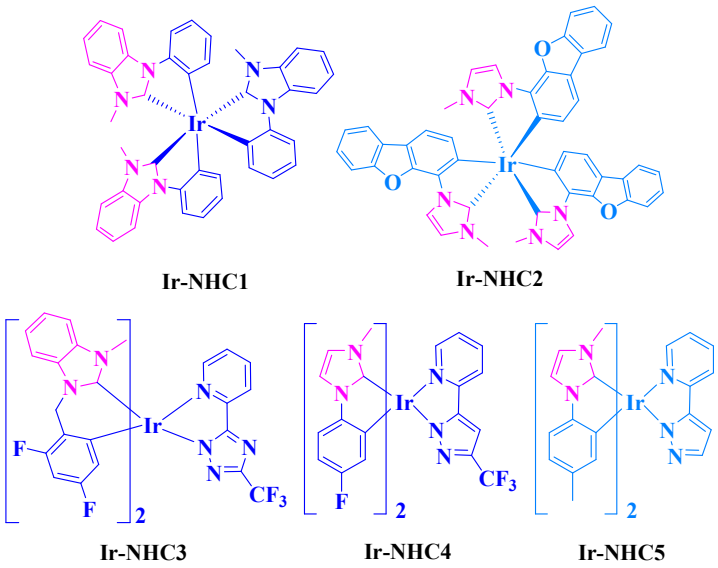

Ir-NHC1; EQE 5.8 %; PE 1.7 lm W^{-1}; CIE (0.17, 0.08)
Ir-NHC2; EQE 18.6 %; CE 28.6 cd A^{-1}; PE 35.9 lm W^{-1}; CIE (0.15, 0.19)
Ir-NHC3; EQE 6.0 %; CE 6.3 cd A^{-1}; PE 4.0 lm W^{-1}; CIE (0.16, 0.13)
Ir-NHC4; EQE 7.6 %; CE 6.5 cd A^{-1}; PE 4.1 lm W^{-1}; CIE (0.14, 0.10)
Ir-NHC5; EQE 15.2%; CE 28.1 cd A^{-1}; PE 19.6 lm W^{-1}; CIE (0.14, 0.27)

Fig. 94 Chemical structures of **Ir-NHC1** – **Ir-NHC5** and peak efficiency data of related OLEDs.

As discussed above, in heteroleptic carbene-based Ir(III) complexes, the auxiliary ligands with insufficient π–π* gaps will cause red-shifted emissions, therefore, using auxiliary ligands with different π–π* gaps can conveniently tune the emission colors of heteroleptic carbene-based Ir(III) complexes. Cheng *et al.* reported several heteroleptic carbene-based Ir(III) complexes which displayed blue to orange-red emission colors depending on the auxiliary ligands.[325] These complexes can give high Φ_P in the range from 0.41 to 0.79 in CH_2Cl_2 at room temperature. As a result, devices based on these complexes exhibit excellent performance. Devices based on **Ir-NHC6** and **Ir-NHC7**

(Fig. 95) display blue emissions with peak EQEs over 15% and PEs above 19 lm W^{-1}. The **Ir-NHC8**-based device emits green light peaking at 520 nm. Besides, this device gives high efficiencies of 24.4%, 91.9 cd A^{-1} and 96.3 lm W^{-1} for peak EQE, CE and PE, respectively. With an isoquinoline-based auxiliary ligand, **Ir-NHC9** displays strong orange-red light (λ_{em} = 592 nm) in solution with a Φ_P of 0.55 (Table 9). The device using **Ir-NHC9** as emitter shows an outstanding performance with a peak EQE of 24.9% and PE of 43.6 lm W^{-1}. The study provides a practical tactic to widely tune the emission color of carbene-based Ir(III) complexes to fulfill full-color display by controlling the E_T through different *N*-containing auxiliary ligands with diverse electronic characters.

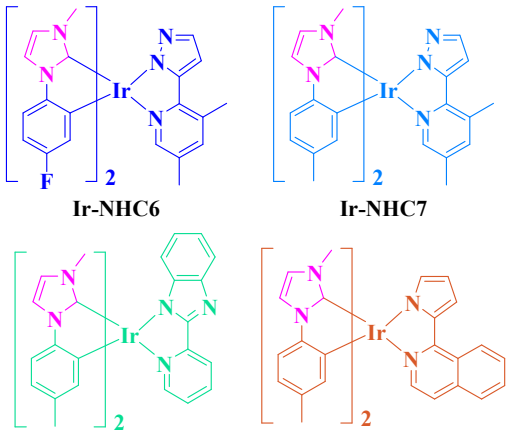

Fig. 95 Chemical structures of **Ir-NHC6** – **Ir-NHC9** and peak efficiency data of related OLEDs.

Table 9. Phosphorescent emitters with *N*-containing functional moieties and their peoperties

Main-group element unit	Metal center	Emitter	Φ_P	$\lambda_{max,em}$ nm	EQE %	CE cd A^{-1}	PE lm W^{-1}	Ref.
triphenylamine	**Pt**	**Pt-Am1**	0.07	540	8.50	29.7	19.7	267
triphenylamine	**Pt**	**Pt-Am4**	0.99	593	7.90	20.5	11.7	289
triphenylamine	**Pt**	**Pt-Am5**	0.019	639	8.46	4.15	–	288
triphenylamine	**Pt**	**Pt-Am6**	0.18	540	3.36	9.55	2.31	280
triphenylamine	**Pt**	**Pt-Am7**	0.17	568	8.3	23.0	17.0	282
triphenylamine	**Pt**	**Pt-Am9**	0.58	621	19.5	–	25.5	284
triphenylamine	**Pt**	**Pt-Am10**	0.58	620	19.3	–	30.3	284
triphenylamine	**Ir**	**Ir-Am1**	0.14	533	10.3	36.9	28.6	31
triphenylamine	**Ir**	**Ir-Am2**	0.13	528	13.9	60.8	49.0	276
triphenylamine	**Ir**	**Ir-Am4**	0.12	571	14.8	40.0	35.9	288
triphenylamine	**Ir**	**Ir-Am6**	0.12	555	9.89	29.8	20.8	289
triphenylamine	**Ir**	**Ir-Am7**	0.21	551	7.04	21.4	2.92	280
triphenylamine	**Ir**	**Ir-Am9**	0.29	561	16.4	40.9	39.5	286
triphenylamine	**Ir**	**Ir-Am10**	0.42	608	15.3	–	–	290
triphenylamine	**Ir**	**Ir-Am11**	0.60	537	15.1	43.8	20.5	291
triphenylamine	**Ir**	**Ir-Am12**	0.40	562	15.6	38.9	38.3	286
triphenylamine	**Ir**	**Ir-Am14**	0.13	636	11.6	5.82	3.65	32
triphenylamine	**Ir**	**Ir-Am15**	0.12	641	7.36	3.72	2.29	32
triphenylamine	**Ir**	**Ir-Am16**	0.62	633	15.2	14.9	10.0	285
triphenylamine	**Au**	**Au-Am1**	–	620	5.50	17.6	14.5	293
triphenylamine	**Au**	**Au-Am2**	0.0085	669	11.5	37.4	26.2	294
triphenylamine	**Au**	**Au-Am3**	0.03	612	0.92	1.04	0.50	295
triphenylamine	**Au**	**Au-Am4**	0.07	685	3.62	3.32	3.47	295
triphenylamine	**Au**	**Au-Am5**	0.03	685	2.33	2.76	2.16	295
triphenylamine	**Au**	**Au-Am6**	0.003	695	7.8	24.0	14.5	296
triphenylamine + carbazole	**Au**	**Au-Am7**	0.10	646	7.0	21.9	16.4	296
triphenylamine + carbazole	**Au**	**Au-Am8**	0.01	620	3.8	11.4	9.60	296
carbazole	**Pt**	**Pt-Cz1**	0.19	560	13.1	35.8	25.0	298
carbazole	**Pt**	**Pt-Cz2**	0.16	493	1.99	5.94	1.44	298
carbazole	**Pt**	**Pt-Cz5**	–	585	9.76	28.1	9.91	300
carbazole	**Pt**	**Pt-Cz6**	–	592	6.63	17.1	5.11	300
carbazole	**Pt**	**Pt-Cz7**	0.86	553	–	74.9	52.1	301
carbazole	**Pt**	**Pt-Cz8**	0.85	449	25.2	–	–	302
carbazole	**Pt**	**Pt-Cz9**	0.89	452	23.7	–	–	302
carbazole	**Pt**	**Pt-Cz10**	0.40	586	12.5	–	–	303
carbazole	**Ir**	**Ir-Cz1**	0.02	594	7.35	12.2	4.63	298
carbazole	**Ir**	**Ir-Cz2**	0.22	511	11.0	31.6	19.0	298
carbazole	**Ir**	**Ir-Cz3**	0.43	515	11.6	38.0	24.0	308

carbazole	**Ir**	**Ir-Cz4**	0.43	515	12.9	43.4	33.4	309
carbazole	**Ir**	**Ir-Cz5**	0.54	504	12.0	40.0	8.50	310
carbazole	**Ir**	**Ir-Cz10**	0.20	622	5.00	3.30	1.30	311
carbazole	**Ir**	**Ir-Cz11**	0.66	580	12.0	31.0	19.0	313
carbazole	**Ir**	**Ir-Cz12**	0.69	476	15.3	31.3	28.9	314
pyrazole	**Pt**	**Pt-Az1**	0.013	520	6.50	–	4.20	315
pyrazole	**Pt**	**Pt-Az2**	0.96	475	31.1	–	50.0	20
triazole	**Pt**	**Pt-Az3**	0.98	480	20.5	–	79.2	327
triazole	**Pt**	**Pt-Az4**	0.02	507	–	15.2	7.01	329
triazole + tetrazole	**Pt**	**Pt-Az6**	0.003	532	5.6	15.5	16.4	330
triazole + tetrazole	**Pt**	**Pt-Az7**	0.05	528	4.9	13.4	13.8	330
imidazole	**Pt**	**Pt-Az8**	–	470	18.1	–	23.3	332
benzimidazole	**Pt**	**Pt-Az9**	0.19	506	11.5	38.9	27.2	318
benzimidazole	**Pt**	**Pt-Az10**	0.25	507	11.8	40.3	28.1	320
benzimidazole	**Pt**	**Pt-Az11**	0.15	530	10.0	34.7	26.4	320
imidazole	**Pt**	**Pt-Az12**	0.64	470	23.1	–	48.8	335
imidazole	**Pt**	**Pt-Az13**	–	490	26.5	69.8	61.4	333
imidazole + pyrazole	**Pt**	**Pt-Az14**	–	480	23.1	64.5	53.5	333
imidazole + pyrazole	**Pt**	**Pt-Az15**	–	476	26.7	80.3	68.3	333
imidazole	**Ir**	**Ir-Az3**	0.52	475	23.1	61.5	43.7	339
imidazole	**Ir**	**Ir-Az5**	0.62	474	33.2	73.6	71.9	341
benzimidazole	**Ir**	**Ir-Az6**	0.73	523	16.7	61.0	20.0	342
benzimidazole	**Ir**	**Ir-Az7**	0.72	524	10.2	10.2	–	342
triazole	**Ir**	**Ir-Az11**	0.73	471	4.6	–	–	321
triazole	**Ir**	**Ir-Az12**	0.76	468	7.9	–	–	321
triazole	**Ir**	**Ir-Az13**	0.59	468	2.1	–	–	321
N-heterocyclic carbene	**Pt**	**Pt-NHC1**	0.90	463	6.2	–	–	348
N-heterocyclic carbene	**Pt**	**Pt-NHC2**	–	448	15.7	–	22.0	332
N-heterocyclic carbene	**Pt**	**Pt-NHC4**	0.08	461	15.0	–	16.6	351
N-heterocyclic carbene	**Pt**	**Pt-NHC6**	0.58	442	4.10	–	3.70	302
N-heterocyclic carbene	**Pt**	**Pt-NHC6**	0.77	472	26.3	–	32.4	352
N-heterocyclic carbene	**Ir**	**Ir-NHC1**	0.002	389	5.8	–	1.7	355
N-heterocyclic carbene	**Ir**	**Ir-NHC2**	0.7	445	18.6	28.6	35.9	356
N-heterocyclic carbene	**Ir**	**Ir-NHC3**	0.73	458	6.0	6.3	4.0	358
N-heterocyclic carbene	**Ir**	**Ir-NHC4**	0.11	456	7.6	6.5	4.1	359
N-heterocyclic carbene	**Ir**	**Ir-NHC5**	0.18	471	15.2	28.1	19.6	359
N-heterocyclic carbene	**Ir**	**Ir-NHC6**	0.59	455	17.1	22.3	19.8	325
N-heterocyclic carbene	**Ir**	**Ir-NHC7**	0.42	466	15.4	21.9	19.1	325
N-heterocyclic carbene	**Ir**	**Ir-NHC8**	0.79	530	24.4	91.9	96.3	325
N-heterocyclic carbene	**Ir**	**Ir-NHC9**	0.55	599	24.9	55.4	43.6	325

4.4 Phosphorescent emitters bearing organic phosphine moieties

4.4.1 Phosphorescent emitters with diphenylphosphoryl groups

Due to its strong electron-deficient properties, diphenylphosphoryl group (Ph_2PO) has been widely used to synthesize ET materials,[360] hosts with EI/ET ability and bipolar host materials.[114] Therefore, incorporating Ph_2PO into Pt(II) and Ir(III) complexes will definitely confer some interesting properties to the resultant phosphorescent emitters, especially the EI/ET feature. Generally, the Ph_2PO group is used to tailor Pt(II) and Ir(III) complexes by attaching Ph_2PO on the HOMO-lying phenyl ring or the LUMO-lying *N*-containing heterocycle moiety of the ligands.[31, 276, 361] Introduction of electron-withdrawing group into the HOMO-lying phenyl ring will blue-shift the emission spectra and attachment of electron-withdrawing group on the LUMO-lying *N*-containing heterocycle moiety will cause red-shift of the emission spectra.[28] However, for these complexes bearing Ph_2PO group, the emissions are red-shifted by introducing Ph_2PO into whether the HOMO-lying phenyl ring or the LUMO-lying *N*-containing heterocycle moiety. For example, the emission peak of **Pt-PO1** (λ_{em} = 500 nm)[267] (Fig. 96) is red-shifted by 19 nm as compared to that of **(ppy)Pt(acac)** (λ_{em} = 481 nm),[362] **Pt-PO2** displays phosphorescent emission in the deeper red region than **Pt-PVP** (646 nm for **Pt-PO2** vs 629 nm for **Pt-PVP**) (Table 10),[274] and the emission peaks of **Ir-PO1** (λ_{em} = 541 nm)[31] and **Ir-PO4** (λ_{em} = 564 nm)[361] are red-shifted by *ca.* 25 nm and 48 nm, respectively, relative to that of **$(ppy)_2$Ir(acac)** (λ_{em} = 516 nm) (Table 10).[28] This phenomenon can be attributed to the larger influence on the LUMO level than HOMO level by introducing Ph_2PO into either the HOMO-lying phenyl ring or the LUMO-lying *N*-containing heterocycle moiety. The LUMO level is significantly reduced by the introduction of Ph_2PO, leading to the narrower energy

gap and thereby red-shifted emission. Therefore, the emission color can be tuned from green (**Pt-PO1**) to red (**Ir-PO5**). Besides, the reduced LUMO level will facilitate the EI/ET properties in related OLEDs. Devices based on these Ph_2PO-containing complexes show good EL performance. A yellow-emitting device based on **Ir-PO4** can ensure high EQE of 14.5% and PE of 27.0 lm W^{-1} at 6 V. Furthermore, the distribution of the LUMO is shifted from the ancillary ligand in FIrpic to the Ph_2PO substituted pyridyl moiety in **Ir-PO3**, indicating the potential of using Ph_2PO to change the excited state properties of the resultant complexes.

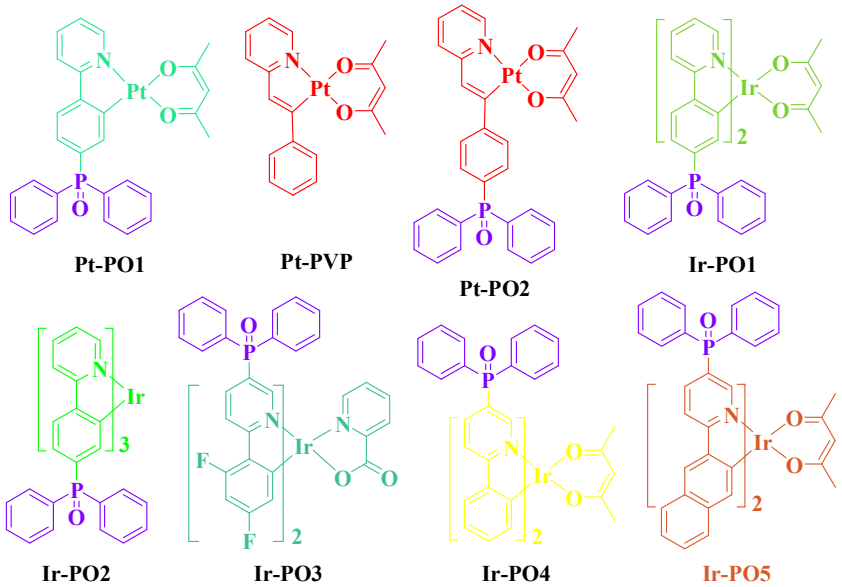

Fig. 96 Chemical structures of Ph_2PO based Pt(II) and Ir(III) complexes and peak efficiency data of the related OLEDs.

4.4.2 Phosphorescent emitters directly chelated with organic phosphine

Due to the lone pair electrons of the sp^3-hybridized phosphorus atom, phenylphosphine groups can directly bond to the transition metal ions, such as Pt(II),[363-365] Ir(III),[366-368] Os(II),[37] *etc.*, to generate strong metal-phosphorus bonds. The saturated character of phenylphosphine group will

keep the electronic transition dipole around the conventional cyclometallating ligand, that is, the contributions from phenylphosphine group to the MOs are greatly suppressed. Therefore, ligands containing phenylphosphine group are usually used as auxiliary ligands in the design of phosphorescent emitters. However, the strong ligand field strength of the phenylphosphine ligand can destabilize the metal-centered d-d excited state and thus suppress the negative influence of metal-centered d-d transition.[369]

Song *et al.* reported a Pt(II) complex **Pt-P1** (Fig. 97) which contained the deprotonated 2-(diphenylphosphino)benzoic acid as auxiliary ligand.[370] This complex adopts a square-planar coordination geometry, similar to the conventional ppy-type Pt(II) complexes. However, the bulky auxiliary ligand can effectively avoid the Pt···Pt interactions as confirmed by the long Pt–Pt distance (9.37 Å) in the crystal of **Pt-P1**. The theoretical calculations also reveal that the HOMO and LUMO have no contribution from this auxiliary ligand, which is consistent with the fact that the emission spectrum of **Pt-P1** is similar to that of **(ppy)Pt(acac)**. However, the PLYQ of **Pt-P1** (Φ_P = 0.18) is slightly higher than that of **(ppy)Pt(acac)** (Φ_P = 0.15) (Table 10). A green-emitting device using **Pt-P1** as emitter gives EQEs of 4.93% for peak value and 4.06% at 1000 cd m^{-2}, indicating that phenylphosphine-type ligand is a good alternative of acac auxiliary ligand.

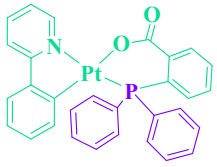

Pt-P1

EQE 4.93 %; PE 14.6 lm W^{-1}

Fig. 97 Chemical structure of **Pt-P1** and peak efficiency data of the related OLED.

Chi *et al.* have done much work on Ir(III) complexes comprising the phenylphosphine moieties

as ligand chelates. These complexes usually consist of two pyridylphenyl-type or pyridylazole-type cyclometallating ligands and one phenylphosphine-containing auxiliary ligand. In order to limit the π-conjugation of the auxiliary ligand and thereby increase the ligand-centered π–π* energy gap, the phenylphosphine moiety is always linked to the phenyl ring or azole ring via a methylene unit or O atom to generate a non-conjugated ancillary phosphine chelate. Therefore, a rigid and stable five-membered metal-chelate bonding interaction is formed when the non-conjugated ancillary phosphine chelate is used to construct Ir(III) complexes. Complexes **Ir-P1** and **Ir-P2** (Fig. 98) have quite similar structures despite the fact that the benzyl moiety in **Ir-P2** substituted by two fluorine atoms slightly blue-shifts the emission peak of 461 nm for **Ir-P1** to 458 nm for **Ir-P2** (Table 10).[371] The theoretical study shows that the HOMO and LUMO have no contribution from the diphenylphosphine moiety. Although the Φ_P of **Ir-P1** and **Ir-P2** are very low (< 0.02) in solutions, but they can be dramatically increased up to 0.58 when **Ir-P2** is doped into **UGH2**. The device based on **Ir-P2** achieves a high peak EQE of 11.9% with a pure blue CIE coordinates of (0.152, 0.110), signaling the advantages of using the non-conjugated, high ligand-field strength benzyl phosphine chelates to synthesize pure blue-emitting Ir(III) complexes. When the phenyl ring in the auxiliary ligand is replaced by an azole moiety, the emission peak of 461 nm for **Ir-P1** is slightly blue-shifted to 458 nm for **Ir-P3** (Table 10).[369] Besides, the Φ_P of **Ir-P3** is slightly increased to 0.024. A blue-emitting device using **Ir-P3** as emitter gives acceptable CIE coordinates of (0.163, 0.145) with a lower peak EQE of 6.9%, which may be attributed to the lower Φ_P of the **Ir-P3** doped **UGH2** film (Φ_P = 0.25). When the cyclometallating ligands, 5-(2-pyridyl)-3-trifluoromethylpyrazole, in **Ir-P3** are changed to 2-phenylpyridyl type ligands, a strong emission peak appears at 488 nm for **Ir-P4**,

and the Φ_P is also significantly increased to 0.72 (Table 10).[369] As a result, the device based on **Ir-P4** realizes an improved peak EQE of 12.6%, but its CIE coordinates of (0.154, 0.215) are beyond the pure blue region. From these results, it can be seen that the emission properties of these Ir(III) complexes are mainly decided by the cyclometallating ligands. However, the diphenylphosphine-based auxiliary ligands can also play the critical role in tuning the phosphorescent features of the concerned Ir(III) complexes. This situation is also consistent with the observations for **Ir-P5** and **Ir-P6**.[367] The emissions and Φ_P of **Ir-P5** and **Ir-P6** are similar in solutions (Table 10), but much different from those of **Ir-P1** due to the different cyclometallating ligands. The emission color of the device based on **Ir-P5** is red-shifted to the sky-blue region with $CIE_x > 0.2$ and $CIE_y > 0.4$ in the range from 100 cd m^{-2} to 10000 cd m^{-2}. However, this device achieves much higher efficiencies of 17.8% and 46.3 lm W^{-1} for peak EQE and PE. Considering the high efficiencies of the sky-blue device based on **Ir-P5**, a two-color WOLED is fabricated using **Ir-P5** as the blue emitter and a phenylphosphine chelated Os(II) phosphor as the orange-red emitter. The resultant device emits warm white light with very high peak EQE of 18.4% and PE of 35.7 lm W^{-1}.

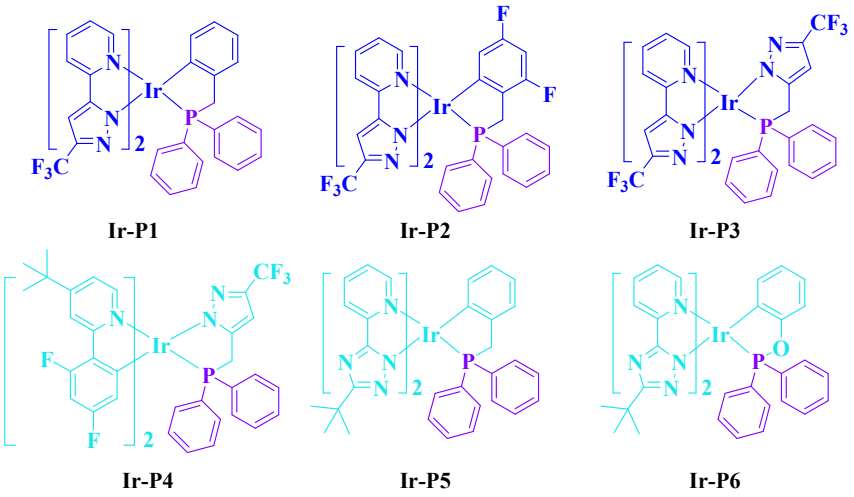

Ir-P2; EQE 11.9 %; CE 11.4 cd A^{-1}; PE 7.90 lm W^{-1}; CIE (0.152, 0.110)
Ir-P3; EQE 6.90 %; CE 8.10 cd A^{-1}; PE 4.90 lm W^{-1}; CIE (0.163, 0.145)
Ir-P4; EQE 12.6 %; CE 20.3 cd A^{-1}; PE 12.6 lm W^{-1}; CIE (0.154, 0.215)
Ir-P5; EQE 17.8 %; CE 44.8 cd A^{-1}; PE 46.3 lm W^{-1}; CIE (0.207, 0.440)

Fig. 98 Chemical structures of **Ir-P1** – **Ir-P6** and peak efficiency data of related OLEDs.

From the abovementioned examples, it can be seen that the electronic transition dipoles are usually maintained around the conventional cyclometallating ligands due to the higher ligand-centered π–π* energy gaps of the phenylphosphine-based auxiliary ligands, which results from the effectively interrupted π-conjugation by the methylene units. However, the methylene unit is an active site which can be oxidized to carbonyl group, as observed in some Ru(II) complexes.[372, 373] Therefore, other strategy should be carried out to break the π-conjugation of the phenylphosphine-based auxiliary ligand. It seems that O atom can be a good candidate as evidenced by **Ir-P6** (Fig. 99) which even shows a slightly blue-shifted emission as compared to **Ir-P5**.[367] Therefore, a series of Ir(III) complexes were designed which consist of a tripodal, facially coordinated phosphite ancillary ligand, a 2-pyridylazolate ligand acting as the blue chromophore, and a monodentate phosphine ligand.[374] These complexes display similar blue emission bands in

solutions. But their Φ_P vary from 0.01 to 0.87 depending on the the Ir-P bond strength. The short Ir-P bond length between the monodentate phosphine ligand PMe_2Ph and Ir(III) center endows **Ir-P7** with high Φ_P of 0.45. As a result, the device based on **Ir-P7** gives a high peak EQE of 11.0%. As for **Ir-P8** and **Ir-P9**, they display slightly lower Φ_P below 0.25 in solutions (Table 10). Devices based on **Ir-P8** and **Ir-P9** also give inferior efficiencies with peak EQEs below 9%. However, the changes of CIE coordinates upon increasing the luminance from 100 cd m^{-2} to 1000 cd m^{-2} are tiny for devices based on **Ir-P8** and **Ir-P9**, but notable for the device based on **Ir-P7**, which can be attributed to the fact that replacing phenoxy (in **Ir-P7**) with phenyl fragment (in **Ir-P8** and **Ir-P9**) and introducing additional ET pyridyl fragment in **Ir-P9** may better match the energy levels between dopant and ET/HT materials.[374] Besides the choice of using phenoxy unit to replace the benzyl group in the phenylphosphine-based auxiliary ligand, 1-(diphenylphosphino)naphthalene and isoquinoline are also suitable to form stable five-membered metallacycles by the C–H activation at the 8-position of both naphthalene and isoquinoline moieties. The resultant Ir(III) complexes **Ir-P10** and **Ir-P11** display intense phosphorescence with Φ_P as high as *ca.* 1.0 (Table 10).[375] The theoretical calculation results show that the diphenylphosphine moieties make no contributions to the HOMOs as well as LUMOs, but the naphthalene and isoquinoline moieties make notable contributions to the HOMOs of **Ir-P10** and **Ir-P11**, indicating that the electronic transitions in these complexes involve the 1-(diphenylphosphino)naphthalene and isoquinoline ligands. Besides, due to the extended conjugation of isoquinoline, the π-π* energy gap of 5-(1-isoquinolyl)-3-*tert*-butyl-1,2,4-triazole is effectively reduced, leading to the low energy emission in the orange region. Nevertheless, devices based on **Ir-P10** and **Ir-P11** produce high efficiencies with peak EQEs above 15% and PEs over 37

lm W^{-1}.

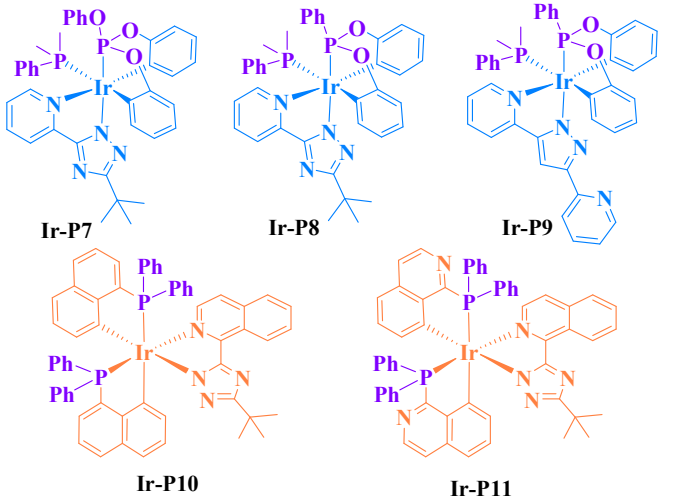

Ir-P7; EQE 11.0 %; CE 22.3 cd A^{-1}; PE 16.7 lm W^{-1}; CIE (0.179, 0.286)
Ir-P8; EQE 8.40 %; CE 17.3 cd A^{-1}; PE 13.2 lm W^{-1}; CIE (0.173, 0.303)
Ir-P9; EQE 8.70 %; CE 14.3 cd A^{-1}; PE 10.8 lm W^{-1}; CIE (0.169, 0.247)
Ir-P10; EQE 17.1 %; CE 47.0 cd A^{-1}; PE 49.3 lm W^{-1}
Ir-P11; EQE 15.0 %; CE 42.6 cd A^{-1}; PE 37.0 lm W^{-1}

Fig. 99 Chemical structures of **Ir-P7** – **Ir-P11** and peak efficiency data of related OLEDs.

Chi *et al.* have also done much work on the neutral osmium(II) complexes containing phenylphosphine groups as monodentate or bidentate ligand.[260, 376-378] Os(II) complexes consisting of monodentate phenylphosphine ligands usually emit red light due to the strong interaction between the Os(II) ion and phenylphosphine group, which can increase the entire transition dipole moment as well as lead to significant red shift due to the enhancement of dative interactions with Os(II).[376] For example, the emission peak of **Os-P2** (λ_{em} = 632 nm) (Fig. 100) is red-shifted as compared to that of **Os-P1** (λ_{em} = 617 nm) due to the stronger electron-donating ability of $PPhMe_2$ ligand than that of PPh_2Me ligand (Table 10). **Os-P3** shows further red-shifted emission peak at 649 nm in solution because of the stronger donor strength of 3-(*tert*-butyl)-5-(2-pyridyl)triazole (bptzH) ligand in **Os-P3** than that of 3-(trifluoromethyl)-5-(2-pyridyl)pyrazole (fppzH) ligand in **Os-P1** (Table 10).[36]

Therefore, the donor strengths of the ligands in these Os(II) complexes show pronounced effects on λ_{em}. **Os-P4** gives the emission peak (λ_{em} = 617 nm) similar to **Os-P1**, but a higher Φ_P (0.62 for **Os-P4** vs 0.50 for **Os-P1** and 0.19 for **Os-P2**) in solution (Table 10), indicating that the donor strengths of the ligands also greatly influence the emission efficiency.[379] By extending the π-conjugation of the cyclometallating ligand, the near-infrared (NIR) emission at 805 nm can even be realized for **Os-P5**.[380] High performance devices can be obtained by using these complexes as triplet emitters. For instance, devices based on **Os-P2** and **Os-P4** achieve very high peak EQEs of 12.8% and *ca.* 20.0%, respectively.[379, 381] Besides, at 20 mA cm^{-2}, the performance of the device based on **Os-P4** still remains attractive in terms of high EQE of 15.3% and CE of 21.3 cd A^{-1}. The device using **Os-P5** as emitter displays NIR emission at 814 nm with EQE of 1.5%, demonstrating the possibility of using Os(II) complexes to fabricate NIR OLEDs. Very recently, the Os(II) complex **Os-P6** which contains a tridentate pyridylazole-based ligand, a monodentate phenylphosphine ligand and a carbonyl ligand was reported to emit yellow light (λ_{em} = 568 nm) with high Φ_P of 0.66 in solution (Table 10).[11] A yellow-emitting device based on **Os-P6** offers a high maximum EQE of 18.3% and PE of 53.8 lm W^{-1}. Besides, a warm white-emitting OLED can be fabricated by using FIrpic, **Os-P6** and **Os-P7** (red emission)[382] as emitters. The resulting device shows attractive efficiencies of 18.0% and 31.2 lm W^{-1} for peak EQE and PE, respectively. Chi *et al.* also designed a tetradentate ligand in which two fppzH chelates are connected by a phenylamino moiety through the 6 position of the pyridyl fragment in fppzH.[378] By cooperating with two monodentate phenylphosphine ligand, this tetradentate ligand can stabilize the Os(II) ion to form efficient red phosphorescent emitter **Os-P8** (λ_{em} = 628 nm, Φ_P = 0.40) (Table 10). The device based on this tetradentate Os(II) complex exhibits

decent performance with a peak EQE of 9.8% and CE of 14.0 cd A^{-1}, which are much higher that that of the reference device using $Ir(piq)_3$ as emitter, indicating the superior EL property of **Os-P8**.

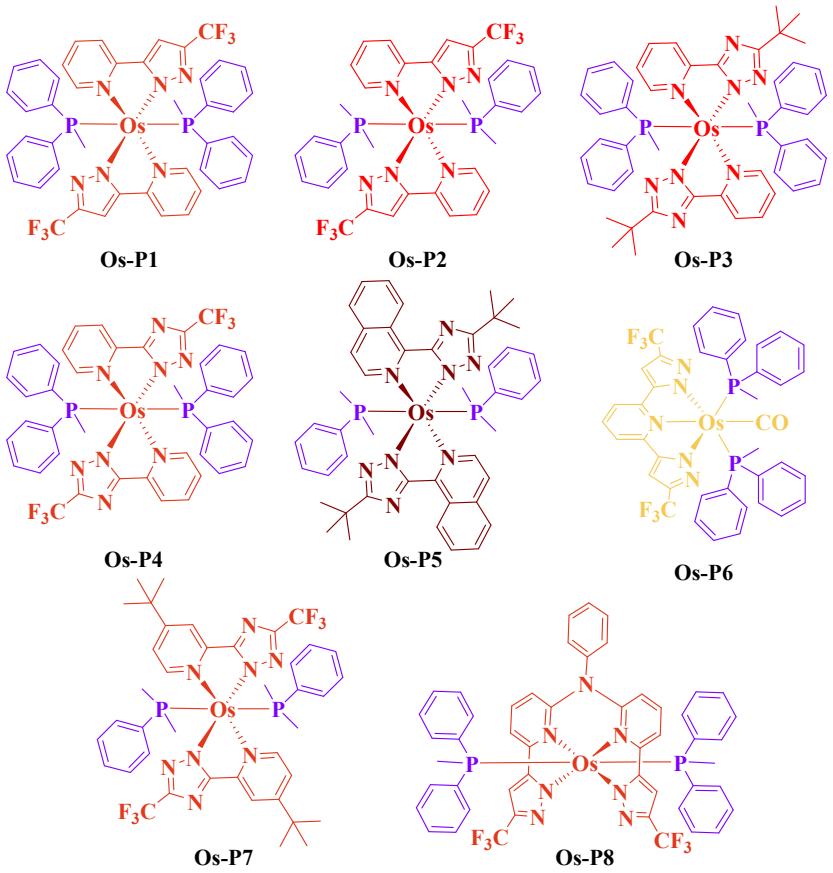

Fig. 100 Chemical structures of **Os-P1** – **Os-P8** and peak efficiency data of related OLEDs.

Apart from the above Os(II) complexes which contain one or two monodentate phenylphosphine ligands in one molecule, Chi *et al.* also developed a lot of Os(II) complexes bearing bidentate ligand including bis(diphenylphosphino)methylene (dppm), *cis*-1,2-bis-(diphenylphosphino)ethene (dppee), 1,2-bis(diphenylphosphino)benzene (dppb), 1,2-bis(dimethylphosphino)benzene (dmpb) and 1,2-bis(phospholano)benzene (pp2b).[251, 377, 380] The resultant Os(II) complexes are more stable than

those containing monodentate phenylphosphine ligands, which mainly results from the improved bonding interaction between the Os(II) ion and chelating phosphines. Furthermore, the emission color of these bidentate phosphine based Os(II) complexes can be tuned in a wider range from green to deep-red by changing the azole chelates. Complex **Os-P10** (λ_{em} = 584 nm) (Fig. 101) shows a slightly blue-shifted emission with respect to **Os-P9** (λ_{em} = 586 nm) (Table 10) because of the more electron-withdrawing *cis*-ethene group in **Os-P10** relative to the methylene linker in **Os-P9**, while complex **Os-P11** (λ_{em} = 572 nm) exhibits blue-shifted emission as compared to **Os-P10** (λ_{em} = 584 nm) due to the weaker donor strength of the 3-(trifluoromethyl)-5-(2-pyridyl)triazole ligand relative to 3-(trifluoromethyl)-5-(2-pyridyl)pyrazole ligand.[36, 377] Due to the extended π-conjugation of isoquinolyl moiety, **Os-P12** emits deep-red light with emission peak at 690 nm. From the emission behaviors of **Os-P9** to **Os-P12**, it is clear that by increasing the donor strength of either the diphosphine ligand or the azole ligand, the emission wavelength is red-shifted, which is consistent with the observations in the monodentate phenylphosphine chelate based Os(II) complexes. This situation is also supported by **Os-P13** (λ_{em} = 618 nm) (Table 10) which displays a red-shifted emission as compared to **Os-P9** and **Os-P10**, because the tetramethylene fragment on phosphole would produce electron-donating character so as to enhance the donor strength of pp2b ligand.[251] Compared to pp2b ligand, dppb ligand shows less electron-donating character because of the two phenyl rings. In addition, the imidazolyl group possesses high electron density, which significantly raises the the π-π* energy of the ligand. Both factors cause blue-shift effects on Os(II) complexes. Hence, **Os-P14** displays green emission with a peak at 538 nm (Table 10).[260] Besides the significant influence on the emission color, these ligands also greatly affect the Φ_P of Os(II) complexes. The Φ_P of these Os(II) complexes vary

from less than 0.01 to 0.95 in solutions. However, in vacuum deposited solid films or doped thin films, almost all these Os(II) complexes can show high Φ_P more than 0.5 due to the suppressed structural distortions or related energy stabilizations of the quenching states in a rigid environment. Therefore, these Os(II) complexes are promising for fabricating highly efficient PHOLEDs. The solution-processed device based on **Os-P11** shows a EL peak at 562 nm with a high maximum EQE of 13.3%. An orange-red device using **Os-P13** as dopant can give a peak EQE of 14.3% and PE of 45.2 lm W^{-1}. As for the green-emitting **Os-P14**, the pertinent solution-processed device shows maximum EQE of 15.6% and PE of 50.9 lm W^{-1}. These results unambiguously demonstate the unique roles played by the bidentate phenylphosphine chelates in tuning phosphorescent characters of Os(II) complexes for fabricating green-to-red OLEDs with high efficiencies.

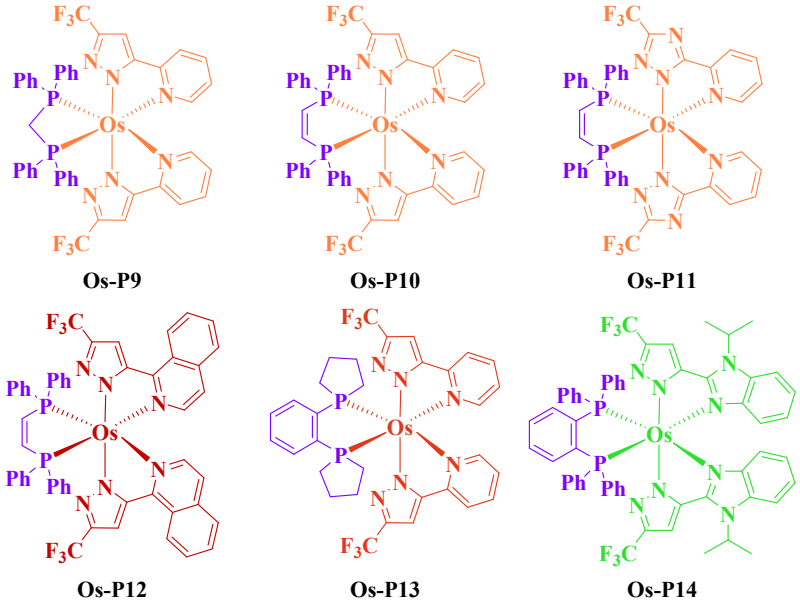

Fig. 101 Chemical structures of **Os-P9** – **Os-P14** and peak efficiency data of related OLEDs.

Locating in the same group as osmium, the second-row ruthenium complexes have also been

used as emitters for OLEDs.[13, 383-385] The early developed Ru(II) complexes are usually charged. Therefore, the devices based on these cationic Ru(II) complexes give relatively low efficiencies due to the inferior charge transporting efficiency induced by the ion-pair structure.[386-388] Hence, rational design of charge neutral Ru(II) complexes for OLEDs is highly desired. Chi *et al.* synthesized a series of neutral Ru(II) complexes bearing azole ligands and mono-/bidentate phenylphosphine chelates.[384, 385] The strong-field phosphine ancillary ligands are used to increase the energy gap of the metal centered d-d transition and thereby suppress the radiationless deactivation associated with metal–metal and/or metal–ligand stretching vibrations. As a result, the Φ_P of these Ru(II) complexes can reach 0.24 in the solid state at room temperature. In addition, the emission color of these Ru(II) complexes can be tuned from yellow to deep-red by changing the azole ligand. For example, **Ru-P1** (Fig. 102) emits yellow light with a peak at 568 nm in the solid state, while **Ru-P2** shows orange-red emission at 571 nm and 589 nm, and the emission peak is shifted to 632 nm for **Ru-P3** (Table 10). Among these Ru(II) complexes, **Ru-P3** gives the highest Φ_P of 0.21 in the solid state and can be used as emitter to fabricate red OLEDs. The pertinent device with a configuration of ITO/NPB (40 nm)/**CBP**:24% **Ru-P3** (30 nm)/BCP (10 nm)/AlQ_3 (30 nm)/Mg:Ag (10:1) (50 nm) shows the EQE of 5.1% at a current density of 20 mA cm^{-2}. The EQE (at 20 mA cm^{-2}) is further improved to 7.03% by the incorporation of a thin layer of poly(styrene sulfonate)-doped poly(3,4-ethylenedioxythiophene) (PEDOT:PSS) to improve the surface smoothness and to serve as a HI layer.[384] The performance of the device based on neutral **Ru-P3** is superior to those of devices based on cationic Ru(II) complexes, indicating the advantages of using neutral Ru(II) complexes as emitters to develop OLEDs. However, the efficiencies of Ru(II) complex based devices are still inferior to those of the devices based on

Os(II) analogues, and the relatively low Φ_P of Ru(II) complexes (vs Os(II) analogues) are presumably one reason for this situation. Therefore, further work can be done to design and synthesize neutral Ru(II) complexes with high Φ_P for application in high efficiency PHOLEDs.

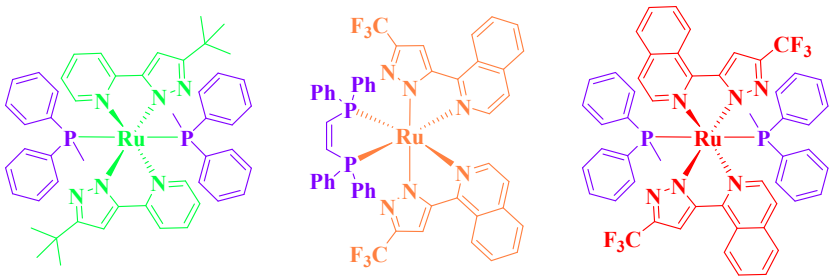

Fig. 102 Chemical structures of **Ru-P1 – Ru-P3** and peak efficiencies of related OLED.

Emissive copper(I) complexes have drawn increased attention in the OLED community because of their high Φ_P as well as much cheaper prices as compared to other transition metal complexes such as Ir(III), Pt(II), Os(II), *etc.*[389-393] To date, most of the Cu(I) complexes used as emitters in OLEDs have a distorted tetrahedral geometry around the Cu(I) atoms bearing a diimine ligand and an ancillary diphosphine ligand. The rigid ancillary diphosphine ligand can effectively suppress the non-radiative pathways and thereby increase Φ_P. Besides, the emission color can also be fine-tuned by modifying the diphosphine ligand. The theoretical calculations on **Cu-P1** and **Cu-P2** (Fig. 103) reveal that the electron density in the HOMO is mainly distributed on the Cu and P atoms, while the LUMO is dominantly localized on the π*-antibonding orbital of diimine ligands.[394, 395] Complexes **Cu-P1** and **Cu-P2** have the same diphosphine ligands but different chromophoric diimine ligands, thus the emissions of **Cu-P1** and **Cu-P2** are different in CH_2Cl_2 solutions (540 nm for **Cu-P1** and 560 nm for **Cu-P2**) (Table 10).[394, 396] Besides, in the solid state, the emissions of both **Cu-P1**

(crystalline powder, λ_{em} = 492 nm) and **Cu-P2** (5 wt% doped PMMA film, λ_{em} = 509 nm) are blue-shifted by *ca.* 50 nm from their respective spectra in a CH_2Cl_2 solution, indicating that the excited state geometry is quite different from the ground state geometry, *i.e.*, involving reorganization from tetrahedral (ground state) to a square-planar geometry (excited state).[394, 395] In addition, it is reported that at room temperature the emission of **Cu-P1** originates from the singlet state which has the contribution from the triplet state *via* reverse intersystem crossing effect,[394] while the ^{3}CT states must be the predominant population excited states among the low-lying excited states in **Cu-P2**,[395] indicating that the chromophoric diimine ligands possess vital influence on the emission nature of Cu(I) complexes. However, in spite of the different sources of their emissions, both **Cu-P1** (crystalline powder) and **Cu-P2** (10 wt% doped 2,6-bis(*N*-carbazolyl)pyridine (26mCPy) film) exhibit high Φ_P values of over 0.5. Devices with the structure of ITO/PEDOT:PSS (40 nm)/20 wt% of **Cu-P1** or 10 wt% of **Cu-P2**:26mCPy (30 nm)/ bis[2-(di-(phenyl)phosphino)-phenyl]ether oxide (DPEPO, 50 nm)/LiF/Al give encouraging performance. The **Cu-P1** based device shows green emission at *ca.* 508 nm with a peak EQE of 8.47 %, while the **Cu-P2** based device with EL at *ca.* 507 nm can produce a maximum EQE of 15.0% with CE of 49.5 cd A^{-1}, which are comparable to those of **Ir(ppy)$_3$** based device.

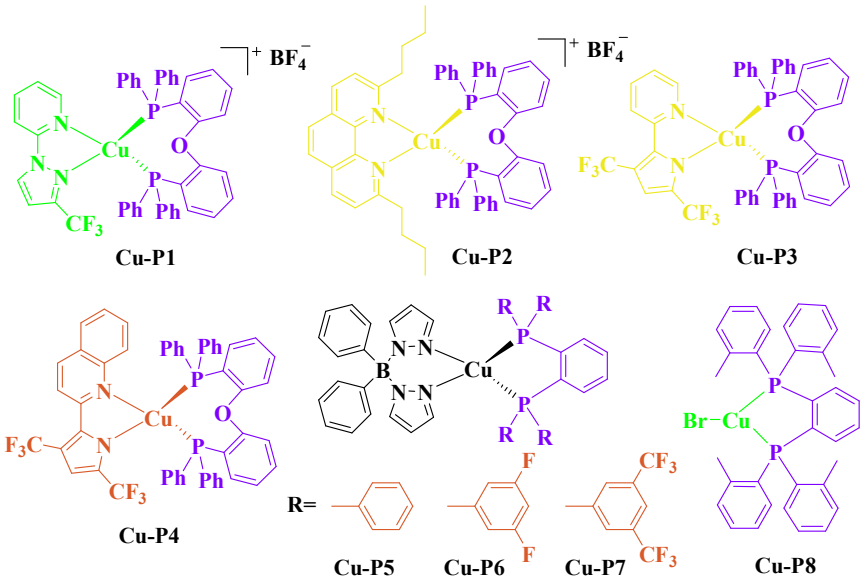

Cu-P1; EQE 8.47 %; CE 23.7 cd A^{-1}
Cu-P2; EQE 15.0 %; CE 49.5 cd A^{-1}; PE 22.3 lm W^{-1}
Cu-P3; EQE 6.60 %; CE 20.0 cd A^{-1}; PE 14.9 lm W^{-1}
Cu-P7; EQE 17.7 %; CE 54.1 cd A^{-1}
Cu-P8; EQE 21.3 %; CE 65.3 cd A^{-1}

Fig. 103 Chemical structures of **Cu-P1 – Cu-P 8** and peak efficiency data of related OLEDs.

Neutal Cu(I) complex **Cu-P3** shows yellow emission (λ_{em} = 559 nm) with a decent Φ_P of 0.34 in degassed CH_2Cl_2 solution at room temperature, while **Cu-P4** emits orange-red light (λ_{em} = 603 nm) with a Φ_P of 0.12 under the same condition (Table 10).[397] The red-shifted emission of **Cu-P4** is due to the elongation of π-conjugation provided by the quinolinyl fragment, indicating that the emission color is significantly affected by the diimine ligand. In addition, similar to the cases of **Cu-P1** and **Cu-P2**, **Cu-P3** and **Cu-P4** also exhibit rigidochromism behaviors, *i.e.*, the emission peaks of **Cu-P3** and **Cu-P4** are blue-shifted by > 50 nm in the solid state at room temperature. Therefore, the device based on **Cu-P3** displays green EL, similar to the observation of **Cu-P1** and **Cu-P2** based devices which also show blue-shifted EL emissions as compared to the PL emissions of **Cu-P1** and **Cu-P2** in solutions. A non-doped device based on **Cu-P3** can give a peak EQE of 7.8% and CE of 23.2 cd A^{-1},

but the efficiencies drastically drop to 0.5% and 1.4 cd A^{-1}at 100 cd m^{-2}. However, the EQE of **Cu-P3** based device at a 8 wt% dopant level is 6.6% for the peak value and decreases to 3.8% at 100 cd m^{-2}, indicating that the host-guest emissive system is indispensable for the **Cu-P3** based device. Complexes **Cu-P5**, **Cu-P6** and **Cu-P7** all display weak red emissions in 2-MeTHF at 293 K, but intense green emissions at 77 K due to the rigidochromic effect.[398] By introducing electron-withdrawing F and CF_3 groups into the diphosphine ligands, the emission peaks are blue-shifted from 524 nm at 77 K for **Cu-P5** to 510 nm and 494 nm of **Cu-P6** and **Cu-P7**, respectively (Table 10). It shows that modification of the diphosphine ligands can fine-tune the emission wavelength of pertinent Cu(I) complexes, since the diphosphine ligands also make contributions to the MOs. Besides, the Φ_P of **Cu-P5**, **Cu-P6** and **Cu-P7** are greatly increased to 0.84, 0.88 and 0.93 at 77 K, respectively. Devices based on **Cu-P5**, **Cu-P6** and **Cu-P7** display very attractive performance with peak EQEs above 11% and CEs exceeding 30 cd A^{-1}. Especially, the green-emitting device based on **Cu-P7** gives remarkably high maximum EQE of 17.7% and CE of 54.1 cd A^{-1}.

From the above examples, it can be seen that four-coordinate Cu(I) complexes show quite different emission properties between solution and solid states because of the rearrangement from a tetrahedral to a square-planar geometry when excited by photon or electrical energy. However, some three-coordinate Cu(I) complexes reported by Osawa *et al.* show little structural change between the ground and excited states as indicated by the small blue-shift from solution emission to solid state emission.[399] These three-coordinate Cu(I) complexes contain a bis(phosphine) ligand and a halogen atom (X = Cl, Br and I). The *o*-methyl groups on bis(phosphine) ligand are critical in determining the

formation of three-coordinate Cu(I) complexes due to its high steric hindrance effect, otherwise only the halogen-bridged binuclear copper complexes are obtained.[400, 401] Furthermore, the steric hindrance induced by the *o*-methyl groups on bis(phosphine) ligand may also be responsible for the little distortion in the excited states of the three-coordinate Cu(I) complexes to furnish high Φ_P exceeding 0.4 in CH_2Cl_2 solutions. The green-emitting device (λ_{em} = 517 nm) using **Cu-P8** as emitter displays prominent performance with peak EQE as high as 21.3% and CE of 65.3 cd A^{-1}, which are comparable to those of the devices based on efficient Ir(III) complexes. This device represents the best performance achieved for Cu(I) complexes based OLEDs so far. This result demonstrates that the judiciously designed bis(phosphine) ligand can show great potential in optimizing the EL performance of the low-cost three-coordinate Cu(I) complexes, which will encouragingly prompt the researchers to develop more efficient Cu(I) complex emitters for OLEDs.

Table 10. Phosphorescent emitters bearing organic phosphine moieties and their properties

Main-group element unit	Metal center	Emitter	Φ_P	$\lambda_{max,em}$ nm	EQE %	CE cd A^{-1}	PE lm W^{-1}	Ref.
diphenylphosphine oxide	**Pt**	**Pt-PO1**	0.93	500	7.9	22.1	13.4	267
diphenylphosphine oxide	**Pt**	**Pt-PO2**	0.08	646	1.2	6.9	2.21	274
diphenylphosphine oxide	**Ir**	**Ir-PO1**	0.19	541	3.49	11.9	2.4	31
diphenylphosphine oxide	**Ir**	**Ir-PO4**	0.20	564	14.5	51.6	27.0	361
phenylphosphine	**Pt**	**Pt-P1**	0.18	482	4.93	–	14.6	370
phenylphosphine	**Ir**	**Ir-P2**	0.01	458	11.9	11.4	7.9	371
phenylphosphine	**Ir**	**Ir-P3**	0.02	458	6.90	8.10	4.9	369
phenylphosphine	**Ir**	**Ir-P4**	0.72	488	12.6	20.3	12.6	369
phenylphosphine	**Ir**	**Ir-P5**	0.04	488	17.8	44.8	46.3	367
phenylphosphine	**Pt**	**Pt-P7**	0.45	473	11.0	22.3	16.7	374
phenylphosphine	**Ir**	**Ir-P8**	0.24	477	8.40	17.3	13.2	374
phenylphosphine	**Ir**	**Ir-P9**	0.18	472	8.70	14.3	10.8	374
phenylphosphine	**Ir**	**Ir-P10**	~1.0	593	17.1	47.0	49.3	375
phenylphosphine	**Ir**	**Ir-P11**	~1.0	591	15.0	42.6	37.0	375

phenylphosphine	**Os**	**Os-P2**	0.19	632	12.8	–	–	376
phenylphosphine	**Os**	**Os-P4**	0.62	617	15.3	21.3	6.34	379
phenylphosphine	**Os**	**Os-P5**	0.002	805	1.5	–	–	380
phenylphosphine	**Os**	**Os-P6**	0.66	568	18.3	61.0	53.8	11
phenylphosphine	**Os**	**Os-P8**	0.40	628	9.80	14.0	9.50	378
diphosphine	**Os**	**Os-P11**	0.90	572	13.9	48.9	16.8	377
diphosphine	**Os**	**Os-P13**	0.73	618	14.3	34.8	45.2	251
diphosphine	**Os**	**Os-P14**	0.003	538	15.6	48.3	50.9	260
phenylphosphine	**Ru**	**Ru-P3**	0.21	632	7.03	8.02	2.74	384
diphosphine	**Cu**	**Cu-P1**	0.30	540	8.47	23.7	–	394
diphosphine	**Cu**	**Cu-P2**	0.16	560	15.0	49.5	22.3	395, 396
diphosphine	**Cu**	**Cu-P3**	0.34	559	6.60	20.0	14.9	397
diphosphine	**Cu**	**Cu-P7**	0.65	485	17.7	54.1	–	398
diphosphine	**Cu**	**Cu-P8**	0.4	517	21.3	65.3	–	399

4.5 Phosphorescent emitters bearing aromatic group 16 moieties

Phenoxy and thienyl groups are good cosmetics to modify the emission properties due to their electron-donating characters. The emission peaks can be red-shifted from 486 nm for **(ppy)Pt(acac)** to 487 and 521 nm for **Pt-O1** (Fig. 104) as well as 510 and 546 nm for **Pt-S1** due to the stronger electron-donating ability of S atom (Table 11).[267] Besides, the Φ_P are also increased from 0.15 for **(ppy)Pt(acac)** to 0.42 for **Pt-O1** as well as 0.27 for **Pt-S1**. When the sulfide atom is oxidized to form benzenesulfonyl group, the LUMO level of **Pt-SO1** (2.69 eV) is significantly lowered as compared to that of (ppy)Pt(acac) (2.41 eV) because of the strongly electron-deficient sulfonyl group, leading to a reduced energy gap and thereby the red-shifted emission of **Pt-SO1** (λ_{em} = 503 and 541 nm) relative to that of **(ppy)Pt(acac)** (Table 11). The reduced LUMO level of **Pt-SO1** can facilitate its EI process while the strongly electron-deficient sulfonyl group can improve the ET property of **Pt-SO1**, which will benefit the charge carrier injection/transport balance in OLEDs using **Pt-SO1** as emitter. Besides as a substituent to fine-tune the complex emission properties, phenoxy-based moieties can

also be used to improve the molecular rigidity by connecting the aromatic rings. The O atom in **Pt-O2** can lock the two phenyl rings in the fluorene-9,9′-xanthene moiety to keep the rigidity of the molecule.[402] The O atoms in **Pt-O3** are also vital to form a tetradentate ligand and thereafter a rigid Pt(II) complex.[334] The rigid molecular configuration can suppress the geometry distortion when the complexes are excited, which may restrain some non-radiative pathways and lead to high Φ_P. As a result, **Pt-O3** possesses a much higher Φ_P of 0.63 in solution relative to **(ppy)Pt(acac)** (Table 11). More importantly, a device using **Pt-O3** as emitter affords a peak EQE of 22.3%, which is comparable to that of the reference device based on **Ir(ppy)$_3$**, indicating that the rigid tetradentate Pt(II) complex is very promising for achieving highly efficient PHOLEDs. The S element also appears in Pt(II) complexes as thiophene ring, *e.g.*, in **Pt-S2** and **Pt-S3**, which can destabilize the *d* orbital of Pt(II) center and raise the HOMO level, leading to low energy emission.[403] As a result, the device based on **Pt-S3** displays red EL emission at 631 nm with a decent peak EQE of 12.6%.

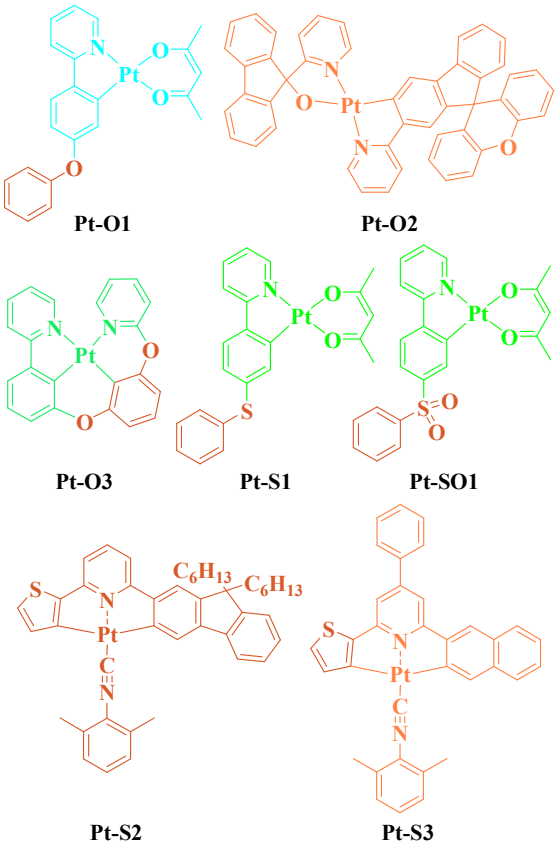

Fig. 104 Chemical structures of some Pt(II) complexes containing aromatic group 16 moieties and peak efficiency data of related OLEDs.

Ppy-type Ir(III) complexes bearing phenoxy and thiophenyl moieties also exhibit red-shifted emissions as compared to the parent **$(ppy)_2$Ir(acac)** or **Ir$(ppy)_3$** due to the electron-donating properties of phenoxy and thienyl group.[31, 276] Because of the methyl group attached to the pyridyl ring, **Ir-O3** and **Ir-O4** (Fig. 105) show slighly blue-shifted emissions.[404] Importantly, the Φ_P of these Ir(III) complexes bearing phenoxy and thiophenyl moieties are higher than that of **$(ppy)_2$Ir(acac)** or **Ir$(ppy)_3$**. For example, **Ir-O3** and **Ir-O4** possess Φ_P over 0.7 in CH_2Cl_2 at room temperature (Table 11). A device using **Ir-O3** as emitter at the dopant concentration of 8 wt% can achieve outstanding

performance with a peak EQE of 24.5% and CE of 84.6 cd A^{-1}, which are two times higher than that of the reference device based on **Ir(ppy)$_3$**. Besides, the **Ir-O3** based devices give similar efficiencies at the doping levels from 4 wt% to 12 wt%, while the Ir(ppy)$_3$ based devices show significantly decreased the efficiencies when the dopant concentration is increased from 4 wt% to 12 wt%. The high efficiencies with less dopant-concentration-dependent character of devices based on **Ir-O3** may be attributed to the suppressed molecular aggregation and self-quenching effects due to the introduction of the phenoxy group and a methyl substituent. When the benzenesulfonyl group is incorporated into **(ppy)$_2$Ir(acac)** or **Ir(ppy)$_3$**, the resulting Ir(III) complexes **Ir-SO1** and **Ir-SO2** also display red-shifted emissions due to the greatly reduced LUMO level caused by the electron-withdrawing benzenesulfonyl unit.[31, 276] The electron-withdrawing benzenesulfonyl unit can improve the EI/ET properties of the related complexes as well.[405, 406] The device based on **Ir-SO1** emits yellow light at 547 nm with a decent peak CE of 35.1 cd A^{-1} and PE of 23.0 lm W^{-1}. Furthermore, a fluorescence/phosphorescence hybrid (F/P) WOLED using the *p*-bis(*p*-*N*,*N*-diphenylaminostyryl)benzene (DSA-Ph) as fluorescent blue emitter and **Ir-SO1** as phosphorescent yellow emitter can realize white emission with CIE coordinates very close to those of the highly desired white-light point at (0.33,0.33) under a wide range of driving voltages.[405] This WOLED also gives encouraging efficiencies of 13.0% for peak EQE and 24.3 lm W^{-1} for maximum PE. The attractive performance achieved by devices based on **Ir-SO1** can be attributed to the improved EI/ET properties endowed by the electron-withdrawing benzenesulfonyl unit.

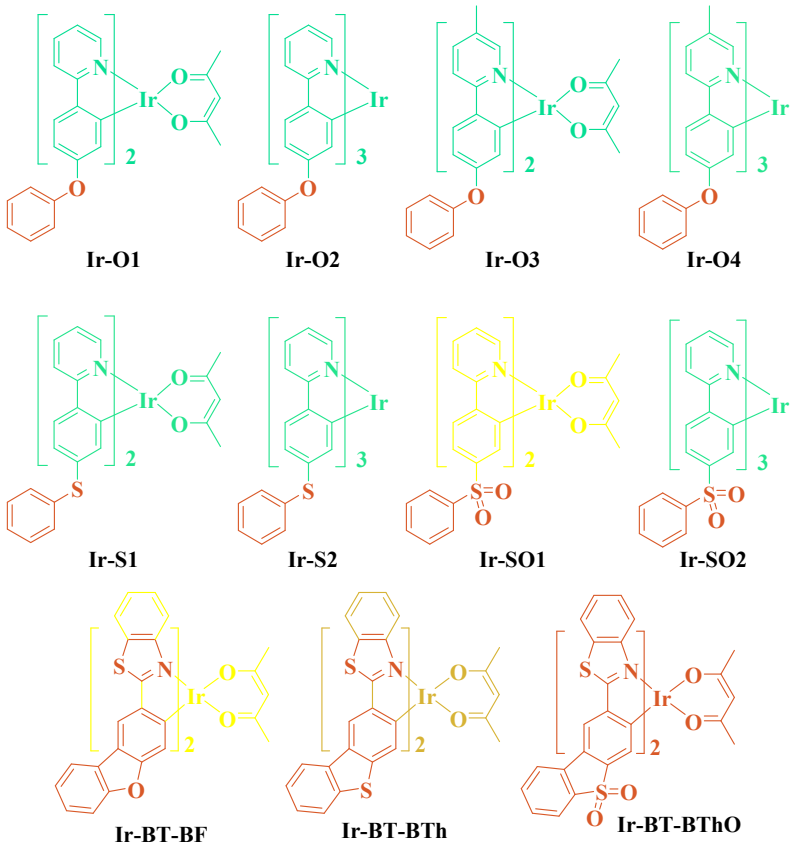

Fig. 105 Chemical structures of some Ir(III) complexes containing aromatic group 16 moieties and peak efficiency data of related OLEDs.

The S atom also appears in thiazole/benzothiazole or thiophene units to tune the emission properties of the corresponding complexes,[342, 407, 408] such as the abovementioned **Ir-PPY-B4** and **Ir-Am4**, as well as **Ir-BT-BF**, **Ir-BT-BTh** and **Ir-BT-BThO**.[409] Besides, the O or S element based dibenzofuran, dibenzothiophene and dibenzothiophene-S,S-dioxide also show notable influence on the emission properties of **Ir-BT-BF**, **Ir-BT-BTh** and **Ir-BT-BThO**, which can be intuitively reflected by their emission peaks. The emission wavelength of these three complexes is in the order

of **Ir-BT-BF** (λ_{em} = 551 nm) < **Ir-BT-BTh** (λ_{em} = 562 nm) < **Ir-BT-BThO** (λ_{em} = 598 nm) (Table 11), because the S atom is more polarizable than O so as to enlarge the π-conjugaton in the ligand of **Ir-BT-BTh** and thus give longer wavelength emission, while the strongly electron-withdrawing sulfonyl moiety will greatly lower the LUMO level of **Ir-BT-BThO**, resulting in reduced energy gap and hence significantly red-shifted emission. Devices based on **Ir-BT-BF** and **Ir-BT-BTh** exhibit very attractive performance with peak EQE of 19.0% and CE exceeding 54 cd A^{-1}, which may result from the well-balanced charge injection/transporting properties induced by the group 16 moieties. The performance of devices based on **Ir-BT-BF** and **Ir-BT-BTh** are among the best for the yellow PHOLED so far. These results have clearly demonstrated the group 16 moieties not only can tune the emission color, but also possess the ability of furnishing EI/ET ability to give highly efficient phosphorescent emitters. Hence, these group 16 building blocks with unique electronic features can show great potential in developing functionalized phosphorescent emitters.

Table 11. Phosphorescent emitters bearing aromatic group 16 moieties and their properties

Main-group element unit	Metal center	Emitter	Φ_P	$\lambda_{max,em}$ nm	EQE %	CE cd A^{-1}	PE lm W^{-1}	Ref.
phenoxyl	**Pt**	**Pt-O1**	0.42	487	5.09	11.4	7.3	267
phenoxyl	**Pt**	**Pt-O3**	0.63	512	22.3	–	–	334
thiophenyl	**Pt**	**Pt-S1**	0.27	510	6.66	16.8	10.1	267
thiophene	**Pt**	**Pt-S3**	0.26	589	12.6	13.4	10.5	403
benzenesulfonyl	**Pt**	**Pt-SO1**	0.95	503	8.35	19.6	7.83	267
phenoxyl	**Ir**	**Ir-O3**	0.73	502	24.5	84.6	77.6	404
thiophenyl	**Ir**	**Ir-S2**	0.42	520	12.5	45.9	35.0	276
benzenesulfonyl	**Ir**	**Ir-SO1**	0.91	527	10.1	37.6	26.0	276
dibenzofuran	**Ir**	**Ir-BT-BF**	0.10	551	19.0	58.4	30.6	409
dibenzothiophene	**Ir**	**Ir-BT-BTh**	0.11	562	19.0	54.1	28.3	409

4.6 Phosphorescent emitters bearing fluorine-modified ligands

Since the early state of development of phosphorescent emitters, fluorine atom has been used to manipulate the properties of pertinent complexes by virtue of its strong electronegativity.[28, 270, 410] Introduction of a C–F bond or CF_3 group may modify the molecular packing style due to the existence of the F···H–C interactions.[411] More importantly, the HOMO and LUMO levels can be adjusted by fluorination, thus allowing the emission color to be tuned conveniently.[412-416] Besides, the charge injection/transporting properties of the related complexes can also be changed due to the altered MO levels. In brief, the strongly electron-withdrawing character confers F atom and CF_3 group with great capability to alter the properties of related phosphorescent emitters, especially fulfilling blue phosphorescence emission by enlarging the E_g.

Incorporating F atoms onto the phenyl ring of the ppy-type ligands significantly blue-shifts the emission peak from 486 nm for **(ppy)Pt(acac)** to 466 nm for **Pt-F1** (Fig. 106) at room temperature.[270] However, the fluorination also notably decreases the Φ_P of **Pt-F1** to 0.02. In order to remedy the adverse effect induced by the F atoms, **Pt-F2** bearing a di(2-pyridyl)benzene-based tridentate ligand (N^C^N) with a more rigid molecular structure is proposed.[417] The Φ_P of **Pt-F2** is dramatically improved to 0.46, while the emission energy of **Pt-F2** is similar to that of **Pt-F1** (Table 12). The greatly enhanced quantum yield of **Pt-F2** is attributed to the more rigid molecular configuration induced by the terdentate ligand over the bidentate ligand, leading to less pronounced distortion of the molecular geometry in the emitting triplet state as compared to the singlet ground state in **Pt-F2**, and thus reducing the non-radiative pathways.[418] Besides, the less distortion results in reduced intensities of the low-energy vibrational satellite bands in the green region of the spectrum,

causing an improved blue color purity as indicated by the smaller CIE coordinates of both *x*- and *y*-conponent for the device based on **Pt-F2** (0.18, 0.32) than those for the one based on **Pt-F1** (0.24, 0.37).[417] Therefore, introducing F atoms onto the phenyl ring of N^C^N-type chelate can blue-shift the emission spectrum without bringing negative effects on the Φ_P. For example, as compared to **Pt-0F** (λ_{em} = 491 nm), the fluorinated **Pt-F3** displays significantly blue-shifted (by *ca.* 30 nm) emission band (Table 12).[419] Theoretical calculation results reveal that the HOMO of the terdentate N^C^N ligand based complex is largely distributed over the metal and the cyclometallating ring, whereas the LUMO is mainly localized on the pyridyl ring.[420, 421] Therefore, introducing F atoms to the phenyl ring will stabilize the HOMO level, but shows little influence on the LUMO level. Accordingly, the E_g is increased and the emission is blue-shifted. Besides, the Φ_P is also increased from 0.73 for **Pt-0F** to 0.87 for **Pt-F3** in CH_2Cl_2 (Table 12). In contrast, the fluorination effect dramatically improves the Φ_P of the neat solid film of **Pt-F3** (0.65 for **Pt-F3** vs 0.05 for **Pt-0F**), indicating that the fluorine atoms show marked influence on the molecular packing of the complexes. Complexes **Pt-F4** (λ_{em} = 465 nm) and **Pt-F5** (λ_{em} = 453 nm) show even bluer emissions as compared to **Pt-F3** (Table 12) due to the respective electron-donating –OMe and $–NMe_2$ groups which will destabilize the LUMO levels without notably changing the HOMO levels.[422, 423] The Φ_P of **Pt-F5** is as high as 0.60 in solution. Due to the intriguing photophysical properties, these fluorinated Pt(II) complexes possess good potential for achieving highly efficient PHOLEDs. At low doping level (≤ 5 wt%), devices based on these Pt(II) complexes show sky-blue emissions with EQE up to 13.0%. With increased doping level, the excimer-based emissions appear in the orange-red to deep-red region of the EL spectra. Especially, at the dopant concentration of 15 wt%, the device based on

Pt-F3 exhibits white emission with the CIE coordinates of (0.33, 0.38) and CRI of 65.[419] This device also gives an attractive EQE of 18.1% at *ca.* 500 cd m^{-2}. When the dopant concentration is increased to 100 wt%, the device based on **Pt-F3** shows red EL emission with a EQE still as high as 14.7% at *ca.* 500 cd m^{-2}, which may result from the high Φ_P of the neat **Pt-F3** film. The device based on **Pt-F4** at the doping level of 20 wt% also shows white emission [CIE of (0.34, 0.35) and CRI of 74] with a nice EQE of 11.5% at *ca.* 500 cd m^{-2}.[422] Surprisingly, when the dopant concentration is increased to 100 wt%, an orange-red emitting device is obtained and the EQE of the device is further increased to 16% at *ca.* 500 cd m^{-2}. These studies show that the fluorinated Pt(II) complexes bearing N^C^N-type chelates are versatile triplet emitters for fabricating color-variable OLEDs. By adjusting the dopant concentration from *ca.* 5 wt% to 100 wt%, the emission colors of the related OLEDs can be tuned from sky-blue to white and final red due to the excimer emissions.

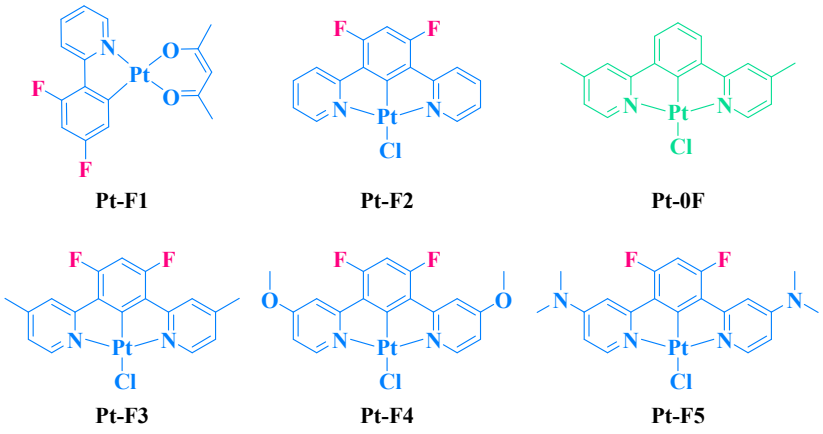

Pt-F2 @ 2 wt %; EQE 12.6 %; CE 20.6 cd A^{-1}; PE 6.40 lm W^{-1}; CIE (0.15, 0.26)
Pt-F2 @ 8 wt %; EQE 9.30 %; CE 13.0 cd A^{-1}; PE 7.30 lm W^{-1}; CIE (0.33, 0.36)
Pt-F3 @ 5 wt %; EQE 13.0 %; CE 26.0 cd A^{-1}; PE 9.30 lm W^{-1}; CIE (0.18, 0.35)
Pt-F3 @ 15 wt %; EQE 18.1 %; CE 29.1 cd A^{-1}; PE 11.8 lm W^{-1}; CIE (0.33, 0.38)
Pt-F4 @ 5 wt %; EQE 6.10 %; CE 10.7 cd A^{-1}; PE 2.80 lm W^{-1}; CIE (0.15, 0.26)
Pt-F4 @ 20 wt %; EQE 11.5 %; CE 21.3 cd A^{-1}; PE 6.80 lm W^{-1}; CIE (0.34, 0.35)

Fig. 106 Chemical structures of **Pt-F1 – Pt-F5** together with **Pt-0F** and peak efficiency data of related OLEDs.

Introducing fluorine atoms into the phenyl ring of ppy-type ligand can also significantly blue-shift the emission band of homoleptic Ir(III) complex (Fig. 107), as evidenced by the comparison between **Ir-F1** (λ_{em} = 468 nm) and **Ir(ppy)$_3$** (λ_{em} = 510 nm) (Table 12).[336] This blue-shift effect is attributed to the electron-withdrawing fluorine atoms which can stabilize the HOMO level more than the LUMO level when they are attached to the phenyl ring of the ligand, leading to larger E_g. With assistance from the strongly electron-withdrawing –CN group, the emission peak can be further blue-shifted to 448 nm for **Ir-F2** (Table 12).[135] As for heteroleptic Ir(III) complexes, such as FIrpic (**Ir-F3**, λ_{em} = 472 nm),[424] **FCNIrpic** (**Ir-F4**, λ_{em} = 465 nm),[425] **Ir-F5** (λ_{em} = 460 nm) and **Ir-F6** (λ_{em} = 459 nm) (Table 12),[426] the fluorine atoms also have a positive influence on enlarging the E_T of these complexes, yet the role of increasing E_T acted by the electron-withdrawing groups, *i.e.*, –CN, phosphoryl (P=O) and sulfonyl (S=O) moieties, is also important. By analyzing these Ir(III) complexes mentioned above, it can be clearly seen that additional introduction of electron-withdrawing groups to the difluorophenyl ring of the ppy-type ligand can further increase the emission energy of the complexes, which is helpful to obtain pure blue-emitting OLEDs. For example, the blue color purity of the device based on **FCNIrpic** is conspicuously improved as compared to that of the device based on FIrpic in terms of the CIE coordinates [(0.14, 0.19)[427] for **FCNIrpic** based device vs (0.16, 0.29)[424] for **FIrpic** based device]. With the assistance of a stronger electron-withdrawing group, trifluoromethyl carbonyl, a bluer emitter **Ir-F7** can be obtained to display an emission peak at 453 nm (Table 12).[428] As a result, the CIE coordinates of (0.141, 0.158) can be realized by the **Ir-F7** based device. Besides, this device shows attractive performance with a peak EQE of 17.1% and PE of 19.0 lm W^{-1}. By replacing the trifluoromethyl carbonyl with

heptafluoropropyl carbonyl almost has no influence on the emission energy, since the emission profiles of **Ir-F7** and **Ir-F8** are almost identical measured either at room temperature or at 77 K. However, the emission peak is further blue-shifted to 447 nm for **Ir-F9** when the auxiliary picolinate ligand is replaced by the trifluoromethyl-substituted triazole ligand (Table 12). The trifluoromethyl-substituted triazole ligand can stabilize the HOMO level more than the LUMO level, leading to the larger energy gap of **Ir-F9**. As a result, deep-blue emission with the CIE coordinates of (0.147, 0.116) can be achieved by the device based on **Ir-F9**, though the peak EQE of this device decreases to 8.4%. This study shows that trifluoromethyl carbonyl exhibits stronger electron-withdrawing ability than –CN, phosphoryl (P=O) and sulfonyl (S=O) moieties. Besides, the use of auxiliary ligands with stronger electron-withdrawing character will further increase the E_T of blue Ir(III) complexes as compared to that of **FIrpic**, which has also been confirmed by **FIr6** (**Ir-F10**, λ_{em} = 457 nm), **Ir-F11** (λ_{em} = 460 nm), **Ir-F12** (λ_{em} = 460 nm), **Ir-F13** (λ_{em} = 459 nm) and **Ir-F14** (λ_{em} = 450 nm) (Table 12).[59, 131, 357, 429] Obviously, these pyridylazole ligands with or without trifluoromethyl substituent show higher abilities to blue-shift the emission of 2-(2,4-difluorophenyl)pyridine based Ir(III) complex in comparison to the picolate of **FIrpic**. Furthermore, devices based on these complexes show encouraging efficiencies with improved color purity. For example, a device using **Ir-F11** as emitter can give a remarkable EQE of 19.3% and CE of 37.8 cd A^{-1}, while the device based on **Ir-F14** gives CIE_y even smaller than 0.2. These studies suggest that with the assistance from pyridylazole based auxiliary ligands, Ir(III) complexes based on 2-(2,4-difluorophenyl)pyridine chromophoric ligands can lead to better blue color purity. Besides, due to the electron-withdrawing properties of pyridylazole based auxiliary ligands, the EI/ET

abilities of the complexes can also be improved, which may benefit the device efficiencies.

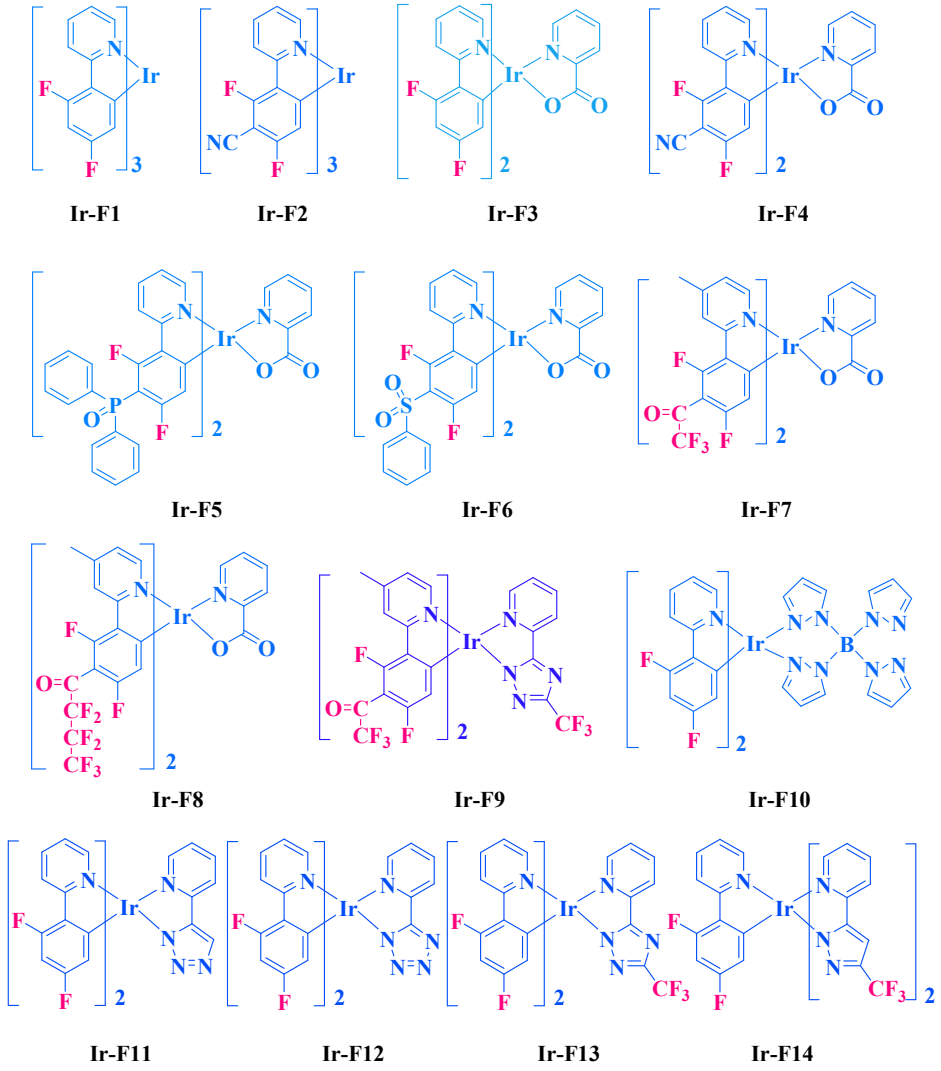

Ir-F4; EQE 22.1 %; CIE (0.14, 0.19)
Ir-F7; EQE 17.1 %; CE 21.7 cd A^{-1}; PE 19.0 lm W^{-1}; CIE (0.141, 0.158)
Ir-F9; EQE 8.40 %; CE 8.60 cd A^{-1}; PE 8.10 lm W^{-1}; CIE (0.147, 0.116)
Ir-F11; EQE 19.3 %; CE 37.8 cd A^{-1}; PE 16.8 lm W^{-1}; CIE (0.15, 0.32)
Ir-F14; EQE 8.50 %; PE 8.50 lm W^{-1}; CIE (0.16, 0.18)

Fig. 107 Chemical structures of **Ir-F1 –Ir-F14** and peak efficiency data of related OLEDs.

Modification of the pyridyl ring is also a popular way to tune the blue emission of the concerned Ir(III) complexes with the aid of the difluorophenyl-based electron-withdrawing moieties.[430-432] The emission profile of the mesityl group modified complex **Ir-F15** (Fig. 108) is similar to that of

FIrpic.[431] Compared with **FIrpic**, the introduction of the bulky mesityl group not only increases the solubility and the Φ_P of **Ir-F15** to 0.92 in toluene (Table 12), but also effectively suppresses the intermolecular aggregation effect. As a result, the solution-processed device based on **Ir-F15** gives much higher efficiencies than the reference one based on **FIrpic**. However, although the peak EQE of the optimized device based on **Ir-F15** is 10.4 %, the *y*-component of the CIE coordinates is as large as 0.4, which is far beyond the deep-blue region. Kim *et al.* decorated the pyridyl ring with a trimethylsilyl group and also used the perfluoropropyl-substituted pyridyltriazole as auxiliary ligand at the same time.[432] The resulting complex **Ir-F16** (λ_{em} = 461 nm) (Table 12) exhibits blue-shifted emission as compared to **FIrpic** because of the lowered HOMO level in **Ir-F16** induced by the trimethylsilyl group as well as perfluoropropyl-substituted triazole moiety. The device using **Ir-F16** as emitter affords not only very high efficiencies with EQE as high as 19.3%, but also improved blue color purity at the CIE coordinates of (0.145, 0.247).

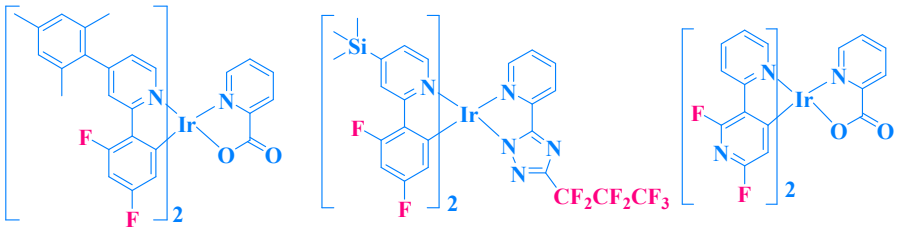

Ir-F15 **Ir-F16** **Ir-F17**

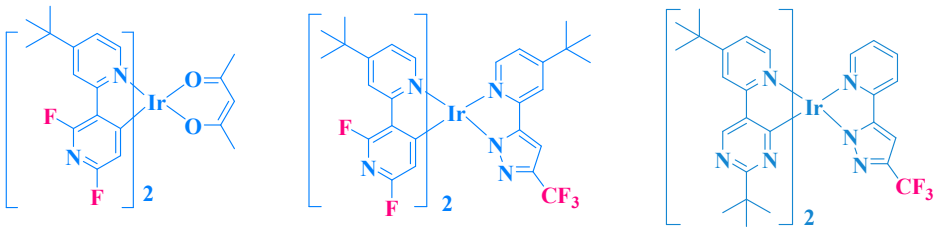

Ir-F18 **Ir-F19** **Ir-F20**

Ir-F15; EQE 10.4 %; CE 23.7 cd A^{-1}; PE 12.6 lm W^{-1}; CIE (0.18, 0.40)
Ir-F16; EQE 19.3 %; CIE (0.145, 0.247)
Ir-F18; EQE 15.3 %; CE 26.1 cd A^{-1}; PE 24.2 lm W^{-1}; CIE (0.16, 0.25)
Ir-F20; EQE 17.9 %; CE 38.0 cd A^{-1}; PE 35.8 lm W^{-1}; CIE (0.19, 0.33)

Fig. 108 Chemical structures of **Ir-F15 – Ir-F20** and peak efficiency data of related OLEDs.

Besides 2-(2,4-difluorophenyl)pyridine and its derivatives, other chromophoric ligands have also been designed to synthesize blue-emitting Ir(III) complexes. By introducing an electron-withdrawing group (e.g., -CN) to the C5-position on the phenyl ring of **FIrpic**, the emission color of the resulting complex (e.g., **FCNIrpic**) can be blue-shifted, and so by directly replacing the carbon atom of C5 position with an electron-withdrawing N atom should also cause bluer phosphorescence, which has been shown by several resultant Ir(III) complexes.[433-435] The emission peak of **Ir-F17** (λ_{em} = 445 nm) is significantly blue-shifted as compared to that of **FIrpic** (Table 12).[434] Even bearing the acac as auxiliary ligand, **Ir-F18** (λ_{em} = 454 nm) still can show bluer phosphorescence than **FIrpic** (Table 12).[435] When a trifluoromethyl substituted pyridylpyrazole serves as the auxiliary ligand, **Ir-F19** can even emit deep-blue phosphorescence at *ca.* 440 nm.[433] Apart from the improved blue color quality of the phosphorescent emission, the fluorine-substituted 2,3′-bipyridine based Ir(III) complexes also give high Φ_P in the range of 0.58-0.95 (Table 12), indicating their great potential in achieving efficient blue-emitting PHOLEDs. The device based on **Ir-F18** can achieve EQE of 15.3% with the CIE coordinates of (0.16, 0.25) at 100 cd m^{-2}.[435] By replacing the fluorine-substituted pyridyl ring with pyrimidyl ring, the resulting complex **Ir-F20** can also emit blue phosphorescence (λ_{em} = 457 nm) with very high Φ_P of 0.85.[436] Sky-blue device based on **Ir-F20** shows an attractive performance with the peak EQE of 17.9% and PE of 35.8 lm W^{-1}(Table 12).

The strongly electron-withdrawing F atom and trifluoromethyl (or other fluorine-containing alkyl) group have been widely used to design blue and deep-blue triplet emitters. Blue PHOLEDs

using these complexes can give attractive EL performance. However, the strongly polarized C−F bonds may degrade during the device operation process or the vacuum-deposition process when fabricating OLEDs as indicated by a study on **FIrpic**.[437] The degradation of the emitter will result in poor device performance in terms of color purity as well as efficiency. Therefore, in view of fabricating the blue-emitting devices with long stability as well as high color purity, the triplet emitters containing aromatic fluorine substituents are less attractive, which in turn make the strategy of using aromatic fluorine-free ligand to synthesize phosphorescent complexes highly desirable. However, without the F atom substituent on the chromophoric ligand, it is not easy to tune the emission color of triplet emitterss to the deep-blue region. For instance, although the aromatic fluorine-free complex **Ir-F20** shows blue emission as well as high EL efficiencies, the color purity still need to be improved. To escape from such dilemma, according to the well-established color-tuning rule,[42] strongly electron-donating group can be attached to the pyridyl moiety of the pyridyl pyrimidine ligand to raise the LUMO level of the related complex, and thereby increase the energy gap. Otherwise, the pyridyl ring can be replaced by other *N*-heterocycle moieties such as azoles and *N*-heterocyclic carbene as discussed in sections 4.3.3 and 4.3.4, respectively.

Table 12. Phosphorescent emitters bearing fluorine-modified ligands and their properties

Main-group element unit	Metal center	Emitter	Φ_P	$\lambda_{max,em}$ nm	EQE %	CE cd A^{-1}	PE lm W^{-1}	Ref.
fluorine atom	**Pt**	**Pt-F2**	0.46	470	12.6	20.6	6.40	417
fluorine atom	**Pt**	**Pt-F3**	0.87	461	18.1	29.1	11.8	419
fluorine atom	**Pt**	**Pt-F4**	0.71	465	11.5	21.3	6.80	422
fluorine atom + cyano	**Ir**	**Ir-F4**	–	465	22.1	–	–	425, 427
fluorine atom + trifluoromethyl carbonyl	**Ir**	**Ir-F7**	0.74	453	17.1	21.7	19.0	428

fluorine atom + trifluoromethyl carbonyl + trifluoromethyl triazole	**Ir**	**Ir-F9**	0.63	447	8.40	8.60	8.10	428
fluorine atom + triazole	**Ir**	**Ir-F11**	–	460	19.3	37.8	16.8	131
fluorine atom + trifluoromethyl	**Ir**	**Ir-F14**	0.50	450	8.50	–	8.50	357
fluorine atom	**Ir**	**Ir-F15**	0.92	473	10.4	23.7	12.6	431
fluorine atom + triazole	**Ir**	**Ir-F16**	0.76	461	19.3	–	–	432
fluorine atom + pyridine	**Ir**	**Ir-F18**	0.78	454	15.3	26.1	24.2	435
trifluoromethyl + pyrimidine	**Ir**	**Ir-F20**	0.85	457	17.9	38.0	35.8	436

4.7 Phosphorescent emitters showing bipolar features

Balanced charge injection/transporting character is vital in improving the device efficiency, especially the efficiency at high luminance. Besides, the long operation stability of a device also requires balanced charge flux in the device. Therefore, in order to realize the goal, much work has been done to develop bipolar host materials (see section 3.7), and some studies have been focused on researching emitters with bipolar features. Out of the questions, endowing complexes with bipolar characters should start by designing ligands with charge injection/transporting properties and properly combining the metal ion and the ligands to synthesize bipolar complexes (Fig. 109). Two design tactics have been successfully implemented. One is to incorporate both HI/HT and EI/ET groups into one single ligand for the subsequent synthesis of the target complexes, *e.g.*, **Pt-NB**,[438] **Ir-NPO1**[361] and **Ir-NPO2**.[439] The other one is to synthesize complexes with asymmetric structures in which one ligand containing ET group and another ligand showing HT property, *e.g.*, **Ir-OSO**, **Ir-NSO1** and **Ir-NSO2**.[440, 441] Whichever the method is adopted, the resulting complexes possess bipolar features as well as high Φ_P, suggesting the great potential of these bipolar phosphorescent

emitters to furnish high performance PHOLEDs. For example, an orange-emitting device using **Pt-NB** as dopant shows an impressive performance with peak CE and PE of 35.0 cd A^{-1} and 36.6 lm W^{-1} (Table 13),[438] respectively, which are much higher than those obtained by the devices based on Pt(II) complexes showing unipolar charge transporting properties (*e.g.*, **Pt-Am1** and **Pt-PPY-B1**). As for **Ir-NPO2**, the related device with non-doped structure of ITO/PEDOT:PSS (50 nm)/**Ir-NPO2** (80 nm)/TPBI (25 nm)/CsF (1.5 nm)/Al (150 nm) gives attractive maximum efficiencies of 8.8% and 12.4 cd A^{-1} for EQE and CE, respectively.[439] More importantly, this device shows very low efficiency roll-off at high luminance, as evidenced by the EQE of 8.2% and CE of 11.5 cd A^{-1} at 1000 cd m^{-2}. For a solution-processed non-doped device, this result is very impressive. The high performance of this device can be attributed to two main factors, one is the large molecular size of the bulky carbazole and diphenylphosphine groups which can effectively suppress intermolecular interactions, while the other is the bipolar charge injection/transporting property of these two groups which can realize balanced charge flux in the device. The devices using asymmetric **Ir-OSO** and **Ir-NSO1** as dopants also display very attractive performance. The peak EQE of 20.2% and CE of 69.4 cd A^{-1} are achieved by **Ir-OSO** based device, while value of 11.0% and 41.2 cd A^{-1} are obtained by **Ir-NSO1** based device (Table 13). In addtion, devices based on **Ir-OSO** and **Ir-NSO1** also display very low efficiency roll-off at high luminance, indicating the merit of using bipolar emitters in fabricating high performance devices with low efficiency roll-off at high luminance.

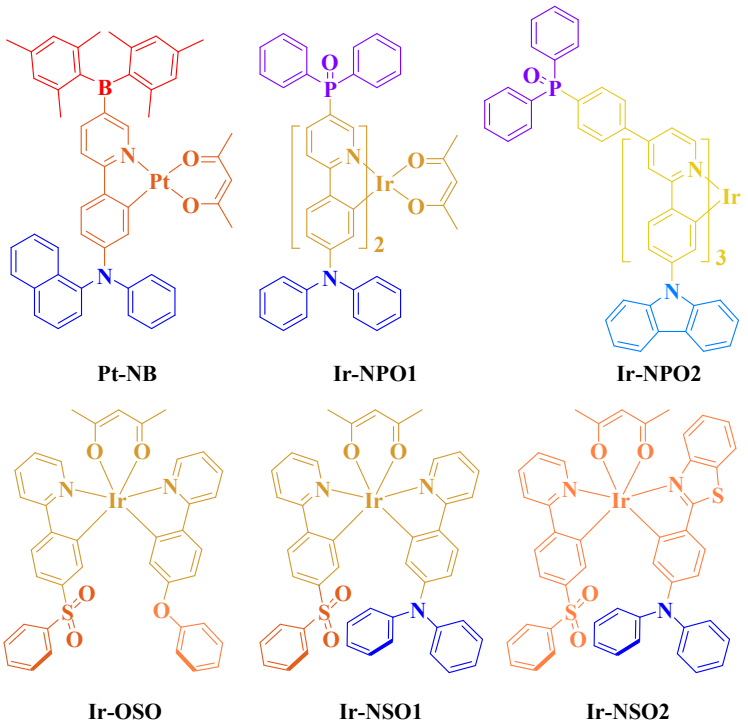

Fig. 109 Chemical structures of some bipolar complexes and peak efficiency data of related OLEDs.

Some bipolar dendritic Ir(III) complexes bearing ET benzimidazole group and HT arylamine group have also been reported.[22, 442, 443] Using these dendrimers as emitters, solution-precessed devices can be fabricated without host materials, *i.e.*, these dendrimers can be used as self-host emitters, which will greatly simplify the device fabrication process and lower the cost. In **Ir-NN1** (Fig. 110), the rigid carbazole dendrons are responsible for HT process as well as effectively suppressing the intermolecular interactions effectively between the emissive cores, while the benzimidazole group can improve the ET ability of **Ir-NN1**.[22] Therefore, the **Ir-NN1** based solution-processed non-doped device can achieve a peak EQE of 10.3% and CE of 34.7 cd A^{-1} (Table 13). Connecting the carbazole dendron and benzimidazole group with a long flexible spacer almost

has no influence on the emission color of **Ir-NN2** as compared to that of **Ir-NN1**, but the Φ_P is significantly decreased from 0.87 for **Ir-NN1** to 0.39 for **Ir-NN2** (Table 13).[442] This reduced Φ_P may be attributed to the more loose molecular structure induced by the long flexible spacer in **Ir-NN2**, which will facilitate the non-radiative pathways and thereby lead to lowered emissive efficiency. As a result, the solution-processed non-doped device based on **Ir-NN2** gives inferior performance with a peak EQE of 5.0% and CE of 17.2 cd A^{-1}. However, the device using **Ir-NN3** as self-host emitter shows an improved peak EQE of 7.4% and CE of 25.5 cd A^{-1}. The notably enhanced device efficiencies can be attributed to the improved EI/ET ability of **Ir-NN3** by introducing two ET oxadiazole groups to furnish more proper bipolar characters, since the Φ_P and E_T of **Ir-NN3** (Φ_P = 0.40, λ_{em} = 512 nm) are much similar to those of **Ir-NN2** (Φ_P = 0.39, λ_{em} = 511 nm) (Table 13). The EQE and CE of the device based on **Ir-NN3** remain as high as 5.7% and 19.8 cd A^{-1}, respectively, even at 5000 cd m^{-2}, indicating the merit of using bipolar phosphorescent dendrimers as self-host emitters for highly efficient solution-processed PHOLEDs. Different from the aforementioned bipolar dendrimers in which the arylamine dendrons are linked to the N atom of the benzimidazole group, dendrimers with arylamine dendrons connected to the phenyl ring of the 2-phenylbenzimidazole have also been reported.[443] Because the bulky arylamine dendrons are located far away from the benzimidazole moiety, the benzimidazole moiety will appear at the molecular surface. Therefore, the EI/ET ability of **Ir-NN4** and **Ir-NN5** may be improved as compared to that of **Ir-NN1-3** in which the benzimidazole moiety is wrapped. As a result, the device with a very simple structure of ITO/PEDOT:PSS/**Ir-NN5**/Cs_2CO_3/Al shows an impressive performance with a peak EQE of 6.12% and PE of 18.35 cd A^{-1}, which are much higher than those of

the device based on **Ir-NN1** with similar device structure (0.19%, and 0.60 cd A^{-1}).[22] Furthermore, this simple device based on **Ir-NN5** can give EQE and CE of 5.51% and 16.52 cd A^{-1} at 1000 cd m^{-2}, 4.37% and 13.11 cd A^{-1} at 10000 cd m^{-2}, indicating the low efficiency roll-off at high luminance.

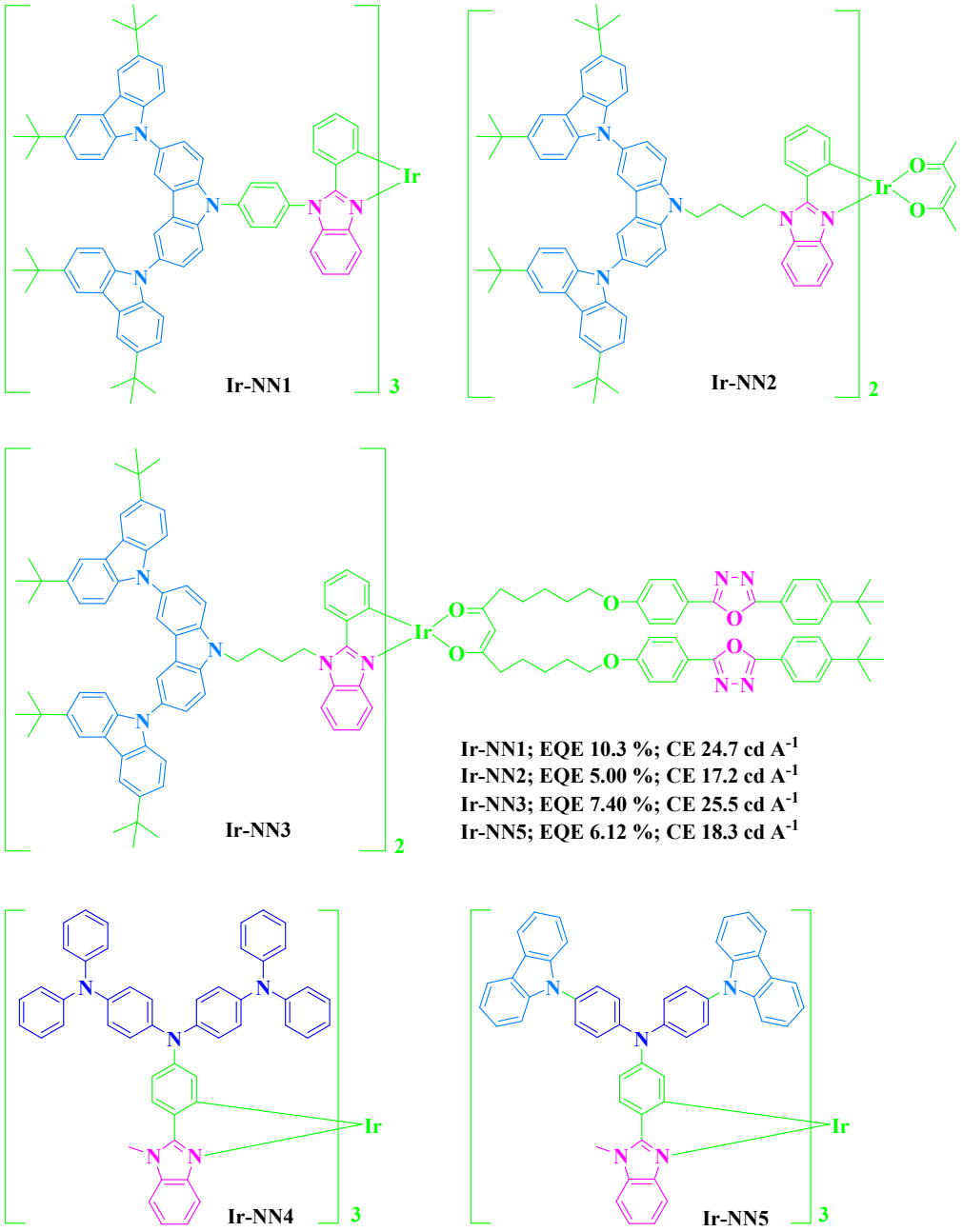

Fig. 110 Chemical structures of some bipolar Ir(III) dendrimers and peak efficiency data of related OLEDs.

Devices based on bipolar phosphorescent emitters can achieve high efficiencies due to the more balanced charge flux within the emissive layers. However, the phosphorescent emitters showing bipolar characters are still limited. Hence, much more work should be devoted to this area to obtain more novel bipolar phosphorescent emitters. Based on the structural features of the bipolar phosphorescent emitters, intraligand charge transfer (ILCT) or ligand-to-ligand charge transfer (LLCT) may occur in the bipolar complexes, which will lead to low energy emissions in the long wavelength region. Hence, developing blue phosphorescent emitters with bipolar character is a big challenge. As for these Ir(III) complexes containing an emissive core based on 2-phenylbenzimidazole ligand and a bulky dendron based on arylamine groups, they exhibit great potential to be applied to high performance green PHOLEDs with simple device structure. However, since the arylamine group based dendrons show negligible influence on the emission energy of the emissive core, the 2-phenylbenzimidazole based Ir(III) dendrimers always show green emissions similar to that of **Ir-Az6** which has no arylamine dendritic group. Therefore, other emissive cores with ET ability should be designed to synthesize the bipolar Ir(III) dendrimers bearing arylamine group based dendrons. Thus the emission color can be shifted to other region in the optical spectrum.

Table 13. Phosphorescent emitters showing bipolar features and their properties

Main-group element unit	Metal center	Emitter	Φ_P	$\lambda_{max,em}$ nm	EQE %	CE cd A^{-1}	PE lm W^{-1}	Ref.
arylborane + phenylamine	**Pt**	**Pt-NB**	0.91	590	10.1	35.0	36.6	438
phenylamine + diphenylphosphine oxide	**Ir**	**Ir-NPO1**	0.14	568	8.8	29.6	15.5	361
carbazole + diphenylphosphine oxide	**Ir**	**Ir-NPO2**	0.43	562	8.80	12.4	6.60	439

phenoxyl + benzenesulfonyl	**Ir**	**Ir-OSO**	0.52	556	20.2	69.4	35.2	440
phenylamine + benzenesulfonyl	**Ir**	**Ir-NSO1**	0.35	564	11.0	41.0	17.3	440
carbazole + benzimidazole	**Ir**	**Ir-NN1**	0.87	522	10.3	24.7	–	22
carbazole + benzimidazole	**Ir**	**Ir-NN2**	0.39	511	5.00	17.2	–	442
carbazole + benzimidazole + oxadiazole	**Ir**	**Ir-NN3**	0.40	512	7.40	25.5	–	422
carbazole + benzimidazole	**Ir**	**Ir-NN5**	0.60	515	6.12	18.3	–	423

4.8 Phosphorescent emitters with main-group unit functionalized auxiliary ligand

From the above Pt(II) complexes and heteroleptic Ir(III) complexes, it can be clearly seen that the auxiliary ligand is acac or its derivatives in most cases. Although the emission property of a complex largely depends on the chromophoric ligands, the auxiliary ligand also has minor but important influence on both the PL and EL properties of related phosphorescent emitters. Therefore, many studies have been focused on designing novel auxiliary ligands for Pt(II) and Ir(III) complexes. Chi *et al.* designed several Pt(II) complexes bearing di-CF_3 substituted 2-pyridylmethanol ligands.[444] The theoretical calculation result reveals that the HOMO of **Pt-PF** (Fig. 111) is distributed on the phenyl ring of the ppy ligand, the Pt(II) center and the O atom in the auxiliary ligand, whereas the LUMO resides on the pyridyl rings of the ppy ligand as well as the auxiliary ligand, indicating that the auxiliary ligand makes significant contributions to both HOMO and LUMO of **Pt-PF**. As a result, the emission peak of **Pt-PF** (λ_{em} = 499 and 525 nm) is red-shifted in CH_2Cl_2 as compared to that of **(ppy)Pt(acac)** (Table 14), which may result from the enhanced LLCT in **Pt-PF**. By replacing the acac ligand in **$(ppy)_2$Ir(acac)** with 2,2′-dipyridylamido (dpa), Hou *et al.* synthesized a neutral dpa-coordinated Ir(III) complex **Ir-dpa** which displayed bluish-green emission with a peak at 480 nm and a shoulder peak at 510 nm in dichloromethane (Table 14).[445] **Ir-dpa** possesses a much higher

Φ_P (Φ_P = 0.87) and a shorter lifetime (τ = 0.17 μs) relative to those of **(ppy)$_2$Ir(acac)** (Φ_P = 0.34, τ = 1.6 μs),[28] indicating that dpa auxiliary ligand affects greatly the emission property of **Ir-dpa**. The optimized device based on **Ir-dpa** leads to an extremely high peak CE of 123.5 cd A^{-1} and a PE of 43.2 lm W^{-1}. Regardless of the high Φ_P and short lifetime, the outstanding performance may also result from the improved EI/ET property as induced by the two pyridyl rings in the dpa ligand, which will ensure balanced charge flux within the device. Zhu *et al.* designed an oxazoline based ligand and a thiazoline based ligand which can serve as auxiliary ligands to replace the acac ligand in **(ppy)$_2$Ir(acac)**.[446] The emissions of **Ir-oz** (λ_{em} = 527 nm) and **Ir-thoz** (λ_{em} = 542 nm) in solution are red-shifted as compared to that of **(ppy)$_2$Ir(acac)** (Table 14), because the phenolate rings in the oxazoline and thiazoline based ligands make notable contribution to the HOMOs, which may destabilize the HOMO levels of **Ir-oz** and **Ir-thoz** and result in the reduced E_g. The green-emitting device based on **Ir-oz** can offer very high peak CE of 66.2 cd A^{-1} and PE of 54 lm W^{-1}. Intriguing EL behavior is observed for the **Ir-thoz** based device with the EL band showing an unusually wide full width at half-maximum (FWHM) of *ca.* 110 nm with the emission maximum at around 540 nm. Considering the decent device efficiencies (8.5%, 27.0 cd A^{-1} and 18.0 lm W^{-1}) as well as the remarkably broadened emission band, **Ir-thoz** is very promising for fabricating two-color WOLED with high CRI.

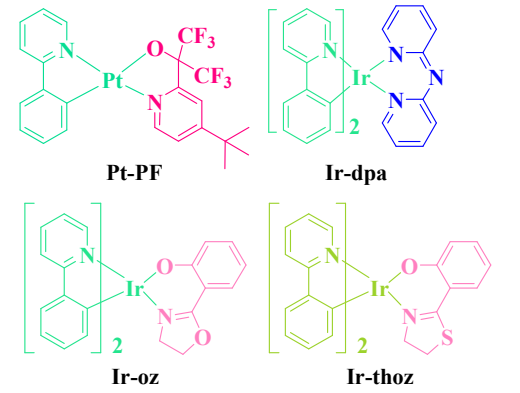

Fig. 111 Chemical structures of some ppy-type Pt(II) and Ir(III) complexes bearing various auxiliary ligands and peak efficiency data of related OLEDs.

Hou *et al.* firstly used an amidinate unit *N*,*N*′-diisopropylbenzamidinate (dipba) as an ancillary ligand to replace the acac ligands in (ppy-type)$_2$Ir(acac) complexes (Fig. 112).[447-450] Theoretical calculation results indicate that the N atoms of the dipba ligand make significant contributions to the HOMOs of the concerned complexes because of the stronger π-bonding ability of the dipba ligand than that of acac, resulting in greatly raised HOMO levels which are also confirmed by the experimental results. Therefore, notable red-shifts in the emissions of these dipba based complexes are observed as compared to those of the respective (ppy-type)$_2$Ir(acac) complexes. For example, **Ir-dipba2** (λ_{em} = 543 nm) displays green-yellow emission in $CHCl_3$ while **(ppy)$_2$Ir(acac)** (λ_{em} = 516 nm) shows green phosphorescence,[447] and **Ir-dipba4** (λ_{em} = 609 nm) emits red phosphorescence while **(bt)$_2$Ir(acac)** (λ_{em} = 557 nm) gives yellow emission (Table 14).[448] Besides the longer phosphorescence wavelength, their higher-lying HOMO levels will also facilitate the HI/HT properties of these dipba based phosphorescent emitters. Furthermore, the bulky dipba ligand can

effectively prevent the intermolecular aggregation behavior and thereby reduce the self-quenching and TTA effects at high concentrations. Therefore, these dipba based complexes can even be used to fabricate non-doped devices. The non-doped device based on **Ir-dipba1** displays green EL emission with a peak PE of 34.6 lm W^{-1} and the yellow-emitting non-doped device based on **Ir-dipba2** gives a peak PE of 32.5 lm W^{-1}. In addition, the efficiency roll-offs at high luminances are very low, as indicated by the high PE of 33.5 lm W^{-1} at 1000 cd m^{-2} for the **Ir-dipba1** based non-doped device.[449] These high PEs are partly attributed to the low driving voltages due to the well-matched MO levels with those of the charge transporting layers. In addition, the comparable HT and ET ability of **Ir-dipba1** (μ_h = 1.1 × 10^{-3} cm^2 V^{-1} s^{-1} and μ_e = 2.1 × 10^{-3} cm^2 V^{-1} s^{-1})[449] is also vital for realizing balanced charge flux within the device and thus achieving high efficiencies. The orange-red PHOLED using **Ir-dipba3** neat film as EML also shows an attractive performance ($V_{turn\text{-}on}$ = 2.5 V, peak PE = 18.7 lm W^{-1}).[450] Moreover, by doping **Ir-dipba3** into a blue fluorescent host, a two-color WOLED achieves an impressive performance with a maximum EQE of 27.8% and PE of 48.8 lm W^{-1}. The CIE coordinates of (0.35 ± 0.02, 0.33 ± 0.02) of this device are quite stable with the increased luminance from 10 to 10000 cd m^{-2}. In addition, the EQE and PE of this deivce remain as high as 26.8% and 37.5 lm W^{-1}, respectively, at 1000 cd m^{-2}, which should be attributed to the balanced charge flux within the device, as indicated by the comparable HT and ET ability of **Ir-dipba3** (μ_h = 6.5 × 10^{-4} cm^2 V^{-1} s^{-1} and μ_e = 8.8 × 10^{-4} cm^2 V^{-1} s^{-1}).[450] These results unambiguously demonstrate that the dipba auxiliary ligand can efficiently tune the phosphorescence wavelength, furnish bipolar features as well as avoid the intermolecular aggregation of the Ir(III) complexes.

By replacing the phenyl ring in dipba with the diphenylamine unit, Hou *et al.* synthesized a new

auxiliary ligand $(N\textit{i}Pr)_2C(NPh_2)$ (dipdpa) for a series of dipdpa-based Ir(III) complexes.[451] The resultant complexes show emission peaks from 505 nm to 655 nm in toluene with Φ_P in the range of 0.18-0.64 depending on the chromophoric ligands. Compared to the dipba based analogues, the dipdpa based Ir(III) complexes show slightly blue-shifted emissions (*e.g.* λ_{em} = 505, 536, 560 and 580 nm for **Ir-dipdpa1**, **Ir-dipdpa2**, **Ir-dipdpa3** and **Ir-dipdpa4**, respectively) (Table 14). Devices using these dipdpa based Ir(III) complexes as dopants can show encouraging performance. Especially, the 5 wt% doped green devices based on **Ir-dipdpa1** and **Ir-dipdpa2** give extremely high CE over 105 cd A^{-1} and high PE exceeding 40 lm W^{-1}, indicating their great potential in fabricating green-emitting PHOLEDs. Hou *et al.* also designed a series of amidinate units bearing different substituents on the central carbon atoms and investigated the influences from these amidinate auxiliary ligands on the emission properties of related Ir(III) complexes.[452] Compared to those of **$(ppy)_2$Ir(acac)** (λ_{em} = 516 nm, τ = 1.6 μs, Φ_P = 0.34),[28] the emission peaks of these Ir(III) complexes are red-shifted (*e.g.* λ_{em} = 528, 530, 548, 548 and 538 nm for **Ir-dipCz**, **Ir-dipPh**, **Ir-dipIp**, **Ir-dipIb** and **Ir-dipSi**, respectively) (Table 14) due to the significantly raised HOMO levels, and the lifetimes are slightly shorter within the range of 0.61-1.42 μs, indicating that these amidinate auxiliary ligands can fine-tune the emission properties of related Ir(III) complexes. Although their Φ_P (*ca.* 0.16-0.37) are slightly lower or comparable to that of $(ppy)_2$Ir(acac), these complexes exhibit impressive EL performance. Devices [ITO/NPB (30 nm)/5 wt% dopant:**CBP** (25 nm)/BCP (6 nm)/Alq_3 (20 nm)/LiF (1 nm)/Al (100 nm)] based on **Ir-dipPh**, **Ir-dipIp**, **Ir-dipIb** and **Ir-dipSi** all afford extremely high CE above 115 cd A^{-1}.[452] With optimized structure of ITO/NPB (35 nm)/15 wt% **Ir-dipIp**:TPBI (25 nm)/TPBI (30 nm)/LiF (0.5 nm)/Al, the yellow-emitting device exhibits an outstanding performance

with a peak EQE of 25.3 % and PE of 93.6 lm W^{-1}, which are the highest value obtained by yellow PHOLEDs so far.[453] In addition, this device can also give remarkably high EQE of 23.2% and PE of 38.7 lm W^{-1} at an extremely high luminance of 10000 cd m^{-2}. This impressive performance can be partly attributed to the suppressed intermolecular interaction between the emitter molecules due to the bulky auxiliary ligand. Besides, the balanced charge transport in this device induced by the bipolar character of **Ir-dipIp** ($\mu_h = 1.2 \times 10^{-3}$ cm^2 V^{-1} s^{-1} and $\mu_e = 3.5 \times 10^{-3}$ cm^2 V^{-1} s^{-1}) also governs such high efficiencies. Thus, the **Ir-dipIp** based non-doped device can also give encouraging efficiencies of 18.5% and 73.8 lm W^{-1} for peak EQE and PE, respectively.

From the results about Ir(III) complexes containing amidinate units as auxiliary ligands, it can be clearly seen that the emission color, Φ_P, τ_P and charge carrier injection/transporting features of the concerned phosphorescent emitters can also be controlled by the judiciously designed auxiliary ligands. In addition, the bulky amidinate auxiliary ligands can effectively restrain the undesired TTA effect in the PHOLEDs. On the whole, the amidinate auxiliary ligands are promising substitutes of acac in heteroleptic Ir(III) complexes, and may also be suitable for synthesizing high performance Pt(II) complexes.

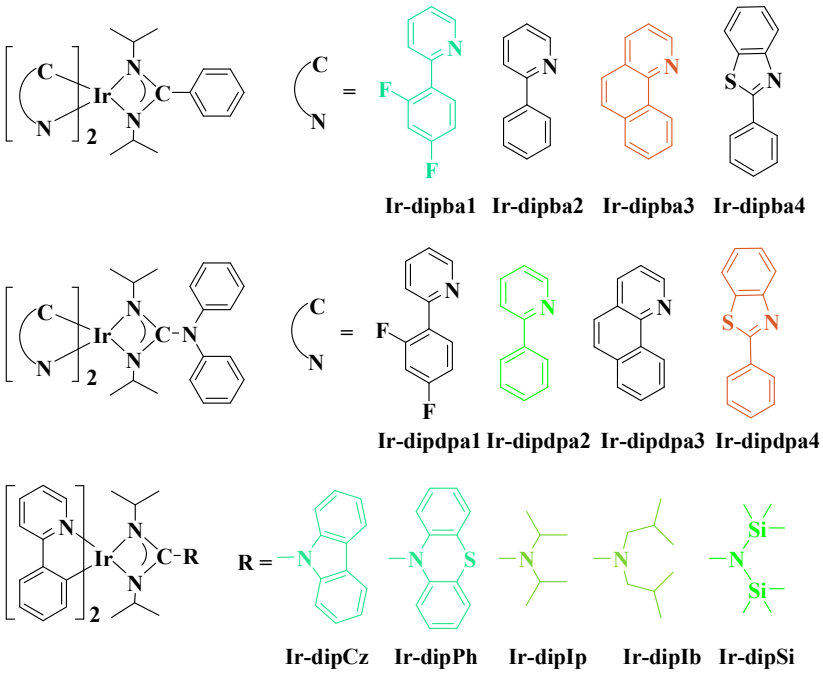

Fig. 112 Chemical structures of Ir(III) complexes bearing amidinate auxiliary ligands and peak efficiency data of related OLEDs.

Zheng *et al.* synthesized several heteroleptic Ir(III) complexes containing tetraphenylimidodiphosphinate unit as auxiliary ligand.[454-456] Compared with its analogue bis[(4,6-difluorophenyl)pyridinato-*N*,$C^{2'}$]iridium(acetylacetonate) [**FIr(acac)**],[424] **Ir-PN1** (Fig. 113) shows slightly red-shifted emission (λ_{em} = 485 nm) with lower quantum yield (Φ_P = 0.038) in solution (Table 14), indicating that the tetraphenylimidodiphosphinate auxiliary ligand has notable influence on the emission properties of the related complex. However, in the solid state **Ir-PN1** gives notably red-shifted emission peak (λ_{em} = 510 nm) with enhanced phosphorescence, which is

attributed to the aggregation-induced phosphorescent emission (AIPE). In dilute solution, the lowest excited state is dominated by the non-emissive triplet auxiliary ligand centered excited state (^{3}LX), leading to the low solution quantum yield. However, in the solid state, the excimeric interactions between the cyclometalating ligands of adjacent complexes will shift the lowest excited state from ^{3}LX to the emissive triplet metal-metal-to-ligand charge transfer (^{3}MMLCT) excited state, resulting in the lower energy emission accompanied by the increased Φ_P. The emission behavior of **Ir-PN2** is similar to that of **Ir-PN1**. When **Ir-PN1** and **Ir-PN2** are used as dopants for OLEDs, the related devices [ITO/TAPC (40 nm)/**Ir-PN1** or **Ir-PN2**:**mCP** (20 nm, *x* wt%)/TPBi (40 nm)/LiF (1 nm)/Al (100 nm)] show impressive performance. The device based on **Ir-PN1** (10 wt%) displays bluish-green emission with the peak PE of 23.52 lm W^{-1} and CE of 25.45 cd A^{-1}, while the device based on **Ir-PN2** (6 wt%) emits green light with the peak PE of 69.90 lm W^{-1} and CE of 67.95 cd A^{-1}.[454] By replacing the LiF layer with a new ET layer which contains an ET material 2,4,7,9-tetraphenyl-1,10-phenanthroline (TPPhen) doped with a molecular n-dopant tetrakis(1,3,4,6,7,8-hexahydro-2H-pyrimido[1,2-a]pyrimidinato)ditungsten(II) ($W_2(hpp)_4$), the device can be further optimized with the device configuration of ITO/MoO_3(1 nm)/**mCP** (60 nm)/**mCP**:TPBI:**Ir-PN2** (20 nm, 1:1, 6 wt%)/TPBI (15 nm)/TPPhen:$W_2(hpp)_4$ (45 nm, 12 wt%)/Al (100 nm).[457] This device furnishes a maximum EQE of 20.8% and CE of 72.9 cd A^{-1}. Besides, the CE remains as high as 69.8 cd A^{-1} at 1000 cd m^{-2} and 60.7 cd A^{-1} at 10000 cd m^{-2}, reflecting the rather low efficiency roll-off at high luminances. Zheng *et al.* also synthesized a heteroleptic Ir(III) complex **Ir-PN3** in which the phenyl rings of the auxiliary ligand were substituted by $-CF_3$ groups.[455] The $-CF_3$ substituted auxiliary ligand stabilizes the HOMO slightly more than the LUMO,

leading to a slightly blue-shifted emission of **Ir-PN3** (λ_{em} = 517 nm) as compared to that of **Ir-PN2** (λ_{em} = 524 nm). Besides, the lower-lying LUMO level will improve the EI/ET property of **Ir-PN3**. As a result, an optimized device based on **Ir-PN3** can lead to an extremely high maximum PE of 113.2 lm W^{-1} and CE of 115.4 cd A^{-1}, declaring the great potential of applying **Ir-PN3** to green-emitting PHOLEDs.

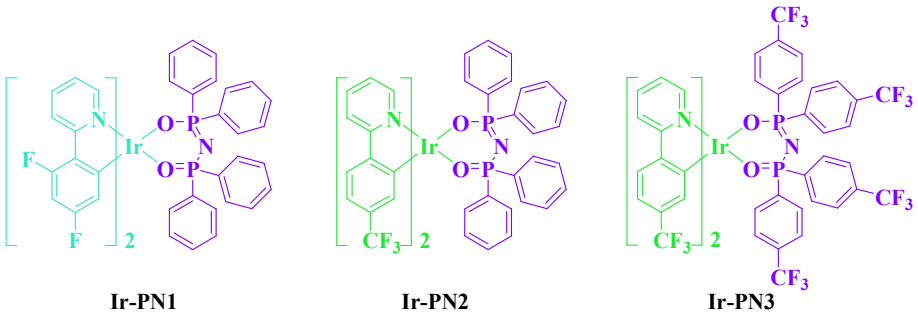

Fig. 113 Chemical structures of **Ir-PN1 – Ir-PN3**and peak efficiency data of related OLEDs.

Table 14. Phosphorescent emitters with main-group unit functionalized auxiliary ligand and their properties

Main-group element unit	Metal center	Emitter	Φ_P	$\lambda_{max,em}$ nm	EQE %	CE cd A^{-1}	PE lm W^{-1}	Ref.
2-pyridylmethanol	**Pt**	**Pt-PF**	0.005	525	4.07	13.5	–	444
2,2′-dipyridylamido	**Ir**	**Ir-dpa**	0.87	480	–	123.5	43.2	445
oxazoline	**Ir**	**Ir-oz**	0.55	527	17.1	66.2	54.0	446
thiazoline	**Ir**	**Ir-thoz**	0.27	542	8.50	27.0	18.0	446
amidinate	**Ir**	**Ir-dipba3**	0.41	572	18.4	21.4	18.7	450
guanidinate	**Ir**	**Ir-dipdpa1**	0.64	505	–	107	40.5	451
guanidinate	**Ir**	**Ir-dipdpa2**	0.42	536	–	125	43.6	451
amidinate	**Ir**	**Ir-dipIp**	0.16	548	25.3	–	93.6	452
amidinate	**Ir**	**Ir-dipIb**	0.17	548	–	137	39.2	452
phenylimidodiphosphinate	**Ir**	**Ir-PN1**	0.038	485	–	25.5	23.5	454
phenylimidodiphosphinate	**Ir**	**Ir-PN2**	0.12	524	20.8	72.9	66.3	457
phenylimidodiphosphinate	**Ir**	**Ir-PN3**	0.09	517	–	115.4	113.2	455

5. Summary and outlook

After years of development, PHOLEDs can emit light covering nearly the whole visible spectrum with high efficiencies to warrant their bright future of their application in new generation full-color display and energy-saving solid-state lighting. The great success of PHOLEDs mainly relies on both the phosphorescent emitters and the advanced host materials. Owing to their diverse electronic features, the moieties containing nonmetallic main-group elements can furnish both the phosphorescent emitters and the host materials with unique properties which can effectively enhance the EL performance of the concerned PHOLEDs. The electron-deficient boron-based groups can not only enhance the EI/ET ability of the hosts and triplet emitters, but can also tune the phosphorescence color as well as significantly increase the Φ_P. The bulky tetrahedral tetraphenylsilane and tetraphenylgermanium groups can effectively limit the π-conjugation elongation, leading to high triplet energies of the host materials. Moreover, the intermolecular interactions between the host molecules or emitter molecules can also be suppressed to improve the device stability. Depending on its hybridization mode, nitrogen-containing group can show either electron-donating or electron-withdrawing ability. Thus, according to their chemical structures, the nitrogen-containing moieties can significantly improve the HI/HT or EI/ET abilities of both the related host materials and triplet emitters. Whatever the nitrogen-containing groups show electron-donating or electron-withdrawing properties, the emission color of the complexes can be widely tuned to cover almost the whole visible spectrum. Falling in the same group as the N element, phosphorus is usually used at its oxidation state, *i.e.*, groups containing strongly polarized P=O moiety are always used to improve the EI/ET capabilities of the related host and emitting materials.

Sometimes, the P atom is directly ligated with the transition metal ion, *i.e.*, the phosphorus-containing ligand can serve as the auxiliary ligand to fine-tune the emission properties of the complexes. The main-group moieties containing oxygen and sulfur atoms can be used to fine-tune the E_T for both host materials and phosphorescent complexes due to their relatively weaker electron-donating abilities as compared with the arylamine groups. Besides, the oxygen-containing moieties can also be employed to construct tetradentate lignds to furnish deep-blue-emitting Pt(II) complexes. Furthermore, when the sulfur atoms are oxidized to form sulfonyl units, the EI/ET abilities of related host materials and phosphorescent emitters can be significantly improved to bring high EL efficiencies. The fluorine-bearing moieties show electron-withdrawing character. Therefore, they play critical role in stabilizing the HOMO levels to bring about blue phosphorescence in triplet emitters, representing their most important application in the field of PHOLEDs. Furthermore, incorporation of the main-group moieties with different charge carrier injection/transporting ability into single host or phosphorescent molecule can furnish bipolar host materials and phosphorescent emitters which can effectively enhance the EL efficiencies and relieve the efficiency roll-off effect. The main-group moieties can also benefit the thermal and morphological stabilities of the hosts and emitters by improving their T_g. Usually, the incorporation of bulky triarylborane, tetraphenylsilane, tetraphenylgermanium, triphenylamine, carbazole and diphenylphosphine oxide groups will increase the molecular weight, especially when the triphenylamine and carbazole units are used to construct the dendrimers. In addition, the incorporation of rigid blocks with optimized substitution position, such as carbazole, carboline, dibenzofuran and dibenzothiophene, can effectively improve the rigidity of the resultant materials. The high molecular weight and the rigid molecular configuration

will show positive effect on increasing the T_g of the materials to benefit their final EL performance. Hence, nonmetallic main-group moieties can play an irreplaceable role in coping with the critical problems in the field of PHOLEDs, which will definitely bring prosperity and bright future to this area.

To date, a lot of monochromatic as well as white PHOLEDs based on main-group element functionalized host materials and phosphorescent emitters have produced encouraging EL performance in terms of EQE (> 20%), CE (> 50 cd A^{-1}) and PE (> 30 lm W^{-1}). Some devices can even give EQE exceeding 30%, CE above 100 cd A^{-1} or PE over 100 lm W^{-1}, fully demonstrating their practical application in display and lighting. However, several challenges of the PHOLEDs also need to be tackled. The efficiency roll-off at high luminances is rather common for most devices due to the exciton quenching effects at high current densities. Fabricating devices with main-group element functionalized host as well as emitting materials to achieve balanced charge flux within the device as far as possible can effectively restrain the efficiency roll-off at high luminance. Considering the higher HT mobility than ET mobility in most PHOLEDs, more attention should be paid to promote the EI/ET capacity of the hosts and phosphorescent emitters through designing more sophisticated main-group moieties with electron-withdrawing characters, such as phosphafluorene oxide moiety. Much more efforts should go to the area of bipolar phosphorescent emitters. For example, the systematic investigations of their sturcture-property relationship, such as different combination of the EI/ET and HI/HT groups, are really needed to provide important guidance for the design and synthesis of high-performance bipolar phosphorescent emitters. Devices based on most of the blue phosphorescent emitters cannot provide desired pure blue CIE coordinates of (0.14, 0.08) as

recommended by the NTSC. To meet the requirement, the blue phosphorescent emitters should possess E_T at least over 2.8 eV with very narrow FWHM (*e.g.*, < 50 nm) at the same time. Besides, the corresponding hosts should have even higher E_T to promote efficient energy transfer from the host to the emitter and/or completely confine the excitons on the emitter molecules. From the results obtained, phosphorescent emitters bearing carbene-based non-conjugated ligands with proper main-group moieties, and well-designed rigid molecular structure have the potential to achieve deep-blue phosphorescence with good quality. This strategy also shows the potential in developing fluorine-free blue phosphorescent emitters with good stabilities. Fabrication of the highly efficient phosphoresccent device with long-term operation stability is still a big challenge to date. To overcome this challenge, both hosts and phosphorescent emitters should show highly balanced charge carrier injection/transporting ability, high chemical stabilities as well as morphological stabilities during the device fabrication and operation processes under electric field. In view of the great achievements realized by the moieties containing non-metallic main-group elements, we are optimistic that all these crucial issues can be properly solved and the PHOLED technology will truly benefit the world widely in the near future.

Acknowledgements

This work was financially supported by Tengfei Project from Xi'an Jiaotong University, the Fundamental Research Funds for the Central Universities (cxtd2015003), The Program for New Century Excellent Talents in University, the Ministry of Education of China (NECT-09-0651), the Key Creative Scientific Research Team in Shaanxi Province (2013KCT-05), the China Postdoctoral

Science Foundation (Grant no. 20130201110034), and the National Natural Science Foundation of China (nos. 20902072 and 51373145). The financial support from State Key Laboratory for Mechanical Behavior of Materials is also acknowledged. W.-Y.W. acknowledges the financial support from the National Basic Research Program of China (973 Program, grant no. 2013CB834702), the Science, Technology and Innovation Committee of Shenzhen Municipality (JCYJ20140419130507116), the Areas of Excellence Scheme, University Grants Committee of HKSAR, China (no. AoE/P-03/08), Hong Kong Research Grants Council (no. HKBU 203313) and Hong Kong Baptist University (no. FRG1/14-15/084).

References

1. C. W. Tang and S. A. Vanslyke, *Appl. Phys. Lett.*, 1987, **51**, 913-915.
2. J. H. Burroughes, D. D. C. Bradley, A. R. Brown, R. N. Marks, K. Mackay, R. H. Friend, P. L. Burns and A. B. Holmes, *Nature*, 1990, **347**, 539-541.
3. C. Adachi, T. Tsutsui and S. Saito, *Appl. Phys. Lett.*, 1990, **56**, 799-801.
4. J. Kido, M. Kimura and K. Nagai, *Science*, 1995, **267**, 1332-1334.
5. A. R. Brown, K. Pichler, N. C. Greenham, D. D. C. Bradley, R. H. Friend and A. B. Holmes, *Chem. Phys. Lett.*, 1993, **210**, 61-66.
6. M. A. Baldo, D. F. O'Brien, M. E. Thompson and S. R. Forrest, *Phys. Rev. B*, 1999, **60**, 14422-14428.
7. Y. G. Ma, H. Y. Zhang, J. C. Shen and C. M. Che, *Synth. Met.*, 1998, **94**, 245-248.
8. M. A. Baldo, D. F. O'Brien, Y. You, A. Shoustikov, S. Sibley, M. E. Thompson and S. R. Forrest, *Nature*, 1998, **395**, 151−154.
9. Y. You and S. Y. Park, *Dalton Trans.*, 2009, 1267-1282.
10. X. L. Yang, C. L. Yao and G. J. Zhou, *Platinum Met. Rev.*, 2013, **57**, 2-16.
11. J.-L. Liao, Y. Chi, Y.-D. Su, H.-X. Huang, C.-H. Chang, S.-H. Liu, G.-H. Lee and P.-T. Chou, *J. Mater. Chem. C*, 2014, **2**, 6269-6282.
12. G. Cheng, K. T. Chan, W. P. To and C. M. Che, *Adv. Mater.*, 2014, **26**, 2540-2546.
13. H. Shahroosvand, L. Najafi, A. Sousaraei, E. Mohajerani and M. Janghouri, *J. Mater. Chem. C*, 2013, **1**, 6970-6980.
14. Z. Liu, J. Qiu, F. Wei, J. Wang, X. Liu, M. G. Helander, S. Rodney, Z. Wang, Z. Bian, Z. Lu, M. E. Thompson and C. Huang, *Chem. Mater.*, 2014, **26**, 2368-2373.
15. H. Yersin, *Top. Curr. Chem.*, 2004, **241**, 1-26.
16. Y. Kawamura, K. Goushi, J. Brooks, J. J. Brown, H. Sasabe and C. Adachi, *Appl. Phys. Lett.*,

2005, **86**, 071104.
17. L. X. Xiao, S. J. Su, Y. Agata, H. L. Lan and J. Kido, *Adv. Mater.*, 2009, **21**, 1271-1274.
18. J. Kwak, Y. Y. Lyu, H. Lee, B. Choi, K. Char and C. Lee, *J. Mater. Chem.*, 2012, **22**, 6351-6355.
19. Q. Wang, I. W. H. Oswald, M. R. Perez, H. Jia, A. A. Shahub, Q. Qiao, B. E. Gnade and M. A. Omary, *Adv. Funct. Mater.*, 2014, **24**, 4746-4752.
20. Q. Wang, I. W. Oswald, X. Yang, G. Zhou, H. Jia, Q. Qiao, Y. Chen, J. Hoshikawa-Halbert and B. E. Gnade, *Adv. Mater.*, 2014, **26**, 8107-8113.
21. Y. H. Song, S. J. Yeh, C. T. Chen, Y. Chi, C. S. Liu, J. K. Yu, Y. H. Hu, P. T. Chou, S. M. Peng and G. H. Lee, *Adv. Funct. Mater.*, 2004, **14**, 1221-1226.
22. J. Q. Ding, J. Gao, Y. X. Cheng, Z. Y. Xie, L. X. Wang, D. G. Ma, X. B. Jing and F. S. Wang, *Adv. Funct. Mater.*, 2006, **16**, 575-581.
23. L. X. Xiao, Z. J. Chen, B. Qu, J. X. Luo, S. Kong, Q. H. Gong and J. J. Kido, *Adv. Mater.*, 2011, **23**, 926-952.
24. Y. T. Tao, C. L. Yang and J. G. Qin, *Chem. Soc. Rev.*, 2011, **40**, 2943-2970.
25. Z. M. Hudson, C. Sun, M. G. Helander, H. Amarne, Z. H. Lu and S. N. Wang, *Adv. Funct. Mater.*, 2010, **20**, 3426-3439.
26. G. Schwartz, S. Reineke, T. C. Rosenow, K. Walzer and K. Leo, *Adv. Funct. Mater.*, 2009, **19**, 1319-1333.
27. S. Reineke, F. Lindner, G. Schwartz, N. Seidler, K. Walzer, B. Lussem and K. Leo, *Nature*, 2009, **459**, 234-239.
28. S. Lamansky, P. Djurovich, D. Murphy, F. Abdel-Razzaq, H. E. Lee, C. Adachi, P. E. Burrows, S. R. Forrest and M. E. Thompson, *J. Am. Chem. Soc.*, 2001, **123**, 4304-4312.
29. P. T. Chou and Y. Chi, *Chem. Eur. J.*, 2007, **13**, 380-395.
30. J. Y. Li, T. Zhang, Y. J. Liang and R. X. Yang, *Adv. Funct. Mater.*, 2013, **23**, 619-628.
31. G. J. Zhou, C. L. Ho, W. Y. Wong, Q. Wang, D. G. Ma, L. X. Wang, Z. Y. Lin, T. B. Marder and A. Beeby, *Adv. Funct. Mater.*, 2008, **18**, 499-511.
32. G. J. Zhou, W. Y. Wong, B. Yao, Z. Y. Xie and L. X. Wang, *Angew. Chem. Int. Ed.*, 2007, **46**, 1149-1151.
33. H. F. Chen, S. J. Yang, Z. H. Tsai, W. Y. Hung, T. C. Wang and K. T. Wong, *J. Mater. Chem.*, 2009, **19**, 8112-8118.
34. T. Y. Hwu, T. C. Tsai, W. Y. Hung, S. Y. Chang, Y. Chi, M. H. Chen, C. I. Wu, K. T. Wong and L. C. Chi, *Chem. Commun.*, 2008, 4956-4958.
35. H. Fukagawa, N. Yokoyama, S. Irisa and S. Tokito, *Adv. Mater.*, 2010, **22**, 4775-4778.
36. Y. Chi and P. T. Chou, *Chem. Soc. Rev.*, 2010, **39**, 638-655.
37. P. T. Chou and Y. Chi, *Eur. J. Inorg. Chem.*, 2006, 3319-3332.
38. C. Fan and C. Yang, *Chem. Soc. Rev.*, 2014, **43**, 6439-6469.
39. C. L. Ho and W. Y. Wong, *New J. Chem.*, 2013, **37**, 1665-1683.
40. K. S. Yook and J. Y. Lee, *Adv. Mater.*, 2014, **26**, 4218-4233.
41. S. C. Lo and P. L. Burn, *Chem. Rev.*, 2007, **107**, 1097-1116.
42. H. B. Wu, L. Ying, W. Yang and Y. Cao, *Chem. Soc. Rev.*, 2009, **38**, 3391-3400.
43. X. L. Yang, G. J. Zhou and W. Y. Wong, *J. Mater. Chem. C*, 2014, **2**, 1760-1778.

44. R. J. Holmes, S. R. Forrest, Y. J. Tung, R. C. Kwong, J. J. Brown, S. Garon and M. E. Thompson, *Appl. Phys. Lett.*, 2003, **82**, 2422-2424.
45. X. Gong, J. C. Ostrowski, D. Moses, G. C. Bazan and A. J. Heeger, *Adv. Funct. Mater.*, 2003, **13**, 439-444.
46. R. Holmes, B. D'Andrade, S. Forrest, X. Ren, J. Li and M. Thompson, *Appl. Phys. Lett.*, 2003, **83**, 3818-3820.
47. X. F. Ren, J. Li, R. J. Holmes, P. I. Djurovich, S. R. Forrest and M. E. Thompson, *Chem. Mater.*, 2004, **16**, 4743-4747.
48. S. Kappaun, C. Slugovc and E. J. W. List, *Int. J. Mol. Sci.*, 2008, **9**, 1527-1547.
49. C. R. Wade, A. E. Broomsgrove, S. Aldridge and F. P. Gabbaï, *Chem. Rev*, 2010, **110**, 3958-3984.
50. Z. M. Hudson and S. Wang, *Acc. Chem. Res.*, 2009, **42**, 1584-1596.
51. T. Noda and Y. Shirota, *J. Am. Chem. Soc.*, 1998, **120**, 9714-9715.
52. S. L. Lin, L. H. Chan, R. H. Lee, M. Y. Yen, W. J. Kuo, C. T. Chen and R. J. Jeng, *Adv. Mater.*, 2008, **20**, 3947-3952.
53. F. Li, W. Jia, S. Wang, Y. Zhao and Z.-H. Lu, *J. Appl. Phys.*, 2008, **103**, 034509.
54. T. Zhang, R. Wang, L. Wang, Q. Wang and J. Li, *Dyes Pigm.*, 2013, **97**, 155-161.
55. P. Erk, M. Bold, M. Egen, E. Fuchs, T. Geßner, K. Kahle, C. Lennartz, O. Molt, S. Nord and H. Reichelt, SID Int. Symp. Dig. Tech., 2006.
56. B. W. DAndrade, S. R. Forrest and A. B. Chwang, *Appl. Phys. Lett.*, 2003, **83**, 3858-3860.
57. P. I. Shih, C. H. Chien, C. Y. Chuang, C. F. Shu, C. H. Yang, J. H. Chen and Y. Chi, *J. Mater. Chem.*, 2007, **17**, 1692-1698.
58. R. J. Holmes, B. W. D'Andrade, S. R. Forrest, X. Ren, J. Li and M. E. Thompson, *Appl. Phys. Lett.*, 2003, **83**, 3818-3820.
59. J. J. Lin, W. S. Liao, H. J. Huang, F. I. Wu and C. H. Cheng, *Adv. Funct. Mater.*, 2008, **18**, 485-491.
60. P. I. Shih, C. H. Chien, T. I. Wu and C. F. Shu, *Adv. Funct. Mater.*, 2007, **17**, 3514-3520.
61. C. H. Wu, P. I. Shih, C. F. Shu and Y. Chi, *Appl. Phys. Lett.*, 2008, **92**, 233303.
62. C. Fan, Y. H. Chen, Z. Q. Jiang, C. L. Yang, C. Zhong, J. G. Qin and D. G. Ma, *J. Mater. Chem.*, 2010, **20**, 3232-3237.
63. Z. Q. Jiang, Y. H. Chen, C. L. Yang, Y. Cao, Y. T. Tao, J. G. Qin and D. G. Ma, *Org. Lett.*, 2009, **11**, 1503-1506.
64. S. H. Ye, Y. Q. Liu, K. Lu, W. P. Wu, C. Y. Du, Y. Liu, H. T. Liu, T. Wu and G. Yu, *Adv. Funct. Mater.*, 2010, **20**, 3125-3135.
65. Y. X. Zhang, L. Zhang, L. S. Cui, C. H. Gao, H. Chen, Q. Li, Z. Q. Jiang and L. S. Liao, *Org. Lett.*, 2014, **16**, 3748-3751.
66. Z. Q. Liu, Q. Fang, D. Wang, D. X. Cao, G. Xue, W. T. Yu and H. Lei, *Chem. Eur. J.*, 2003, **9**, 5074-5084.
67. O. Kwon, S. Barlow, S. A. Odom, L. Beverina, N. J. Thompson, E. Zojer, J. L. Bredas and S. R. Marder, *J. Phys. Chem. A*, 2005, **109**, 9346-9352.
68. Z. Gao, Y. L. Liu, Z. M. Wang, F. Z. Shen, H. Liu, G. N. Sun, L. Yao, Y. Lv, P. Lu and Y. G. Ma, *Chem. Eur. J.*, 2013, **19**, 2602-2605.

69. Y. Zhang, S. L. Lai, Q. X. Tong, M. F. Lo, T. W. Ng, M. Y. Chan, Z. C. Wen, J. He, K. S. Jeff, X. L. Tang, W. M. Liu, C. C. Ko, P. F. Wang and C. S. Lee, *Chem. Mater.*, 2012, **24**, 61-70.
70. Z. Jiang, T. Ye, C. Yang, D. Yang, M. Zhu, C. Zhong, J. Qin and D. Ma, *Chem. Mater.*, 2011, **23**, 771-777.
71. D. F. O'Brien, M. A. Baldo, M. E. Thompson and S. R. Forrest, *Appl. Phys. Lett.*, 1999, **74**, 442-444.
72. S. Tokito, T. Iijima, Y. Suzuri, H. Kita, T. Tsuzuki and F. Sato, *Appl. Phys. Lett.*, 2003, **83**, 569-571.
73. K. Brunner, A. van Dijken, H. Borner, J. J. A. M. Bastiaansen, N. M. M. Kiggen and B. M. W. Langeveld, *J. Am. Chem. Soc.*, 2004, **126**, 6035-6042.
74. L. S. Cui, S. C. Dong, Y. Liu, Q. Li, Z. Q. Jiang and L. S. Liao, *J. Mater. Chem. C*, 2013, **1**, 3967-3975.
75. S. L. Gong, X. He, Y. H. Chen, Z. Q. Jiang, C. Zhong, D. G. Ma, J. G. Qin and C. L. Yang, *J. Mater. Chem.*, 2012, **22**, 2894-2899.
76. L. Deng, X. Wang, Z. Zhang and J. Li, *J. Mater. Chem.*, 2012, **22**, 19700-19708.
77. K. R. Wee, Y. J. Cho, S. Jeong, S. Kwon, J. D. Lee, I. H. Suh and S. O. Kang, *J. Am. Chem. Soc.*, 2012, **134**, 17982-17990.
78. J. H. Jou, S. M. Shen, S. H. Chen, M. H. Wu, W. B. Wang, H. C. Wang, C. R. Lin, Y. C. Chou, P. H. Wu and J. J. Shyue, *Appl. Phys. Lett.*, 2010, **96**, 143306.
79. T. Sakai, H. Seo, S. Aihara, M. Kubota and M. Furuta, *IS&T/SPIE Electronic Imaging*, 2013.
80. S. J. Su, C. Cai and J. Kido, *J. Mater. Chem.*, 2012, **22**, 3447-3456.
81. L. S. Cui, Y. Liu, Q. Li, Z. Q. Jiang and L. S. Liao, *Org. Electron.*, 2014, **15**, 1368-1377.
82. X. D. Yuan, J. Liang, Y. C. He, Q. Li, C. Zhong, Z. Q. Jiang and L. S. Liao, *J. Mater. Chem. C*, 2014, **2**, 6387-6394.
83. H. Sasabe, Y. J. Pu, K. Nakayama and J. Kido, *Chem. Commun.*, 2009, 6655-6657.
84. C. L. Ho, L. C. Chi, W. Y. Hung, W. J. Chen, Y. C. Lin, H. Wu, E. Mondal, G. J. Zhou, K. T. Wong and W. Y. Wong, *J. Mater. Chem.*, 2012, **22**, 215-224.
85. S. Y. Chen, J. B. Wei, K. Wang, C. G. Wang, D. Chen, Y. Liu and Y. Wang, *J. Mater. Chem. C*, 2013, **1**, 6594-6602.
86. M. H. Tsai, Y. H. Hong, C. H. Chang, H. C. Su, C. C. Wu, A. Matoliukstyte, J. Simokaitiene, S. Grigalevicius, J. V. Grazulevicius and C. P. Hsu, *Adv. Mater.*, 2007, **19**, 862-866.
87. W. Jiang, L. A. Duan, J. A. Qiao, G. F. Dong, D. Q. Zhang, L. D. Wang and Y. Qiu, *J. Mater. Chem.*, 2011, **21**, 4918-4926.
88. W. Jiang, Z. J. Ge, P. Y. Cai, B. Huang, Y. Q. Dai, Y. M. Sun, J. Qiao, L. D. Wang, L. Duan and Y. Qiu, *J. Mater. Chem.*, 2012, **22**, 12016-12022.
89. J. Q. Ding, B. H. Zhang, J. H. Lu, Z. Y. Xie, L. X. Wang, X. B. Jing and F. S. Wang, *Adv. Mater.*, 2009, **21**, 4983-4986.
90. B. H. Zhang, G. P. Tan, C. S. Lam, B. Yao, C. L. Ho, L. H. Liu, Z. Y. Xie, W. Y. Wong, J. Q. Ding and L. X. Wang, *Adv. Mater.*, 2012, **24**, 1873-1877.
91. X. D. Wang, S. M. Wang, Z. H. Ma, J. Q. Ding, L. X. Wang, X. B. Jing and F. S. Wang, *Adv. Funct. Mater.*, 2014, **24**, 3413-3421.
92. A. P. Kulkarni, C. J. Tonzola, A. Babel and S. A. Jenekhe, *Chem. Mater.*, 2004, **16**,

4556-4573.
93. G. Hughes and M. R. Bryce, *J. Mater. Chem.*, 2005, **15**, 94-107.
94. Y. T. Chang, J. K. Chang, Y. T. Lee, P. S. Wang, J. L. Wu, C. C. Hsu, I. W. Wu, W. H. Tseng, T. W. Pi, C. T. Chen and C. I. Wu, *ACS Appl. Mater. Interfaces*, 2013, **5**, 10614-10622.
95. J. H. Ahn, C. Wang, C. Pearson, M. R. Bryce and M. C. Petty, *Appl. Phys. Lett.*, 2004, **85**, 1283-1285.
96. S. Oyston, C. Wang, G. Hughes, A. S. Batsanov, I. F. Perepichka, M. R. Bryce, J. H. Ahn, C. Pearson and M. C. Petty, *J. Mater. Chem.*, 2005, **15**, 194-203.
97. S. Y. Chen, X. J. Xu, Y. Q. Liu, W. F. Qiu, G. Yu, X. B. Sun, H. J. Zhang, T. Qi, K. Lu, X. Gao, Y. Liu and D. B. Zhu, *J. Mater. Chem.*, 2007, **17**, 3788-3795.
98. M. K. Leung, C. C. Yang, J. H. Lee, H. H. Tsai, C. F. Lin, C. Y. Huang, Y. O. Su and C. F. Chiu, *Org. Lett.*, 2007, **9**, 235-238.
99. P. Venkatakrishnan, P. Natarajan, J. N. Moorthy, Z. H. Lin and T. J. Chow, *Tetrahedron*, 2012, **68**, 7502-7508.
100. T.-L. Chiu, P.-Y. Lee, J.-H. Lee, C.-H. Hsiao, M.-K. Leung, C.-C. Lee, C.-Y. Chen and C.-C. Yang, *J. Appl. Phys.*, 2011, **109**, 084520.
101. Y. T. Tao, L. Ao, Q. Wang, C. Zhong, C. L. Yang, J. G. Qin and D. G. Ma, *Chem. Asian J.*, 2010, **5**, 278-284.
102. H. Inomata, K. Goushi, T. Masuko, T. Konno, T. Imai, H. Sasabe, J. J. Brown and C. Adachi, *Chem. Mater.*, 2004, **16**, 1285-1291.
103. R. A. Klenkler, H. Aziz, A. Tran, Z. D. Popovic and G. Xu, *Org. Electron.*, 2008, **9**, 285-290.
104. C. Sun, Z. M. Hudson, M. G. Helander, Z. H. Lu and S. N. Wang, *Organometallics*, 2011, **30**, 5552-5555.
105. S. J. Su, H. Sasabe, Y. J. Pu, K. Nakayama and J. Kido, *Adv. Mater.*, 2010, **22**, 3311-3316.
106. H.-F. Chen, S.-J. Yang, Z.-H. Tsai, W.-Y. Hung, T.-C. Wang and K.-T. Wong, *J. Mater. Chem.*, 2009, **19**, 8112-8118.
107. H. F. Chen, T. C. Wang, S. W. Lin, W. Y. Hung, H. C. Dai, H. C. Chiu, K. T. Wong, M. H. Ho, T. Y. Cho, C. W. Chen and C. C. Lee, *J. Mater. Chem.*, 2012, **22**, 15620-15627.
108. T. Motoyama, H. Sasabe, Y. Seino, J. Takamatsu and J. Kido, *Chem. Lett.*, 2011, **40**, 306-308.
109. C. W. Lee and J. Y. Lee, *Adv. Mater.*, 2013, **25**, 5450-5454.
110. C. W. Lee, Y. Im, J. A. Seo and J. Y. Lee, *Chem. Commun.*, 2013, **49**, 9860-9862.
111. T. Matsushima and C. Adachi, *Appl. Phys. Lett.*, 2006, **89**, 253506.
112. M. Y. Ha and D. G. Moon, *Appl. Phys. Lett.*, 2008, **93**, 043306.
113. S. O. Jeon, K. S. Yook, C. W. Joo and J. Y. Lee, *J. Mater. Chem.*, 2009, **19**, 5940-5944.
114. S. O. Jeon and J. Y. Lee, *J. Mater. Chem.*, 2012, **22**, 4233-4243.
115. W. Jiang, H. G. Xu, X. X. Ban, G. L. Yuan, Y. M. Sun, B. Huang, L. Duan and Y. Qiu, *Org. Lett.*, 2014, **16**, 1140-1143.
116. P. E. Burrows, A. B. Padmaperuma, L. S. Sapochak, P. Djurovich and M. E. Thompson, *Appl. Phys. Lett.*, 2006, **88**, 183503.
117. S. O. Jeon, K. S. Yook, C. W. Joo and J. Y. Lee, *Appl. Phys. Lett.*, 2009, **94**, 013301.
118. A. B. Padmaperuma, L. S. Sapochak and P. E. Burrows, *Chem. Mater.*, 2006, **18**, 2389-2396.
119. D. H. Yu, Y. B. A. Zhao, H. Xu, C. M. Han, D. G. Ma, Z. P. Deng, S. Gao and P. F. Yan, *Chem.*

Eur. J., 2011, **17**, 2592-2596.
120. S. E. Jang, K. S. Yook and J. Y. Lee, *Org. Electron.*, 2010, **11**, 1154-1157.
121. S. E. Jang, C. W. Joo, S. O. Jeon, K. S. Yook and J. Y. Lee, *Org. Electron.*, 2010, **11**, 1059-1065.
122. S. O. Jeon, K. S. Yook, C. W. Joo, H. S. Son, S. E. Jang and J. Y. Lee, *Org. Electron.*, 2009, **10**, 998-1000.
123. L. S. Cui, S. C. Dong, Y. Liu, M. F. Xu, Q. Li, Z. Q. Jiang and L. S. Liao, *Org. Electron.*, 2013, **14**, 1924-1930.
124. K. S. Yook and J. Y. Lee, *Adv. Mater.*, 2012, **24**, 3169-3190.
125. X. Y. Cai, A. B. Padmaperuma, L. S. Sapochak, P. A. Vecchi and P. E. Burrows, *Appl. Phys. Lett.*, 2008, **92**, 083308.
126. S. C. Dong, C. H. Gao, X. D. Yuan, L. S. Cui, Z. Q. Jiang, S. T. Lee and L. S. Liao, *Org. Electron.*, 2013, **14**, 902-908.
127. S. C. Dong, L. Zhang, J. Liang, L. S. Cui, Q. Li, Z. Q. Jiang and L. S. Liao, *J. Phys. Chem. C*, 2014, **118**, 2375-2384.
128. S. J. Kim, J. Leroy, C. Zuniga, Y. D. Zhang, L. Y. Zhu, J. S. Sears, S. Barlow, J. L. Bredas, S. R. Marder and B. Kippelen, *Org. Electron.*, 2011, **12**, 1314-1318.
129. X. X. Ban, H. G. Xu, G. L. Yuan, W. Jiang, B. Huang and Y. M. Sun, *Org. Electron.*, 2014, **15**, 1678-1686.
130. H. Sasabe, Y. Seino, M. Kimura and J. Kido, *Chem. Mater.*, 2012, **24**, 1404-1406.
131. S. J. Yeh, M. F. Wu, C. T. Chen, Y. H. Song, Y. Chi, M. H. Ho, S. F. Hsu and C. H. Chen, *Adv. Mater.*, 2005, **17**, 285-289.
132. M. T. Wu, S. J. Yeh, C. T. Chen, H. Murayama, T. Tsuboi, W. S. Li, I. Chao, S. W. Liu and J. K. Wang, *Adv. Funct. Mater.*, 2007, **17**, 1887-1895.
133. T. Tsuboi, S. W. Liu, M. F. Wu and C. T. Chen, *Org. Electron.*, 2009, **10**, 1372-1377.
134. M. H. Tsai, H. W. Lin, H. C. Su, T. H. Ke, C. C. Wu, F. C. Fang, Y. L. Liao, K. T. Wong and C. I. Wu, *Adv. Mater.*, 2006, **18**, 1216-1220.
135. S. H. Kim, J. Jang, S. J. Lee and J. Y. Lee, *Thin Solid Films*, 2008, **517**, 722-726.
136. M. H. Tsai, T. H. Ke, H. W. Lin, C. C. Wu, S. F. Chiu, F. C. Fang, Y. L. Liao, K. T. Wong, Y. H. Chen and C. I. Wu, *ACS Appl. Mater. Interfaces*, 2009, **1**, 567-574.
137. Z. Q. Jiang, Y. H. Chen, C. Fan, C. L. Yang, Q. Wang, Y. T. Tao, Z. Q. Zhang, J. G. Qin and D. G. Ma, *Chem. Commun.*, 2009, 3398-3400.
138. C. Fan, Y. H. Chen, Z. Y. Liu, Z. Q. Jiang, C. Zhong, D. G. Ma, J. G. Qin and C. L. Yang, *J. Mater. Chem. C*, 2013, **1**, 463-469.
139. H. Chen, Z. Q. Jiang, C. H. Gao, M. F. Xu, S. C. Dong, L. S. Cui, S. J. Ji and L. S. Liao, *Chem. Eur. J.*, 2013, **19**, 11791-11797.
140. M. K. Leung, W. H. Yang, C. N. Chuang, J. H. Lee, C. F. Lin, M. K. Wei and Y. H. Liu, *Org. Lett.*, 2012, **14**, 4986-4989.
141. P. A. Vecchi, A. B. Padmaperuma, H. Qiao, L. S. Sapochak and P. E. Burrows, *Org. Lett.*, 2006, **8**, 4211-4214.
142. C. M. Han, G. H. Xie, J. Li, Z. S. Zhang, H. Xu, Z. P. Deng, Y. Zhao, P. F. Yan and S. Y. Liu, *Chem. Eur. J.*, 2011, **17**, 8947-8956.

143. S. H. Jeong and J. Y. Lee, *J. Mater. Chem.*, 2011, **21**, 14604-14609.
144. C. M. Han, Z. S. Zhang, H. Xu, S. Z. Yue, J. Li, P. R. Yan, Z. P. Deng, Y. Zhao, P. F. Yan and S. Y. Liu, *J. Am. Chem. Soc.*, 2012, **134**, 19179-19188.
145. A. Chaskar, H. F. Chen and K. T. Wong, *Adv. Mater.*, 2011, **23**, 3876-3895.
146. U. S. Bhansali, H. P. Jia, M. A. Q. Lopez, B. E. Gnade, W. H. Chen and M. A. Omary, *Appl. Phys. Lett.*, 2009, **94**, 203501.
147. K. S. Yook, S. O. Jeon, C. W. Joo and J. Y. Lee, *Appl. Phys. Lett.*, 2009, **94**, 093501.
148. V. I. Adamovich, S. R. Cordero, P. I. Djurovich, A. Tamayo, M. E. Thompson, B. W. D'Andrade and S. R. Forrest, *Org. Electron.*, 2003, **4**, 77-87.
149. J. A. Hagen, W. Li, J. Steckl and J. G. Grote, *Appl. Phys. Lett.*, 2006, **88**, 171109.
150. N. Chopra, J. S. Swensen, E. Polikarpov, L. Cosimbescu, F. So and A. B. Padmaperuma, *Appl. Phys. Lett.*, 2010, **97**, 033304.
151. S. J. Su, H. Sasabe, T. Takeda and J. Kido, *Chem. Mater.*, 2008, **20**, 1691-1693.
152. C. W. Lee and J. Y. Lee, *Adv. Mater.*, 2013, **25**, 596-600.
153. B. Pan, B. Wang, Y. X. Wang, P. Xu, L. Wang, J. S. Chen and D. G. Ma, *J. Mater. Chem. C*, 2014, **2**, 2466-2469.
154. C. Fan, L. P. Zhu, T. X. Liu, B. Jiang, D. G. Ma, J. G. Qin and C. L. Yang, *Angew. Chem. Int. Ed.*, 2014, **53**, 2147-2151.
155. W. Y. Hung, T. H. Ke, Y. T. Lin, C. C. Wu, T. H. Hung, T. C. Chao, K. T. Wong and C. I. Wu, *Appl. Phys. Lett.*, 2006, **88**, 064102.
156. M. Y. Lai, C. H. Chen, W. S. Huang, J. T. Lin, T. H. Ke, L. Y. Chen, M. H. Tsai and C. C. Wu, *Angew. Chem. Int. Ed.*, 2008, **47**, 581-585.
157. C. H. Chen, W. S. Huang, M. Y. Lai, W. C. Tsao, J. T. Lin, Y. H. Wu, T. H. Ke, L. Y. Chen and C. C. Wu, *Adv. Funct. Mater.*, 2009, **19**, 2661-2670.
158. Z. Y. Ge, T. Hayakawa, S. Ando, M. Ueda, T. Akiike, H. Miyamoto, T. Kajita and M. A. Kakimoto, *Adv. Funct. Mater.*, 2008, **18**, 584-590.
159. S. L. Gong, C. Zhong, Q. Fu, D. G. Ma, J. G. Qin and C. L. Yang, *J. Phys. Chem. C*, 2013, **117**, 549-555.
160. S. Y. Takizawa, V. A. Montes and P. Anzenbacher, *Chem. Mater.*, 2009, **21**, 2452-2458.
161. S. L. Gong, Y. B. A. Zhao, M. Wang, C. L. Yang, C. Zhong, J. G. Qin and D. G. Ma, *Chem. Asian J.*, 2010, **5**, 2093-2099.
162. S. L. Gong, Y. H. Chen, C. L. Yang, C. Zhong, J. G. Qin and D. G. Ma, *Adv. Mater.*, 2010, **22**, 5370-5373.
163. Y. T. Tao, Q. Wang, Y. Shang, C. L. Yang, L. Ao, J. G. Qin, D. G. Ma and Z. G. Shuai, *Chem. Commun.*, 2009, 77-79.
164. F. Dumur and F. Goubard, *New J. Chem.*, 2014, **38**, 2204-2224.
165. S. L. Gong, Q. Fu, W. X. Zeng, C. Zhong, C. L. Yang, D. G. Ma and J. G. Qin, *Chem. Mater.*, 2012, **24**, 3120-3127.
166. Y. T. Tao, Q. Wang, L. Ao, C. Zhong, J. G. Qin, C. L. Yang and D. G. Ma, *J. Mater. Chem.*, 2010, **20**, 1759-1765.
167. Y. T. Tao, Q. A. Wang, C. L. Yang, J. G. Qin and D. G. Ma, *ACS Appl. Mater. Interfaces*, 2010, **2**, 2813-2818.

168. Y. T. Tao, Q. A. Wang, C. L. Yang, C. Zhong, J. G. Qin and D. G. Ma, *Adv. Funct. Mater.*, 2010, **20**, 2923-2929.
169. S. L. Gong, Y. H. Chen, J. J. Luo, C. L. Yang, C. Zhong, J. G. Qin and D. G. Ma, *Adv. Funct. Mater.*, 2011, **21**, 1168-1178.
170. S. L. Gong, Q. Fu, Q. Wang, C. L. Yang, C. Zhong, J. G. Qin and D. G. Ma, *Adv. Mater.*, 2011, **23**, 4956-4959.
171. Y. H. Son, Y. J. Kim, M. J. Park, H. Y. Oh, J. S. Park, J. H. Yang, M. C. Suh and J. H. Kwon, *J. Mater. Chem. C*, 2013, **1**, 5008-5014.
172. H. Sasabe, D. Tanaka, D. Yokoyama, T. Chiba, Y. J. Pu, K. Nakayama, M. Yokoyama and J. Kido, *Adv. Funct. Mater.*, 2011, **21**, 336-342.
173. L. X. Xiao, B. Y. Qi, X. Xing, L. L. Zheng, S. Kong, Z. J. Chen, B. Qu, L. P. Zhang, Z. W. Ji and Q. H. Gong, *J. Mater. Chem.*, 2011, **21**, 19058-19062.
174. M. Ichikawa, T. Yamamoto, H. G. Jeon, K. Kase, S. Hayashi, M. Nagaoka and N. Yokoyama, *J. Mater. Chem.*, 2012, **22**, 6765-6773.
175. M. Kim and J. Y. Lee, *Chem. Asian J.*, 2012, **7**, 899-902.
176. X. K. Liu, C. J. Zheng, M. F. Lo, J. Xiao, Z. Chen, C. L. Liu, C. S. Lee, M. K. Fung and X. H. Zhang, *Chem. Mater.*, 2013, **25**, 4454-4459.
177. E. Polikarpov, J. S. Swensen, N. Chopra, F. So and A. B. Padmaperuma, *Appl. Phys. Lett.*, 2009, **94**, 223304.
178. U. S. Bhansali, E. Polikarpov, J. S. Swensen, W. H. Chen, H. P. Jia, D. J. Gaspar, B. E. Gnade, A. B. Padmaperuma and M. A. Omary, *Appl. Phys. Lett.*, 2009, **95**, 233304.
179. X. K. Liu, C. J. Zheng, M. F. Lo, J. Xiao, C. S. Lee, M. K. Fung and X. H. Zhang, *Chem. Commun.*, 2014, **50**, 2027-2029.
180. S. L. Gong, Y. L. Chang, K. L. Wu, R. White, Z. H. Lu, D. T. Song and C. L. Yang, *Chem. Mater.*, 2014, **26**, 1463-1470.
181. F. M. Hsu, C. H. Chien, C. F. Shu, C. H. Lai, C. C. Hsieh, K. W. Wang and P. T. Chou, *Adv. Funct. Mater.*, 2009, **19**, 2834-2843.
182. C. H. Chien, F. M. Hsu, C. F. Shu and Y. Chi, *Org. Electron.*, 2009, **10**, 871-876.
183. S. C. Dong, Y. Liu, Q. Li, L. S. Cui, H. Chen, Z. Q. Jiang and L. S. Liao, *J. Mater. Chem. C*, 2013, **1**, 6575-6584.
184. F. M. Hsu, C. H. Chien, Y. J. Hsieh, C. H. Wu, C. F. Shu, S. W. Liu and C. T. Chen, *J. Mater. Chem.*, 2009, **19**, 8002-8008.
185. J. Ye, Z. Chen, K. Wang, F. An, Y. Yuan, W. Chen, Q. Yang, X. Zhang and C.-S. Lee, *Chem. Eur. J.*, 2014, **20**, 13762–13769.
186. S. Yamaguchi, S. Akiyama and K. Tamao, *J. Am. Chem. Soc.*, 2001, **123**, 11372-11375.
187. H. G. Jang, B. S. Kim, J. Y. Lee and S. H. Hwang, *Dalton Trans.*, 2014, **43**, 7712-7715.
188. H. P. Shi, D. H. Xin, X. Q. Dong, J. X. Dai, X. H. Wu, Y. Q. Miao, L. Fang, H. Wang and M. M. F. Choi, *J. Mater. Chem. C*, 2014, **2**, 2160-2168.
189. W. Y. Hung, L. C. Chi, W. J. Chen, E. Mondal, S. H. Chou, K. T. Wong and Y. Chi, *J. Mater. Chem.*, 2011, **21**, 19249-19256.
190. Y. M. Chen, W. Y. Hung, H. W. You, A. Chaskar, H. C. Ting, H. F. Chen, K. T. Wong and Y. H. Liu, *J. Mater. Chem.*, 2011, **21**, 14971-14978.

191. S. H. Chou, W. Y. Hung, C. M. Chen, Q. Y. Liu, Y. H. Liu and K. T. Wong, *RSC Adv.*, 2013, **3**, 13891-13900.
192. H. Huang, X. Yang, B. Pan, L. Wang, J. S. Chen, D. H. Ma and C. L. Yang, *J. Mater. Chem.*, 2012, **22**, 13223-13230.
193. H. Huang, Y. X. Wang, S. Q. Zhuang, X. Yang, L. Wang and C. L. Yang, *J. Phys. Chem. C*, 2012, **116**, 19458-19466.
194. H. Huang, Y. X. Wang, B. Wang, S. Q. Zhuang, B. Pan, X. Yang, L. Wang and C. L. Yang, *J. Mater. Chem. C*, 2013, **1**, 5899-5908.
195. E. Mondal, W. Y. Hung, Y. H. Chen, M. H. Cheng and K. T. Wong, *Chem. Eur. J.*, 2013, **19**, 10563-10572.
196. S.-H. Cheng, W.-Y. Hung, M.-H. Cheng, H.-F. Chen, A. Chaskar, G.-H. Lee, S.-H. Chou and K.-T. Wong, *J. Mater. Chem. C*, 2014, **2**, 8554-8563.
197. H. Huang, Y. X. Wang, B. Pan, X. Yang, L. Wang, J. S. Chen, D. G. Ma and C. L. Yang, *Chem. Eur. J.*, 2013, **19**, 1828-1834.
198. H. C. Ting, Y. M. Chen, H. W. You, W. Y. Hung, S. H. Lin, A. Chaskar, S. H. Chou, Y. Chi, R. H. Liu and K. T. Wong, *J. Mater. Chem.*, 2012, **22**, 8399-8407.
199. Y. T. Tao, Q. Wang, C. L. Yang, Q. Wang, Z. Q. Zhang, T. T. Zou, J. G. Qin and D. G. Ma, *Angew. Chem. Int. Ed.*, 2008, **47**, 8104-8107.
200. Y. T. Tao, Q. Wang, C. L. Yang, C. Zhong, K. Zhang, J. G. Qin and D. G. Ma, *Adv. Funct. Mater.*, 2010, **20**, 304-311.
201. E. Mondal, W. Y. Hung, H. C. Dai and K. T. Wong, *Adv. Funct. Mater.*, 2013, **23**, 3096-3105.
202. Q. Li, L. S. Cui, C. Zhong, X. D. Yuan, S. C. Dong, Z. Q. Jiang and L. S. Liao, *Dyes Pigm.*, 2014, **101**, 142-149.
203. Q. Li, L. S. Cui, C. Zhong, Z. Q. Jiang and L. S. Liao, *Org. Lett.*, 2014, **16**, 1622-1625.
204. J. J. Jin, W. Z. Zhang, B. Wang, G. Y. Mu, P. Xu, L. Wang, H. Huang, J. S. Chen and D. G. Ma, *Chem. Mater.*, 2014, **26**, 2388-2395.
205. C. S. Wu, J. W. Wu and Y. Chen, *J. Mater. Chem.*, 2012, **22**, 23877-23884.
206. M. K. Kim, J. Kwon, T. H. Kwon and J. I. Hong, *New J. Chem.*, 2010, **34**, 1317-1322.
207. Y. T. Tao, Q. Wang, L. Ao, C. Zhong, C. L. Yang, J. G. Qin and D. G. Ma, *J. Phys. Chem. C*, 2010, **114**, 601-609.
208. J. H. Kim, D. Y. Yoon, J. W. Kim and J. J. Kim, *Synth. Met.*, 2007, **157**, 743-750.
209. J. Y. Zhuang, W. M. Su, W. F. Li, Y. Y. Zhou, Q. Shen and M. Zhou, *Org. Electron.*, 2012, **13**, 2210-2219.
210. J. Y. Zhuang, W. F. Li, W. M. Su, M. Zhou and Z. Cui, *New J. Chem.*, 2014, **38**, 650-656.
211. M. K. Leung, Y. H. Hsieh, T. Y. Kuo, P. T. Chou, J. H. Lee, T. L. Chiu and H. J. Chen, *Org. Lett.*, 2013, **15**, 4694-4697.
212. X. H. Zhao, Z. S. Zhang, Y. Qian, M. D. Yi, L. H. Xie, C. P. Hu, G. H. Xie, H. Xu, C. M. Han, Y. Zhao and W. Huang, *J. Mater. Chem. C*, 2013, **1**, 3482-3490.
213. D. Wagner, S. T. Hoffmann, U. Heinemeyer, I. Munster, A. Kohler and P. Strohriegl, *Chem. Mater.*, 2013, **25**, 3758-3765.
214. Z. F. An, R. F. Chen, J. Yin, G. H. Xie, H. F. Shi, T. Tsuboi and W. Huang, *Chem. Eur. J.*, 2011, **17**, 10871-10878.

215. M. M. Rothmann, S. Haneder, E. Da Como, C. Lennartz, C. Schildknecht and P. Strohriegl, *Chem. Mater.*, 2010, **22**, 2403-2410.
216. M. M. Rothmann, E. Fuchs, C. Schildknecht, N. Langer, C. Lennartz, I. Munster and P. Strohriegl, *Org. Electron.*, 2011, **12**, 1192-1197.
217. Z. M. Hudson, Z. B. Wang, M. G. Helander, Z. H. Lu and S. N. Wang, *Adv. Mater.*, 2012, **24**, 2922-2928.
218. S. J. Su, C. Cai and J. Kido, *Chem. Mater.*, 2011, **23**, 274-284.
219. C. W. Lee and J. Y. Lee, *Dyes Pigm.*, 2014, **109**, 1-5.
220. C. W. Lee and J. Y. Lee, *Dyes Pigm.*, 2014, **103**, 34-38.
221. M. S. Park and J. Y. Lee, *Org. Electron.*, 2013, **14**, 1291-1296.
222. C. H. Chen, L. C. Hsu, P. Rajamalli, Y. W. Chang, F. I. Wu, C. Y. Liao, M. J. Chiu, P. Y. Chou, M. J. Huang, L. K. Chu and C. H. Cheng, *J. Mater. Chem. C*, 2014, **2**, 6183-6191.
223. D. D. Zhang, L. Duan, D. Q. Zhang, J. Qiao, G. F. Dong, L. D. Wang and Y. Qiu, *Org. Electron.*, 2013, **14**, 260-266.
224. C. H. Chang, M. C. Kuo, W. C. Lin, Y. T. Chen, K. T. Wong, S. H. Chou, E. Mondal, R. C. Kwong, S. A. Xia, T. Nakagawa and C. Adachi, *J. Mater. Chem.*, 2012, **22**, 3832-3838.
225. X. K. Liu, C. J. Zheng, J. Xiao, J. Ye, C. L. Liu, S. D. Wang, W. M. Zhao and X. H. Zhang, *Phys. Chem. Chem. Phys.*, 2012, **14**, 14255-14261.
226. Y. Im and J. Y. Lee, *Chem. Commun.*, 2013, **49**, 5948-5950.
227. S. J. Kim, Y. J. Kim, Y. H. Son, J. A. Hur, H. A. Um, J. Shin, T. W. Lee, M. J. Cho, J. K. Kim, S. Joo, J. H. Yang, G. S. Chae, K. Choi, J. H. Kwon and D. H. Choi, *Chem. Commun.*, 2013, **49**, 6788-6790.
228. C. W. Lee and J. Y. Lee, *Chem. Mater.*, 2014, **26**, 1616-1621.
229. C. W. Lee, Y. Im, J. A. Seo and J. Y. Lee, *Org. Electron.*, 2013, **14**, 2687-2691.
230. M. S. Liu, X. Jiang, P. Herguth and A. K. Jen, *Chem. Mater.*, 2001, **13**, 3820-3822.
231. M. S. Liu, X. Jiang, S. Liu, P. Herguth and A. K.-Y. Jen, *Macromolecules*, 2002, **35**, 3532-3538.
232. M. S. Lin, S. J. Yang, H. W. Chang, Y. H. Huang, Y. T. Tsai, C. C. Wu, S. H. Chou, E. Mondal and K. T. Wong, *J. Mater. Chem.*, 2012, **22**, 16114-16120.
233. T. Zhang, Y. J. Liang, J. L. Cheng and J. Y. Li, *J. Mater. Chem. C*, 2013, **1**, 757-764.
234. S. Y. Ku, W. Y. Hung, C. W. Chen, S. W. Yang, E. Mondal, Y. Chi and K. T. Wong, *Chem. Asian J.*, 2012, **7**, 133-142.
235. E. Mondal, W. Y. Hung, H. C. Dai, H. F. Chen, P. Y. Hung and K. T. Wong, *Tetrahedron*, 2014, **70**, 6328-6336.
236. J. A. Seo, M. S. Gong and J. Y. Lee, *Org. Electron.*, 2014, **15**, 1843-1848.
237. M. Kim and J. Y. Lee, *ACS Appl. Mater. Interfaces*, 2014, **6**, 14874-14880.
238. S. O. Jeon, K. S. Yook, C. W. Joo and J. Y. Lee, *Adv. Funct. Mater.*, 2009, **19**, 3644-3649.
239. W. Jiang, L. Duan, J. Qiao, G. F. Dong, L. D. Wang and Y. Qiu, *Org. Lett.*, 2011, **13**, 3146-3149.
240. Y. J. Cho and J. Y. Lee, *Chem. Eur. J.*, 2011, **17**, 11415-11418.
241. S. O. Jeon, S. E. Jang, H. S. Son and J. Y. Lee, *Adv. Mater.*, 2011, **23**, 1436-1441.
242. S. O. Jeon and J. Y. Lee, *J. Mater. Chem.*, 2012, **22**, 7239-7244.

243. H. Huang, X. Yang, Y. X. Wang, B. Pan, L. Wang, J. S. Chen, D. G. Ma and C. L. Yang, *Org. Electron.*, 2013, **14**, 2573-2581.
244. A. Wada, T. Yasuda, Q. S. Zhang, Y. S. Yang, I. Takasu, S. Enomoto and C. Adachi, *J. Mater. Chem. C*, 2013, **1**, 2404-2407.
245. C. Fan, F. C. Zhao, P. Gan, S. F. Yang, T. X. Liu, C. Zhong, D. G. Ma, J. G. Qin and C. L. Yang, *Chem. Eur. J.*, 2012, **18**, 5510-5514.
246. S. O. Jeon, K. S. Yook, C. W. Joo and J. Y. Lee, *Adv. Mater.*, 2010, **22**, 1872-1876.
247. H. S. Son, C. W. Seo and J. Y. Lee, *J. Mater. Chem.*, 2011, **21**, 5638-5644.
248. M. Kim and J. Y. Lee, *Adv. Funct. Mater.*, 2014, **24**, 4164-4169.
249. J. Q. Ding, Q. Wang, L. Zhao, D. G. Ma, L. X. Wang, X. B. Jing and F. S. Wang, *J. Mater. Chem.*, 2010, **20**, 8126-8133.
250. H. H. Chou and C. H. Cheng, *Adv. Mater.*, 2010, **22**, 2468-2471.
251. C. H. Lin, C. W. Hsu, J. L. Liao, Y. M. Cheng, Y. Chi, T. Y. Lin, M. W. Chung, P. T. Chou, G. H. Lee, C. H. Chang, C. Y. Shih and C. L. Ho, *J. Mater. Chem.*, 2012, **22**, 10684-10694.
252. C. M. Han, Z. S. Zhang, H. Xu, J. Li, G. H. Xie, R. F. Chen, Y. Zhao and W. Huang, *Angew. Chem. Int. Ed.*, 2012, **51**, 10104-10108.
253. S. H. Jeong, C. W. Seo, J. Y. Lee, N. S. Cho, J. K. Kim and J. H. Yang, *Chem. Asian J.*, 2011, **6**, 2895-2898.
254. C. M. Han, Z. S. Zhang, H. Xu, J. Li, Y. Zhao, P. F. Yan and S. Y. Liu, *Chem. Eur. J.*, 2013, **19**, 1385-1396.
255. S. O. Jeon and J. Y. Lee, *J. Mater. Chem.*, 2012, **22**, 10537-10541.
256. J. K. Bin, J. Yang and J. I. Hong, *J. Mater. Chem.*, 2012, **22**, 21720-21726.
257. C. W. Lee, J. A. Seo, M. S. Gong and J. Y. Lee, *Chem. Eur. J.*, 2013, **19**, 1194-1198.
258. C. W. Lee, K. S. Yook and J. Y. Lee, *Org. Electron.*, 2013, **14**, 1009-1014.
259. W. C. Lin, W. C. Huang, M. H. Huang, C. C. Fan, H. W. Lin, L. Y. Chen, Y. W. Liu, J. S. Lin, T. C. Chao and M. R. Tseng, *J. Mater. Chem. C*, 2013, **1**, 6835-6841.
260. B. S. Du, J. L. Liao, M. H. Huang, C. H. Lin, H. W. Lin, Y. Chi, H. A. Pan, G. L. Fan, K. T. Wong, G. H. Lee and P. T. Chou, *Adv. Funct. Mater.*, 2012, **22**, 3491-3499.
261. C. W. Lee and J. Y. Lee, *Chem. Commun.*, 2013, **49**, 1446-1448.
262. C. W. Lee and J. Y. Lee, *Chem. Commun.*, 2013, **49**, 6185-6187.
263. X. L. Yang, Z. Huang, J. S. Dang, C. L. Ho, G. J. Zhou and W. Y. Wong, *Chem. Commun.*, 2013, **49**, 4406-4408.
264. X. L. Yang, N. Sun, J. S. Dang, Z. Huang, C. L. Yao, X. B. Xu, C. L. Ho, G. J. Zhou, D. G. Ma, X. Zhao and W. Y. Wong, *J. Mater. Chem. C*, 2013, **1**, 3317-3326.
265. X. L. Yang, Z. Huang, C. L. Ho, G. J. Zhou, D. R. Whang, C. L. Yao, X. B. Xu, S. Y. Park, C. H. Chui and W. Y. Wong, *RSC Adv.*, 2013, **3**, 6553-6563.
266. Y. L. Rao, D. Schoenmakers, Y. L. Chang, J. S. Lu, Z. H. Lu, Y. Kang and S. N. Wang, *Chem. Eur. J.*, 2012, **18**, 11306-11316.
267. G. J. Zhou, Q. Wang, X. Z. Wang, C. L. Ho, W. Y. Wong, D. G. Ma, L. X. Wang and Z. Y. Lin, *J. Mater. Chem.*, 2010, **20**, 7472-7484.
268. Z. B. Wang, M. G. Helander, Z. M. Hudson, J. Qiu, S. Wang and Z. H. Lu, *Appl. Phys. Lett.*, 2011, **98**.

269. Z. M. Hudson, C. Sun, M. G. Helander, Y. L. Chang, Z. H. Lu and S. N. Wang, *J. Am. Chem. Soc.*, 2012, **134**, 13930-13933.
270. J. Brooks, Y. Babayan, S. Lamansky, P. I. Djurovich, I. Tsyba, R. Bau and M. E. Thompson, *Inorg. Chem.*, 2002, **41**, 3055-3066.
271. Y. M. You and S. Y. Park, *Adv. Mater.*, 2008, **20**, 3820-3826.
272. C. L. Ho, B. Yao, B. H. Zhang, K. L. Wong, W. Y. Wong, Z. Y. Xie, L. X. Wang and Z. Y. Lin, *J. Organomet. Chem.*, 2013, **730**, 144-155.
273. G. J. Zhou, Q. Wang, C. L. Ho, W. Y. Wong, D. G. Ma and L. X. Wang, *Chem. Commun.*, 2009, 3574-3576.
274. X. Yang, X. Xu, J. Zhao, J.-S. Dang, Z. Huang, X. Yan, G. Zhou and D. Wang, *Inorg. Chem.*, 2014, **53**, 12986-13000.
275. Y. M. You, C. G. An, D. S. Lee, J. J. Kim and S. Y. Park, *J. Mater. Chem.*, 2006, **16**, 4706-4713.
276. G. J. Zhou, Q. Wang, C. L. Ho, W. Y. Wong, D. G. Ma, L. X. Wang and Z. Y. Lin, *Chem. Asian J.*, 2008, **3**, 1830-1841.
277. S. O. Kim, Q. Zhao, K. Thangaraju, J. J. Kim, Y. H. Kim and S. K. Kwon, *Dyes Pigm.*, 2011, **90**, 139-145.
278. W. T. Wu, C. H. Cheng, W. H. Wu, H. M. Guo, S. M. Ji, P. Song, K. L. Han, J. Z. Zhao, X. Zhang, Y. B. Wu and G. T. Du, *Eur. J. Inorg. Chem.*, 2010, 4683-4696.
279. G. J. Zhou, X. Z. Wang, W. Y. Wong, X. M. Yu, H. S. Kwok and Z. Y. Lin, *J. Organomet. Chem.*, 2007, **692**, 3461-3473.
280. G. J. Zhou, W. Y. Wong, B. Yao, Z. Xie and L. Wang, *J. Mater. Chem.*, 2008, **18**, 1799-1809.
281. B. W. D'Andrade, J. Brooks, V. Adamovich, M. E. Thompson and S. R. Forrest, *Adv. Mater.*, 2002, **14**, 1032-1036.
282. J. Zhang, F. C. Zhao, X. J. Zhu, W. K. Wong, D. G. Ma and W. Y. Wong, *J. Mater. Chem.*, 2012, **22**, 16448-16457.
283. D. A. K. Vezzu, J. C. Deaton, J. S. Jones, L. Bartolotti, C. F. Harris, A. P. Marchetti, M. Kondakova, R. D. Pike and S. Q. Huo, *Inorg. Chem.*, 2010, **49**, 5107-5119.
284. H. Fukagawa, T. Shimizu, H. Hanashima, Y. Osada, M. Suzuki and H. Fujikake, *Adv. Mater.*, 2012, **24**, 5099-5103.
285. N. M. Hsu and W. R. Li, *Angew. Chem. Int. Ed.*, 2006, **45**, 4138-4142.
286. M. R. Zhu, J. H. Zou, X. He, C. L. Yang, H. B. Wu, C. Zhong, J. G. Qin and Y. Cao, *Chem. Mater.*, 2012, **24**, 174-180.
287. Q. B. Mei, L. X. Wang, Y. H. Guo, J. E. N. Weng, F. Yan, B. Tian and B. H. Tong, *J. Mater. Chem.*, 2012, **22**, 6878-6884.
288. X. L. Yang, Y. B. Zhao, X. W. Zhang, R. Li, J. S. Dang, Y. Li, G. J. Zhou, Z. X. Wu, D. G. Ma, W. Y. Wong, X. Zhao, A. M. Ren, L. X. Wang and X. Hou, *J. Mater. Chem.*, 2012, **22**, 7136-7148.
289. W. Y. Wong, G. J. Zhou, X. M. Yu, H. S. Kwok and B. Z. Tang, *Adv. Funct. Mater.*, 2006, **16**, 838-846.
290. M. R. Zhu, Y. H. Li, S. J. Hu, C. G. Li, C. L. Yang, H. B. Wu, J. G. Qin and Y. Cao, *Chem. Commun.*, 2012, **48**, 2695-2697.

291. M. R. Zhu, Y. H. Li, C. G. Li, C. Zhong, C. L. Yang, H. B. Wu, J. G. Qin and Y. Cao, *J. Mater. Chem.*, 2012, **22**, 11128-11133.
292. V. W. W. Yam, K. M. C. Wong, L. L. Hung and N. Y. Zhu, *Angew. Chem. Int. Ed.*, 2005, **44**, 3107-3110.
293. K. M. C. Wong, X. L. Zhu, L. L. Hung, N. Y. Zhu, V. W. W. Yam and H. S. Kwok, *Chem. Commun.*, 2005, 2906-2908.
294. V. K. M. Au, K. M. C. Wong, D. P. K. Tsang, M. Y. Chan, N. Y. Zhu and V. W. W. Yam, *J. Am. Chem. Soc.*, 2010, **132**, 14273-14278.
295. M.-C. Tang, C. K.-M. Chan, D. P.-K. Tsang, Y.-C. Wong, M. M.-Y. Chan, K. M.-C. Wong and V. W.-W. Yam, *Chem. Eur. J.*, 2014, **20**, 15233-15241.
296. M. C. Tang, D. P. K. Tsang, M. M. Y. Chan, K. M. C. Wong and V. W. W. Yam, *Angew. Chem. Int. Ed.*, 2013, **52**, 446-449.
297. K. Albrecht and K. Yamamoto, *J. Am. Chem. Soc.*, 2009, **131**, 2244-2251.
298. C. L. Yang, X. W. Zhang, H. You, L. Y. Zhu, L. Q. Chen, L. N. Zhu, Y. T. Tao, D. G. Ma, Z. G. Shuai and J. G. Qin, *Adv. Funct. Mater.*, 2007, **17**, 651-661.
299. C. L. Ho, W. Y. Wong, B. Yao, Z. Y. Xie, L. X. Wang and Z. Y. Lin, *J. Organomet. Chem.*, 2009, **694**, 2735-2749.
300. C. H. Chen, F. I. Wu, Y. Y. Tsai and C. H. Cheng, *Adv. Funct. Mater.*, 2011, **21**, 3150-3158.
301. S. L. Lai, W. Y. Tong, S. C. F. Kui, M. Y. Chan, C. C. Kwok and C. M. Che, *Adv. Funct. Mater.*, 2013, **23**, 5168-5176.
302. X. C. Hang, T. Fleetham, E. Turner, J. Brooks and J. Li, *Angew. Chem. Int. Ed.*, 2013, **52**, 6753-6756.
303. G. Li, J. Ecton, B. O'Brien and J. Li, *Org. Electron.*, 2014, **15**, 1862-1867.
304. S. J. Lee, J. S. Park, M. Song, I. A. Shin, Y. I. Kim, J. W. Lee, J. W. Kang, Y. S. Gal, S. Kang, J. Y. Lee, S. H. Jung, H. S. Kim, M. Y. Chae and S. H. Jin, *Adv. Funct. Mater.*, 2009, **19**, 2205-2212.
305. M. Song, J. S. Park, Y. S. Gal, S. Kang, J. Y. Lee, J. W. Lee and S. H. Jin, *J. Phys. Chem. C*, 2012, **116**, 7526-7533.
306. N. Tian, Y. V. Aulin, D. Lenkeit, S. Pelz, O. V. Mikhnenko, P. W. M. Blom, M. A. Loi and E. Holder, *Dalton Trans.*, 2010, **39**, 8613-8615.
307. N. Tian, A. Thiessen, R. Schiewek, O. J. Schmitz, D. Hertel, K. Meerholz and E. Holder, *J. Org. Chem.*, 2009, **74**, 2718-2725.
308. W. Y. Wong, C. L. Ho, Z. Q. Gao, B. X. Mi, C. H. Chen, K. W. Cheah and Z. Lin, *Angew. Chem. Int. Ed. Engl.*, 2006, **45**, 7800-7803.
309. C. L. Ho, Q. Wang, C. S. Lam, W. Y. Wong, D. Ma, L. Wang, Z. Q. Gao, C. H. Chen, K. W. Cheah and Z. Lin, *Chem. Asian J.*, 2009, **4**, 89-103.
310. M. Tavasli, T. N. Moore, Y. Zheng, M. R. Bryce, M. A. Fox, G. C. Griffiths, V. Jankus, H. A. Al-Attar and A. P. Monkman, *J. Mater. Chem.*, 2012, **22**, 6419-6428.
311. J. Q. Ding, J. H. Lu, Y. X. Cheng, Z. Y. Xie, L. X. Wang, X. B. Jing and F. S. Wang, *Adv. Funct. Mater.*, 2008, **18**, 2754-2762.
312. T. D. Anthopoulos, M. J. Frampton, E. B. Namdas, P. L. Burn and I. D. W. Samuel, *Adv. Mater.*, 2004, **16**, 557-560.

313. Y. J. Pu, N. Iguchi, N. Aizawa, H. Sasabe, K. Nakayama and J. Kido, *Org. Electron.*, 2011, **12**, 2103-2110.
314. D. B. Xia, B. Wang, B. Chen, S. M. Wang, B. H. Zhang, J. Q. Ding, L. X. Wang, X. B. Jing and F. S. Wang, *Angew. Chem. Int. Ed.*, 2014, **53**, 1048-1052.
315. J. L. Chen, S. Y. Chang, Y. Chi, K. Chen, Y. M. Cheng, C. W. Lin, G. H. Lee, P. T. Chou, C. H. Wu, P. I. Shih and C. F. Shu, *Chem. Asian J.*, 2008, **3**, 2112-2123.
316. S. Y. Chang, J. Kavitha, J. Y. Hung and Y. Chi, *Inorg. Chem.*, 2007, **46**, 7064-7074.
317. B. W. Ma, B. J. Kim, D. A. Poulsen, S. J. Pastine and J. M. J. Frechet, *Adv. Funct. Mater.*, 2009, **19**, 1024-1031.
318. A. Y. Y. Tam, D. P. K. Tsang, M. Y. Chan, N. Y. Zhu and V. W. W. Yam, *Chem. Commun.*, 2011, **47**, 3383-3385.
319. W. S. Huang, J. T. Lin, C. H. Chien, Y. T. Tao, S. S. Sun and Y. S. Wen, *Chem. Mater.*, 2004, **16**, 2480-2488.
320. E. S. H. Lam, D. P. K. Tsang, W. H. Lam, A. Y. Y. Tam, M. Y. Chan, W. T. Wong and V. W. W. Yam, *Chem. Eur. J.*, 2013, **19**, 6385-6397.
321. S. C. Lo, R. N. Bera, R. E. Harding, P. L. Burn and I. D. W. Samuel, *Adv. Funct. Mater.*, 2008, **18**, 3080-3090.
322. S. Y. Chang, J. Kavitha, S. W. Li, C. S. Hsu, Y. Chi, Y. S. Yeh, P. T. Chou, G. H. Lee, A. J. Carty, Y. T. Tao and C. H. Chien, *Inorg. Chem.*, 2006, **45**, 137-146.
323. U. S. Bhansali, E. Polikarpov, J. S. Swensen, W. H. Chen, H. P. Jia, D. J. Gaspar, B. E. Gnade, A. B. Padmaperuma and M. A. Omary, *Appl. Phys. Lett.*, 2009, **95**.
324. K.-H. Kim, C.-K. Moon, J.-H. Lee, S.-Y. Kim and J.-J. Kim, *Adv. Mater.*, 2014, **26**, 3844-3847.
325. K.-Y. Lu, H.-H. Chou, C.-H. Hsieh, Y.-H. O. Yang, H.-R. Tsai, H.-Y. Tsai, L.-C. Hsu, C.-Y. Chen, I. C. Chen and C.-H. Cheng, *Adv. Mater.*, 2011, **23**, 4933-4937.
326. M. H. Li, W. H. Chen, M. T. Lin, M. A. Omary and N. D. Shepherd, *Org. Electron.*, 2009, **10**, 863-870.
327. Q. Wang, I. W. H. Oswald, M. R. Perez, H. P. Jia, A. A. Shahub, Q. Q. Qiao, B. E. Gnade and M. A. Omary, *Adv. Funct. Mater.*, 2014, **24**, 4746-4752.
328. Q. Wang, I. W. H. Oswald, M. R. Perez, H. Jia, B. E. Gnade and M. A. Omary, *Adv. Funct. Mater.*, 2013, **23**, 5420-5428.
329. M. Mydlak, M. Mauro, F. Polo, M. Felicetti, J. Leonhardt, G. Diener, L. De Cola and C. A. Strassert, *Chem. Mater.*, 2011, **23**, 3659-3667.
330. C. Cebrian, M. Mauro, D. Kourkoulos, P. Mercandelli, D. Hertel, K. Meerholz, C. A. Strassert and L. De Cola, *Adv. Mater.*, 2013, **25**, 437-442.
331. H. Li, J. Q. Ding, Z. Y. Xie, Y. X. Cheng and L. X. Wang, *J. Organomet. Chem.*, 2009, **694**, 2777-2785.
332. T. Fleetham, Z. X. Wang and J. Li, *Org. Electron.*, 2012, **13**, 1430-1435.
333. T. Fleetham, L. Huang and J. Li, *Adv. Funct. Mater.*, 2014, **24**, 6066-6073.
334. E. Turner, N. Bakken and J. Li, *Inorg. Chem.*, 2013, **52**, 7344-7351.
335. J. Ecton, T. Fleetham, X. Hang and J. Li, *SID Int. Symp. Dig. Tech.*, 2013, **44**, 152-155.
336. A. B. Tamayo, B. D. Alleyne, P. I. Djurovich, S. Lamansky, I. Tsyba, N. N. Ho, R. Bau and M.

E. Thompson, *J. Am. Chem. Soc.*, 2003, **125**, 7377-7387.
337. T. Sajoto, P. I. Djurovich, A. B. Tamayo, J. Oxgaard, W. A. Goddard and M. E. Thompson, *J. Am. Chem. Soc.*, 2009, **131**, 9813-9822.
338. H. J. Bolink, F. De Angelis, E. Baranoff, C. Klein, S. Fantacci, E. Coronado, M. Sessolo, K. Kalyanasundaram, M. Gratzel and M. K. Nazeeruddin, *Chem. Commun.*, 2009, 4672-4674.
339. J. Y. Zhuang, W. F. Li, W. M. Su, Y. Liu, Q. Shen, L. S. Liao and M. Zhou, *Org. Electron.*, 2013, **14**, 2596-2601.
340. K. P. Klubek, S.-C. Dong, L.-S. Liao, C. W. Tang and L. J. Rothberg, *Org. Electron.*, 2014, **15**, 3127-3136.
341. K. Udagawa, H. Sasabe, C. Cai and J. Kido, *Adv. Mater.*, 2014, **26**, 5062-5066.
342. X. Q. Wei, J. B. Peng, J. B. Cheng, M. G. Xie, Z. Y. Lu, C. Li and Y. Cao, *Adv. Funct. Mater.*, 2007, **17**, 3319-3325.
343. H. T. Cao, G. G. Shan, X. M. Wen, H. Z. Sun, Z. M. Su, R. L. Zhong, W. F. Xie, P. Li and D. X. Zhu, *J. Mater. Chem. C*, 2013, **1**, 7371-7379.
344. Q. Wang, J. Q. Ding, D. G. Ma, Y. X. Cheng, L. X. Wang, X. B. Jing and F. S. Wang, *Adv. Funct. Mater.*, 2009, **19**, 84-95.
345. S. C. Lo, C. P. Shipley, R. N. Bera, R. E. Harding, A. R. Cowley, P. L. Burn and I. D. W. Samuel, *Chem. Mater.*, 2006, **18**, 5119-5129.
346. S. C. Lo, R. E. Harding, C. P. Shipley, S. G. Stevenson, P. L. Burn and I. D. W. Samuel, *J. Am. Chem. Soc.*, 2009, **131**, 16681-16688.
347. K. Li, G. Cheng, C. S. Ma, X. G. Guan, W. M. Kwok, Y. Chen, W. Lu and C. M. Che, *Chem. Sci.*, 2013, **4**, 2630-2644.
348. Y. Unger, D. Meyer, O. Molt, C. Schildknecht, I. Munster, G. Wagenblast and T. Strassner, *Angew. Chem. Int. Ed.*, 2010, **49**, 10214-10216.
349. T. Fleetham, J. Ecton, Z. X. Wang, N. Bakken and J. Li, *Adv. Mater.*, 2013, **25**, 2573-2576.
350. A. Tronnier, A. Pöthig, S. Metz, G. Wagenblast, I. Münster and T. Strassner, *Inorg. Chem.*, 2014, **53**, 6346-6356.
351. K. Li, X. G. Guan, C. W. Ma, W. Lu, Y. Chen and C. M. Che, *Chem. Commun.*, 2011, **47**, 9075-9077.
352. G. J. Li, T. Fleetham and J. Li, *Adv. Mater.*, 2014, **26**, 2931-2936.
353. S. K. Kim, B. Yang, Y. Ma, J. H. Lee and J. W. Park, *J. Mater. Chem.*, 2008, **18**, 3376-3384.
354. T. Sajoto, P. I. Djurovich, A. Tamayo, M. Yousufuddin, R. Bau, M. E. Thompson, R. J. Holmes and S. R. Forrest, *Inorg. Chem.*, 2005, **44**, 7992-8003.
355. R. J. Holmes, S. R. Forrest, T. Sajoto, A. Tamayo, P. I. Djurovich, M. E. Thompson, J. Brooks, Y. J. Tung, B. W. D'Andrade, M. S. Weaver, R. C. Kwong and J. J. Brown, *Appl. Phys. Lett.*, 2005, **87**, 243507.
356. H. Sasabe, J. Takamatsu, T. Motoyama, S. Watanabe, G. Wagenblast, N. Langer, O. Molt, E. Fuchs, C. Lennartz and J. Kido, *Adv. Mater.*, 2010, **22**, 5003-5007.
357. C. H. Yang, Y. M. Cheng, Y. Chi, C. J. Hsu, F. C. Fang, K. T. Wong, P. T. Chou, C. H. Chang, M. H. Tsai and C. C. Wu, *Angew. Chem. Int. Ed.*, 2007, **46**, 2418-2421.
358. C. F. Chang, Y. M. Cheng, Y. Chi, Y. C. Chiu, C. C. Lin, G. H. Lee, P. T. Chou, C. C. Chen, C. H. Chang and C. C. Wu, *Angew. Chem. Int. Ed.*, 2008, **47**, 4542-4545.

359. C. H. Hsieh, F. I. Wu, C. H. Fan, M. J. Huang, K. Y. Lu, P. Y. Chou, Y. H. O. Yang, S. H. Wu, I. C. Chen, S. H. Chou, K. T. Wong and C. H. Cheng, *Chem. Eur. J.*, 2011, **17**, 9180-9187.
360. S. J. Yoo, H. J. Yun, I. Kang, K. Thangaraju, S. K. Kwon and Y. H. Kim, *J. Mater. Chem. C*, 2013, **1**, 2217-2223.
361. L. J. Deng, T. Zhang, R. J. Wang and J. Y. Li, *J. Mater. Chem.*, 2012, **22**, 15910-15918.
362. Z. He, W. Y. Wong, X. M. Yu, H. S. Kwok and Z. Y. Lin, *Inorg. Chem.*, 2006, **45**, 10922-10937.
363. W. Lu, M. C. W. Chan, N. Y. Zhu, C. M. Che, C. N. Li and Z. Hui, *J. Am. Chem. Soc.*, 2004, **126**, 7639-7651.
364. M. S. Eum, C. S. Chin, S. Y. Kim, C. Kim, S. K. Kang, N. H. Hur, J. H. Seo, G. Y. Kim and Y. K. Kim, *Inorg. Chem.*, 2008, **47**, 6289-6295.
365. J. Braddock-Wilking, L. B. Gao and N. P. Rath, *Dalton Trans.*, 2010, **39**, 9321-9328.
366. T. C. Lee, C. F. Chang, Y. C. Chiu, Y. Chi, T. Y. Chan, Y. M. Cheng, C. H. Lai, P. T. Chou, G. H. Lee, C. H. Chien, C. F. Shu and J. Leonhardt, *Chem. Asian J.*, 2009, **4**, 742-753.
367. C. H. Chang, C. L. Ho, Y. S. Chang, I. C. Lien, C. H. Lin, Y. W. Yang, J. L. Liao and Y. Chi, *J. Mater. Chem. C*, 2013, **1**, 2639-2647.
368. F. S. Zhang, L. D. Wang, S. H. Chang, K. L. Huang, Y. Chi, W. Y. Hung, C. M. Chen, G. H. Lee and P. T. Chou, *Dalton Trans.*, 2013, **42**, 7111-7119.
369. Y. C. Chiu, Y. Chi, J. Y. Hung, Y. M. Cheng, Y. C. Yu, M. W. Chung, G. H. Lee, P. T. Chou, C. C. Chen, C. C. Wu and H. Y. Hsieh, *ACS Appl. Mater. Interfaces*, 2009, **1**, 433-442.
370. B. Zhang, L. N. Zhang, C. M. Liu, Y. Y. Zhu, M. S. Tang, C. X. Du and M. P. Song, *Dalton Trans.*, 2014, **43**, 7704-7707.
371. Y. C. Chiu, J. Y. Hung, Y. Chi, C. C. Chen, C. H. Chang, C. C. Wu, Y. M. Cheng, Y. C. Yu, G. H. Lee and P. T. Chou, *Adv. Mater.*, 2009, **21**, 2221-2225.
372. M. Abrahamsson, M. J. Lundqvist, H. Wolpher, O. Johansson, L. Eriksson, J. Bergquist, T. Rasmussen, H.-C. Becker, L. Hammarström, P.-O. Norrby, B. Åkermark and P. Persson, *Inorg. Chem.*, 2008, **47**, 3540-3548.
373. F. Schramm, V. Meded, H. Fliegl, K. Fink, O. Fuhr, Z. Qu, W. Klopper, S. Finn, T. E. Keyes and M. Ruben, *Inorg. Chem.*, 2009, **48**, 5677-5684.
374. C. H. Lin, Y. Y. Chang, J. Y. Hung, C. Y. Lin, Y. Chi, M. W. Chung, C. L. Lin, P. T. Chou, G. H. Lee, C. H. Chang and W. C. Lin, *Angew. Chem. Int. Ed.*, 2011, **50**, 3182-3186.
375. C. H. Lin, Y. Chi, M. W. Chung, Y. J. Chen, K. W. Wang, G. H. Lee, P. T. Chou, W. Y. Hung and H. C. Chiu, *Dalton Trans.*, 2011, **40**, 1132-1143.
376. Y. L. Tung, P. C. Wu, C. S. Liu, Y. Chi, J. K. Yu, Y. H. Hu, P. T. Chou, S. M. Peng, G. H. Lee, Y. Tao, A. J. Carty, C. F. Shu and F. I. Wu, *Organometallics*, 2004, **23**, 3745-3748.
377. Y. M. Cheng, G. H. Lee, P. T. Chou, L. S. Chen, Y. Chi, C. H. Yang, Y. H. Song, S. Y. Chang, P. I. Shih and C. F. Shu, *Adv. Funct. Mater.*, 2008, **18**, 183-194.
378. S. H. Chang, C. F. Chang, J. L. Liao, Y. Chi, D. Y. Zhou, L. S. Liao, T. Y. Jiang, T. P. Chou, E. Y. Li, G. H. Lee, T. Y. Kuo and P. T. Chou, *Inorg. Chem.*, 2013, **52**, 5867-5875.
379. Y. L. Tung, S. W. Lee, Y. Chi, Y. T. Tao, C. H. Chien, Y. M. Cheng, P. T. Chou, S. M. Peng and C. S. Liu, *J. Mater. Chem.*, 2005, **15**, 460-464.
380. T. C. Lee, J. Y. Hung, Y. Chi, Y. M. Cheng, G. H. Lee, P. T. Chou, C. C. Chen, C. H. Chang

and C. C. Wu, *Adv. Funct. Mater.*, 2009, **19**, 2639-2647.
381. Y. H. Niu, Y. L. Tung, Y. Chi, C. F. Shu, J. H. Kim, B. Q. Chen, J. D. Luo, A. J. Carty and A. K. Y. Jen, *Chem. Mater.*, 2005, **17**, 3532-3536.
382. C. H. Chien, S. F. Liao, C. H. Wu, C. F. Shu, S. Y. Chang, Y. Chi, P. T. Chou and C. H. Lai, *Adv. Funct. Mater.*, 2008, **18**, 1430-1439.
383. H. Rudmann, S. Shimada and M. F. Rubner, *J. Am. Chem. Soc.*, 2002, **124**, 4918-4921.
384. Y. L. Tung, L. S. Chen, Y. Chi, P. T. Chou, Y. M. Cheng, E. Y. Li, G. H. Lee, C. F. Shu, T. I. Wu and A. J. Carty, *Adv. Funct. Mater.*, 2006, **16**, 1615-1626.
385. Y. L. Tung, S. W. Lee, Y. Chi, L. S. Chen, C. F. Shu, F. I. Wu, A. J. Carty, P. T. Chou, S. M. Peng and G. M. Lee, *Adv. Mater.*, 2005, **17**, 1059-1064.
386. D. A. Bernards, J. D. Slinker, G. G. Malliaras, S. Flores-Torres and H. D. Abruna, *Appl. Phys. Lett.*, 2004, **84**, 4980-4982.
387. H. Xia, C. Zhang, X. Liu, S. Qiu, P. Lu, F. Shen, J. Zhang and Y. Ma, *J. Phys. Chem. B*, 2004, **108**, 3185-3190.
388. H. Xia, Y. Zhu, D. Lu, M. Li, C. Zhang, B. Yang and Y. Ma, *J. Phys. Chem. B*, 2006, **110**, 18718-18723.
389. Q. Zhang, Q. Zhou, Y. Cheng, L. Wang, D. Ma, X. Jing and F. Wang, *Adv. Mater.*, 2004, **16**, 432-436.
390. Q. S. Zhang, J. Q. Ding, Y. X. Cheng, L. X. Wang, Z. Y. Xie, X. B. Jing and F. S. Wang, *Adv. Funct. Mater.*, 2007, **17**, 2983-2990.
391. J. C. Deaton, S. C. Switalski, D. Y. Kondakov, R. H. Young, T. D. Pawlik, D. J. Giesen, S. B. Harkins, A. J. M. Miller, S. F. Mickenberg and J. C. Peters, *J. Am. Chem. Soc.*, 2010, **132**, 9499-9508.
392. Z. W. Liu, M. F. Qayyum, C. Wu, M. T. Whited, P. I. Djurovich, K. O. Hodgson, B. Hedman, E. I. Solomon and M. E. Thompson, *J. Am. Chem. Soc.*, 2011, **133**, 3700-3703.
393. A. Wada, Q. S. Zhang, T. Yasuda, I. Takasu, S. Enomoto and C. Adachi, *Chem. Commun.*, 2012, **48**, 5340-5342.
394. X. L. Chen, R. M. Yu, Q. K. Zhang, L. J. Zhou, C. Y. Wu, Q. Zhang and C. Z. Lu, *Chem. Mater.*, 2013, **25**, 3910-3920.
395. Q. S. Zhang, T. Komino, S. P. Huang, S. Matsunami, K. Goushi and C. Adachi, *Adv. Funct. Mater.*, 2012, **22**, 2327-2336.
396. S.-M. Kuang, D. G. Cuttell, D. R. McMillin, P. E. Fanwick and R. A. Walton, *Inorg. Chem.*, 2002, **41**, 3313-3322.
397. C. W. Hsu, C. C. Lin, M. W. Chung, Y. Chi, G. H. Lee, P. T. Chou, C. H. Chang and P. Y. Chen, *J. Am. Chem. Soc.*, 2011, **133**, 12085-12099.
398. S. Igawa, M. Hashimoto, I. Kawata, M. Yashima, M. Hoshino and M. Osawa, *J. Mater. Chem. C*, 2013, **1**, 542-551.
399. M. Hashimoto, S. Igawa, M. Yashima, I. Kawata, M. Hoshino and M. Osawa, *J. Am. Chem. Soc.*, 2011, **133**, 10348-10351.
400. A. Tsuboyama, K. Kuge, M. Furugori, S. Okada, M. Hoshino and K. Ueno, *Inorg. Chem.*, 2007, **46**, 1992-2001.
401. V. A. Krylova, P. I. Djurovich, M. T. Whited and M. E. Thompson, *Chem. Commun.*, 2010, **46**,

6696-6698.
402. X. H. Zhao, G. H. Xie, Z. D. Liu, W. J. Li, M. D. Yi, L. H. Xie, C. P. Hu, R. Zhu, Q. Zhao, Y. Zhao, J. F. Zhao, Y. Qian and W. Huang, *Chem. Commun.*, 2012, **48**, 3854-3856.
403. S. C. F. Kui, F. F. Hung, S. L. Lai, M. Y. Yuen, C. C. Kwok, K. H. Low, S. S. Y. Chui and C. M. Che, *Chem. Eur. J.*, 2012, **18**, 96-109.
404. G. P. Tan, S. M. Chen, N. Sun, Y. H. Li, D. Fortin, W. Y. Wong, H. S. Kwok, D. G. Ma, H. B. Wu, L. X. Wang and P. D. Harvey, *J. Mater. Chem. C*, 2013, **1**, 808-821.
405. G. J. Zhou, X. L. Yang, W. Y. Wong, Q. Wang, S. Suo, D. G. Ma, J. K. Feng and L. X. Wang, *ChemPhysChem*, 2011, **12**, 2836-2843.
406. C. L. Ho, C. S. Lam, N. Sun, D. Ma, L. Liu, Z. Q. Yu, L. Xue, Z. Lin, H. Li and Y. H. Lo, *Isr. J. Chem.*, 2014, **54**, 999-1014.
407. C. Fan, L. P. Zhu, B. Jiang, Y. F. Li, F. C. Zhao, D. G. Ma, J. G. Qin and C. L. Yang, *J. Phys. Chem. C*, 2013, **117**, 19134-19141.
408. J. H. Jou, S. H. Peng, C. I. Chiang, Y. L. Chen, Y. X. Lin, Y. C. Jou, C. H. Chen, C. J. Li, W. B. Wang, S. M. Shen, S. Z. Chen, M. K. Wei, Y. S. Sun, H. W. Hung, M. C. Liu, Y. P. Lin, J. Y. Li and C. W. Wang, *J. Mater. Chem. C*, 2013, **1**, 1680-1686.
409. D. Liu, H. Ren, L. Deng and T. Zhang, *ACS Appl. Mater. Interfaces*, 2013, **5**, 4937-4944.
410. S. Lamansky, P. Djurovich, D. Murphy, F. Abdel-Razzaq, R. Kwong, I. Tsyba, M. Bortz, B. Mui, R. Bau and M. E. Thompson, *Inorg. Chem.*, 2001, **40**, 1704-1711.
411. C. L. Yao, B. Jiao, X. L. Yang, X. B. Xu, J. S. Dang, G. J. Zhou, Z. X. Wu, X. Q. Lv, Y. Zeng and W. Y. Wong, *Eur. J. Inorg. Chem.*, 2013, **2013**, 4754-4763.
412. T. Tsuzuki, N. Shirasawa, T. Suzuki and S. Tokito, *Adv. Mater.*, 2003, **15**, 1455-1458.
413. S. M. Chen, G. P. Tan, W. Y. Wong and H. S. Kwok, *Adv. Funct. Mater.*, 2011, **21**, 3785-3793.
414. J. M. Fernandez-Hernandez, J. I. Beltran, V. Lemaur, M. D. Galvez-Lopez, C. H. Chien, F. Polo, E. Orselli, R. Frohlich, J. Cornil and L. De Cola, *Inorg. Chem.*, 2013, **52**, 1812-1824.
415. C. Fan, L. P. Zhu, B. Jiang, C. Zhong, D. G. Ma, J. G. Qin and C. L. Yang, *Org. Electron.*, 2013, **14**, 3163-3171.
416. M. S. Park, H. J. Park, O. Y. Kim and J. Y. Lee, *Org. Electron.*, 2013, **14**, 1504-1509.
417. X. H. Yang, Z. X. Wang, S. Madakuni, J. Li and G. E. Jabbour, *Adv. Mater.*, 2008, **20**, 2405-2409.
418. A. F. Rausch, L. Murphy, J. A. G. Williams and H. Yersin, *Inorg. Chem.*, 2012, **51**, 312-319.
419. M. Cocchi, J. Kalinowski, V. Fattori, J. A. G. Williams and L. Murphy, *Appl. Phys. Lett.*, 2009, **94**, 073309.
420. W. Sotoyama, T. Satoh, H. Sato, A. Matsuura and N. Sawatari, *J. Phys. Chem. A*, 2005, **109**, 9760-9766.
421. D. L. Rochester, S. Develay, S. Zalis and J. A. G. Williams, *Dalton Trans.*, 2009, 1728-1741.
422. M. Cocchi, J. Kalinowski, L. Murphy, J. A. G. Williams and V. Fattori, *Org. Electron.*, 2010, **11**, 388-396.
423. L. Murphy, P. Brulatti, V. Fattori, M. Cocchi and J. A. G. Williams, *Chem. Commun.*, 2012, **48**, 5817-5819.
424. C. Adachi, R. C. Kwong, P. Djurovich, V. Adamovich, M. A. Baldo, M. E. Thompson and S. R. Forrest, *Appl. Phys. Lett.*, 2001, **79**, 2082-2084.

425. J. H. Seo, G. Y. Kim, J. H. Kim, J. S. Park, B. M. Seo, K. H. Lee, S. S. Yoon and Y. K. Kim, *Jpn. J. Appl. Phys.*, 2009, **48**, 082103.
426. C. Fan, Y. H. Li, C. L. Yang, H. B. Wu, J. G. Qin and Y. Cao, *Chem. Mater.*, 2012, **24**, 4581-4587.
427. K. S. Yook and J. Y. Lee, *Org. Electron.*, 2011, **12**, 1711-1715.
428. S. Lee, S. O. Kim, H. Shin, H. J. Yun, K. Yang, S. K. Kwon, J. J. Kim and Y. H. Kim, *J. Am. Chem. Soc.*, 2013, **135**, 14321-14328.
429. R. J. Holmes, B. W. D'Andrade, S. R. Forrest, X. Ren, J. Li and M. E. Thompson, *Appl. Phys. Lett.*, 2003, **83**, 3818-3820.
430. S. C. Lo, G. J. Richards, J. P. J. Markham, E. B. Namdas, S. Sharma, P. L. Burn and I. D. W. Samuel, *Adv. Funct. Mater.*, 2005, **15**, 1451-1458.
431. V. N. Kozhevnikov, Y. H. Zheng, M. Clough, H. A. Al-Attar, G. C. Griffiths, K. Abdullah, S. Raisys, V. Jankus, M. R. Bryce and A. P. Monkman, *Chem. Mater.*, 2013, **25**, 2352-2358.
432. C. Y. Kim, D. G. Ha, H. H. Kang, H. J. Yun, S. K. Kwon, J. J. Kim and Y. H. Kim, *J. Mater. Chem.*, 2012, **22**, 22721-22726.
433. C. H. Yang, M. Mauro, F. Polo, S. Watanabe, I. Muenster, R. Frohlich and L. De Cola, *Chem. Mater.*, 2012, **24**, 3684-3695.
434. Y. Kang, Y. L. Chang, J. S. Lu, S. B. Ko, Y. L. Rao, M. Varlan, Z. H. Lu and S. N. Wang, *J. Mater. Chem. C*, 2013, **1**, 441-450.
435. F. Kessler, Y. Watanabe, H. Sasabe, H. Katagiri, M. K. Nazeeruddin, M. Gratzel and J. Kido, *J. Mater. Chem. C*, 2013, **1**, 1070-1075.
436. C. H. Chang, Z. J. Wu, C. H. Chiu, Y. H. Liang, Y. S. Tsai, J. L. Liao, Y. Chi, H. Y. Hsieh, T. Y. Kuo, G. H. Lee, H. A. Pan, P. T. Chou, J. S. Lin and M. R. Tseng, *ACS Appl. Mater. Interfaces*, 2013, **5**, 7341-7351.
437. V. Sivasubramaniam, F. Brodkorb, S. Hanning, H. P. Loebl, V. van Elsbergen, H. Boerner, U. Scherf and M. Kreyenschmidt, *J. Fluorine Chem.*, 2009, **130**, 640-649.
438. Z. M. Hudson, M. G. Helander, Z. H. Lu and S. N. Wang, *Chem. Commun.*, 2011, **47**, 755-757.
439. M. R. Zhu, Y. H. Li, J. S. Miao, B. Jiang, C. L. Yang, H. Wu, J. G. Qin and Y. Cao, *Org. Electron.*, 2014, **15**, 1598-1606.
440. X. B. Xu, X. L. Yang, J. S. Dang, G. J. Zhou, Y. Wu, H. Li and W. Y. Wong, *Chem. Commun.*, 2014, **50**, 2473-2476.
441. X. Xu, X. Yang, Y. Wu, G. Zhou, C. Wu and W. Y. Wong, *Chem. Asian J.*, 2015, **10**, 252-262.
442. L. C. Chen, J. Q. Ding, Y. X. Cheng, Z. Y. Xie, L. X. Wang, X. B. Jing and F. S. Wang, *Chem. Asian J.*, 2011, **6**, 1372-1380.
443. W. W. Tian, C. Yi, B. Song, Q. Qi, W. Jiang, Y. P. Zheng, Z. J. Qi and Y. M. Sun, *J. Mater. Chem. C*, 2014, **2**, 1104-1115.
444. S. Y. Chang, Y. M. Cheng, Y. Chi, Y. C. Lin, C. M. Jiang, G. H. Lee and P. T. Chou, *Dalton Trans.*, 2008, 6901-6911.
445. V. K. Rai, M. Nishiura, M. Takimoto and Z. M. Hou, *Chem. Commun.*, 2011, **47**, 5726-5728.
446. K. Chao, K. Z. Shao, T. Peng, D. X. Zhu, Y. Wang, Y. Liu, Z. M. Su and M. R. Bryce, *J. Mater. Chem. C*, 2013, **1**, 6800-6806.

447. Y. Liu, K. Q. Ye, Y. Fan, W. F. Song, Y. Wang and Z. M. Hou, *Chem. Commun.*, 2009, 3699-3701.
448. T. Peng, H. Bi, Y. Liu, Y. Fan, H. Z. Gao, Y. Wang and Z. M. Hou, *J. Mater. Chem.*, 2009, **19**, 8072-8074.
449. T. Peng, Y. Yang, Y. Liu, D. G. Ma, Z. M. Hou and Y. Wang, *Chem. Commun.*, 2011, **47**, 3150-3152.
450. T. Peng, Y. Yang, H. Bi, Y. Liu, Z. M. Hou and Y. Wang, *J. Mater. Chem.*, 2011, **21**, 3551-3553.
451. V. K. Rai, M. Nishiura, M. Takimoto and Z. M. Hou, *J. Mater. Chem. C*, 2013, **1**, 677-689.
452. V. K. Rai, M. Nishiura, M. Takimoto, S. S. Zhao, Y. Liu and Z. M. Hou, *Inorg. Chem.*, 2012, **51**, 822-835.
453. T. Peng, G. M. Li, K. Q. Ye, C. G. Wang, S. S. Zhao, Y. Liu, Z. M. Hou and Y. Wang, *J. Mater. Chem. C*, 2013, **1**, 2920-2926.
454. Y. C. Zhu, L. Zhou, H. Y. Li, Q. L. Xu, M. Y. Teng, Y. X. Zheng, J. L. Zuo, H. J. Zhang and X. Z. You, *Adv. Mater.*, 2011, **23**, 4041-4046.
455. H. Y. Li, L. Zhou, M. Y. Teng, Q. L. Xu, C. Lin, Y. X. Zheng, J. L. Zuo, H. J. Zhang and X. Z. You, *J. Mater. Chem. C*, 2013, **1**, 560-565.
456. Q. L. Xu, C. C. Wang, T. Y. Li, M. Y. Teng, S. Zhang, Y. M. Jing, X. Yang, W. N. Li, C. Lin, Y. X. Zheng, J. L. Zuo and X. Z. You, *Inorg. Chem.*, 2013, **52**, 4916-4925.
457. J. Wang, J. Liu, S. J. Huang, X. K. Wu, X. D. Shi, C. P. Chen, Z. C. Ye, J. G. Lu, Y. K. Su, G. F. He and Y. X. Zheng, *Org. Electron.*, 2013, **14**, 2854-2858.